

## Applications of Dynamic Covalent Bonds in Chemical Reaction Networks

Spitzbarth, B.

**DOI**

[10.4233/uuid:a26f9d02-74db-4f87-b99b-5b226065c598](https://doi.org/10.4233/uuid:a26f9d02-74db-4f87-b99b-5b226065c598)

**Publication date**

2024

**Document Version**

Final published version

**Citation (APA)**

Spitzbarth, B. (2024). *Applications of Dynamic Covalent Bonds in Chemical Reaction Networks*. [Dissertation (TU Delft), Delft University of Technology]. <https://doi.org/10.4233/uuid:a26f9d02-74db-4f87-b99b-5b226065c598>

**Important note**

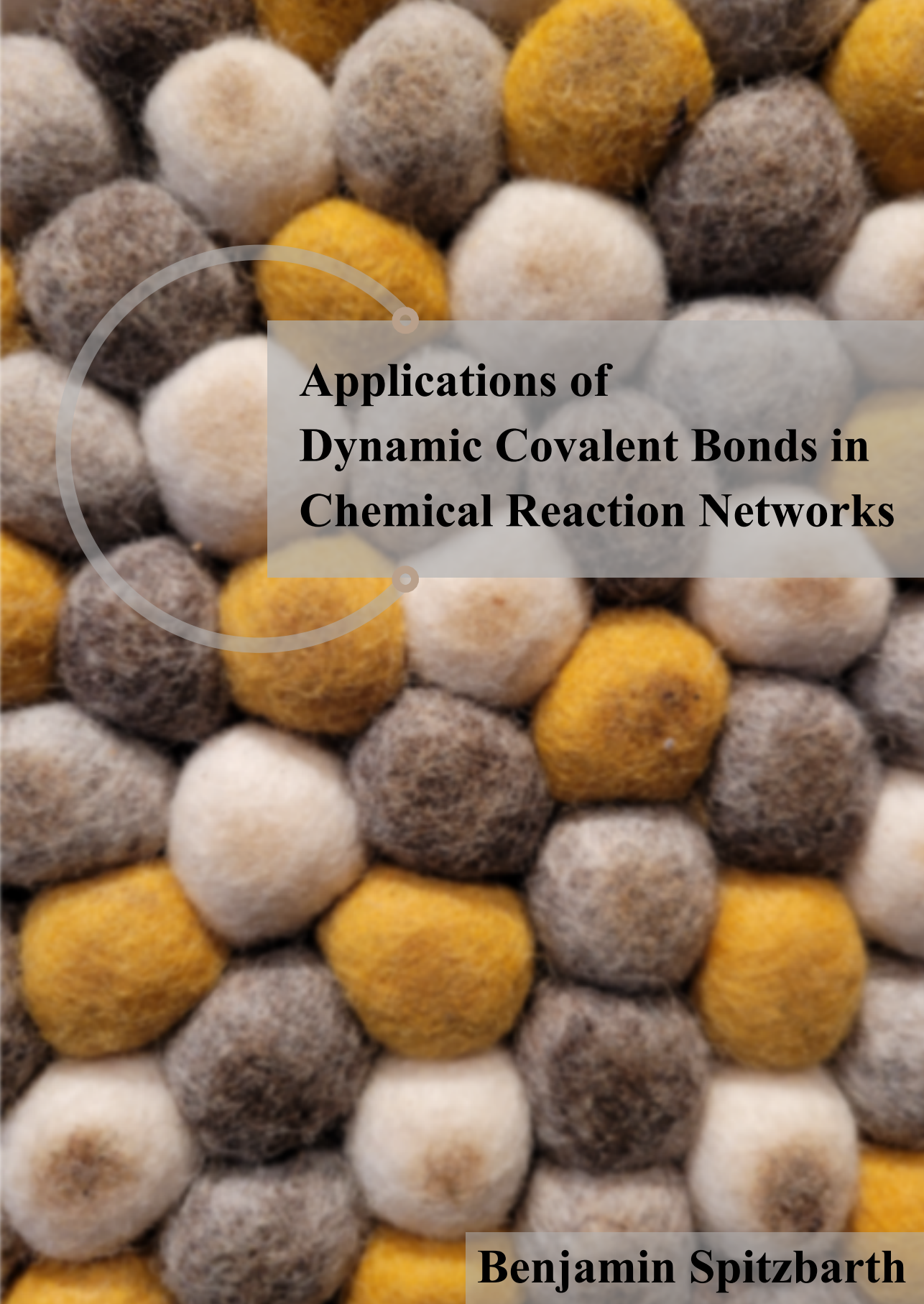
To cite this publication, please use the final published version (if applicable). Please check the document version above.

**Copyright**

Other than for strictly personal use, it is not permitted to download, forward or distribute the text or part of it, without the consent of the author(s) and/or copyright holder(s), unless the work is under an open content license such as Creative Commons.

**Takedown policy**

Please contact us and provide details if you believe this document breaches copyrights. We will remove access to the work immediately and investigate your claim.

The background of the entire page is a dense, close-up photograph of numerous small, spherical objects. These spheres are in various colors, including bright yellow, off-white, and a dark charcoal grey. They appear to be made of a porous, fibrous material, possibly microbeads or small pieces of polymer. The lighting is soft, creating subtle shadows and highlights on the surfaces of the spheres, giving them a three-dimensional appearance. A semi-transparent grey rectangular box is overlaid on the right side of the image, containing the title text. A thin, light grey circular line is also present, partially overlapping the box and the background spheres.

# **Applications of Dynamic Covalent Bonds in Chemical Reaction Networks**

**Benjamin Spitzbarth**

## Propositions

accompanying the dissertation with the title

*Applications of Dynamic Covalent Bonds in Chemical Reaction Networks*

by Benjamin Spitzbarth

1. The choice of solvent is one of the most important, yet underestimated, factors in the kinetics of chemical reactions.  
Chapters 3, 4, and 6 of this Thesis
2. Under- and misreported synthesis procedures cause massive time and resource losses in research.  
Chapters 4 and 6 of this Thesis
3. “To affirm or deny is to limit; to limit is to shut out the light of truth.” From ‘The Zen Teaching of Huang Po’, John Blofeld Translator’s Introduction.  
— Science, by affirming or denying, is inherently self-limiting.
4. Every knowingly unhealthful choice is an act of self-violence.
5. The modern carbohydrate-rich diet in conjunction with conventional farming practices are destroying the health of our land and bodies.
6. The majority of medical interventions cause more disease burden than they alleviate, due to lack of a holistic, individual-oriented approach.
7. “To know nothing about yourself is to live. To know yourself badly is to think.” From ‘The Book of Disquiet’ by Fernando Pessoa, Chapter 39.  
— The current mental health crisis indicates that we are not ready for dealing with the information age in a sane way.
8. CO<sub>2</sub> emissions are an entirely insufficient measure of environmental burden.
9. The burden of changing the planet (e.g. the climate) must be on the system, not the individual.
10. Being absolutely sure is the safest way to be wrong.

*These propositions are regarded as opposable and defensible, and have been approved as such by the promotor Dr. Rienk Eelkema and promotor Prof. dr. Jan H. van Esch.*

# **Applications of Dynamic Covalent Bonds in Chemical Reaction Networks**

Dissertation

for the purpose of obtaining the degree of doctor  
at Delft University of Technology

by the authority of the Rector Magnificus, Prof. dr. ir. T.H.J.J. van der Hagen,  
chair of the Board for Doctorates

to be defended publicly on

Thursday 8 February 2024 at 12:30 o'clock

by

**Benjamin SPITZBARTH**

Master of Science in Chemistry, Johannes-Gutenberg-Universität Mainz, Germany,  
born in Frankfurt am Main, Germany

This dissertation has been approved by the promotor.

Composition of the doctoral committee:

Rector Magnificus	chairperson
Dr. R. Eelkema	Delft University of Technology, promotor
Prof. dr. J. H. van Esch	Delft University of Technology, promotor

Independent members:

Prof. dr. E. A. Pidko	Delft University of Technology
Prof. dr. U. Hanefeld	Delft University of Technology
Prof. dr. R. V. Ulijn	City University of New York, ASRC
Prof. dr. F. Du Prez	Ghent University
Dr. G. A. Filonenko	Delft University of Technology

The experiments described in this thesis were primarily conducted in the Advanced Soft Matter Group of the Department of Chemical Engineering, Faculty of Applied Science of the Delft University of Technology, and partly in the laboratories of the research group of Prof. dr. Thomas Hermans at the University of Strasbourg. Funding was received from the European Union's Horizon 2020 research and innovation programme under the Marie Skłodowska-Curie grant agreement No 812868.

Cover: Dynamic Covalent Chemistry, photo taken by Benjamin Spitzbarth

Printed by: Proefschriftspecialist, Zaandam, the Netherlands

Copyright © 2023 by Benjamin Spitzbarth

This dissertation is available (open access) online at <https://repository.tudelft.nl/>

*“Breathing in, I calm body and mind.*

*Breathing out, I smile.*

*Dwelling in the present moment,*

*I know this is the only moment.”*

*— Thich Nhat Hanh, Being Peace*

# Table of Contents

<b>Chapter 1: General Introduction</b> .....	1
Dynamic Covalent Chemistry .....	1
Research Goals .....	2
Thesis Outline .....	3
References .....	4
<b>Chapter 2: Dynamic Covalent Ureas: Properties and Applications</b> .....	7
Abstract .....	7
Availability and Contributions .....	7
Introduction .....	8
Historical context .....	8
Properties of DCv ureas .....	10
Stability trends and reactivity .....	10
Challenges and limitations .....	14
DCv urea network properties and requirements .....	14
Applications .....	15
Materials .....	15
Encapsulation and delivery of biological cargo .....	16
Catalysis .....	16
Synthesis.....	17
Urea-derived DCv bonds.....	17
Conclusion and Outlook.....	17
Conflicts of interest .....	18
Acknowledgements .....	18
References .....	18
<b>Chapter 3: On-Demand Release of Secondary Amine Bases for the Activation of Catalysts and Crosslinkers</b> .....	24
Abstract .....	24
Availability and Contributions .....	24
Introduction .....	25
Results and Discussion.....	26

Choice of ureas and triggering conditions .....	27
Triggered Fmoc deprotection for catalyst release.....	27
Triggered acylhydrazone formation.....	31
Triggered elimination for the release of nitrile- <i>N</i> -oxides .....	33
Conclusion .....	34
Experimental Section.....	35
Acknowledgements .....	35
References .....	35
Supporting Information .....	38
General Information.....	38
Experimental Procedures .....	38
Fmoc deprotection with different bases.....	39
Side reaction of benzyl isocyanate with aniline.....	40
Fmoc deprotection with DCv ureas U1 and U2.....	40
Reference test: Fmoc deprotection with non-DCv urea U3.....	44
Acylhydrazone formation .....	44
<sup>1</sup> H-NMR analysis .....	44
Excluding catalytic effect of non-DCv urea U3 .....	45
Determination of maximum rate and activation time .....	46
Catalytic effect of benzyl amine side product and addition of hydrazone formation rates.....	46
DLS: Excluding the formation of supramolecular structures .....	47
Synthesis .....	49
References.....	52
<b>Chapter 4: Dynamic Covalent Urea-Catalysed Self-Healing of Thiol-Maleimide Networks.....</b>	<b>53</b>
Abstract.....	53
Availability and Contributions .....	53
Introduction .....	54
Results and Discussion .....	55
Choice of Michael acceptor, nucleophile, and solvent .....	55
Effect of temperature and DCv urea stability on kinetics.....	56
DCv urea catalysed dual self-healing networks.....	58

Conclusion.....	60
Methods.....	60
Polymer synthesis.....	60
NMR kinetics.....	60
Rheology.....	61
Acknowledgments.....	61
Competing interests.....	61
References.....	61
Supporting Information.....	67
General Information.....	67
NMR measurements.....	67
GPC measurements.....	67
Rheology measurements.....	68
ESI-LC/MS measurements.....	68
Synthesis.....	68
T1 Measurements.....	71
Side Reactivity of DIPU.....	71
References.....	74
<b>Chapter 5: Chemical Reaction Networks based on Conjugate Additions on <math>\beta'</math>-substituted Michael Acceptors.....</b>	<b>75</b>
Abstract.....	75
Availability and Contributions.....	75
Introduction.....	76
Systems chemistry: chemical toolbox to understand and mimic Nature.....	76
Versatility and drawbacks of conjugate additions.....	78
$\beta'$ -substituted Michael acceptors: addition-elimination reactions.....	79
MAs as a basis for CRN chemistry and their reactivity.....	82
MA-based CRNs for material applications.....	83
MA-based CRNs for signal amplification.....	89
MA-based CRNs for oxidation-driven pathway control and MA recovery.....	90
Conclusions.....	92
Conflicts of interest.....	92
Acknowledgements.....	92

Notes .....	93
References .....	93
<b>Chapter 6: Redox-controlled shunts in a synthetic chemical reaction cycle .....</b>	<b>102</b>
Abstract.....	102
Availability and Contributions .....	102
Introduction .....	103
Results and Discussion .....	104
Choice of chemistry and reagents.....	104
Sulfone cycle .....	105
Sulfoxide shunt .....	106
Sulfide shunt .....	108
Reversibility and recycling strategy .....	109
Conclusions .....	110
Acknowledgment.....	111
Conflict of Interest.....	111
References .....	111
Supporting Information .....	116
General Information.....	116
NMR measurements .....	116
LC-HRMS measurements.....	116
Ultimate Scheme: sulfone CRN.....	117
Synthesis .....	119
Supplementary experiments.....	122
T1 measurements .....	122
Half-lives of individual CRN reactions .....	123
Sulfide Oxidation at different pH values .....	125
Sulfone-MA + nucleophiles.....	126
Sulfone-MA 4 + additional proline: substitution reversibility and the fate of the sulfinate.....	130
Sulfone-MA 4 + thiol(s) .....	131
Sulfoxide-MA 3 + thiol .....	133
Sulfone network: simultaneous addition of MBA and Oxone.....	133
Oxone: reference reactions .....	134

Recovery of Proline-MA 1 from Ox-Proline-MA.....	136
Stepwise addition: comparison of oxidants.....	136
Sulfoxide-MA stability study .....	138
Bromate: reference reactions.....	139
Addition reactions without substitution: Loss of double bond functionality .....	141
Phosphine + MA.....	142
Bromate RC with aliphatic thiol.....	143
References .....	144
Summary .....	146
Samenvatting.....	148
Acknowledgement.....	150
About the author.....	152
List of Publications.....	152

## General Introduction

Historically, chemistry has evolved as a science of studying the conversion of a discrete set of starting compounds to a discrete set of products.<sup>1</sup> In recent decades however, more emphasis has been placed on the study of complexity in chemical reactions, as well as networks of several reactions, and the resulting application possibilities.<sup>2-5</sup> This trend has mostly been inspired by nature, where complex behaviour emerges from simple, basic building blocks.<sup>4</sup> These more complex systems are typically based on chemical reaction networks (CRNs), which describe any set of reactions that influence each other, making them intrinsically connected, such as chemical reaction cycles, sets of competing reactions, or reaction cascades (Figure 1.1 a).<sup>5-7</sup> Apart from insights in fundamental science, some examples of applications of such CRNs are sensors,<sup>8-10</sup> transient materials,<sup>11-14</sup> self-healing materials,<sup>15-17</sup> triggered drug release systems,<sup>18-21</sup> and chemical oscillators such as clock reactions.<sup>4,6,22</sup>

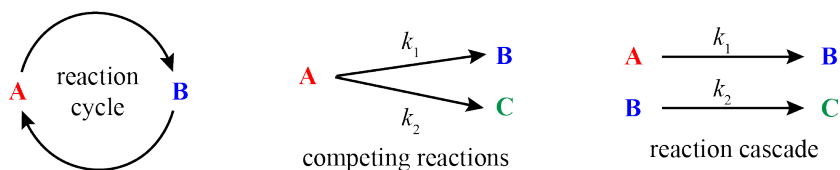
### Dynamic Covalent Chemistry

One way to realise systems that show complex behaviour such as self-healing, triggered degradability, malleability, and recyclability is Dynamic Covalent (DCv) chemistry. This branch of chemistry has developed rapidly especially since the late 20<sup>th</sup> century and led to many new developments, mainly in the fields of self-healing materials, as well as dynamic combinatorial chemistry.<sup>15,16,23,24</sup> DCv chemistry encompasses all reactions where the bond formation process is reversible on a reasonable timescale under the relevant conditions (Figure 1.1 b, c).<sup>25</sup> For example, a reaction that is reversible at 200 °C would not be considered to belong to the field of DCv chemistry, if the objective is to make a material that can undergo exchange reactions (i.e. self-healing) at 50 °C. As such, DCv chemistry offers an important bridge between relatively weak, intermolecular bonds (with bond energies for example for standard H-bonds ranging from 4 to 40 kJ/mol),<sup>26</sup> and stable, covalent bonds (with bond energies ranging from 151 kJ/mol for weak bonds such as in I<sub>2</sub> to 945 kJ/mol for strong bonds such as in N<sub>2</sub>),<sup>27</sup> as judged by the timescale of their exchange processes (Figure 1.1 b).<sup>28</sup> This allows researchers to utilise DCv chemistry in areas where a compromise of stability and dynamicity is required, offering a unique overlap between traditional organic chemistry, and highly dynamic supramolecular chemistry.<sup>25</sup>

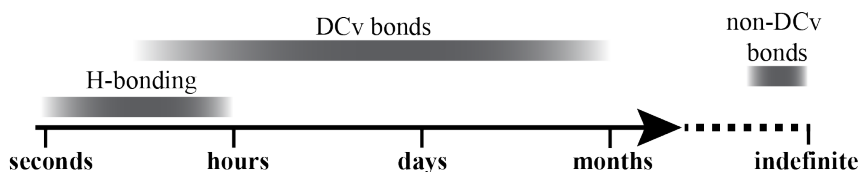
Some of the key systems developed in the field of DCv chemistry are based on disulfides,<sup>29</sup> vinylogous urethane<sup>30</sup> and urea bonds,<sup>31</sup> boronate esters,<sup>32</sup> and Diels-Alder adducts,<sup>33</sup> among others.<sup>15,34-36</sup> Two further DCv groups of central importance to this thesis are DCv ureas,<sup>37</sup> as well as DCv Michael adducts.<sup>20,38-40</sup>

This wealth of new findings in the field of DCv chemistry and its applications in CRNs offers many new leads to make fundamental progress and find new applications for this emerging discipline of chemistry.

a) different Chemical Reaction Networks (CRNs)



b) exchange timescales in different bonding modes



c) general principle of Dynamic Covalent Chemistry (DCvC)

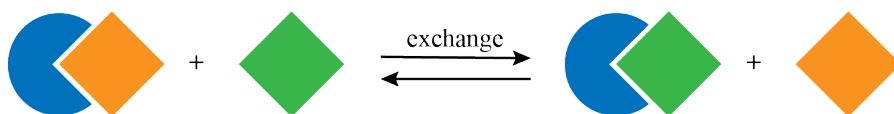


**Figure 1.1:** a) three different types of CRNs.<sup>5-7</sup> b) timescale of bond exchange of three different bond types under ambient conditions (i.e. 25 °C, 1 atm).<sup>28</sup> c) general principle of DCvC: adducts that are bound via covalent bonds can exchange.

## Research Goals

The aim of this thesis is to showcase how DCv ureas and DCv Michael adducts can be used in a new context. These chemistries have enjoyed much attention for their applications in self-healing materials and dynamic combinatorial libraries. We want to demonstrate that the chemical nature of the species involved in the equilibria of these DCv molecules allows them to further expand their applications. Specifically, we envisioned that

- i. the amine present in the equilibrium of DCv ureas can be used as a latent reagent, allowing for triggered catalysis.
- ii.  $\beta'$ -substituted Michael acceptors (MAs) can be used as species to design a new CRN that enables the efficient, controlled recovery of these MAs.

In this way, we aim to expand the knowledge about the reactivity and behaviour of these two different DCv chemical species, as well as the extent of their area of applications.

## Thesis Outline

Based on the research goals, this thesis is divided into *two major parts*: the first part (chapters 2, 3, and 4) is about DCv ureas, whereas the second part (chapters 5 and 6) discusses DCv  $\beta'$ -substituted MAs.

More specifically, in **chapter 2**, an introduction on the properties, and current state-of-the-art of DCv ureas will be given in the form of a literature review.

In **chapter 3**, we show that besides their traditional applications in the field of self-healing materials, DCv ureas can be used as heat-triggered catalytic species to trigger reaction cascades, and as equimolar reagents to trigger, as well as influence the kinetics of the formation of organogels.

In **chapter 4**, we build on the findings from the previous chapter, and integrate DCv ureas together with DCv thiol-maleimide adducts into a synergistic dual self-healing covalent adaptable networks (CAN). This allows the amine present in the DCv urea network to catalyse the thiol-maleimide exchange reaction and effectively reduce the self-healing temperature of these networks.

To introduce the second part of this thesis, in **chapter 5**, a literature review of the properties and state-of-the-art of  $\beta'$ -substituted MAs is given, followed by a summary of the applications of this chemistry.

**Chapter 6** shows our findings on how  $\beta'$ -substituted MAs can be integrated into a CRN, and how the choice of reagents can be utilised to gain control over the pathway, side reactions, and kinetics that govern this CRN, both in a closed system, as well as under flow conditions.

Finally, the implications of our findings are summarised and an outlook on potential future developments is given.

## References

1. Wentrup, C. Origins of Organic Chemistry and Organic Synthesis. *European J. Org. Chem.* **2022**, e202101492 (2022).
2. Whitesides, G. M. & Ismagilov, R. F. Complexity in chemistry. *Science.* **284**, 89–92 (1999).
3. Singh, N., Formon, G. J. M., De Piccoli, S. & Hermans, T. M. Devising Synthetic Reaction Cycles for Dissipative Nonequilibrium Self-Assembly. *Adv. Mater.* **32**, 1906834 (2020).
4. Ashkenasy, G., Hermans, T. M., Otto, S. & Taylor, A. F. Systems chemistry. *Chem. Soc. Rev.* **46**, 2543–2554 (2017).
5. Wang, Z., Xiao, J., Zhao, T., Zhang, C., Wang, L., He, N., Kong, Q. & Wang, X. Transient regulation of gel properties by chemical reaction networks. *Chem. Commun.* **59**, 9818–9831 (2023).
6. Semenov, S. N. De novo Design of Chemical Reaction Networks and Oscillators and Their Relation to Emergent Properties. in *Out-of-Equilibrium (Supra)molecular Systems and Materials* 91–130 (John Wiley & Sons, Ltd, 2021). doi:10.1002/9783527821990.CH4.
7. Plasson, R. Chemical Reaction Network. in *Encyclopedia of Astrobiology* (eds. Gargaud, M. et al.) 287–288 (Springer Berlin Heidelberg, 2011). doi:10.1007/978-3-642-11274-4\_269.
8. Fabbri, L. & Poggi, A. Sensors and switches from supramolecular chemistry. *Chem. Soc. Rev.* **24**, 197–202 (1995).
9. Frisch, H., Unsleber, J. P., Lüdeker, D., Peterlechner, M., Brunklau, G., Waller, M. & Besenius, P. PH-switchable ampholytic supramolecular copolymers. *Angew. Chem. Int. Ed.* **52**, 10097–10101 (2013).
10. Heuser, T., Weyandt, E. & Walther, A. Biocatalytic Feedback-Driven Temporal Programming of Self-Regulating Peptide Hydrogels. *Angew. Chem. Int. Ed.* **54**, 13258–13262 (2015).
11. De, S. & Klajn, R. Dissipative Self-Assembly Driven by the Consumption of Chemical Fuels. *Adv. Mater.* **30**, 1706750 (2018).
12. Sharko, A., Livitz, D., De Piccoli, S., Bishop, K. J. M. & Hermans, T. M. Insights into Chemically Fueled Supramolecular Polymers. *Chem. Rev.* **122**, 11759–11777 (2022).
13. Würbser, M. A., Schwarz, P. S., Heckel, J., Bergmann, A. M., Walther, A. & Boekhoven, J. Chemically Fueled Block Copolymer Self-Assembly into Transient Nanoreactors. *ChemSystemsChem* **3**, e2100015 (2021).
14. Klemm, B., Lewis, R. W., Piergentili, I. & Eelkema, R. Temporally programmed polymer – solvent interactions using a chemical reaction network. *Nat. Commun.* **13**, 6242 (2022).

15. García, F. & Smulders, M. M. J. Dynamic covalent polymers. *J. Polym. Sci. Part A Polym. Chem.* **54**, 3551–3577 (2016).
16. Chakma, P. & Konkolewicz, D. Dynamic Covalent Bonds in Polymeric Materials. *Angew. Chem. Int. Ed.* **58**, 9682–9695 (2019).
17. Li, B., Cao, P.-F., Saito, T. & Sokolov, A. P. Intrinsically Self-Healing Polymers: From Mechanistic Insight to Current Challenges. *Chem. Rev.* **123**, 701–735 (2023).
18. Hu, X., Zeng, T., Husic, C. C. & Robb, M. J. Mechanically Triggered Small Molecule Release from a Masked Furfuryl Carbonate. *J. Am. Chem. Soc.* **141**, 15018–15023 (2019).
19. Shi, Z., Wu, J., Song, Q., Göstl, R. & Herrmann, A. Toward Drug Release Using Polymer Mechanochemical Disulfide Scission. *J. Am. Chem. Soc.* **142**, 14725–14732 (2020).
20. Zhuang, J., Zhao, B., Meng, X., Schi, D., Perry, S. L., Vachet, W. & Thayumanavan, S. Chemical Science A programmable chemical switch based on triggerable Michael acceptors. *Chem. Sci.* **11**, 2103–2111 (2020).
21. Fan, B., Zhang, K., Liu, Q. & Eelkema, R. Self-Healing Injectable Polymer Hydrogel via Dynamic Thiol-Alkynone Double Addition Cross-Links. *ACS Macro Lett.* **9**, 776–780 (2020).
22. Horváth, A. K. & Nagypál, I. Classification of clock reactions. *ChemPhysChem* **16**, 588–594 (2015).
23. Corbett, P. T., Leclaire, J., Vial, L., West, K. R., Wietor, J. L., Sanders, J. K. M. & Otto, S. Dynamic combinatorial chemistry. *Chem. Rev.* **106**, 3652–3711 (2006).
24. Komáromy, D., Nowak, P. & Otto, S. Dynamic Combinatorial Libraries. in *Dynamic Covalent Chemistry - Principles, Reactions and Applications* 31–119 (John Wiley & Sons, Inc., 2017). doi:10.1002/9781119075738.ch2.
25. Schaufelberger, F., Timmer, B. J. J. & Ramström, O. Principles of Dynamic Covalent Chemistry. in *Dynamic Covalent Chemistry: Principles, Reactions, and Applications* (eds. Zhang, W. & Jin, Y.) 1–30 (John Wiley & Sons Ltd., 2017). doi:10.1002/9781119075738.ch1.
26. Gokel, G. W. 1.01 - Introduction and Overview of Supramolecular Receptor Types. in *Comprehensive Supramolecular Chemistry II* (ed. Atwood, J. L.) 1–10 (Elsevier Ltd., 2017).
27. Huber, K. P. & Herzberg, G. Constants of diatomic molecules. in *Molecular Spectra and Molecular Structure* (eds. Huber, K. P. & Herzberg, G.) 8–689 (Springer US, 1979). doi:10.1007/978-1-4757-0961-2\_2.
28. Wanasinghe, S. V., Dodo, O. J. & Konkolewicz, D. Dynamic Bonds: Adaptable Timescales for Responsive Materials. *Angew. Chem. Int. Ed.* **61**, e202206938 (2022).

29. Li, J., Carnall, J. M. A., Stuart, M. C. A. & Otto, S. Hydrogel formation upon photoinduced covalent capture of macrocycle stacks from dynamic combinatorial libraries. *Angew. Chem. Int. Ed.* **50**, 8384–8386 (2011).
30. Denissen, W., Rivero, G., Nicolaÿ, R., Leibler, L., Winne, J. M. & Du Prez, F. E. Vinylogous urethane vitrimers. *Adv. Funct. Mater.* **25**, 2451–2457 (2015).
31. Denissen, W., De Baere, I., Van Paepegem, W., Leibler, L., Winne, J. & Du Prez, F. E. Vinylogous Urea Vitrimers and Their Application in Fiber Reinforced Composites. *Macromolecules* **51**, 2054–2064 (2018).
32. Nishiyabu, R., Kubo, Y., James, T. D. & Fossey, J. S. Boronic acid building blocks: tools for self assembly. *Chem. Commun* **47**, 1124–1150 (2011).
33. Chen, X., Dam, M. A., Ono, K., Mal, A., Shen, H., Nutt, S. R., Sheran, K. & Wudl, F. A thermally re-mendable cross-linked polymeric material. *Science*. **295**, 1698–1702 (2002).
34. Jin, Y., Yu, C., Denman, R. J. & Zhang, W. Recent advances in dynamic covalent chemistry. *Chem. Soc. Rev.* **42**, 6634–6654 (2013).
35. Winne, J. M., Leibler, L. & Du Prez, F. E. Dynamic covalent chemistry in polymer networks: A mechanistic perspective. *Polym. Chem.* **10**, 6091–6108 (2019).
36. Kloxin, C. J. & Bowman, C. N. Covalent adaptable networks: Smart, reconfigurable and responsive network systems. *Chem. Soc. Rev.* **42**, 7161–7173 (2013).
37. Ying, H., Zhang, Y. & Cheng, J. Dynamic urea bond for the design of reversible and self-healing polymers. *Nat. Commun.* **5**, 3218 (2014).
38. Baldwin, A. D. & Kiick, K. L. Tunable degradation of maleimide-Thiol adducts in reducing environments. *Bioconjug. Chem.* **22**, 1946–1953 (2011).
39. Nelson, R. P. & Lawton, R. G. On the alpha,alpha' Annelation of Cyclic Ketones. *J. Am. Chem. Soc.* **88**, 3884–3885 (1966).
40. Crolais, A. E., Dolinski, N. D., Boynton, N. R., Radhakrishnan, J. M., Snyder, S. A. & Rowan, S. J. Enhancing the Equilibrium of Dynamic Thia-Michael Reactions through Heterocyclic Design. *J. Am. Chem. Soc.* **145**, 14427–14434 (2023).

# Dynamic Covalent Ureas: Properties and Applications

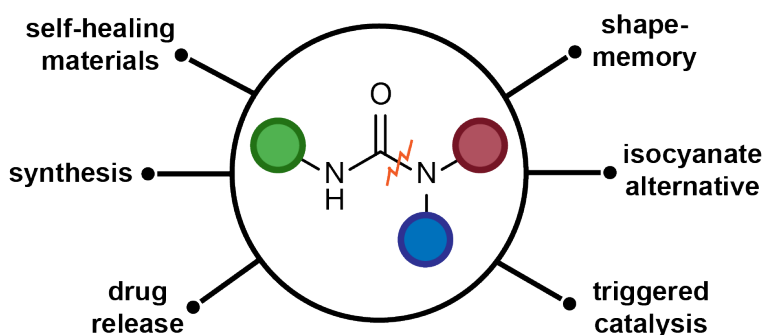
## Abstract

Dynamic Covalent (DCv) ureas are a class of compounds undergoing exchange reactions under conditions near room temperature. As such, they have been applied extensively over the last decade in different fields and have become one of the key motifs in DCv chemistry (DCvC). We provide here an overview over the historical development of DCv ureas, their properties, both on a small molecule and material scale, limitations, and give a guide for the reader on how to design DCv ureas of different stabilities. Further, we summarise the key applications of DCv ureas in recent decades in material science, reversible encapsulation of cargo, catalysis, and synthesis, and conclude by offering an outlook on potential future directions that the research on and applications of DCv ureas may take.

## Availability and Contributions

This chapter is based on a review article by B. Spitzbarth and R. Eelkema currently in preparation for submission.

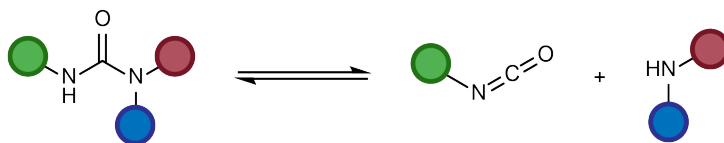
B.S. conducted the literature search, designed the schemes and figures, and summarised the findings into the paper draft. R.E. aided in figure design, corrected the manuscript draft and secured funding.



## Introduction

Dynamic Covalent Chemistry (DCvC) has taken major strides over the last few decades.<sup>1</sup> The key characteristic of DCv bonds is that they undergo exchange reactions under relatively mild conditions, allowing covalent bonds, which are typically stable, to undergo exchange reactions.<sup>2-4</sup> This feature leads to interesting applications such as in malleable, recyclable, and self-healing materials, dynamic combinatorial libraries, and more.<sup>1,5-9</sup> Some of the bonds that are typically utilised in DCvC are Diels-Alder adducts,<sup>10</sup> boronic esters,<sup>11</sup> or disulfides.<sup>12</sup> Unlike some species such as Diels-Alder adducts, DCv ureas (Scheme 2.1) exhibit self-healing under exceptionally mild conditions near room temperature,<sup>13</sup> offering a valuable addition to the toolkit of DCvC. Apart from exhibiting self-healing near room temperature, the commercial availability of their starting materials, their ease of synthesis, and chemical nature makes them stand out in the field of DCvC, which is why they have received increased attention over the last 10 years, starting with pioneering efforts from the group around J. Cheng.<sup>13</sup>

The aim of this literature review is to offer a comprehensive guide to understand how DCv ureas were developed, where their strengths and challenges lie and how they are applied today. We will conclude by offering our view on how researchers can use DCv ureas' properties for future directions of research into this emerging field of DCvC.

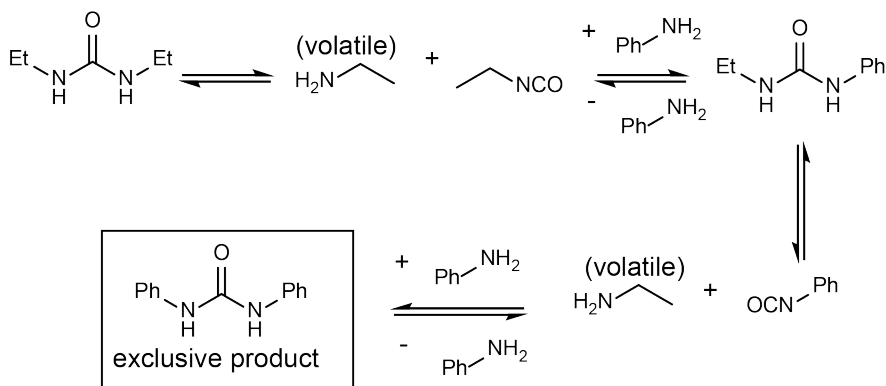


**Scheme 2.1:** general equilibrium of a DCv urea species with its corresponding isocyanate and primary or secondary amine. Where the equilibrium lies depends majorly on the nature of substituents, solvent, and the conditions.

## Historical context

The history of urea dates to the founding fathers of organic chemistry, Friedrich Wöhler and Justus von Liebig. They had already discovered feasible, albeit harsh, routes of how urea can degrade, under the influence of nitrous acid, in the early 19<sup>th</sup> century.<sup>14</sup> In 1893, it was found that aromatic ureas release their corresponding isocyanates upon heating above their melting point.<sup>15</sup> The first tangible findings however, which indicate that ureas as well as thioureas are in equilibrium with their corresponding isocyanates (or isothiocyanates, respectively) and amines upon heating were shown in 1922.<sup>16</sup> This was demonstrated by heating crude urea and aniline, yielding phenylurea at 160 °C. It was concluded that this transformation is possible due to the reaction of aniline with isocyanic acid present in urea's dissociative equilibrium. Further studies revealed that these transformations also take place in boiling water, yielding phenylurea and *sym*-diphenylurea from urea and aniline hydrochloride while expelling ammonia from the solution.<sup>17</sup> Asymmetrically substituted *N,N*-alkyl-aryl ureas were found to dissociate

exclusively into isocyanic acid and secondary amines, and the presence of an excess of amines did not yield tetrasubstituted ureas, corroborating the hypothesis that free isocyanates are part of the transformation. Importantly, it was found that the product formation can be controlled via the volatility of the released species. Heating diethylurea with aniline will progressively yield *N,N'*-ethylphenylurea and *sym*-diphenylurea, respectively.<sup>17</sup> While *N,N'*-ethylphenylurea can in principle dissociate via two pathways, the exclusive formation of *sym*-diphenylurea was observed due to the higher volatility of ethyl amine, escaping the solution (Scheme 2.2).

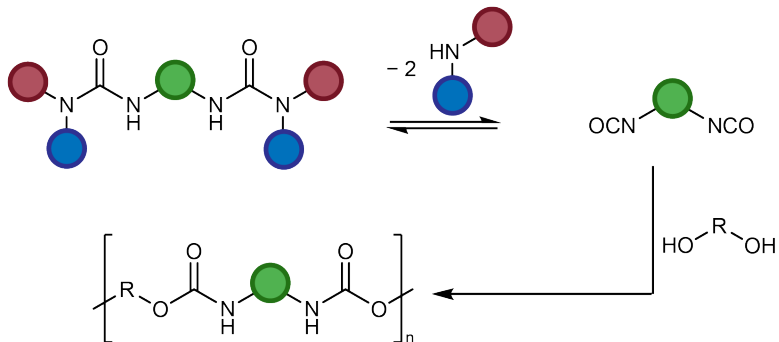


**Scheme 2.2:** When *sym*-diethylurea is heated with aniline, *sym*-diphenylurea will form exclusively, due to the dynamic nature of all species involved and the higher volatility of ethylamine.<sup>17</sup>

Further studies to investigate the lability of ureas with varying substitution degree, substituent properties, and solvent properties to elucidate the kinetics of the involved dissociation processes were undertaken in the 1950s by T. Mukaiyama and coworkers.<sup>18–23</sup> While previous examples demonstrated the dissociation of non-hindered ureas under harsh conditions, these studies began to show that hindered ureas dissociate into their isocyanates and amines under relatively mild conditions, with a strong dependence on the bulkiness of the substituents. Further studies in the 1970s corroborated these discoveries with findings that ureas<sup>24</sup> and semicarbazides<sup>25</sup> with hindered substituents dissociate appreciably into isocyanates and the corresponding amines or hydrazines, respectively, even at room temperature. Stowell and Padegimas generalised these findings in 1974 to derive a method of estimating sterical hindrance of secondary amines by observing the dissociation equilibria of the corresponding ureas formed with 2,6-dimethylphenylisocyanate.<sup>26</sup>

The first industrial applicability for ureas' dissociation properties came with the advent of "blocked isocyanates". Isocyanates are extremely versatile reagents and are widely used in academia and industry.<sup>27,28</sup> However, due to their high reactivity and long list of health concerns,<sup>29</sup> it is generally desirable to work with reagents that can release isocyanates on demand. While "blocked isocyanates" have been reviewed elsewhere in depth,<sup>27</sup> ureas, which may in this context be referred to as "amine-blocked isocyanates", comprise a notable subclass of these compounds. The introduction of ureas as a further

group of compounds that are labile enough to release isocyanates, widened the accessible conditions for polymerisation reactions involving “blocked isocyanates”. Among the first examples of studies investigating the feasibility of DCv ureas for their application in curing reactions of polyurethanes are the works by A. Sultan Nasar and coworkers in 1999 and the years thereafter (Scheme 2.3).<sup>30–32</sup>



**Scheme 2.3:** The use of blocked isocyanates as pioneered by A. Sultan Nasar and colleagues. A DCv urea made from secondary aromatic amines and a bisfunctional aromatic isocyanate can release the isocyanate upon heating, leading to a curing reaction with a diol, forming polyurethanes without the direct need for isocyanates.<sup>30</sup>

More recently, the group of J. Cheng pioneered the detailed investigation of hindered ureas in a different context, going beyond their usage as a synthetical or polymerisation starting point and exploiting their reversibility for material/self-healing applications.<sup>13</sup> This quest for the application of the desirable properties of DCv (hindered) ureas in a material context has sparked the research into and development of a whole range of interesting materials and other uses in recent years, which will be discussed in detail.

## Properties of DCv ureas

### Stability trends and reactivity

In general, amides and ureas are known to be highly stable functional groups and degradation is usually achieved only under prolonged heating in strongly acidic or basic conditions.<sup>26,33</sup> However, both can be envisioned to dissociate into ketenes and amines or isocyanates and amines respectively.<sup>13</sup> These unfavourable reaction pathways require structural manipulations to make them more feasible. One of the key factors leading to the high stability of amides and ureas is the conjugation of the nitrogen lone pairs with the carbonyl centres. Partly breaking this conjugation under loss of coplanarity and endowing the carbonyl centre with more ketone-like properties enables a fast and efficient degradation. For urea itself, such a dissociation requires harsh conditions,<sup>14</sup> while for tetrasubstituted ureas this dissociative pathway is not possible due to the absence of a proton that can be transferred during the dissociation step. Alkyl-substituted species are still highly stable species which require harsh conditions to dissociate, while aryl-substituted ureas dissociate more easily into the resonance-stabilised isocyanates and

amines.<sup>15,17</sup> The species that dissociate most easily into isocyanates and amines are trisubstituted ureas with sterically highly demanding substituents (Figure 2.1).

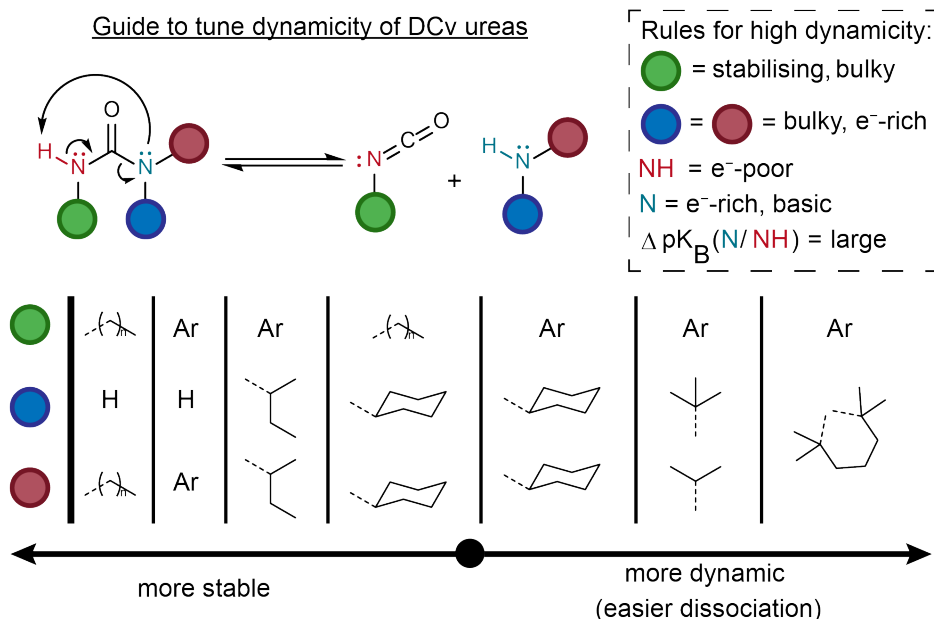


**Figure 2.1:** stability of urea derivatives with different substitution patterns and general guidelines to design a DCv urea with high lability (i.e. easy dissociation). With decreasing stability from left to right in the table, the ease of the DCv urea's dissociation and the basicity of the free base increase. While for non-hindered ureas (first 2 entries, left to right), resonance stabilisation of the species plays a big role, for hindered ureas the bulkiness and hence torsion of C-N bond play a more important role.

For the first two non-hindered urea derivatives in Figure 1, resonance stabilization of the fragments plays an important role. Aromatic amines and isocyanates are more stable and hence the corresponding ureas dissociate more readily than aliphatic ones. For hindered ureas, steric bulk is one of the key factors that influence urea stability. An especially noteworthy observation is the large difference in stability between bis-secondary (e.g. *N,N*-ethyl-*iso*-propyl) ureas and primary-tertiary (e.g. *N,N*-ethyl-*tert*-butyl) ureas.<sup>13,26</sup> Introducing tertiary alkyl groups has a large impact on the stability of the hindered urea. Furthermore, the basicity of the urea nitrogen atoms is important in estimating stability. Generally, a more basic secondary amine, assuming similar steric hindrance, will form less stable ureas, as the more basic nitrogen will facilitate the proton transfer required for the dissociation process to take place. Similarly, the difference of basicity between the two nitrogen atoms plays a role as well, as a less basic NH-moiety will further facilitate proton transfer to a highly basic NR<sub>2</sub>-unit.<sup>21</sup> The general rules, in order of decreasing influence, to design a highly dynamic urea would hence be as follows:

- 1) Choose trisubstituted ureas over mono- and disubstituted species (tetrasubstituted ureas are not dynamic),

- 2) Use a highly basic, sterically demanding secondary amine with at least one tertiary substituent,
- 3) Pick a resonance-stabilised, electron-deficient isocyanate (ideally hindered, e.g. 2,6-dimethylphenylisocyanate<sup>26</sup>).

These general guidelines (Figure 2.1, top right) enable researchers to design urea structures meeting a wide range of stability and dynamicity demands.

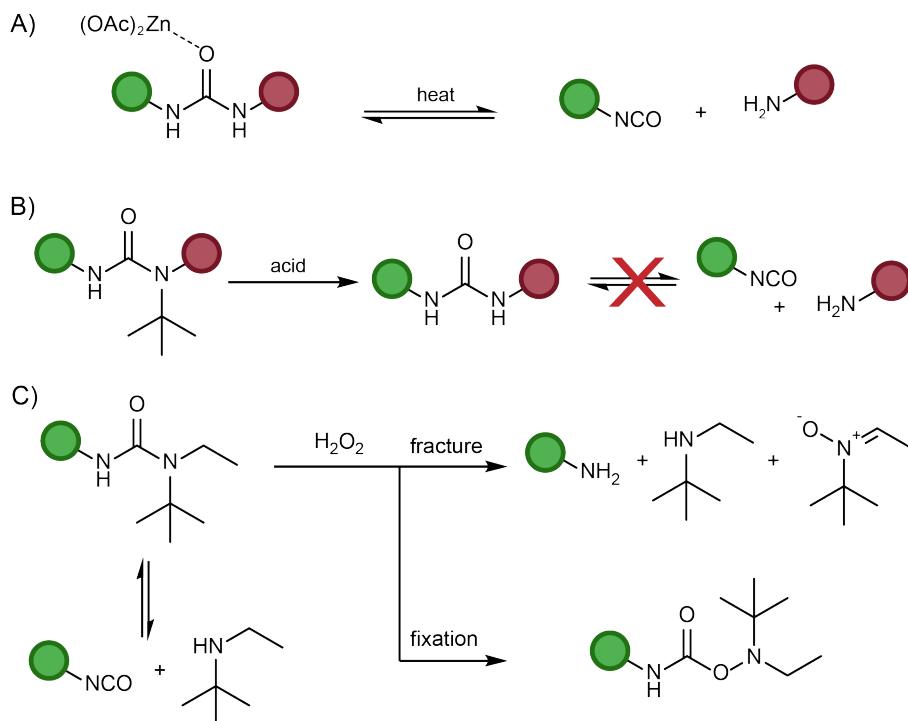
However, as basicity and steric hindrance of an amine do not always go hand in hand, there are some exceptions to the generally expected stability trends. Padegimas and Stowell used the  $E_s$  values (steric substituent constants) of the Taft equation to define the expected trends of urea stability. They found that, in line with  $E_s$  values, amines with the sterically more demanding 3-pentyl group form ureas with 2,6-dimethylphenylisocyanate more slowly than amines with a cyclohexyl residue. On the contrary, their dissociation follows the inverse trend, showing a slower dissociation for the 3-pentyl-substituted urea than for the cyclohexyl-substituted urea.<sup>26</sup>

While most recent publications involve highly hindered DCv ureas due to their significant dissociation under ambient or near-ambient conditions and the interesting properties that come with this dynamicity, there are some notable examples of non-hindered DCv ureas. Aromatically trisubstituted ureas have been extensively employed as amine-blocked isocyanates for polymerisations.<sup>30,31</sup> Typically, these DCv ureas can cure in polymerization reactions with deblocking temperatures of roughly 120–150 °C.

Recently, the group of Hesheng Xia explored different ways of making non-hindered ureas more dynamic. They found that disubstituted aliphatic ureas, which are highly stable under ambient conditions, can undergo exchange reactions via a dissociative pathway in the presence of zinc acetate at elevated temperatures (70–90 °C).<sup>34</sup> The formation of an *O*-bound zinc complex accelerates the dissociation of these urea species by several orders of magnitude (Scheme 2.4 A). This is a significant finding as it widens the scope of urea motifs that can be used for applications in which fast exchange kinetics are required. In another recent work, the group discovered that NIR irradiation of urea-based networks can enable self-healing of these polymers.<sup>35</sup> It is hypothesised that the high, localised heat generation from the NIR radiation as well as entropy changes in the polymer system favour the dissociation of the stable urea bonds, leading to a temporary depolymerisation of the network.

On the contrary, Cheng and colleagues have recently introduced a strategy to “switch off” the dynamic behaviour of DCv ureas carrying a *tert*-butyl group on one of the nitrogens.<sup>36</sup> By adding acid, the *tert*-butyl group of the dynamic urea can be removed, forming a non-dynamic urea moiety (Scheme 2.4 B). This on demand off-switch for the dynamicity of different DCv ureas could dramatically widen their applications by increasing the stability of the material when needed.

Another interesting feature of DCv ureas is their reactivity towards hydrogen peroxide. While perhydrolysis of the free isocyanate in the urea’s equilibrium leads to bond fracture, oxidation of the amine can lead to formation of a urethane-like product which does not show dynamic behaviour (Scheme 2.4 C).<sup>37</sup> It was however not possible to achieve control over which pathway dominates.



**Scheme 2.4:** Reactivity of DCv urea units under different conditions. A) Despite not showing dynamic behaviour under standard conditions, aliphatic ureas can undergo dissociative exchange in the presence of zinc catalysts.<sup>34</sup> B) Dynamic ureas carrying a *tert*-butyl group can be converted into non-DCv ureas via *de-tert*-butylation in the presence of acid.<sup>36</sup> C) DCv ureas show different reactions in the presence of hydrogen peroxide, leading both to non-reversible fracture, as well as permanent fixation of the bond.<sup>37</sup>

The previous examples focused exclusively on the reactivity of DCv ureas in a dissociative fashion, forming a free isocyanate and amine in the reaction. However, a far less common associative pathway is also possible. In 1992 it was found that aryl-substituted ureas undergo a second-order nucleophilic substitution at carbonyl centre of the urea via attack of primary or secondary amines and subsequent displacement.<sup>38</sup> This method works especially well with monosubstituted ureas as the steric hindrance for the nucleophilic attack is minimal and the released ammonia can easily be expelled from solution due to its high volatility. While this work technically does not fall into the realm of DCvC due to the non-reversibility of the process, it is worth mentioning as it provides an easy synthetic route to substituted ureas and proceeds via an associative pathway which will be discussed in more depth at a later point.

## Challenges and limitations

While DCv ureas are applicable under a wide range of conditions and in a wide range of solvents, there are some factors that do need to be considered when working with these compounds. One of the downsides is the use of isocyanates in the synthesis of DCv ureas. They are highly toxic compounds, that can lead to many chronic health issues.<sup>29</sup> While their use during synthesis can be handled safely, the presence of free isocyanates in the equilibrium of DCv ureas may limit their area of applications. The high reactivity of isocyanates presents another more practical challenge. DCv ureas have been shown to be labile towards solvolysis, for example in water or alcohols, due to the degradation of isocyanates.<sup>39-41</sup> This feature can however also be a desirable behaviour, leading to new applications such as solvent-triggered release systems (see below). Another potential limitation is the relatively high oxidative lability of the secondary amines present in the DCv urea equilibrium. We have observed in our laboratory the discoloration of highly dynamic ureas upon prolonged storage, due to degradation of both amine and isocyanate, as observed in <sup>1</sup>H-NMR spectroscopy.

## DCv urea network properties and requirements

The properties of DCv urea networks mostly reflect their molecular properties. As previously indicated, the exchange mechanism of DCv urea is typically dissociative in nature.<sup>13</sup> There is however a limited number of examples of associative DCv urea networks.<sup>42,43</sup> This expands the application scope of DCv ureas further, as it allows access to dissociative as well as vitrimer networks (i.e. networks with a constant crosslinking density throughout the whole self-healing process<sup>44,45</sup>). Apart from the small number of vitrimer-like DCv urea networks, typical requirements for dissociative DCv urea networks with good stability, reprocessability, self-healing, and malleability are a large equilibrium constant  $K_{eq}$ , as well as fast kinetics of both the dissociation, as well as association process.<sup>13</sup> This means that the exchange process must be fast, and the equilibrium of the dissociation process must be mostly on the side of the urea, and not isocyanate and amine, to construct a useable material. As discussed above, the dynamicity can be regulated relatively easily by changing the steric demand of the amine in the DCv urea equilibrium.<sup>13,46</sup> It was found that sterically more demanding amines lead to a decrease in flow temperature of the networks, as well lower degree of connectivity and hence improved self-healing in the order of ethyl-, *iso*-propyl-, *tert*-butyl-, and tetramethylpiperidiny-based substituents.<sup>46</sup> Another important factor that can influence the properties of DCv urea networks is the concentration of DCv urea bonds in the network. It was found that typically, > 50 % of DCv urea bonds (in urea-urethane networks, i.e. as a fraction of urea bonds compared to all functional groups) are needed to allow for good self-healing, whereas < 50 % DCv urea bonds lead to suboptimal reprocessability.<sup>47</sup>

## Applications

### Materials

Due to their dynamic exchange reactions, the most widespread application of DCv ureas is in self-healing materials. When a damage, such as a scratch, cut, or in general any mechanical failure is inflicted upon the material, the DCv urea moieties near the interfaces at the site of damage can exchange between those interfaces, leading to a healed material (Figure 2.2).

#### General principle of self-healing DCv-urea-based materials

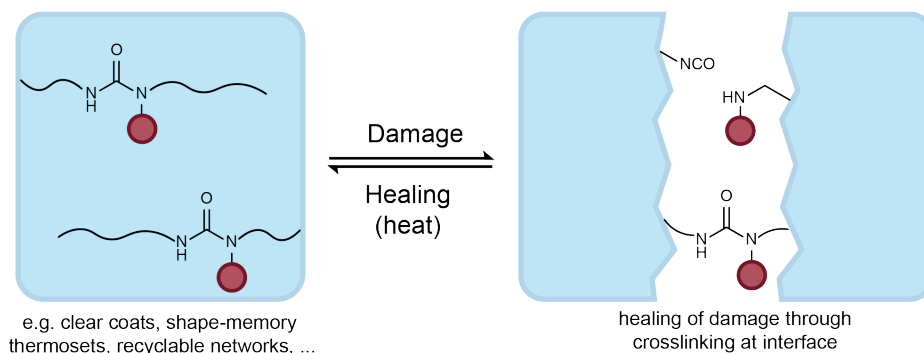


**Figure 2.2:** General principle of self-healing materials based on DCv ureas. Exchange reaction between interfaces lead to the material growing back together and recovering its initial mechanical properties.

Since the introduction into this field in 2014 by the group of J. Cheng, many works exploring the scope of these materials have been published. Typically, a large part of recent research focuses on improving the mechanical characteristics such as malleability, as well as the recyclability of these materials.<sup>48-50</sup> These findings have significantly improved the diversity and properties of DCv urea materials and expand their accessibility by exploring different, commercially available monomers. A common example of where DCv urea materials can find applications is in self-healing clear coats. In one example, a self-healing clear coat, containing DCv ureas and a polysiloxane was fabricated.<sup>51</sup> While the DCv urea moieties endowed the clear coat with its self-healing properties, the polysiloxane offered self-cleaning properties such as repellence of water, oil, as well as ink. In addition, the clear coat showed excellent optical and mechanical properties. In other examples, DCv ureas were incorporated into polycarbonates and polyurethanes to make clear coats with applications such as automotive coatings.<sup>52,53</sup> Further, in one instance, silver nanowires were incorporated into a self-healing DCv urea network, which allowed for healable and stretchable electrodes.<sup>54</sup> Upon cutting the electrode in half, the team demonstrated that it can be reused within 30 minutes of healing at 60 °C.

In another work, hindered urea bonds were incorporated into shape memory thermosets, based on poly(urea-urethane) polymers.<sup>55</sup> Not only did this endow the original shape-memory thermoset with self-healing properties, but it also endowed the material with triple-shape-memory performance under very mild conditions without the need for conventional curing in a mould.

Despite their degradability in aqueous conditions, advances were also made in applying DCv urea polymers as self-healing tubes for flowing water.<sup>56</sup> It was shown while flowing water with a temperature of 37 °C, tubes that were scratched showed self-healing behaviour upon wetting the scratched area. The group explained this behaviour with the formation of free isocyanate units which can hydrolyse and react with further free isocyanate to form non-DCv ureas, thereby using water to render the tubes self-reinforcing.

### **Encapsulation and delivery of biological cargo**

Besides these more material-focused works, further advances were made in the fields of drug, as well as stem cell delivery. Here, the hydrolysis of the isocyanate from the DCv urea's equilibrium plays a crucial role in controlling the degradation kinetics of the encapsulation matrix. In one instance, a hindered urea-based polymer was pegylated on both chain ends to form micelles which could incorporate the chemotherapy drug paclitaxel.<sup>57</sup> The group demonstrated the entry of these drug-loaded micelles into breast cancer cells in mice and subsequent inhibition of tumour growth. The tuneable release kinetics of these micelles by variation of the DCv urea structure provides another way to achieve controlled drug release, with boronates and esters offering similar options.<sup>58,59</sup> In another example, crosslinked hydrogels containing hindered urea bonds were prepared and loaded with stem cells. The networks were found to be biocompatible and the hydrolytic release of these cells could be tuned over 5 days by changing the structure of the DCv ureas.<sup>60</sup>

### **Catalysis**

In our group, we recently showed that DCv ureas can also be applied as latent amine catalysts and reagents (see Chapter 3 of this Thesis). The concentration of free base present in the equilibrium of hindered ureas can be raised by increasing the temperature to 45 °C or adding water to induce isocyanate hydrolysis. This effectively creates a temperature- and solvent-triggered base release system. We showed that this base can be used catalytically to release Fmoc-protected aniline, which can in turn catalyse the formation of acylhydrazones. The action of aniline as well as bulky base in response to heat or solvent greatly enhance the formation of acylhydrazones over the background reaction. Further, we showed that DCv ureas can be used to release highly reactive nitrile-*N*-oxides from chlorooximes via elimination of hydrogen chloride. These nitrile-*N*-oxides can undergo cycloadditions with tetrafunctional acrylates to form organogels in response to a thermal stimulus. In addition, the bulkiness of the DCv urea can be used to tune the gelation kinetics.<sup>61</sup>

## Synthesis

DCv ureas have also been used as precursors in several synthesis procedures. Recently, the group of J. Cheng has demonstrated the first high-yielding synthesis of macrocycles with high reaction concentrations, utilising *tert*-butyl substituted hindered ureas as the template.<sup>62</sup> Further, unsymmetrical ureas can be synthesised by reacting primary or secondary amines with phenylurea, displacing ammonia in the process.<sup>63</sup> The solvolysis of DCv ureas, discussed as one of the downsides above, can also be utilised as a synthetic procedure. Alcohols can be carbamoylated efficiently in the presence of DCv ureas under mild conditions without the need for free isocyanates.<sup>41</sup> Lastly, low-boiling isocyanates can be generated via distillative removal from the equilibrium of DCv ureas under heating.<sup>64,65</sup>

## Urea-derived DCv bonds

The increased attention that DCv ureas have received over the last years has also led to the development of other, urea-derived DCv bonds. Among these are pyrazole-blocked isocyanates,<sup>66,67</sup> imidazole-blocked isocyanates,<sup>32</sup> polyacylsemicarbazides,<sup>68,69</sup> DCv thioureas,<sup>70,71</sup> as well as isoureas used for their ability to generate radicals during their bond cleavage.<sup>72</sup>

## Conclusion and Outlook

The field of Dynamic Covalent Chemistry (DCvC) has made large strides over the last few decades and continues to gain importance with the rising need for more sustainable materials which show properties such as reprocessability and recyclability. DCv ureas are an important addition to the field of DCvC because of their widely tuneable dynamicity, making them applicable over a large range of conditions. Despite some downsides such as solvolytic lability, and the presence of toxic isocyanates in their equilibrium, they have found widespread use in different fields such as drug and stem cell delivery systems, self-healing electrodes, clear coats, recyclable and malleable networks, triple-shape-memory networks, triggered catalysis, and synthesis. With the knowledge gathered about the properties of DCv ureas, the future will see further developments utilising these moieties. Their ability to release isocyanates in situ makes them interesting candidates for further applications replacing the direct need for isocyanates. Furthermore, the wide range of self-healing polymers with different properties and the easy tuneability of their stability presupposes DCv ureas for more applications in material science, such as coatings, or sensors for detecting mechanical stress. Their more recent development in the release of biological cargo also offers further options in the field of drug delivery. Lastly, the extremely wide chemical versatility of the amine species present in DCv ureas' equilibria offers many possible applications in reactions where amines participate as substrates or catalysts, as recently shown with their applications as heat-triggered catalysts and reagents. As such, hindered ureas offer a general method to replace amines with a heat- or solvent-triggered alternative that can release amines on demand.

## Conflicts of interest

There are no conflicts to declare.

## Acknowledgements

This work has received funding from the European Union's Horizon 2020 research and innovation programme under the Marie Skłodowska-Curie grant agreement No 812868.

## References

1. Jin, Y., Yu, C., Denman, R. J. & Zhang, W. Recent advances in dynamic covalent chemistry. *Chem. Soc. Rev.* **42**, 6634–6654 (2013).
2. Li, B., Cao, P.-F., Saito, T. & Sokolov, A. P. Intrinsically Self-Healing Polymers: From Mechanistic Insight to Current Challenges. *Chem. Rev.* **123**, 701–735 (2023).
3. Furgal, J. C., Dunn, M., Wei, T. & Scott, T. F. Emerging Applications of Dynamic Covalent Chemistry from Macro- to Nanoscopic Length Scales. in *Dynamic Covalent Chemistry: Principles, Reactions, and Applications* (eds. Zhang, W. & Jin, Y.) 389–434 (John Wiley & Sons Ltd., 2018). doi:10.1002/9781119075738.ch10.
4. Kloxin, C. J. & Bowman, C. N. Covalent adaptable networks: Smart, reconfigurable and responsive network systems. *Chem. Soc. Rev.* **42**, 7161–7173 (2013).
5. Komáromy, D., Nowak, P. & Otto, S. Dynamic Combinatorial Libraries. in *Dynamic Covalent Chemistry - Principles, Reactions and Applications* (eds. Zhang, W. & Jin, Y.) 31–119 (John Wiley & Sons, Inc., 2018). doi:10.1002/9781119075738.ch2.
6. Lehn, J. M. Dynamic combinatorial chemistry and virtual combinatorial libraries. *Chem. Eur. J.* **5**, 2455–2463 (1999).
7. Corbett, P. T., Leclaire, J., Vial, L., West, K. R., Wietor, J. L., Sanders, J. K. M. & Otto, S. Dynamic combinatorial chemistry. *Chem. Rev.* **106**, 3652–3711 (2006).
8. Yuan, Y. C., Yin, T., Rong, M. Z. & Zhang, M. Q. Self healing in polymers and polymer composites. Concepts, realization and outlook: A review. *Express Polym. Lett.* **2**, 238–250 (2008).
9. Aïssa, B., Therriault, D., Haddad, E. & Jamroz, W. Self-healing materials systems: Overview of major approaches and recent developed technologies. *Adv. Mater. Sci. Eng.* **2012**, 854203 (2012).

10. Chen, X., Dam, M. A., Ono, K., Mal, A., Shen, H., Nutt, S. R., Sheran, K. & Wudl, F. A thermally re-mendable cross-linked polymeric material. *Science*. **295**, 1698–1702 (2002).
11. Nishiyabu, R., Kubo, Y., James, T. D. & Fossey, J. S. Boronic acid building blocks: tools for self assembly. *Chem. Commun* **47**, 1124–1150 (2011).
12. Li, J., Carnall, J. M. A., Stuart, M. C. A. & Otto, S. Hydrogel formation upon photoinduced covalent capture of macrocycle stacks from dynamic combinatorial libraries. *Angew. Chem. Int. Ed.* **50**, 8384–8386 (2011).
13. Ying, H., Zhang, Y. & Cheng, J. Dynamic urea bond for the design of reversible and self-healing polymers. *Nat. Commun.* **5**, 3218 (2014).
14. Wöhler, F. & Liebig, J. Untersuchungen über die Natur der Harnsäure. *Ann. der Pharm.* **26**, 241–336 (1838).
15. Eckenroth, H. & Wolf, M. Ueber Phenyl-, alpha- und beta-naphthylester der Salicylsäure. *Berichte der Dtsch. Chem. Gesellschaft* **26**, 1463–1470 (1893).
16. Davis, T. L. & Underwood, H. W. The Urea Rearrangement. *J. Am. Chem. Soc.* **44**, 2595–2604 (1922).
17. Tenney, L., Blanchard, D. & Blanchard, K. C. The Urea Rearrangement. II. *J. Am. Chem. Soc.* **45**, 1816–1820 (1923).
18. Mukaiyama, T. & Fujita, Y. On the Thermal Dissociation of Organic Compounds. IX. The Urea Linkage (1,3-Di-substituted Ureas in Alcohols). *Bull. Chem. Soc. Jpn.* **29**, 54–57 (1956).
19. Mukaiyama, T. On the Thermal Dissociation of Organic Compounds. VII. The Urea Linkage (1,3-Dibenzylurea and 1-isopropyl-3,3-diethylurea in Alcohols). *Bull. Chem. Soc. Jpn.* **28**, 253–258 (1955).
20. Mukaiyama, T., Ozaki, S. & Hoshino, T. On the Thermal Dissociation of Organic Compounds. VI. The Effect of the Substituent and That of the Solvent on the Thermal Dissociation of Ureas. *Bull. Chem. Soc. Jpn.* **27**, 578–582 (1954).
21. Mukaiyama, T. & Iwanami, M. On the Thermal Dissociation of Organic Compounds. VIII. The Effects of the Substituents on the Thermal Dissociation of Urethans in Amine Solvent. *Bull. Chem. Soc. Jpn.* **29**, 51–54 (1956).
22. Mukaiyama, T., Matsunaga, T. & Hoshino, H. On the Thermal Dissociation of Organic Compounds. (1) The Urea Linkage (Diphenylurea in Fatty Acids). *J. Am. Chem. Soc.* **74**, 3097–3100 (1952).
23. Mukaiyama, T. & Matsunaga, T. On the Thermal Dissociation of Organic Compounds. V. The Effect of the Solvent (Fatty Acids) on the Thermal Dissociation of Urea. *J. Am. Chem. Soc.* **75**, 6209–6212 (1953).
24. Aurich, H. G., Scharpenberg, H. G. & Kabs, K. Umlagerung von H-Hydroxyharnstoffen. *Tetrahedron Lett.* **11**, 3559–3562 (1970).

25. Greene, F. D., Stowell, J. C. & Bergmark, W. R. Diaziridinones (2,3-Diazacyclopropanones). II. Synthesis, Properties, and Reactions. *J. Org. Chem.* **34**, 2254–2262 (1969).
26. Stowell, J. C. & Padegimas, S. J. Urea Dissociation. A Measure of Steric Hindrance in Secondary Amines. *J. Org. Chem.* **39**, 2448–2449 (1974).
27. Rolph, M. S., Markowska, A. L. J., Warriner, C. N. & O'Reilly, R. K. Blocked isocyanates: From analytical and experimental considerations to non-polyurethane applications. *Polym. Chem.* **7**, 7351–7364 (2016).
28. Delebecq, E., Pascault, J. P., Boutevin, B. & Ganachaud, F. On the versatility of urethane/urea bonds: Reversibility, blocked isocyanate, and non-isocyanate polyurethane. *Chem. Rev.* **113**, 80–118 (2013).
29. Nakashima, K., Takeshita, T. & Morimoto, K. Review of the occupational exposure to isocyanates: Mechanisms of action. *Environ. Health Prev. Med.* **7**, 1–6 (2002).
30. Sultan Nasar, A., Subramani, S. & Radhakrishnan, G. Synthesis and Properties of Aromatic Secondary Amine-Blocked Isocyanates. *J. Polym. Sci. Part A Polym. Chem.* **37**, 1815–1821 (1999).
31. Sankar, G. & Sultan Nasar, A. Amine-Blocked Polyisocyanates. I. Synthesis of Novel N-Methylaniline-Blocked Polyisocyanates and Deblocking Studies Using Hot-Stage Fourier Transform Infrared Spectroscopy. *J. Polym. Sci. Part A Polym. Chem.* **45**, 1557–1570 (2007).
32. Sultan Nasar, A., Subramani, S. & Radhakrishnan, G. Synthesis and properties of imidazole-blocked diisocyanates. *Polym. Int.* **48**, 614–620 (1999).
33. Hutchby, M., Houlden, C. E., Haddow, M. F., Tyler, S. N. G., Lloyd-Jones, G. C. & Booker-Milburn, K. I. Switching pathways: Room-temperature neutral solvolysis and substitution of amides. *Angew. Chem. Int. Ed.* **51**, 548–551 (2012).
34. Wang, Z., Gangarapu, S., Escorihuela, J., Fei, G., Zuilhof, H. & Xia, H. Dynamic covalent urea bonds and their potential for development of self-healing polymer materials. *J. Mater. Chem. A* **7**, 15933–15943 (2019).
35. Wang, Z., Yang, M., Wang, X., Fei, G., Zheng, Z. & Xia, H. NIR driven fast macro-damage repair and shear-free reprocessing of thermoset elastomers: Via dynamic covalent urea bonds. *J. Mater. Chem. A* **8**, 25047–25052 (2020).
36. Yang, Y., Ying, H., Jia, Y., Chen, Y. & Cheng, J. Stabilization of the hindered urea bond through de-tert-butylation. *Chem. Commun.* **57**, 3812–3815 (2021).
37. Ying, H., Yang, Y., Cai, K. & Cheng, J. Hindered urea bond: A bilaterally responsive chemistry to hydrogen peroxide. *European J. Org. Chem.* **2019**, 728–731 (2019).
38. Hackl, K. A. & Falk, H. The synthesis of N-substituted ureas II: Nucleophilic substitution of ureas at the carbonyl group. *Monatshefte für Chem. Chem. Mon.* **123**, 607–615 (1992).

39. Ying, H. & Cheng, J. Hydrolyzable polyureas bearing hindered urea bonds. *J. Am. Chem. Soc.* **136**, 16974–16977 (2014).
40. Cai, K., Ying, H. & Cheng, J. Dynamic Ureas with Fast and pH-Independent Hydrolytic Kinetics. *Chem. Eur. J.* **24**, 7345–7348 (2018).
41. Hutchby, M., Houlden, C. E., Gair Ford, J., Tyler, S. N. G., Gagné, M. R., Lloyd-Jones, G. C. & Booker-Milburn, K. I. Hindered ureas as masked isocyanates: Facile carbamoylation of nucleophiles under neutral conditions. *Angew. Chem. Int. Ed.* **48**, 8721–8724 (2009).
42. Erice, A., Ruiz de Luzuriaga, A., Matxain, J. M., Ruipérez, F., Asua, J. M., Grande, H. J. & Rekondo, A. Reprocessable and recyclable crosslinked poly(urea-urethane)s based on dynamic amine/urea exchange. *Polymer*. **145**, 127–136 (2018).
43. Erice, A., Azcune, I., Ruiz de Luzuriaga, A., Ruipérez, F., Irigoyen, M., Matxain, J. M., Asua, J. M., Grande, H.-J. & Rekondo, A. Effect of Regioisomerism on Processability and Mechanical Properties of Amine/Urea Exchange Based Poly(urea-urethane) Vitrimers. *ACS Appl. Polym. Mater.* **1**, 2472–2481 (2019).
44. Montarnal, D., Capelot, M., Tournilhac, F. & Leibler, L. Silica-like malleable materials from permanent organic networks. *Science*. **334**, 965–968 (2011).
45. Denissen, W., Winne, J. M. & Du Prez, F. E. Vitrimers: Permanent organic networks with glass-like fluidity. *Chem. Sci.* **7**, 30–38 (2016).
46. Zhang, L. & Rowan, S. J. Effect of Sterics and Degree of Cross-Linking on the Mechanical Properties of Dynamic Poly(alkylurea-urethane) Networks. *Macromolecules* **50**, 5051–5060 (2017).
47. Chen, L., Zhang, L., Griffin, P. J. & Rowan, S. J. Impact of Dynamic Bond Concentration on the Viscoelastic and Mechanical Properties of Dynamic Poly(alkylurea-co-urethane) Networks. *Macromol. Chem. Phys.* **221**, 1900440 (2020).
48. Zhang, Y., Ying, H., Hart, K. R., Wu, Y., Hsu, A. J., Coppola, A. M., Kim, T. A., Yang, K., Sottos, N. R., White, S. R. & Cheng, J. Malleable and Recyclable Poly(urea-urethane) Thermosets bearing Hindered Urea Bonds. *Adv. Mater.* **28**, 7646–7651 (2016).
49. Wang, S., Yang, Y., Ying, H., Jing, X., Wang, B., Zhang, Y. & Cheng, J. Recyclable, self-healable, and highly malleable poly(urethane-urea)s with improved thermal and mechanical performances. *ACS Appl. Mater. Interfaces* **12**, 35403–35414 (2020).
50. Jiang, L., Lei, Y., Xiao, Y., Fu, X., Kong, W., Wang, Y. & Lei, J. Mechanically robust, exceptionally recyclable and shape memory cross-linked network based on reversible dynamic urea bonds. *J. Mater. Chem. A* **8**, 22369–22378 (2020).
51. Khan, A., Huang, K., Sarwar, M. G., Cheng, K., Li, Z., Tuhin, M. O. & Rabnawaz, M. Self-healing and self-cleaning clear coating. *J. Colloid Interface*

- Sci.* **577**, 311–318 (2020).
52. Lee, D. G., Sung, S., Oh, D. G., Park, Y. Il, Lee, S. H., Kim, J. C., Noh, S. M. & Jung, H. W. Application of polycarbonate diol containing hindered urea to polyurethane-based clearcoats for tuning of scratch-healing properties. *J. Coatings Technol. Res.* **17**, 963–976 (2020).
  53. Kim, G. Y., Sung, S., Kim, M. P., Kim, S. C., Lee, S. H., Park, Y. Il, Noh, S. M., Cheong, I. W. & Kim, J. C. Reversible polymer networks based on the dynamic hindered urea bond for scratch healing in automotive clearcoats. *Appl. Surf. Sci.* **505**, 144546 (2020).
  54. Liu, S., Chen, S., Shi, W., Peng, Z., Luo, K., Xing, S., Li, J., Liu, Z. & Liu, L. Self-Healing, Robust, and Stretchable Electrode by Direct Printing on Dynamic Polyurea Surface at Slightly Elevated Temperature. *Adv. Funct. Mater.* **31**, 1–8 (2021).
  55. Jia, Y., Ying, H., Zhang, Y., He, H. & Cheng, J. Reconfigurable Poly(urea-urethane) Thermoset Based on Hindered Urea Bonds with Triple-Shape-Memory Performance. *Macromol. Chem. Phys.* **220**, 1900148 (2019).
  56. Park, J. I., Choe, A., Kim, M. P., Ko, H., Lee, T. H., Noh, S. M., Kim, J. C. & Cheong, I. W. Water-adaptive and repeatable self-healing polymers bearing bulky urea bonds. *Polym. Chem.* **9**, 11–19 (2018).
  57. Chen, M., Feng, X., Xu, W., Wang, Y., Yang, Y., Jiang, Z. & Ding, J. Pegylated polyurea bearing hindered urea bond for drug delivery. *Molecules* **24**, 1538 (2019).
  58. Jäger, E., Humajová, J., Dölen, Y., Kučka, J., Jäger, A., Konefał, R., Pankrác, J., Pavlova, E., Heizer, T., Šefc, L., Hrubý, M., Figdor, C. G. & Verdoes, M. Enhanced Antitumor Efficacy through an “AND gate” Reactive Oxygen-Species-Dependent pH-Responsive Nanomedicine Approach. *Adv. Healthc. Mater.* **10**, (2021).
  59. Piergentili, I., Bouwmans, P. R., Reinalda, L., Lewis, R. W., Klemm, B., Liu, H., De Kruijff, R. M., Denkova, A. G. & Eelkema, R. Thioanisole ester based logic gate cascade to control ROS-triggered micellar degradation. *Polym. Chem* **13**, 2383–2390 (2022).
  60. Ying, H., Yen, J., Wang, R., Lai, Y., Hsu, J. L. A., Hu, Y. & Cheng, J. Degradable and biocompatible hydrogels bearing a hindered urea bond. *Biomater. Sci.* **5**, 2398–2402 (2017).
  61. Spitzbarth, B. & Eelkema, R. On-Demand Release of Secondary Amine Bases for the Activation of Catalysts and Crosslinkers. *Chem. Eur. J.* **29**, e202203028 (2023).
  62. Yang, Y., Ying, H., Li, Z., Wang, J., Chen, Y., Luo, B., Gray, D. L., Ferguson, A., Chen, Q., Z, Y. & Cheng, J. Near quantitative synthesis of urea macrocycles enabled by bulky N-substituent. *Nat. Commun.* **12**, 1572 (2021).

63. Hosseinzadeh, R., Sarrafi, Y. & Aghili, N. An efficient and mild protocol for the synthesis of unsymmetrical ureas in the absence of catalyst and additives. *Chinese Chem. Lett.* **21**, 1171–1174 (2010).
64. Bennet, W. B., Saunders, J. H. & Hardy, E. E. The Preparation of Isocyanates by the Thermal Decomposition of Substituted Ureas. *J. Am. Chem. Soc.* **75**, 2101–2103 (1953).
65. Bunge, W. Einfache Laboratoriumsmethode zur Herstellung niedrigsiedender Isocyanate. *Angew. Chem.* **72**, 1002 (1960).
66. Rolph, M. S., Inam, M. & O'Reilly, R. K. The application of blocked isocyanate chemistry in the development of tunable thermoresponsive crosslinkers. *Polym. Chem.* **8**, 7229–7239 (2017).
67. Liu, W. X., Yang, Z., Qiao, Z., Zhang, L., Zhao, N., Luo, S. & Xu, J. Dynamic multiphase semi-crystalline polymers based on thermally reversible pyrazole-urea bonds. *Nat. Commun.* **10**, 4753 (2019).
68. Wang, S., Fu, D., Wang, X., Pu, W., Martone, A., Lu, X., Lavorgna, M., Wang, Z., Amendola, E. & Xia, H. High performance dynamic covalent crosslinked polyacylesemicarbazide composites with self-healing and recycling capabilities. *J. Mater. Chem. A* **9**, 4055–4065 (2021).
69. Yang, M., Lu, X., Wang, Z., Fei, G. & Xia, H. A novel self-catalytic cooperative multiple dynamic moiety: towards rigid and tough but more healable polymer networks. *J. Mater. Chem. A* **9**, 16759–16768 (2021).
70. Lee, D. S., Choi, Y.-S., Hwang, J. H., Lee, J.-H., Lee, W., Ahn, S., Park, S., Lee, J.-H., Kim, Y. S. & Kim, D.-G. Weldable and Reprocessable Biomimetic Polymer Networks Based on a Hydrogen Bonding and Dynamic Covalent Thiourea Motif. *ACS Appl. Polym. Mater.* **3**, 3714–3720 (2021).
71. Vlatković, M. & Feringa, B. L. Unclicking of thioureas: Base catalyzed elimination of anilines and isothiocyanates from thioureas. *Tetrahedron* **75**, 2188–2192 (2019).
72. Jung, K. I., Kim, B., Lee, D. G., Lee, T. H., Choi, S. Y., Kim, J. C., Noh, S. M., Park, Y. II & Jung, H. W. Characteristics of dual-curable blocked isocyanate with thermal radical initiator for low-temperature curing of automotive coatings. *Prog. Org. Coatings* **125**, 160–166 (2018).

# On-Demand Release of Secondary Amine Bases for the Activation of Catalysts and Crosslinkers

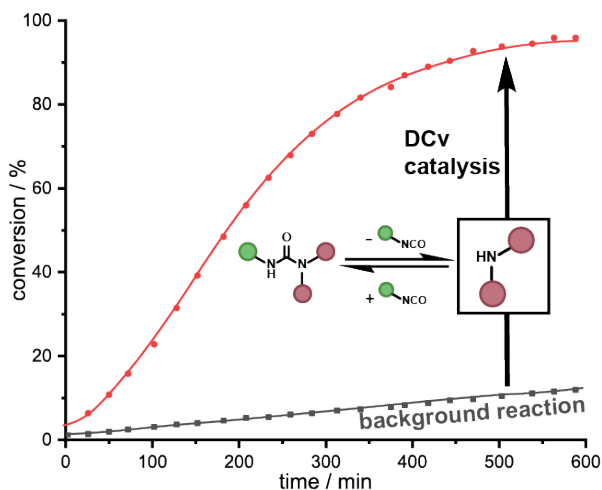
## Abstract

Dynamic covalent (DCv) ureas have been used abundantly to design self-healing materials. We demonstrate that apart from self-healing materials, the species present in the equilibrium of DCv ureas can be employed as responsive organocatalysts. Easily controllable stimuli like heat or addition of water shift the equilibrium towards isocyanate and free base which can function as an in situ released reagent. We demonstrate this application of DCv ureas with two examples. Firstly, we use the liberated base to catalytically activate a latent organocatalyst for acylhydrazone formation. Secondly, this base can be employed in an equimolar manner to trigger the release of nitrile-*N*-oxides from chlorooximes, which react with acrylates to form an isoxazoline polymer gel.

## Availability and Contributions

This chapter is based on an article published as: B. Spitzbarth, R. Eelkema. *Chem. Eur. J.* **29**, e202203028 (2023). It is reprinted with permission from Wiley VCH. DOI: 10.1002/chem.202203028

B.S and R.E. developed the project idea. B.S. conducted all experiments, wrote the initial draft, and designed figures and schemes. R.E. supervised the research, secured funding, and corrected the manuscript.



## Introduction

Dynamic Covalent (DCv) ureas have been shown by the group of J. Cheng to be a versatile motif in the development of reversible and self-healing poly(ureaurethanes).<sup>1</sup> Such dynamic motifs have been extensively used for a wide range of applications in materials, imparting polymer networks with desirable properties like self-healing.<sup>2,3</sup> Generally, amides (and ureas) are considered to be very stable and are frequently employed as protecting groups in organic synthesis due to their inertness under a wide range of conditions.<sup>4</sup> However, substituting the nitrogen in amides with increasingly bulky substituents weakens the C-N bond due to torsion and therefore reduced conjugation.<sup>5</sup>

The concept of reversible amide, urea and urethane bonds has been widely employed in the form of ‘blocked isocyanates’ as a procedure to access hyperbranched polyurethanes,<sup>6,7</sup> as well as routes to post-polymerization modifications.<sup>8,9</sup> Besides these material applications however, DCv ureas have found little use, yet they appear to be attractive dormant base release reagents.

The activation of dormant reagents has previously found some application, for instance in mechanocatalytic polymerization,<sup>10</sup> or the time-controlled pH lowering through the hydrolysis of glucono- $\delta$ -lactone.<sup>11</sup> Inspired by these works, the findings in this paper focus on the reversible, as well as irreversible, controlled release of the secondary, bulky amine base present in dynamic urea equilibria and demonstration of its application as a triggering reagent in two different reaction cascades. In addition, we show that under the application of heat as a stimulus, the secondary amine can be used directly as a transient, catalytic species and return to its original, dormant urea state upon removal of the stimulus (Figure 3.1, Scheme 3.1 A). We demonstrate, by means of triggered catalysis as well as triggered gelation (Scheme 3.1 B, C), the versatility of the DCv urea equilibrium as a starting point for a diverse range of reaction cascades. This concept of using species which are present in DCv equilibria to trigger a reaction cascade opens up new possibilities of making use of an on demand change in chemical reactivity upon a change in conditions.

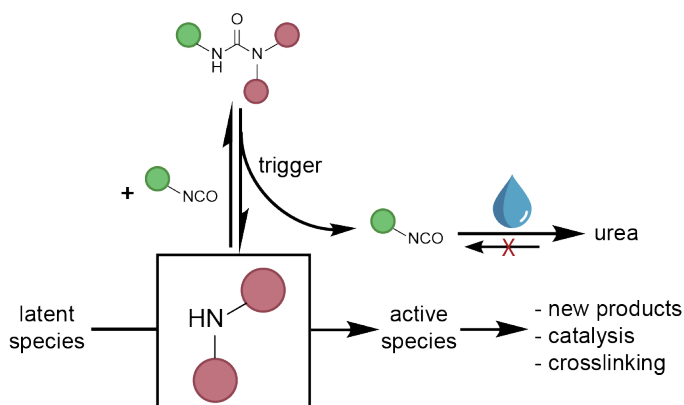
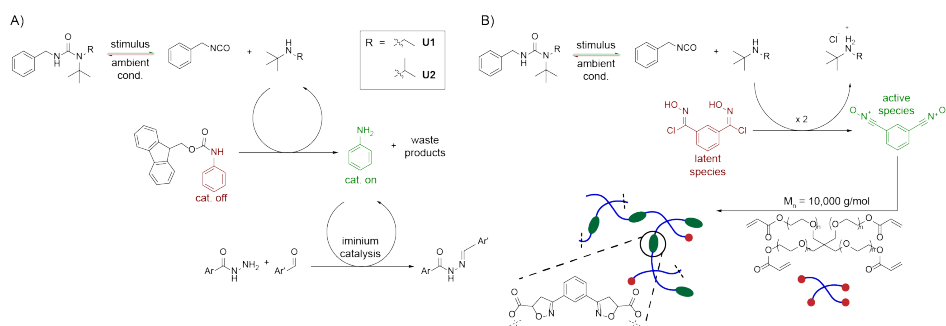


**Figure 3.1:** Base present in the equilibrium of DCv ureas can be used to deprotect a blocked organocatalyst. This can happen reversibly under application of heat or irreversibly in the presence of water or alcohols.

## Results and Discussion

We chose two different reactions to showcase the versatility that such an on demand release system of secondary amines can have. First, secondary amine bases are routinely used to remove protecting groups like the base-labile fluorenyl-methyloxycarbonyl (Fmoc) group.<sup>12</sup> This group can be used to block catalytically active species. The Fmoc group is also well known to be cleaved by catalytic amounts of base and has been applied along those lines, such as for the amplification of organic amines.<sup>13</sup> This sets up Fmoc-blocked catalysts as good candidates for a triggered deprotection by the small amounts of base released in the equilibrium of DCv ureas upon heating or addition of water. Potential candidates for reversible blockage by the Fmoc group include nitrogen-bearing catalysts like amines. Compounds such as anilines and pyrrolidine derivatives like proline or indolines, to name a few, have been extensively studied for their catalytic function in iminium- and enamine-catalysed reactions, such as the formation of acylhydrazones from aldehydes and acylhydrazides.<sup>14–19</sup>



**Scheme 3.1:** A) DCv urea equilibrium to release a bulky base. Studied reaction cascades in which B) liberated base from DCv ureas U1 and U2 is used for the in situ release of aniline which in turn catalyses acylhydrazone formation and C) liberated base is used for the in situ generation of nitrile-N-oxides which leads to the formation of an isoxazoline gel in the presence of 4-arm acrylates.

Hence, we chose to apply DCv ureas as dormant reagents for a triggered Fmoc deprotection, releasing an amine catalyst on demand, which can then catalyse the formation of acylhydrazones (Scheme 3.1 B). Second, another reaction in which the basicity of the liberated secondary amine bases can be applied is the elimination of hydrogen chloride from chlorooximes to generate highly reactive nitrile-*N*-oxides in situ.<sup>20</sup> This reaction has found widespread use, for example in the recently developed bioorthogonal isonitrile-chlorooxime ligation,<sup>21</sup> or the synthesis of polyisoxazoles via click polymerisation.<sup>22</sup> The reactivity of nitrile-*N*-oxides towards many species like alkenes and thiols makes them an attractive intermediate in reaction cascades for the formation of new species and materials alike.<sup>23,24</sup> We describe their application for the formation of an isoxazoline polymer gel triggered by the in situ release of secondary amine bases, which generate nitrile-*N*-oxides that proceed to form an organogel by crosslinking with a 4-arm PEG acrylate (Scheme 3.1 C).

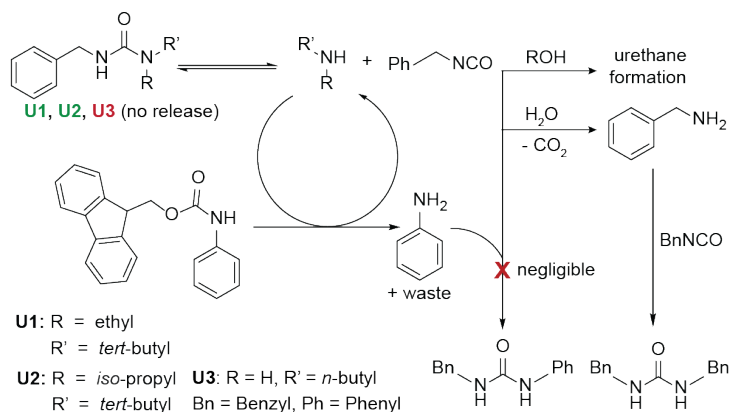
## Choice of ureas and triggering conditions

To examine the DCv equilibrium of bulky ureas under varying conditions, small molecule models had to be synthesised and tested. The group of J. Cheng showed that various bulky ureas, e.g. those based on benzyl isocyanate and two different bulky secondary amine bases, *N-tert*-butylethylamine (base **1**) and *N-tert*-butylisopropylamine (base **2**), have fast equilibration kinetics (approx.  $0.2 \text{ h}^{-1}$ , at  $37 \text{ }^\circ\text{C}$ ) and a low concentration of free base under ambient conditions ( $20 \text{ }^\circ\text{C}$ ,  $K_{\text{eq}} < 10^{-4} \text{ M}^{-1}$ ).<sup>1,25</sup> Furthermore, it was shown that the equilibrium reaction between isocyanate and amine base shows a temperature dependence with Arrhenius-like behaviour,<sup>1</sup> thus making it attractive for a temperature-triggered reversible base release system. The low concentration of free base under ambient conditions is essential to avoid initiating the reaction cascades in the absence of a trigger. One way to irreversibly trigger the release of base is by adding intercepting agents like water or alcohols which react with the generated isocyanate and hence drive the equilibrium towards free base (Scheme 3.2).

These triggers of applying heat and adding intercepting agents can be combined to tune the time scale and reversibility of the base release.

## Triggered Fmoc deprotection for catalyst release

To study the catalyst release, we decided to test whether the Fmoc group is also cleavable under our conditions, yet remains untouched by the miniscule amounts of base present at ambient conditions. We synthesised Fmoc-protected aniline as a model compound, probing the release of aniline via  $^1\text{H-NMR}$ . We chose aniline as a substrate due to its easily trackable chemical shift in the  $^1\text{H-NMR}$  spectra, as well as its low basicity and nucleophilicity. The low basicity avoids the Fmoc-deprotection becoming self-catalysed and allows us to explicitly study the effect that the free base in the DCv urea equilibrium has without the interference of a potential second base, released in the deprotection step.



**Scheme 3.2:** The isocyanate released in the DCv urea equilibrium of **U1** and **U2** can react with alcohols to form urethanes and with water to form benzylamine, which can further react to *N,N'*-dibenzylurea. The reaction of the isocyanate with aniline is negligible under these conditions (see S.I., Figure S3.2). Non-DCv **U3** does not release any amine.

As potential solvent systems DMSO-*d*<sub>6</sub> and DMSO-*d*<sub>6</sub>/D<sub>2</sub>O (4:1) were tested. The solutions of Fmoc-aniline and the ethyl-based DCv urea **U1** were heated to 40 °C. Indeed, in pure DMSO-*d*<sub>6</sub>, an accumulation of aniline could be observed, driven by the catalytic and fully reversible release of base from DCv urea **U1** (Figure 3.2 B). The free base **1** can recombine with the free isocyanate—which is stable in non-aqueous conditions—upon performing the deprotection step and hence does not accumulate over time. In DMSO-*d*<sub>6</sub>/D<sub>2</sub>O (4:1), a more pronounced release of aniline could be observed along with an irreversible accumulation of bulky base **1** (Figure 3.2 C). The irreversible release of base over time in the DMSO-*d*<sub>6</sub>/D<sub>2</sub>O-system can be attributed to the hydrolysis and subsequent decarboxylation of the free isocyanate to form benzyl amine and *N,N'*-dibenzylurea, accelerating the further reaction (Scheme 3.2, Figure 3.2 C).<sup>1</sup> We anticipated that free aniline would also be consumed due to reaction with free benzyl isocyanate for form a non-DCv side product. However, no such side reaction was found, likely due to the much higher reactivity of the benzylamine (Scheme 3.2 and S.I., Figure S3.2). Hence, choosing a weakly nucleophilic catalyst also aids in preventing side reactions with the free isocyanate.

These results show that by increasing the temperature as well as adding an intercepting agent, in this case water, the DCv urea equilibrium can be manipulated sufficiently to trigger the Fmoc-deprotection. Under ambient conditions, no such release was observed on the same timescale in both solvent systems.

To further demonstrate that the release of aniline truly proceeds due to the presence of base released from the DCv urea species, we synthesised a non-bulky non-DCv urea (*N*-Benzyl-*N'*-*n*-butyl urea) and subjected a solution of this urea **U3** with Fmoc-aniline to the same conditions (see S.I., Figure S3.6). Indeed, we found no release of aniline over 48 hours at 40 °C, offering further proof that the DCv properties of ureas **U1** and **U2** are responsible for the observed release of aniline.

To get more clarity about what role the structure of the free base and the solvent play, we studied the influence of the base substituents as well as the effect of adding water to the solvent system on the deprotection rates. The results (Table 1) show that adding D<sub>2</sub>O to DMSO-*d*<sub>6</sub> decreases the reaction rate, while less bulky substituents on the amines increase the rate of aniline release. Specifically, 1-butylamine in pure DMSO-*d*<sub>6</sub> leads to the fastest release, whereas *N*-*tert*-butylisopropylamine (base **2**) with its two bulky residues and rotational freedom leads to the slowest release of aniline.

Having understood how the base structure and presence of water influence the rate of the deprotection step, we proceeded to study the effect that varying the bulk on the DCv ureas (ethyl-based DCv urea **U1** versus isopropyl-based DCv Urea **U2**) has on the release of base and aniline over time (Figure 3.2 C, D). While in experiment C (DCv urea **U1**), the base is released more slowly than in experiment D (DCv urea **U2**), the release of cargo still occurs on a similar time scale. This effect is caused by two counteracting influences. Firstly, the equilibrium is shifted towards the urea more strongly in the case of less hindered urea **U1**. Thus, less free isocyanate is present at equilibrium which slows down the irreversible isocyanate hydrolysis, hence releasing the base over a longer time span. Secondly, the Fmoc deprotection proceeds faster with less bulky bases, as can be seen from comparing bases **1** and **2** in Table 3.1, thus releasing aniline faster than in the presence of equal amounts of a bulkier base. These findings suggest that besides

temperature and the presence of water, the bulkiness of the DCv ureas (**U1** and **U2**) can also be used to tune the release kinetics of the cargo.

**Table 3.1:** Rate constants for the Fmoc-deprotection of Fmoc-aniline with varying bases and solvents, determined via  $^1\text{H-NMR}$ . The rate constants were retrieved by assuming pseudo first order kinetics (see S.I., Figure S3.1). Conditions: 5 mM Fmoc-aniline, 50 mM base, 40 °C.

Entry	Base, solvent	Rate constant ( $\text{min}^{-1}$ )
1	1-butylamine, $\text{DMSO-}d_6$	$0.81 \pm 0.01$
2	Base <b>1</b> , $\text{DMSO-}d_6$	$0.15 \pm 0.01$
3	2,2,6,6-Tetramethylpiperidine, $\text{DMSO-}d_6$	$0.0508 \pm 0.0008$
4	Base <b>2</b> , $\text{DMSO-}d_6$	$0.034 \pm 0.003$
5	Base <b>1</b> , $\text{DMSO-}d_6/\text{D}_2\text{O}$ (4/1)	$0.062 \pm 0.006$

In Figure 3.2 C, D, it can also be seen that the release of aniline proceeds with an ‘activation time’, during which the rate at which aniline is released is increasing. For Figure 3.2 B, this initial increase in rate cannot be observed.

The presence of this inflection could also be explained by reaction of benzyl isocyanate with released aniline (Scheme 3.2), however this side reaction was not observed (see S.I., Figure S3.2). When plotting the first derivative of the conversion graphs over time (see S.I., Figure S3.5), a characteristic peak, after which the change in rate decreases, can be seen. We used this peak to define an ‘activation time’ for the system. This simple method of observing the effect that triggered DCv ureas have on a different reaction offers a way to determine the dynamicity of DCv ureas relative to one another. The different values for the two DCv systems show that the more dynamic urea **U2** leads to a significantly shorter activation time. Since this behaviour cannot be observed for the water-free system (Figure 3.2 B), we hypothesise that the reason for this activation time is the delayed accumulation of base over time. In the water-free environment, only the equilibration between DCv urea and free base, which happens on a relatively fast time scale,<sup>1</sup> is required for the deprotection step to proceed.

In addition, we subjected the aniline release system with DCv urea **U1** to a temperature ramp programme where we varied the temperature between 25 °C and 40 °C (Figure 3.2 E). In an aqueous environment, the accumulation of base is negligible under ambient conditions but leads to an irreversible accumulation at 40 °C. This leads to a great degree of control over the release of precise amounts of base even through a relatively small change in temperature. Furthermore, the release of aniline is also significantly retarded initially. During the first heating cycle, the release of aniline can be observed. However, even after the first heating cycle, the release of aniline continues slowly even under ambient conditions due to the irreversible release of base, which continues to react with Fmoc-aniline to produce aniline.

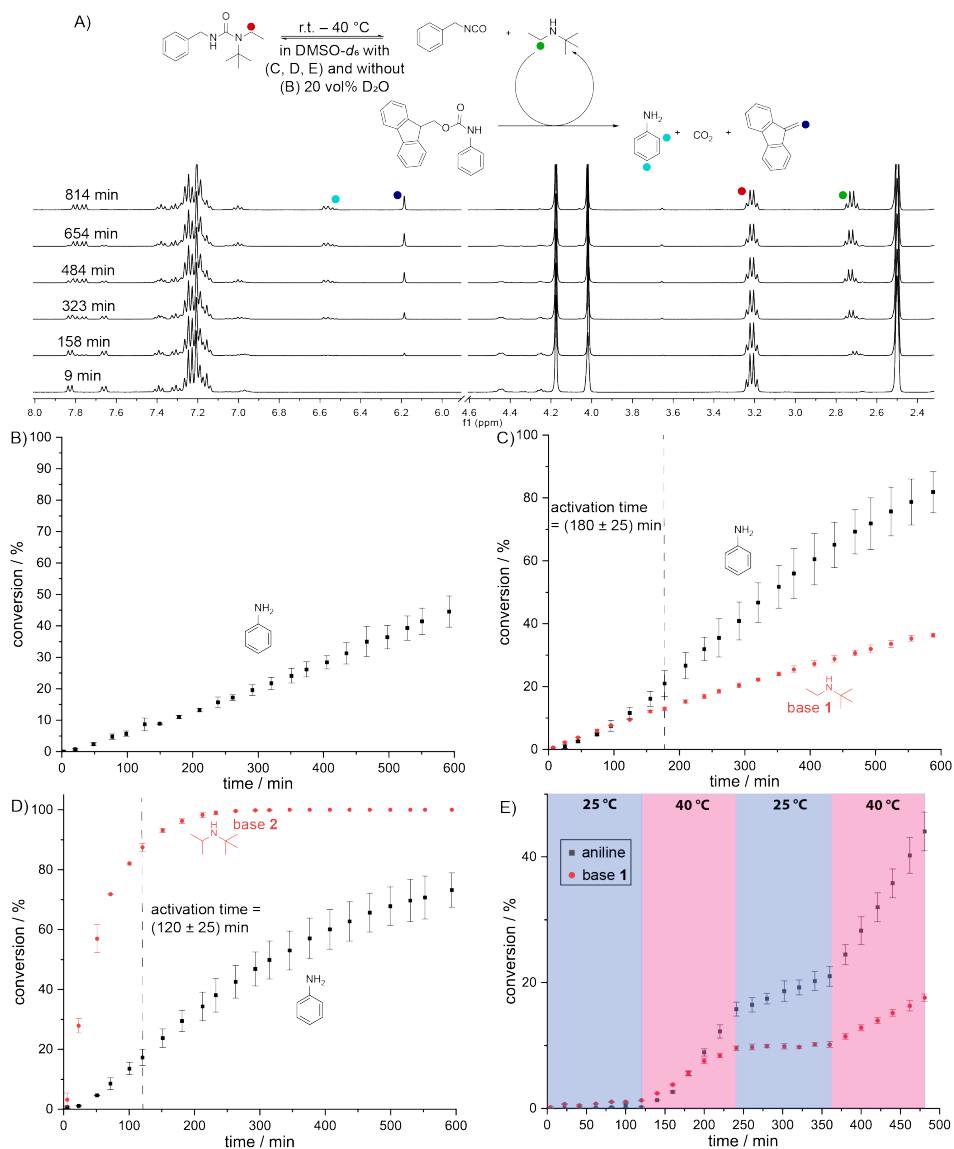


**Figure 3.2:** **A)** Reaction cascade (Scheme 3.1-B) studied via  $^1\text{H-NMR}$  with application of temperature and water as triggers. **B)** Conversion of Fmoc-aniline (5 mM) to aniline in  $\text{DMSO-}d_6$  at  $40^\circ\text{C}$  in the presence of ethyl-based DCv urea **U1** (50 mM). No base release could be observed. **C)** conversion of Fmoc-aniline (5 mM) to aniline and irreversible release of  $N$ -tert-butylethylamine from ethyl-based DCv urea **U1** (50 mM) in  $\text{DMSO-}d_6/\text{D}_2\text{O}$  (4:1) at  $40^\circ\text{C}$ . **D)** conversion of Fmoc-aniline (5 mM) to aniline and irreversible release of  $N$ -tert-butylisopropylamine from isopropyl-based DCv urea **U2** (50 mM) in  $\text{DMSO-}d_6/\text{D}_2\text{O}$  (4:1) at  $40^\circ\text{C}$ . The dashed line marks the activation time of the DCv systems in C) and D) (see S.I., Figure S3.5). **E)** conversion of Fmoc-aniline (5 mM) to aniline and irreversible release of  $N$ -tert-butylethylamine from ethyl-based DCv urea **U1** (50 mM) in  $\text{DMSO-}d_6/\text{D}_2\text{O}$  (4:1) at varying temperature over time.

## Triggered acylhydrazone formation

The triggered aniline release system was then applied to the formation of acylhydrazones as a triggered catalysis system (Scheme 3.1 B).<sup>26-28</sup> Specifically, we chose to study the formation of the acylhydrazone formed from benzhydrazide and 4-nitrobenzaldehyde, which has been studied in our group and shown to proceed significantly faster in the presence of aniline.<sup>29</sup> We studied the formation in the absence of catalysts (i.e. background reaction), the direct influence of 100 mol% catalyst (i.e. aniline), the influence of 5 eq. DCv hindered urea in combination with 100 mol% blocked catalyst (i.e. Fmoc-aniline), the influence of 5 eq. DCv hindered urea without addition of any (pre-)catalyst, as well as the influence of 100 mol% benzyl amine waste product. The results of these studies (Figure 3.3, Figure S3.9) show that the addition of aniline as a catalyst significantly speeds up the formation of acylhydrazone over the background reaction, as expected. However, even the DCv hindered urea **U1** by itself speeds up the reaction and a combination of **U1** with pre-catalyst Fmoc-aniline as a triggered release system leads to the largest increase in reaction rate. This surprising result suggests that another catalytically active species must be present or produced in the early stages of the release reactions. While the catalytic action of the aniline that is released from Fmoc-aniline is well understood,<sup>19</sup> we decided to test whether the bulky base **1** released from DCv urea **U1** as well as a simple non-dynamic urea moiety **U3** (i.e. H-bonding catalyst) can also catalyse the acylhydrazone formation. While the non-dynamic urea **U3** showed no formation above background levels (see S.I., Figure S3.8), the free bulky base **1** showed a catalytic effect on the acylhydrazone formation (Figure 3.3). This observation explains why the reaction catalysed by a combination of Fmoc-aniline and DCv urea **U1** shows a higher maximum rate than the aniline-catalysed reaction alone.

Furthermore, we found the same phenomenon as the previously defined ‘activation time’ in the triggered systems where the acylhydrazone formation was tracked. For the system with the addition of the DCv hindered urea **U1** (Figure 3.3, blue triangles), we observed an activation time of  $100 \pm 25$  min, whereas for the system with the addition of DCv hindered urea **U1** and Fmoc-aniline (Figure 3.3, red squares), we observed an activation time of  $130 \pm 25$  min, which can be attributed to the delayed release of free bulky base **1** and aniline, respectively. For the aniline-catalysed reaction we observed a relatively short activation time of  $50 \pm 25$  min, attributed to the initial reaction between aniline and 4-nitrobenzaldehyde to form the corresponding imine as a catalytic intermediate. Additionally, we decided to compare the maximum rates of the triggered and non-triggered systems to quantify the differences (Table 3.2). It can be seen that the triggered aniline-release system shows a roughly two-fold increase in maximum rate of product formation compared to the traditional aniline-catalysed system, whereas it is roughly 12.5-times faster than the background reaction. These findings show that DCv ureas can not only be used for the triggered release of catalysts protected with the Fmoc-group, but can also enhance traditional catalysis by releasing a second, catalytically active species and increase reaction rates above the rate observed for each individual catalyst alone.

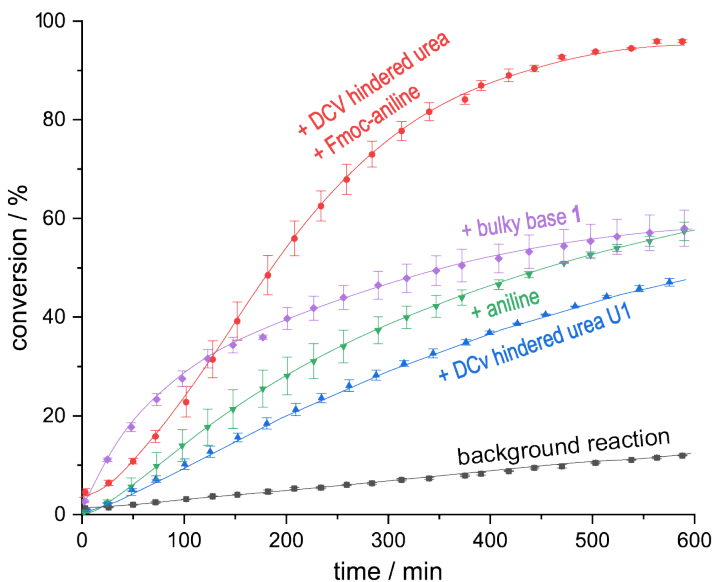


**Figure 3.3:** Formation of acylhydrazone from benzhydrazide and 4-nitrobenzaldehyde over time in 4:1 DMSO- $d_6$ /D $_2$ O at 40 °C. Black squares: background reaction between benzhydrazide (10 mM) and 4-nitrobenzaldehyde (10 mM). Green inverted triangles: addition of 100 mol% aniline. Red circles: addition of 5 mM Fmoc-aniline and 50 mM DCv urea **U1**. Blue triangles: addition of 50 mM DCv urea **U1**. Violet squares: addition of 50 mM bulky base **1**. The data points are connected to guide the eye.

**Table 3.2:** Maximum rates and activation times of formation of acylhydrazone from benzhydrazide (10 mM) and 4-nitrobenzaldehyde (10 mM) in the presence of different catalytically active species as well as without catalysts (background reaction) in 4/1 DMSO- $d_6$ /D $_2$ O, derived from the conversion graphs in Figure 3.3. For systems where no initial increase in reaction rate is observed, an activation time is not applicable (N/A).

System	Maximum rate (mM/min)	Activation time (min)
DCv urea <b>U1</b> + Fmoc aniline	$0.033 \pm 0.001$	$130 \pm 25$
Bulky base <b>1</b>	$0.036 \pm 0.001$	N/A
Aniline	$0.017 \pm 0.003$	$50 \pm 25$
DCv urea <b>U1</b>	$0.0116 \pm 0.0003$	$100 \pm 25$
Background reaction	$0.00264 \pm 0.00003$	N/A

## Triggered elimination for the release of nitrile-*N*-oxides

Next, we use an example in soft material formation to demonstrate the broad application area of DCv ureas as dormant base release reagents. Here, the base eliminates hydrogen chloride from bis-chlorooximes to release nitrile-*N*-oxides in situ. These highly reactive nitrile-*N*-oxides can react with acrylates to form isoxazolines, which we apply as a crosslinking reaction in the formation of a polymer gel (Scheme 3.1 C). To demonstrate this concept, we probed the formation of isoxazolines via <sup>1</sup>H-NMR spectroscopy in a small molecule test at elevated temperature. The result can be seen in Figure 3.4 A. As base **1** is released from DCv urea **U1**, the formation of nitrile-*N*-oxide starts and leads to the cycloaddition with methyl acrylate, resulting in the formation of the bis-cycloaddition product (orange squares, Figure 3.4 A, in good agreement with literature data for aromatic isoxazolines)<sup>30</sup> over time. The hydrochloride salt of bulky base **1** is among the waste species formed.

To put the concept of the in situ formation of nitrile-*N*-oxides to use, we decided to test the heat-triggered gelation of the generated bisfunctional nitrile-*N*-oxides with tetrafunctional 4-arm PEG acrylates ( $M_n = 10$  kg/mol). Tests were performed with the ethyl-based **U1** and *iso*-propyl-based **U2** DCv ureas. The 5% w/v solutions in 9/1 CHCl<sub>3</sub>/DMSO were kept at room temperature for 24 h and heated to 45 °C thereafter. Figure 3.4 B shows that the ethyl-based DCv urea **U1** is a good candidate to enable a temperature-triggered gelation via isoxazoline formation. All experiments start with a clear solution of bischlorooxime, additive and 4-arm PEG acrylate. In the case of the *iso*-propyl based DCv urea **U2**, a colourless transparent gel is formed within 12 h at room temperature, whereas in the experiment with the ethyl-based DCv urea **U1**, the solution does not gel under the same conditions even after 24 hours. Upon heating the latter sample to 45 °C for 3 hours, a transparent gel ultimately forms as well. These findings can be attributed to the different equilibrium constants of the DCv ureas. For DCv urea **U2**, where the equilibrium is more on the side of the free base than for DCv urea **U1**, gelation can occur faster. The reference sample without additives on the other hand remained a colourless solution over weeks. We performed a control by adding triethylamine as a free base to the solution. In this case, we observed gelation within 90 minutes under ambient conditions to form a transparent gel, suggesting that the gelation times can be tuned over a wide range, depending on whether a free base or DCv ureas with varying bulkiness are added to the solution of bischlorooxime and 4-arm PEG acrylate.

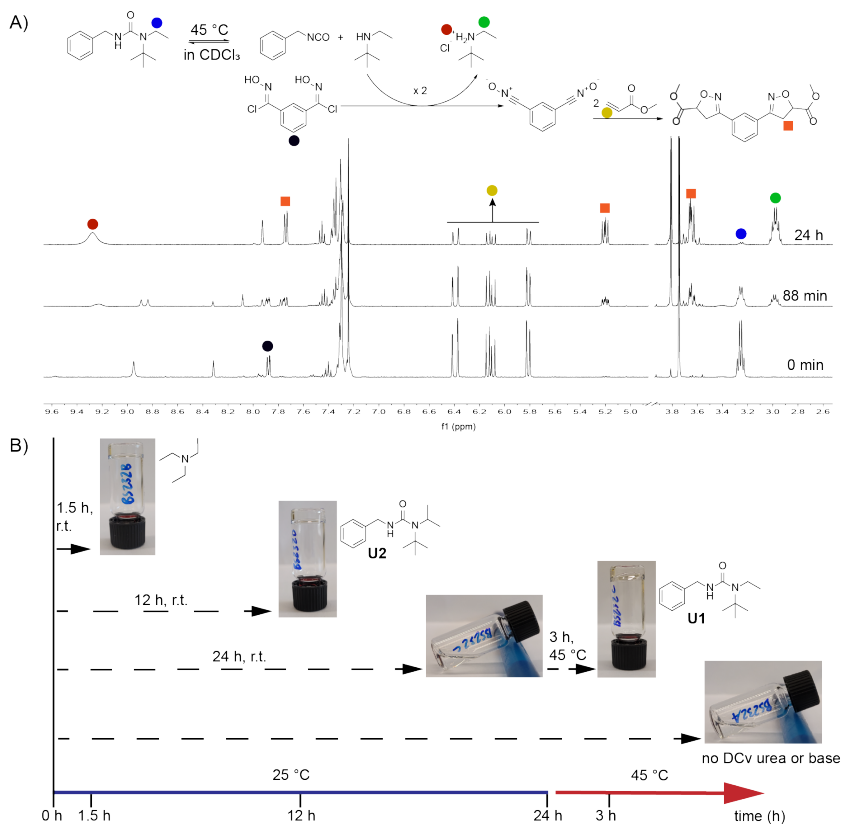


**Figure 3.4:** Temperature-dependent gelation of a 5% w/v solution of bis-chlorooxime (2.0 eq.) and 4-arm PEG acrylate (1.0 eq.) in chloroform with the addition of 5 eq. (1.25 eq. relative to acrylate and chlorooxime groups) of DCv ureas with different substituents. **A)** Reaction with a small molecule acrylate tracked via  $^1\text{H-NMR}$ , 45 °C, in  $\text{CDCl}_3$ . **B)** Time- and temperature-dependent gelation upon addition of a free base and DCv ureas **U1** and **U2** to bis-chlorooxime.

## Conclusion

We demonstrated that the species present in the equilibrium of DCv ureas can be used in reaction cascades and as organocatalysts on demand. We show that the base released in the urea equilibrium can be applied to 1) catalytically cleave the base-labile Fmoc protecting group, releasing active organocatalysts which in turn catalyse the formation of acylhydrazones above levels found for the free catalyst alone and 2) form highly reactive nitrile-*N*-oxides in situ which can lead to the gelation with acrylates present in solution, forming an isoxazoline polymer gel.

Further, we demonstrated that the temperature- and bulk-dependence of the urea equilibrium as well as the reactivity of the released isocyanate species towards nucleophiles can be employed to tune the urea equilibrium, reversibly and irreversibly, in

a way that allows great control over the release of Fmoc-blocked aniline and nitrile-*N*-oxides on demand.

We envisage that these findings have great potential in the design of responsive materials which possess useful functionalities on demand. Especially the sensitivity of the urea equilibrium at or near body temperature sets these triggered release-systems up for potential uses in biomedical materials.

Our group is currently working on applying these equilibria in crosslinked materials to design triggered, self-healing networks.

## Experimental Section

Triggered hydrazone formation: Benzhydrazide (10 mM) and 4-nitrobenzaldehyde (10 mM) were dissolved in 4/1 DMSO-*d*<sub>6</sub>/D<sub>2</sub>O. The corresponding catalyst or DCv urea was added and the solution was heated to 40 °C in a water bath and <sup>1</sup>H-NMR spectra were recorded over time with the probe head heated to 40 °C.

Triggered gelation: 200 μL of a 9/1 CHCl<sub>3</sub>/DMSO 5% w/v solution of 4-arm PEG acrylate (*M*<sub>n</sub> = 10 kg/mol, 1.0 μmol, 10 mg) and bischlorooxime (2.0 eq., 2.0 μmol, 0.47 mg) was prepared. 5.0 eq. triethylamine or DCv urea were added and the solution were kept at room temperature. Gelation was probed via inverted vial test. After 24 hours, the samples were heated in a water bath to 45 °C. A reference sample without base additive was prepared.

Further experimental details, analysis and spectra can be found in the Supporting Information.

## Acknowledgements

This work has received funding from the European Union's Horizon 2020 research and innovation programme under the Marie Skłodowska-Curie grant agreement No 812868. We thank Dr. Stephen Eustace for help with the NMR measurements.

## References

1. Ying, H., Zhang, Y. & Cheng, J. Dynamic urea bond for the design of reversible and self-healing polymers. *Nat. Commun.* **5**, 3218 (2014).
2. Jin, Y., Yu, C., Denman, R. J. & Zhang, W. Recent advances in dynamic covalent chemistry. *Chem. Soc. Rev.* **42**, 6634–6654 (2013).
3. Winne, J. M., Leibler, L. & Du Prez, F. E. Dynamic covalent chemistry in polymer networks: A mechanistic perspective. *Polym. Chem.* **10**, 6091–6108 (2019).

4. Wuts, P. G. M. & Greene, T. M. *Greene's Protective Groups in Organic Synthesis*. (John Wiley & Sons, Inc., 2007). doi:10.1021/jm068051f.
5. Hutchby, M., Houlden, C. E., Haddow, M. F., Tyler, S. N. G., Lloyd-Jones, G. C. & Booker-Milburn, K. I. Switching pathways: Room-temperature neutral solvolysis and substitution of amides. *Angew. Chem. Int. Ed.* **51**, 548–551 (2012).
6. Shanmugam, T. & Nasar, A. S. Novel Hyperbranched Poly(aryl ether urethane)s Using AB<sub>2</sub>-Type Blocked Isocyanate Monomers and Copolymerization with AB-Type Monomers. *Macromol. Chem. Phys.* **209**, 651–665 (2008).
7. Spindler, R. & Fréchet, J. M. J. Synthesis and Characterization of Hyperbranched Polyurethanes Prepared from Blocked Isocyanate Monomers by Step-Growth Polymerization. *Macromolecules* **26**, 4809–4813 (1993).
8. Günay, K. A., Theato, P. & Klok, H. A. Standing on the shoulders of hermann staudinger: Post-polymerization modification from past to present. *J. Polym. Sci. Part A Polym. Chem.* **51**, 1–28 (2013).
9. Rolph, M. S., Markowska, A. L. J., Warriner, C. N. & O'Reilly, R. K. Blocked isocyanates: From analytical and experimental considerations to non-polyurethane applications. *Polym. Chem.* **7**, 7351–7364 (2016).
10. Jakobs, R. T. M., Ma, S. & Sijbesma, R. P. Mechanocatalytic polymerization and cross-linking in a polymeric matrix. *ACS Macro Lett.* **2**, 613–616 (2013).
11. Adams, D. J., Butler, M. F., Frith, W. J., Kirkland, M., Mullen, L. & Sanderson, P. A new method for maintaining homogeneity during liquid-hydrogel transitions using low molecular weight hydrogelators. *Soft Matter* **5**, 1856–1862 (2009).
12. Carpino, L. A. & Han, G. Y. The 9-Fluorenylmethoxycarbonyl Amino-Protecting Group. *J. Org. Chem.* **37**, 3404–3409 (1972).
13. Arimitsu, K., Miyamoto, M. & Ichimura, K. Applications of a nonlinear organic reaction of carbamates to proliferate aliphatic amines. *Angew. Chem. Int. Ed.* **39**, 3425–3428 (2000).
14. Pihko, P. M., Majander, I. & Erkkilä, A. Enamine Catalysis. *Top. Curr. Chem.* **291**, 29–75 (2009).
15. Erkkilä, A., Majander, I. & Pihko, P. M. Iminium catalysis. *Chem. Rev.* **107**, 5416–5470 (2007).
16. Zhou, Y., Piergentili, I., Hong, J., van der Helm, M. P., Macchione, M., Li, Y., Eelkema, R. & Luo, S. Indoline Catalyzed Acylhydrazone/Oxime Condensation under Neutral Aqueous Conditions. *Org. Lett.* **22**, 6035–6040 (2020).
17. Trausel, F., Maity, C., Poolman, J. M., Kouwenberg, D. S. J., Versluis, F., Van Esch, J. H. & Eelkema, R. Chemical signal activation of an organocatalyst enables control over soft material formation. *Nat. Commun.* **8**, 1–7 (2017).
18. van der Helm, M. P., Klemm, B. & Eelkema, R. Organocatalysis in aqueous media. *Nat. Rev. Chem.* **3**, 491–508 (2019).

19. Kölmel, D. K. & Kool, E. T. Oximes and Hydrazones in Bioconjugation: Mechanism and Catalysis. *Chem. Rev.* **117**, 10358–10376 (2017).
20. Cerniauskaite, D., Rousseau, J., Sackus, A., Rollin, P. & Tatibouët, A. Glucosinolate synthesis: A hydroxamic acid approach. *Eur. J. Org. Chem.* 2293–2300 (2011) doi:10.1002/ejoc.201001438.
21. Schaefer, R., Monaco, M. R., Li, M., Tirla, A., Rivera-Fuentes, P. & Wennemers, H. The Bioorthogonal Isonitrile–Chlorooxime Ligation. *J. Am. Chem. Soc.* **141**, 18644–18648 (2019).
22. Matsumura, T., Koyama, Y., Uchida, S., Yonekawa, M., Yui, T., Ishitani, O. & Takata, T. Fluorescent poly(boron enaminoketonate): Synthesis via the direct modification of polyisoxazoles obtained from the click polymerization of a homoditopic nitrile N-oxide and diynes. *Polym. J.* **46**, 609–616 (2014).
23. Benn, M. H. Synthesis of thiohydroximates - The Addition of Thiols to Nitrile Oxides. *Can. J. Chem.* **42**, 2393–2397 (1964).
24. Lee, Y. G., Koyama, Y., Yonekawa, M. & Takata, T. New click chemistry: Polymerization based on 1,3-dipolar cycloaddition of a homo ditopic nitrile N-oxide and transformation of the resulting polymers into reactive polymers. *Macromolecules* **42**, 7709–7717 (2009).
25. Ying, H. & Cheng, J. Hydrolyzable polyureas bearing hindered urea bonds. *J. Am. Chem. Soc.* **136**, 16974–16977 (2014).
26. Maity, C., Trausel, F. & Eelkema, R. Selective activation of organocatalysts by specific signals. *Chem. Sci.* **9**, 5999–6005 (2018).
27. Xi, W., Krieger, M., Kloxin, C. J. & Bowman, C. N. A new photoclick reaction strategy: Photo-induced catalysis of the thiol-Michael addition via a caged primary amine. *Chem. Commun.* **49**, 4504–4506 (2013).
28. Li, G., Trausel, F., van der Helm, M., Klemm, B., Breve, T., van Rossum, S., Hartono, M., Gerlings, H., Lovrak, M., van Esch, J. & Eelkema, R. Tuneable control over organocatalytic activity through host guest chemistry. *Angew. Chem. Int. Ed.* **60**, 14022–14029 (2021).
29. Trausel, F., Fan, B., van Rossum, S. A. P., van Esch, J. H. & Eelkema, R. Aniline Catalysed Hydrazone Formation Reactions Show a Large Variation in Reaction Rates and Catalytic Effects. *Adv. Synth. Catal.* **360**, 2571–2576 (2018).
30. Iwakura, Y., Shiraishi, S., Akiyama, M. & Yuyama, M. Polymerizations by 1,3-Dipolar Cycloaddition Reactions. V. The 1,3-Dipolar Polycycloadditions of Dinitrile N-Oxides with Diolefins. *Bull. Chem. Soc. Jpn.* **41**, 1648–1653 (1968).

## Supporting Information

### General Information

Benzyl isocyanate and *N,N*-*tert*-butylethylamine were purchased from TCI Europe. *N,N*-*tert*-butylisopropylamine and *N*-chlorosuccinimide were purchased from Thermo Fisher. Butylamine, isophthalaldehyde, DMF and hydroxylamine hydrochloride were purchased from Sigma Aldrich. 4arm PEG acrylate ( $M_n = 10$  kg/mol) was purchased from JenKem Technology USA. Ethyl acetate and ethanol were purchased from VWR International. D<sub>2</sub>O and DMSO-*d*<sub>6</sub> were purchased from Eurisotop. Deionised water was made in our laboratory. Unless stated otherwise, all chemicals were used as received. For water-free experiments, anhydrous solvents were used. NMR spectra were recorded on an Agilent-400 MR DD2 (399.67 MHz) instrument. Room temperature measurements were taken at 298 K. Heated experiments were performed and measured at 313 K. All quantified NMR experiments were conducted as duplicates and the mean values were used. For DLS experiments, a Malvern Zetasizer Nano ZS employing a 633 nm laser at a back-scattering angle of 173° was used. Each data point was acquired from two measurements with at least 10 runs each. The temperature in the cell was 25 °C.

### Experimental Procedures

NMR experiments were performed by weighing out compounds, dissolving them in the applicable solvent or solvent mixture and starting the measurements as soon as all compounds had dissolved. For heated experiments, the probe head of the NMR spectrometer was pre-heated to 40 °C before dissolving all compounds. Measurements of <sup>1</sup>H-NMR spectra (8 scans) were taken at intervals of 2 to 30 minutes. The spectra were analysed in Mestrenova after automated baseline- and phase-correction. For the conversion of Fmoc-aniline, the olefinic dibenzofulvene protons as well as the aromatic ortho- and para-protons of aniline were tracked. For the irreversible release of base from DCv urea **U1** and DCv urea **U2**, the CH<sub>2</sub>-protons in the ethyl residue and the CH-proton in the *iso*-propyl residue were tracked respectively. For the conversion in the acylhydrazone experiments, the ortho-protons of 4-nitrobenzaldehyde were tracked. For an explanation of the NMR-analysis in detail, refer to the corresponding section below. For all NMR-experiments, samples with a volume of 0.6 mL were prepared. For all Fmoc-release studies, solutions with final concentrations of 5 mM Fmoc-aniline and 50 mM DCv and non-DCv urea were prepared. For acylhydrazone formation-tests, solutions with final concentrations of 10 mM 4-nitrobenzaldehyde, 10 mM benzhydrazide, 10 mM Fmoc-aniline and 50 mM DCv or non-DCv urea were prepared.

Gelation experiments were performed by dissolving the bischlorooxime (0.47 mg, 2.0 μmol, 2.0 eq.) and 4-arm PEG acrylate ( $M_n = 10$  kg/mol, 10.0 mg, 1.0 μmol, 1.0 eq.) in 150 μL 9/1 chloroform/DMSO (the final solution equated to 5% w/v). In different vials, solutions of DCv urea **U1** (1.2 mg, 5.0 μmol, 5.0 eq.), DCv urea **U2** (1.2 mg, 5.0 μmol, 5.0 eq.) and triethylamine (0.69 μL, 5.0 μmol, 5.0 eq.) in 50 μL of the solvent mixture were prepared and added to each polymer solution. Gelation was tested via the inverted

vial test. For heated gelation tests, the vials with the prepared solutions were submerged in a water bath at the desired temperature.

### Fmoc deprotection with different bases

To determine the rate constants of the Fmoc deprotection of Fmoc-aniline with varying bases and solvent systems, the natural logarithm of the concentration of Fmoc-aniline was plotted over time and a linear fit was performed. These experiments were performed twice for each condition and the mean value of the rate constants and their standard deviation were determined. For purpose of clarity, the mean value of each dataset (duplicates) was plotted.

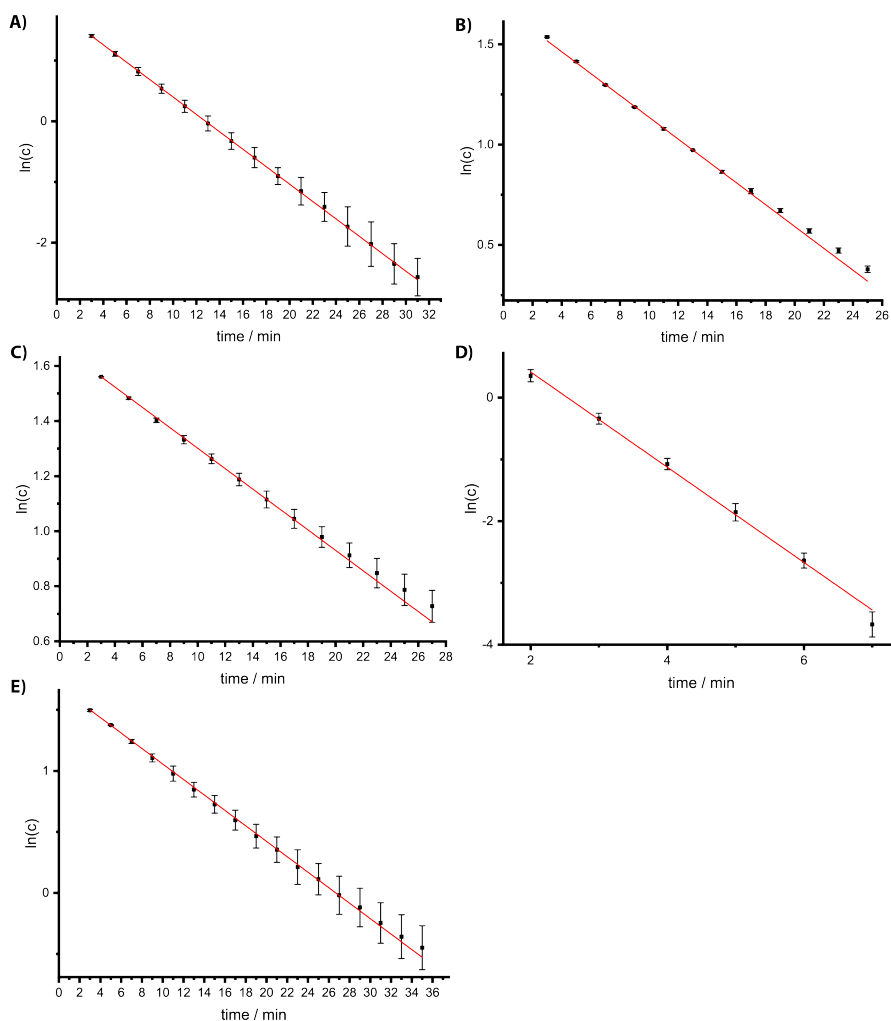


**Figure S3.1:** natural logarithm of concentration of Fmoc-aniline over time in the presence of different bases in DMSO- $d_6$ , at 40 °C, monitored via  $^1\text{H-NMR}$ . A) 50 mM base 2, B) 50 mM base 3, C) 50 mM base 4, D) 50 mM base 1, E) base 2 in 4/1 DMSO- $d_6$ /D $_2$ O.

## Side reaction of benzyl isocyanate with aniline

To rule out that the presence of an inflection point in the release kinetics of bulky bases **1** and **2** as well as aniline was due to the consumption of aniline by benzyl isocyanate, we reacted benzyl isocyanate directly with aniline. To our surprise, this reaction proceeded very slowly. The signals of *N,N'*-dibenzylurea are in accordance with literature<sup>1</sup> and were not detected in our temperature-triggered release studies, ruling out the possibility of aniline consumption by urea having an impact on the release kinetics.

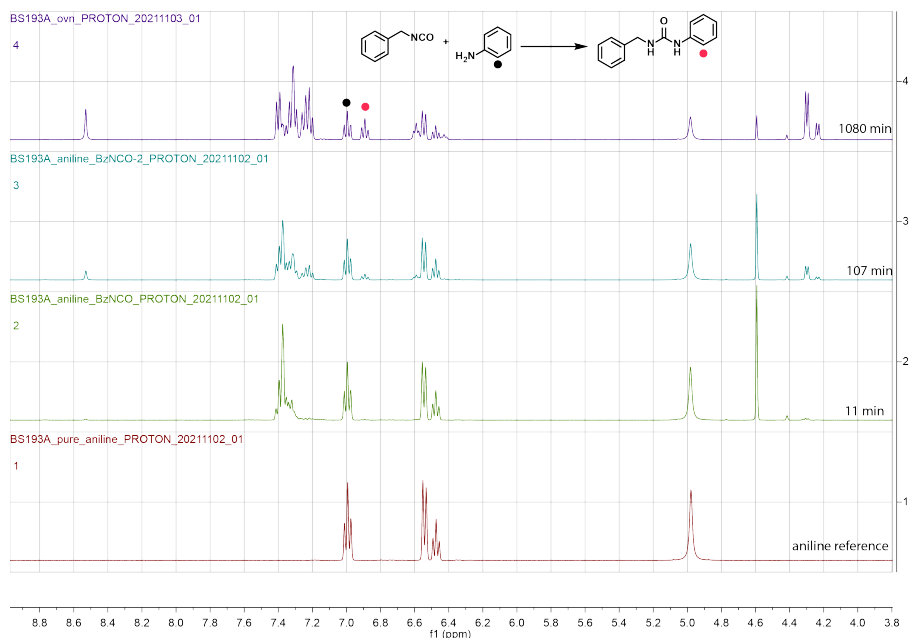


**Figure S3.2:** Cutout of <sup>1</sup>H-NMR spectrum, showing reaction of aniline (50 mM) with benzyl isocyanate (50 mM) in DMSO-*d*<sub>6</sub>. Compared to the reaction with benzyl amine (main text Scheme 2), the reaction with aniline is negligible and the product signals were not found in the experiments of triggered aniline release as well as acylhydrazone formation.

## Fmoc deprotection with DCv ureas **U1** and **U2**

After determination of the rate constants of Fmoc deprotections with varying bases, the deprotection was tested with DCv ureas **U1** and **U2** via <sup>1</sup>H-NMR spectroscopy. For the irreversible release of base in aqueous conditions, the CH<sub>2</sub>-signal of the ethyl group and the CH-signal of the *iso*-propyl group in DCv ureas **U1** and **U2** were tracked respectively. The conversion – in this and all following experiments – was calculated as follows:

$$\text{conversion} = \frac{\text{integral}(\text{product})}{\text{integral}(\text{product}) + \text{integral}(\text{starting material})} \times 100\%$$

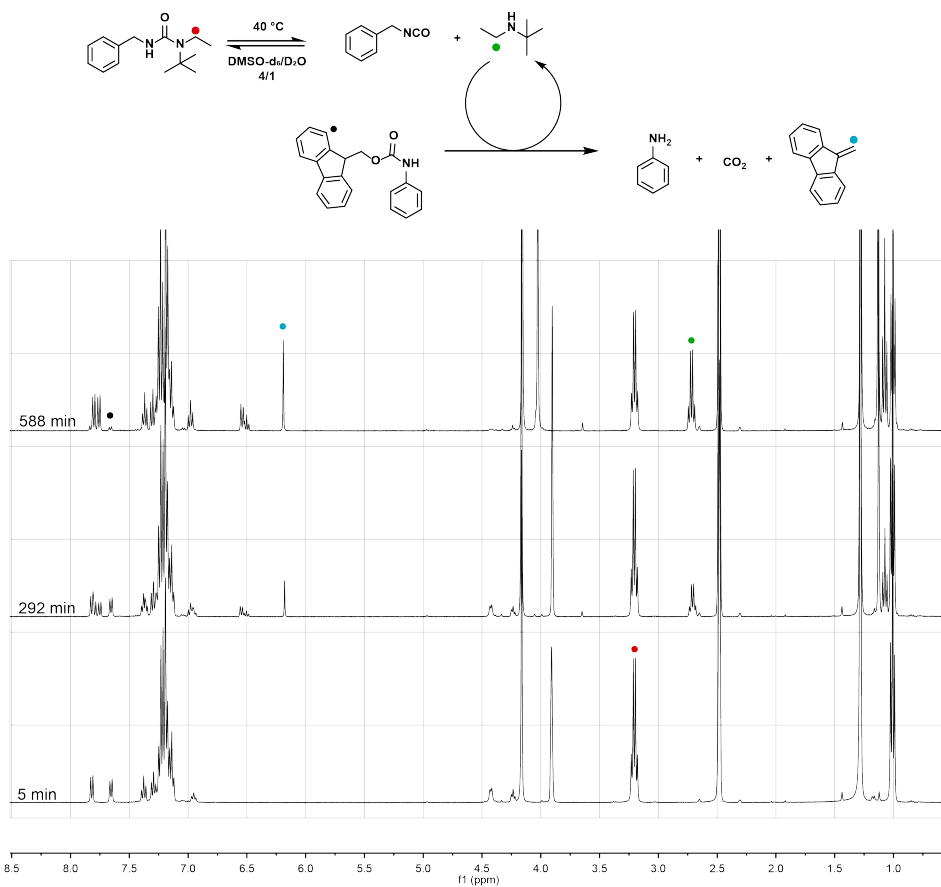


**Figure S3.3:** reaction scheme and cutout of a selection of  $^1\text{H-NMR}$  spectra of DCv urea U1 (50 mM) with Fmoc-aniline (5 mM) in 4/1 DMSO/ $\text{D}_2\text{O}$  (0.6 mL) at  $40\text{ }^\circ\text{C}$  over time. The signals indicated by a black and blue dot were used to track the conversion of Fmoc-aniline to aniline, whereas the signals indicated by a red and green dot were used to track the irreversible release of bulky base over time.

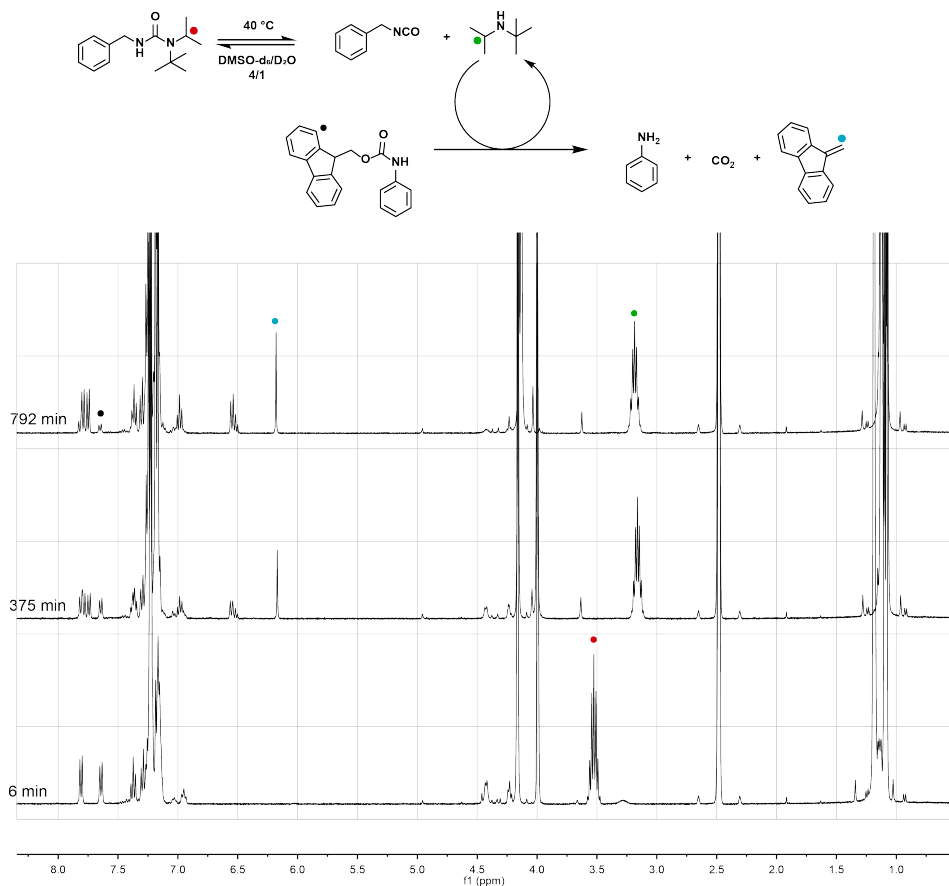


**Figure S3.4:** reaction scheme and cutout of a selection of <sup>1</sup>H-NMR spectra of DCv urea **U2** (50 mM) with Fmoc-aniline (5 mM) in 4/1 DMSO/D<sub>2</sub>O (0.6 mL) at 40 °C over time. The signals indicated by a black and blue dot were used to track the conversion of Fmoc-aniline to aniline, whereas the signals indicated by a red and green dot were used to track the irreversible release of bulky base over time.

For the experiment under water-free conditions, the data was treated the same, however no release of bulky base over time could be observed, hence only the degradation of Fmoc-aniline over time was plotted, whereas the DCv urea **U1** remained intact over the course of the experiment.

To define the activation time of the irreversible water-containing release systems, the derivative of conversion with time was plotted. The time when a global maximum and hence the maximum conversion per time unit was reached, is defined as the activation time of the system. This time gives an estimate of how sensitive the DCv ureas are to the application of a trigger. The system with DCv urea **U1** has a longer activation time compared to the system containing DCv urea **U2** due to its larger equilibrium constant.

This is shown exemplary for the release of aniline through the irreversible release of base from DCv urea **U2**. The error of the activation time is defined as the time between two measurement points.

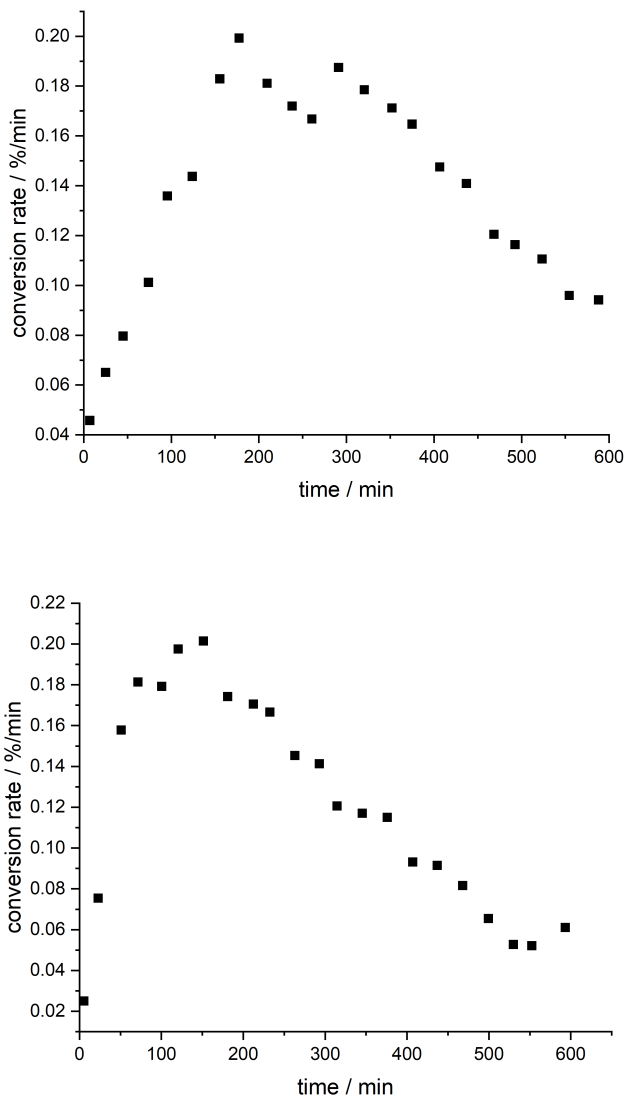


**Figure S3.5:** derivation of the conversion graph of the release of aniline from Fmoc-aniline (5 mM) in the presence of DCv urea **U1** (50 mM, top) and DCv urea **U2** (50 mM, bottom) at 40 °C in 4/1 DMSO- $d_6$ /D $_2$ O (0.6 mL). The point with the highest conversion rate is defined as the activation time of the system.

### Reference test: Fmoc deprotection with non-DCv urea U3

To confirm that the release of aniline from Fmoc-aniline is linked to the release of base from DCv ureas **U1** and **U2**, the same experiment was performed with a non-DCv urea **U3**, which was synthesised from a primary amine and hence no release of base at elevated temperature or in water is expected. In the  $^1\text{H-NMR}$  spectra, neither the characteristic olefinic signal of dibenzofulvene, nor the release of aniline or the accumulation of butylamine could be observed over 24 hours at  $40\text{ }^\circ\text{C}$ , showing that the DCv properties of **U1** and **U2** are responsible for the release of aniline over time.

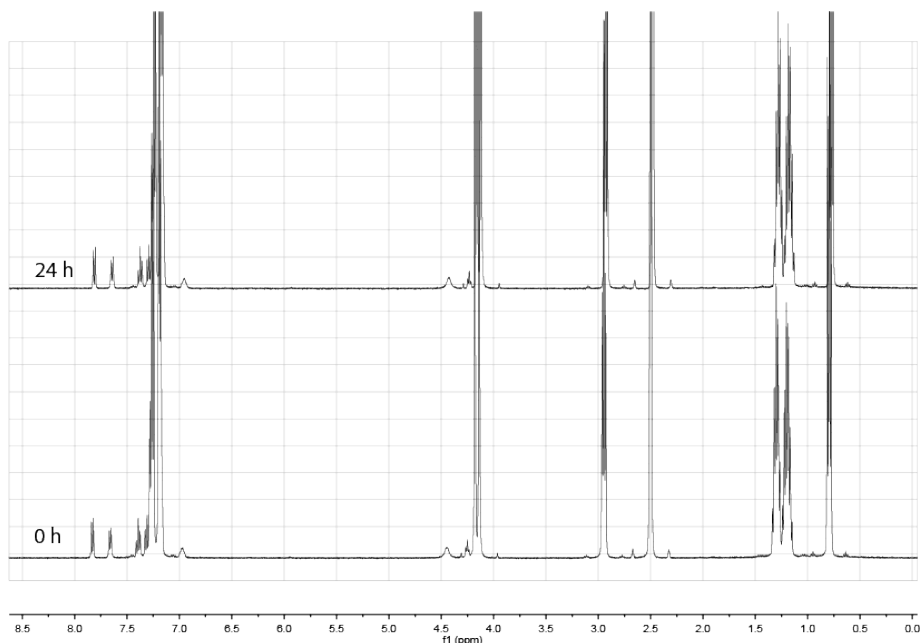


**Figure S3.6:** cutout of  $^1\text{H-NMR}$  spectrum of non-DCv urea **U3** with Fmoc-aniline in 4/1 DMSO/D<sub>2</sub>O at  $40\text{ }^\circ\text{C}$  over time.

### Acylhydrazone formation

#### $^1\text{H-NMR}$ analysis

As in previous experiments, the analysis of the conversion of 4-nitrobenzaldehyde and benzhydrazide to form the acylhydrazone was performed via  $^1\text{H-NMR}$  spectroscopy. For this, the proton signals in *ortho*-position of the aldehyde group and acylhydrazone group were tracked respectively.

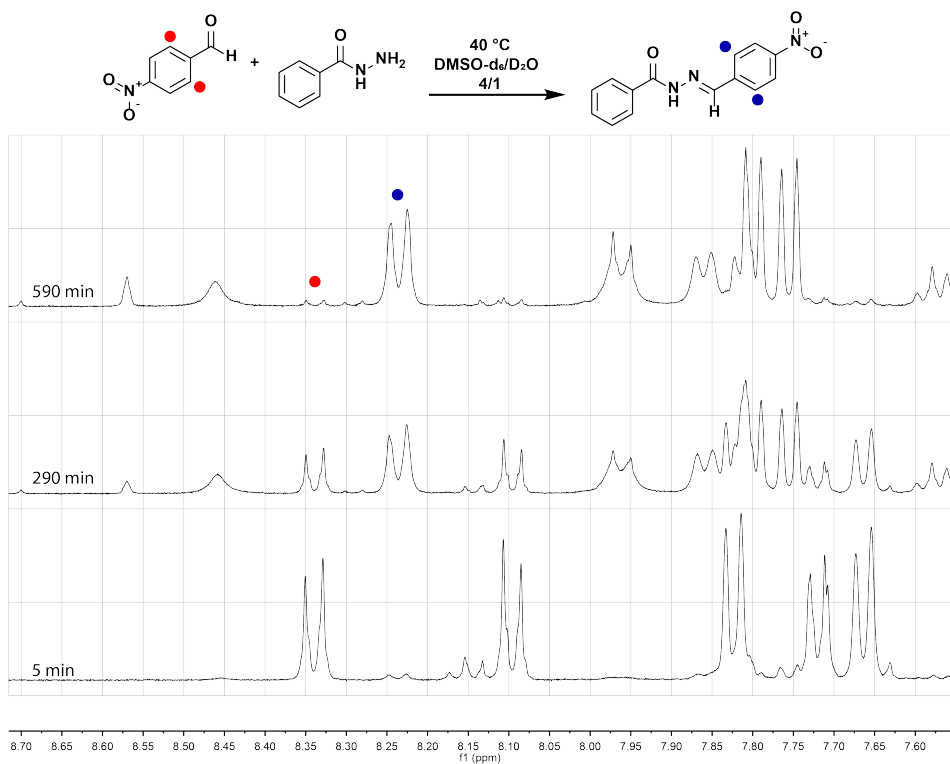


**Figure S3.7:** reaction scheme and cutout of a selection of <sup>1</sup>H-NMR spectra of the formation of acylhydrazone from 4-nitrobenzaldehyde (10 mM) and benzhydrazide (10 mM) with 100 mol% aniline as a catalyst in 4/1 DMSO/D<sub>2</sub>O (0.6 mL) at 40 °C over time. The signals indicated by a red dot belong to the starting material (4-nitrobenzaldehyde) and the signals indicated by a blue dot belong to the product.

### Excluding catalytic effect of non-DCv urea U3

Due to the hydrolysis of the benzyl isocyanate that is present in the equilibria of DCv ureas **U1** and **U2**, dibenzylurea can form over time under aqueous conditions. To ensure that the catalytic effects observed are exclusively due to the presence of aniline as well as a bulky base and not the presence of a urea moiety, the acylhydrazone formation was repeated in the presence of a non-DCv urea **U3**, added to the experiment in the same concentration as the DCv ureas **U1** and **U2** in previous experiments (50 mM). The results in comparison to the background show that no significant deviation is found. This lets us conclude that the catalytic effect seen in experiments with DCv ureas **U1** and **U2** is due to the irreversible release of a bulky base, as well as aniline, which both act as catalysts in the formation of acylhydrazone.

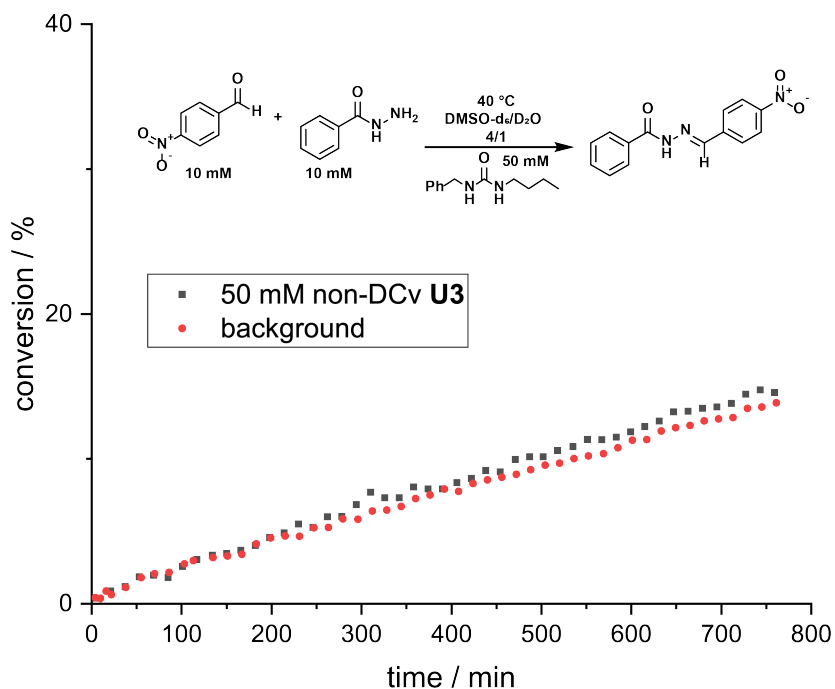


**Figure S3.8:** conversion of 4-nitrobenzaldehyde and benzhydrazide in 4/1 DMSO-d<sub>6</sub>/D<sub>2</sub>O over time at 40 °C without the addition of catalytically active species, compared to the formation over time in the presence of 5 eq. non-DCv urea **U3**. No significant catalytic effect could be observed.

### Determination of maximum rate and activation time

The activation times for the acylhydrazone system were determined analogously to the Fmoc release system by plotting the derivative of conversion with time and determining at what point in time the maximum rate was reached. These maximum rates for all systems derived from these derivatives were compared to one another for a quantitative analysis of the catalytic effect of the different systems (main text, Table 2).

### Catalytic effect of benzyl amine side product and addition of hydrazone formation rates

To better understand the combined effects that all different species have on the formation of the hydrazone product, we decided to first overlay some of the rates from Figure 3.3 in the main text. To compare the rate of the triggered system to the individual rates of different species, we combined the rate of the experiment with 100 mol% of aniline and the experiment with 5.0 eq. DCv urea **U1**. The addition of conversions of those two graphs are relatively close to the rates of the triggered system, showing that the triggered system reflects a combined catalysis of the species involved in the individual experiments

(compare red and green data points in Figure S3.9). To further look into how exactly the catalysis of DCv urea **U1** functions, we decided to also look into the catalytic effect that the benzyl amine side product can have. Benzyl amine is, along with the bulky base, released in the hydrolysis step of the isocyanate (Scheme 2, main text). We found that benzyl amine also is an excellent catalyst, catalysing the reaction significantly over the background reaction. However, in the triggered release system, benzyl amine is only slowly released over time. This explains the comparatively low formation rate for the DCv urea **U1** alone, which combines the effect of bulky base and benzyl amine being released over time (Figure 3.3, main text).

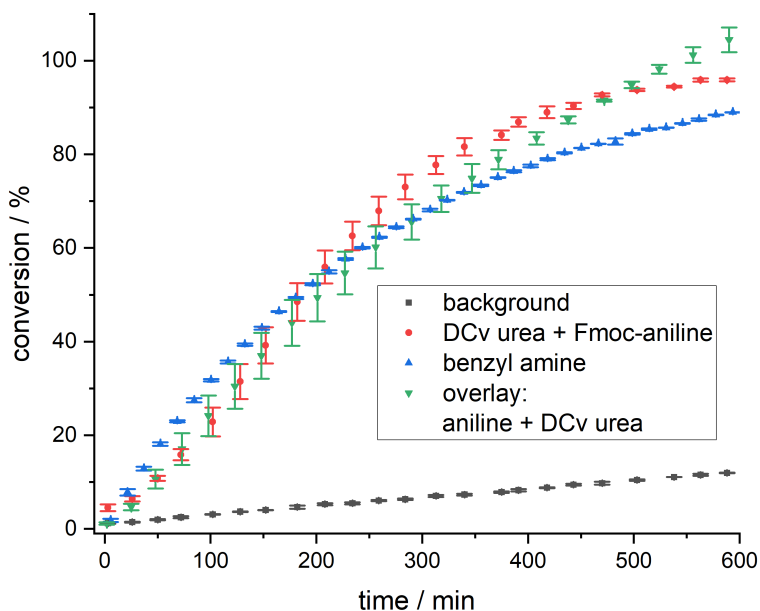


**Figure S3.9:** background reaction in 4/1 DMSO- $d_6$ /D $_2$ O at 40 °C of benzhydrazide (10 mM) and 4-nitrobenzaldehyde (10 mM) (grey squares), in the presence of 10 mM Fmoc-aniline and 50 mM DCv urea **U1** (red circles) and 100 mol% benzyl amine (blue triangles). The green, inverted triangles represent an overlay of the rates of hydrazone formation of the experiment with 100 mol% aniline and that with 50 mM DCv urea **U1**.

### DLS: Excluding the formation of supramolecular structures

To ensure that Fmoc-aniline or DCv ureas do not form any supramolecular structures which may have an impact on the overall reaction rates or modes of catalysis, we performed DLS measurements. We ran all samples in duplicates, both in unfiltered and filtered (0.45  $\mu$ m PTFE filter) states. For all samples and the solvent reference, we found nearly identical results and very low scatter counts ( $\sim$  200 kcps with the highest laser attenuation possible). We only observed the presence of low levels of particles with a size of approximately 1000 nm. These are very likely dust particles, as they appear in all samples.

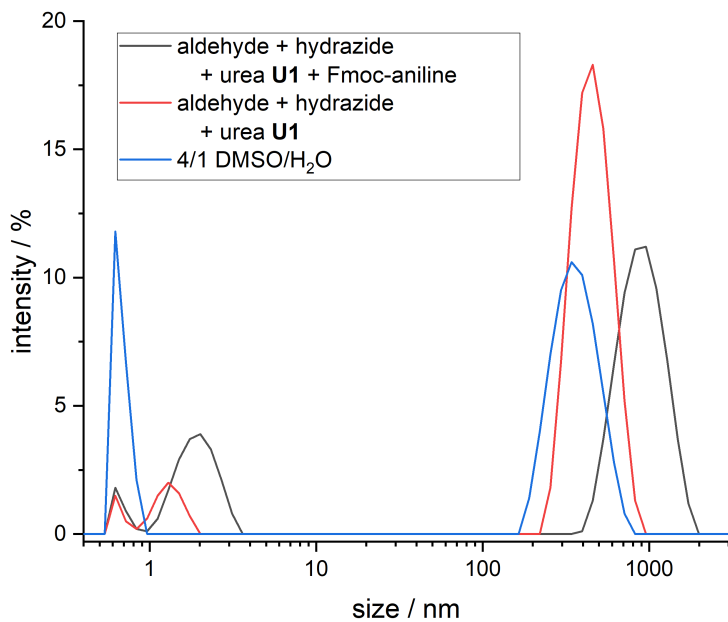
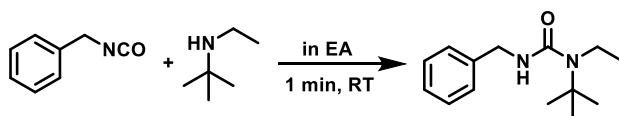


**Figure S3.10:** DLS measurements. Intensity (%) plotted against size for pure solvent (4/1 DMSO/H<sub>2</sub>O, blue line), 10 mM benzhydrazide with 10 mM 4-nitrobenzaldehyde, and 50 mM DCv urea **U1** (red line) and the same sample but additionally with 10 mM Fmoc-aniline (grey line).

## Synthesis



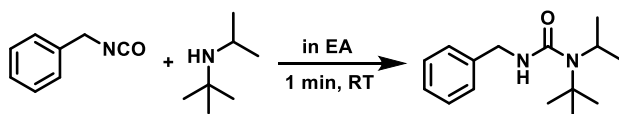
DCv urea **U1** was prepared by dissolving 0.492 mL (4.0 mmol, 1.0 eq.) benzyl isocyanate in 4 mL ethyl acetate and adding 0.664 mL (4.8 mmol, 1.2 eq.) *N,N*-tert-butylethylamine (base **1**) dropwise to the solution. After cooling to room temperature, the solution was filtered through a silica plug with ethyl acetate to remove excess amine. The solvent was removed under reduced pressure to yield 0.929 g (99%, 4.0 mmol) analytically pure compound as a colourless solid.

$^1\text{H-NMR}$  (400 MHz,  $\text{CDCl}_3$ )  $\delta$  = 7.32 – 7.15 (m, 5H,  $\text{CH}_{\text{aromatic}}$ ), 4.56 (s, 1H, NH), 4.36 (d,  $J$  = 5.4 Hz, 2H,  $\text{NHCH}_2$ ), 3.21 (q,  $J$  = 7.1 Hz, 2H,  $\text{NCH}_2$ ), 1.40 (s, 9H,  $\text{C}(\text{CH}_3)_3$ ), 1.10 (t,  $J$  = 7.2 Hz, 3H,  $\text{NCH}_2\text{CH}_3$ ).

$^{13}\text{C-NMR}$  (101 MHz,  $\text{CDCl}_3$ )  $\delta$  = 158.49, 140.14, 128.70, 127.73, 127.21, 56.23, 44.89, 39.21, 29.81, 16.78.

ESI-MS: calculated for  $[\text{C}_{14}\text{H}_{23}\text{N}_2\text{O}]^+$ : 235.18; found: 235.01.

The data is in accordance with literature.<sup>2</sup>



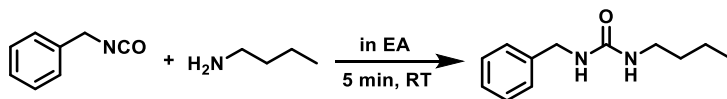
DCv urea **U2** compound was prepared by dissolving 0.494 mL (4.0 mmol, 1.0 eq.) benzyl isocyanate in 4 mL ethyl acetate and adding 0.761 mL (4.8 mmol, 1.2 eq.) *N,N*-tert-butylisopropylamine dropwise to the solution. After cooling to room temperature, the solution was filtered through a silica plug with ethyl acetate to remove excess amine. The solvent was removed under reduced pressure to yield 0.993 g (quant., 4.0 mmol) analytically pure compound as a colourless solid.

$^1\text{H NMR}$  (400 MHz,  $\text{CDCl}_3$ )  $\delta$  = 7.41 – 7.21 (m, 5H,  $\text{CH}_{\text{aromatic}}$ ), 4.78 (s, 1H, NH), 4.41 (d,  $J$  = 5.6 Hz, 2H,  $\text{NHCH}_2$ ), 3.65 (hept,  $J$  = 6.9 Hz, 1H,  $\text{NCH}$ ), 1.36 (s, 9H,  $\text{C}(\text{CH}_3)_3$ ), 1.26 (d,  $J$  = 6.9 Hz, 6H,  $\text{CH}(\text{CH}_3)_2$ ).

$^{13}\text{C NMR}$  (101 MHz,  $\text{CDCl}_3$ )  $\delta$  = 160.46, 139.48, 128.68, 127.90, 127.49, 127.27, 56.17, 45.91, 44.61, 29.11, 23.55.

ESI-MS: calculated for  $[\text{C}_{15}\text{H}_{25}\text{N}_2\text{O}]^+$ : 249.19; found: 248.94.

The data is in accordance with literature.<sup>2</sup>



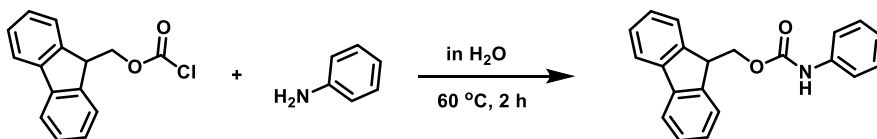
Non-DCv urea **U3** was prepared by dissolving 0.494 mL (4.0 mmol, 1.0 eq.) benzyl isocyanate in 10 mL ethyl acetate and adding 0.475 mL (4.8 mmol, 1.2 eq.) 1-butylamine dropwise to the solution. After cooling in an ice-bath for 15 minutes, the precipitate was filtered and washed with cold EA to yield 0.250 g (30%, 1.2 mmol) analytically pure compound as a colourless solid.

$^1\text{H}$  NMR (400 MHz,  $\text{CDCl}_3$ )  $\delta$  = 7.36 – 7.25 (m, 5H,  $\text{CH}_{\text{aromatic}}$ ), 4.65 (s, 1H,  $\text{PhCH}_2\text{NH}$ ), 4.40 – 4.30 (m, 3H,  $\text{PhCH}_2$ ,  $\text{NHCH}_2\text{CH}_2$ ), 3.16 (td,  $J$  = 7.1, 5.7 Hz, 2H,  $\text{NHCH}_2$ ), 1.51 – 1.41 (m, 2H,  $\text{NCH}_2\text{CH}_2$ ), 1.38 – 1.25 (m, 2H,  $\text{CH}_3\text{CH}_2$ ), 0.90 (t,  $J$  = 7.3 Hz, 3H,  $\text{CH}_3$ ).

$^{13}\text{C}$  NMR (101 MHz,  $\text{CDCl}_3$ )  $\delta$  = 158.47, 139.43, 128.75, 127.56, 127.41, 44.66, 40.46, 32.39, 20.12, 13.90.

ESI-MS: calculated for  $[\text{C}_{12}\text{H}_{19}\text{N}_2\text{O}]^+$ : 207.15; found: 207.17.

The data is in accordance with literature.<sup>3</sup>



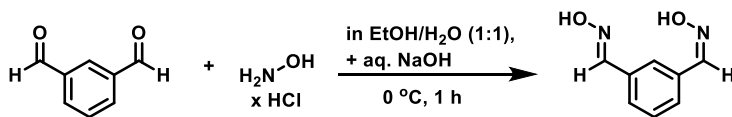
An adapted literature procedure was followed.<sup>4</sup> Fmoc-aniline was prepared by adding 0.181 mL (0.186 g, 2.0 mmol, 1.0 eq.) aniline and 0.621 g (2.4 mmol, 1.2 eq.) Fmoc-chloride to 3 mL water. The reaction mixture was heated to 60 °C and stirred for 2 hours. The precipitate was filtered after cooling the reaction mixture to room temperature. The slightly yellow solid was then recrystallized from ethanol to yield 0.283 g (45%, 0.9 mmol) analytically pure product as colourless needles.

$^1\text{H}$  NMR (400 MHz,  $\text{CDCl}_3$ )  $\delta$  = 7.79 (d,  $J$  = 7.6 Hz, 2H,  $\text{CH}_{\text{aromatic}}$ ), 7.62 (d,  $J$  = 7.5 Hz, 2H,  $\text{CH}_{\text{aromatic}}$ ), 7.47 – 7.27 (m, 8H,  $\text{CH}_{\text{aromatic}}$ ), 7.08 (td,  $J$  = 7.2, 1.3 Hz, 1H,  $\text{CH}_{\text{aromatic}}$ ), 6.65 (s, 1H,  $\text{NH}$ ), 4.55 (d,  $J$  = 6.6 Hz, 2H,  $\text{CH}_2\text{O}$ ), 4.29 (t,  $J$  = 6.6 Hz, 1H,  $\text{CHCH}_2\text{O}$ ).

$^{13}\text{C}$  NMR (101 MHz,  $\text{CDCl}_3$ )  $\delta$  = 143.89, 141.52, 129.22, 127.93, 127.27, 125.09, 123.76, 120.19, 66.98, 47.29.

ESI-MS: calculated for  $[\text{C}_{21}\text{H}_{18}\text{NO}_2]^+$ : 316.13; found: 315.74.

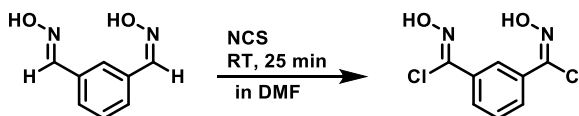
The data is in accordance with literature.<sup>4</sup>



The bisoxime of isophthalaldehyde was prepared according to a modified literature procedure.<sup>5</sup> 2.50 g (18.6 mmol, 1.0 eq.) isophthalaldehyde and 3.03 g (43.6 mmol, 2.34 eq.) hydroxylamine hydrochloride were dissolved in 19 mL 1:1 EtOH/H<sub>2</sub>O. After cooling to 0 °C, an aqueous solution of 3.9 g sodium hydroxide was added and the mixture stirred for one hour. It was cooled for one hour at –20 °C and the resulting precipitate was filtered and recrystallized from methanol to yield 1.99 g (65%, 12.1 mmol) of an off-white powder.

<sup>1</sup>H NMR (400 MHz, CDCl<sub>3</sub>) δ = 11.30 (d, J = 2.2 Hz, 2H, OH), 8.16 (s, 2H, COH), 7.80 (s, 1H, CH<sub>aromatic</sub>), 7.59 (d, J = 7.7 Hz, 2H, CH<sub>aromatic</sub>), 7.42 (t, J = 8.0 Hz, 1H, CH<sub>aromatic</sub>).

The data is in accordance with literature.<sup>5</sup> The second synthetical step was conducted without further analysis.



The bischlorooxime of isophthalaldehyde was prepared according to literature procedure.<sup>5</sup> 0.820 g (5.0 mmol, 1.0 eq.) of isophthalaldehyde bisoxime was dissolved in 1.65 mL anhydrous DMF. *N*-chlorosuccinimide (1.402 g, 10.5 mmol, 2.1 eq.) were added and the slightly yellow suspension was stirred at room temperature for 25 minutes, upon which the suspension cleared up under a release of heat. The solution was cooled to room temperature and poured into 15 mL of H<sub>2</sub>O. The aqueous phase was extracted twice with 15 mL EA each. The organic phase was then washed twice with 25 mL H<sub>2</sub>O each and dried over anhydrous MgSO<sub>4</sub>. The solvent was removed under reduced pressure to yield 934.7 mg (80%, 4.0 mmol) of analytically pure product as a colourless solid.

<sup>1</sup>H NMR (400 MHz, DMSO-*d*<sub>6</sub>) δ = 12.58 (s, 2H, OH), 8.21 (br s, 1H, CH<sub>aromatic</sub>), 7.91 (br s, 2H, CH<sub>aromatic</sub>), 7.59 (t, J = 7.9 Hz, 1H, CH<sub>aromatic</sub>).

<sup>13</sup>C NMR (101 MHz, DMSO-*d*<sub>6</sub>) δ = 134.70, 133.08, 129.46, 128.26, 124.34.

The data is in accordance with literature.<sup>5</sup>

## References

1. Song, S., Feng, P., Zou, M. & Jiao, N. KI Catalyzed Nitrogenation of Aldehydes and Alcohols: Direct Synthesis of Carbamoyl Azides and Ureas. *Chinese J. Chem.* **35**, 845–848 (2017).
2. Ying, H. & Cheng, J. Hydrolyzable polyureas bearing hindered urea bonds. *J. Am. Chem. Soc.* **136**, 16974–16977 (2014).
3. Zhao, J., Li, Z., Yan, S., Xu, S., Wang, M. A., Fu, B. & Zhang, Z. Pd/C Catalyzed Carbonylation of Azides in the Presence of Amines. *Org. Lett.* **18**, 1736–1739 (2016).
4. Gawande, M. B. & Branco, P. S. An efficient and expeditious Fmoc protection of amines and amino acids in aqueous media. *Green Chem.* **13**, 3355–3359 (2011).
5. Byeang Hyeon Kim, Eun Jeong Jeong, Gil Tae Hwang & Venkatesan, N. Multiple cycloadditive macrocyclization: An efficient method for crown ether-type cyclophanes, bis-calix[4]arenes and silamacrocycles. *Synthesis (Stuttg.)* **4**, 2191–2202 (2001).

# Dynamic Covalent Urea-Catalysed Self-Healing of Thiol-Maleimide Networks

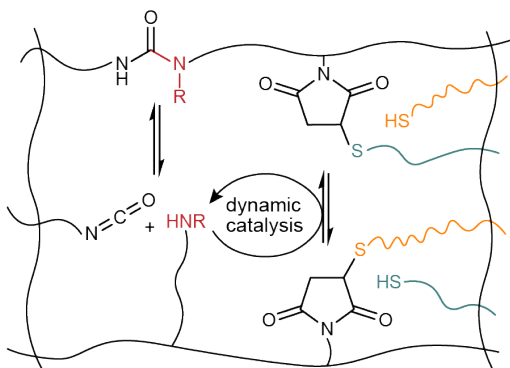
## Abstract

Covalent adaptable networks (CANs) offer promising features such as self-healing, malleability, and recyclability. Yet, some of the chemistries used in CANs suffer from downsides such as high self-healing temperatures or low mechanical strength. Here, we introduce a synergistic dual CAN based on a DCv thiol-maleimide network with a catalytic amount of DCv urea bonds in the backbone. The base present in the DCv urea equilibrium acts as heat-triggered catalyst to accelerate the thiol-maleimide exchange, leading to improved self-healing at lower temperatures without the need for externally added catalysts. This concept offers a new pathway towards CANs which are stable at room temperature, yet exhibit excellent self-healing capabilities at temperatures far below the 90 °C required for uncatalysed DCv thiol-maleimide CANs.

## Availability and Contributions

This chapter is based on an article currently in preparation for submission, in collaboration with the authors Lotte Sünnen, Steffen Lohrmann, Mélodie Ardoin, and Rienk Eelkema.

B.S. and R.E. developed the project idea. B.S. conducted the majority of experiments, wrote the manuscript, and designed figures and schemes. R.E. supervised the research, revised the manuscript, and secured funding. L.S. helped in conducting kinetic experiments, synthesis, polymerisation reactions, and analysing NMR data. S.L. helped in resolving issues with the maleimide monomer synthesis and optimising the polymerisation. M.A. helped in conducting polymerisations and rheology experiments.



## Introduction

Self-healing materials are a promising field of research, as they demonstrate sought after properties such as degradability, reprocessability and healing after damage.<sup>1–10</sup> Although there are distinct ways to design and realise self-healing materials such as the microencapsulation of a healing agent,<sup>11</sup> presence of excess monomer,<sup>12</sup> photo-induced crack healing,<sup>13</sup> or through intrinsically dynamic supramolecular chemistry,<sup>14</sup> Dynamic Covalent Chemistry (DCvC) has emerged as the primary toolkit to engineer materials on a molecular level so that they demonstrate self-healing properties.<sup>4,10,15</sup> DCvC describes any chemistry in which bonds can be reversibly broken and formed again, such as disulfide,<sup>16</sup> boronic ester,<sup>17</sup> or vinylogous urethane linkages,<sup>18</sup> among many others.<sup>7,15,19–28</sup> Self-healing materials based on DCvC are typically referred to as covalent adaptable networks (CANs).<sup>4,9</sup>

Downsides of many CANs are that high temperatures are necessary to effectively induce self-healing,<sup>5</sup> and that materials exhibiting self-healing at lower temperatures typically tend to be weaker due to a higher dynamicity of the bonds.<sup>29</sup> Some strategies exist to tune the kinetics of self-healing and the temperature at which self-healing occurs for a given chemistry, such as the introduction of external catalysts,<sup>30–32</sup> internal catalysts built into the polymer network and neighbouring group participation,<sup>33–38</sup> the introduction of several synergistic DCv bonds,<sup>39</sup> molecular design,<sup>32,40</sup> as well as variations of the macromolecular architecture of a network.<sup>41</sup> However, precise tuning of self-healing kinetics and temperatures still remains a challenge and the addition of external catalysts often suffers from significant downsides such as leaching over time.<sup>38</sup>

We sought two chemistries that can be combined into one CAN, where a catalytic species that is latently present in one dynamic bond can catalyse the exchange of the other moiety. Two promising DCv units that have recently been applied to realise CANs are Dynamic Covalent (DCv) ureas,<sup>29</sup> as well as DCv thiol-maleimide adducts.<sup>42,43</sup> On the one hand, DCv ureas (Figure 4.1a) have been introduced in a material context by J. Cheng and coworkers in 2014.<sup>29</sup> Ureas are typically thought to be highly stable and typically only dissociate in harsh conditions.<sup>44</sup> Due to the steric bulk that has been introduced on one of the nitrogen atoms, the C-N bond is weakened and the formation of the urea from amine and isocyanate becomes highly reversible. The group around J. Cheng used this feature to develop a material which could be degraded, reprocessed, as well as healed under relatively mild conditions.<sup>29</sup> Since then, DCv ureas have been applied in diverse, self-healing materials (see also Chapter 2 and 3 of this Thesis).<sup>45–49</sup> On the other hand, thiol-Michael adducts have already been found to be reversible decades ago,<sup>50</sup> and studied for use in dynamic combinatorial chemistry and self-healing materials since then.<sup>51–56</sup> Despite the success of thiol-Michael reactions in general and the thiol-maleimide click reaction specifically,<sup>57</sup> thiol-maleimide adducts have received relatively sparse attention in the field of self-healing materials and have only recently been observed to be dynamic as well (Figure 4.1b).<sup>42</sup> They have subsequently been applied in materials that can exchange and self-heal at increased temperature, in response to a thiol signal, or at high pH.<sup>41,43,58,59</sup>

Here, we introduce a strategy to combine these two DCv self-healing units, DCv ureas and DCv thiol-maleimide adducts, into one synergistic dual CAN, where one moiety catalyses the exchange of the other. Specifically, we will incorporate a catalytic amount of DCv urea units into a thiol-maleimide-based network, to enable the free base in the DCv urea equilibrium to catalyse the thiol-maleimide exchange reaction and effectively reduce the self-healing temperature of these networks upon applying heat as a trigger (Figure 4.1c). This strategy overcomes the problem of catalyst leaching and endows the DCv urea moieties in the network both with a catalytic, as well as self-healing function which becomes more pronounced at elevated temperature where urea dissociation into isocyanate and catalytically active amine is favoured. We study the kinetics of this system on a small-molecule scale to understand the role that the bulkiness of the DCv urea plays and compare a synergistic dual CAN with a thiol-maleimide network containing an externally added base catalyst, as well as with a thiol-maleimide network without the addition of any catalysts, to understand the role that each species plays in the self-healing process.

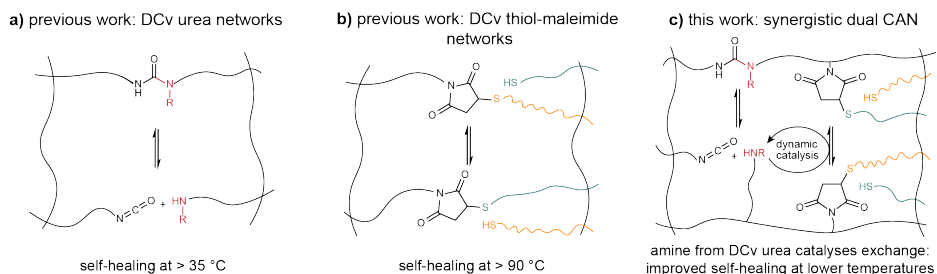


**Figure 4.1:** Self-healing networks applied in this work. **a)** Dynamic covalent (DCv) urea CAN.<sup>29</sup> **b)** DCv thiol-maleimide CAN.<sup>42,43</sup> **c)** this work: combination of both DCv urea and thiol-maleimide units into a synergistic dual CAN.

## Results and Discussion

### Choice of Michael acceptor, nucleophile, and solvent

In previous work, we have shown that the base in the equilibrium of DCv ureas can be utilised as catalytic species and latent reagents.<sup>60</sup> One of the challenges remaining in this work was the fact that to trigger the crosslinking of a material, equimolar amounts of an external DCv urea species had to be added to the system, and the resulting network was not dynamic. We envisioned that by finding another class of reactions where DCv ureas can act as heat-triggered exchange catalysts, we could develop a synergistic dual CAN, offering control over the self-healing kinetics and overcoming catalyst leaching. The addition of thiols on Michael acceptors has received copious attention in the past years,<sup>57</sup> with extensive studies on the impact of different thiols, Michael acceptors and catalysts on the overall reaction rates.<sup>40,58,61–64</sup> These addition reactions are typically catalysed by

an amine base, which makes them an interesting choice for applying DCv ureas as heat-triggered, catalytic species. In initial tests we found that less reactive Michael acceptors such as fumarates or acrylamides are not suitable candidates for a heat-triggered synergistic dual CAN. We eventually settled on the addition of  $\beta$ -mercapto esters on maleimides (Figure 4.2b, c). This reaction proceeds smoothly and with high yields and the resulting thiol-maleimide adducts can undergo exchange reactions in the presence of thiols, making them dynamic.<sup>41,43,58</sup> Furthermore, the kinetics can be tuned with the choice of solvent, with more polar solvents stabilising the charged intermediate and enhancing the rates of both the addition, as well as the exchange reaction, offering another level of control.<sup>58,61–63</sup>

### Effect of temperature and DCv urea stability on kinetics

To understand how to design a polymer containing both DCv ureas and DCv thiol-maleimide units, we determined the thiol-maleimide addition and exchange kinetics at two different temperatures via <sup>1</sup>H-NMR spectroscopy in the presence of catalytic amounts of three different DCv ureas with vastly different equilibrium constants, ranging from 5600 to  $> 10^7 \text{ M}^{-1}$ ,<sup>29,47</sup> and their corresponding free bases (Figure 4.2a). Testing different DCv urea structures allows us to decide which bulkiness is suitable for sufficient stability, yet good catalytic action in the thiol-maleimide exchange reaction.

For the thiol-maleimide addition, we studied the reaction of ethyl 3-mercaptopropionate **2** with *N*-methylmaleimide **1** in dimethyl carbonate (DMC) (Figure 4.2b) to yield adduct **3**. The least stable DCv urea TBIPU and its free base TBIPA showed the fastest kinetics as expected (Figure 4.2c). However, due to significant side reactivity of the thiol with the free isocyanate in the DCv urea equilibrium (see SI), TBIPU was eliminated as a potential candidate for a material application. The other two DCv ureas, TBEU and DIPU, showed no side reactivity under the same conditions. This is likely due to the negligible amount of free isocyanate and the slower addition kinetics of thiols on isocyanates compared with maleimides.<sup>61</sup> The reaction in the presence of TBEU and DIPU demonstrated a low reactivity at 25 °C, and a roughly 2.5-fold decrease in the maleimide half-life at 45 °C for TBEU and an approximately 12.5-fold decrease for DIPU, demonstrating that these two urea moieties are promising candidates for heat-triggered addition reactions.

Upon establishing the kinetics of the addition reaction in the presence of DCv ureas, we proceeded to study the thiol-maleimide exchange. For this, we investigated the exchange of an aromatic thiol-maleimide adduct **4** with thiol **2** to yield adduct **3** and thiol **5** in 2/1 DMC/DMSO as a model to simulate the exchange process in a thiol-maleimide material (Figure 4.2d). The more polar solvent mixture was needed to facilitate the exchange process which is much slower than the addition reaction. This is in alignment with previous literature which has shown that the retro-Michael addition is the rate-determining step, with polar solvents stabilising the charged intermediate.<sup>58</sup> Looking at the results (Figure 4.2e), we observed similar trends as for the addition reaction. The exchange reaction in the presence of TBEU shows slow kinetics at 25 °C ( $t_{1/2} = 738 \pm 21 \text{ h}$ ), whereas the reaction with DIPU as well as the uncatalysed reaction show no significant reactivity over 1 month. At 45 °C, the exchange with TBEU shows a 9-fold decrease in half-life of **4**, with DIPU also showing a catalytic activity at 45 °C, despite

not exhibiting any reactivity at 25 °C. Compared to the uncatalysed exchange reaction, a 10-fold and 5-fold decrease in half-life can be observed in the presence of TBEU and DIPU at 45 °C, respectively.

Combined, these findings show that DCv ureas of medium (TBEU) and high stability (DIPU) are suitable candidates for the heat-triggered catalysis of thiol-maleimide addition and exchange reactions, whereas DCv ureas of low stability (TBIPU) show significant side reactivity and are thus not suitable. Both TBEU and DIPU show very low to no catalytic effect at 25 °C and exhibit a 5- to 10-fold acceleration of the thiol-maleimide exchange process at 45 °C, compared to the uncatalysed reaction. Further, this shows that the bulkiness of the DCv urea can be used to tune both the overall kinetics of thiol-maleimide addition and exchange reactions as well as the responsiveness to a change in temperature, with more stable DCv ureas leading to a larger increase in reaction rates at elevated temperatures compared with ambient conditions.

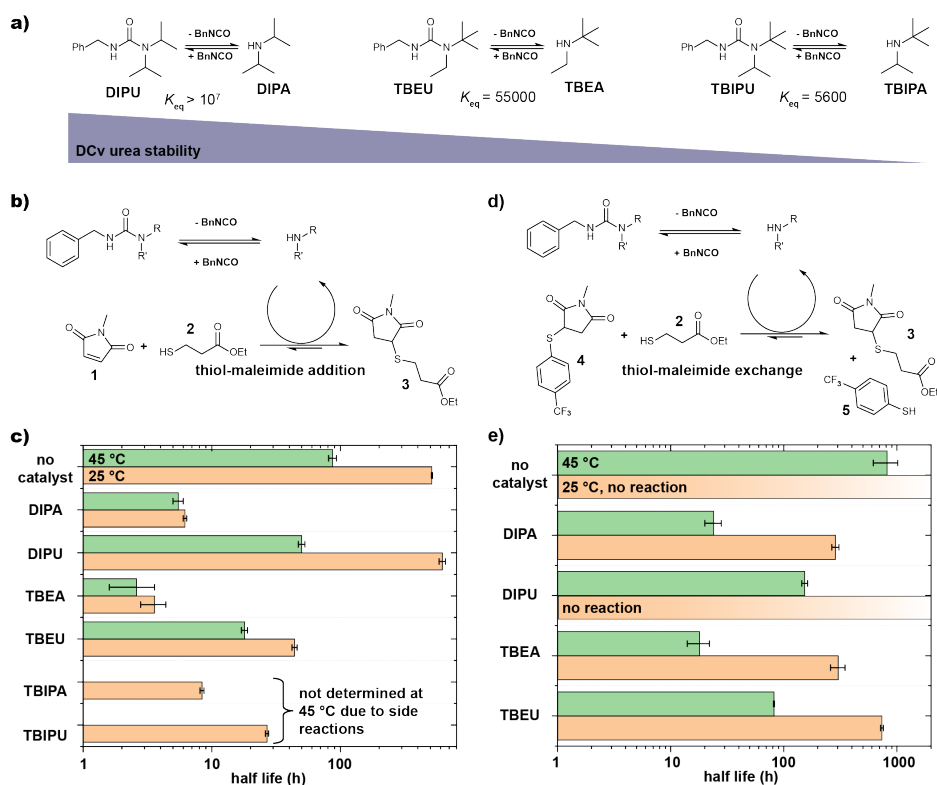


**Figure 4.2:** half-life of thiol-maleimide addition and exchange reactions in the presence of different catalysts at 25 °C and 45 °C. **a)** The different DCv ureas and free bases used to study their impact on the addition and exchange kinetics, and the DCv ureas' corresponding equilibrium constants, as determined by J. Cheng and coworkers, for TBEU,<sup>47</sup> DIPU, and TBIPU (different substituents on NH).<sup>29</sup> **b)** DCv urea-catalysed thiol-maleimide addition. **c)** Half-life of *N*-methylmaleimide **1** with thiol **2** in the presence of

50 mol% different bases and DCv ureas at 25 °C (orange) and 45 °C (green). **d**) DCv urea-catalysed thiol-maleimide exchange. **e**) Half-life of aromatic thiol-maleimide adduct **4** with thiol **2** in the presence of different bases and DCv ureas at 25 °C (orange) and 45 °C (green). All error bars were determined as the standard deviation from duplicates of <sup>1</sup>H-NMR kinetic experiments.

### DCv urea catalysed dual self-healing networks

Next, we implemented these findings from small-molecule DCv ureas and thiol-maleimide adducts into a crosslinked, synergistic dual CAN. For this, a linear, maleimide-functionalised DCv poly(ureaurethane) was prepared, which can subsequently be crosslinked with bis- or polyfunctional thiols. The polymer was synthesised according to general literature procedures for DCv poly(ureas) and poly(urethanes) (see Methods).<sup>65-67</sup> For our synergistic dual CAN (Figure 4.3a), we chose to incorporate a catalytic amount of 5% bulky base and 95% maleimide-functionalised diol as crosslinking sites relative to the diisocyanate. As a reference material, we synthesised the same polymer, but replaced the bulky base with triethylene glycol as a chain extender (80% total), and lowered the maleimide content to 20%. The higher maleimide-content of the synergistic dual CAN does somewhat limit the comparability of the two materials, but was necessary to synthesise a polymer that would crosslink. A maleimide content where both the synergistic CAN and the reference network form chains of similar length and undergo crosslinking needs to be determined and more experiments with the same maleimide content in both materials will need to be performed to verify the findings further. The reference polymer was tested uncatalysed, as well as in the presence of 5% externally added bulky base (same amount as in the synergistic dual CAN, Figure 4.3a). To each sample, bithiol (ethylene glycol bis(3-mercaptopropionate), see Figure 4.3a) was added to crosslink the maleimide-functionalised polymer in situ on the rheometer. The gelation was tracked via a time sweep at 50 °C. Upon reaching a plateau, stress relaxation tests were conducted at 45 °C. It can be seen (Figure 4.3c) that the dual synergistic CAN shows the fastest, most efficient stress relaxation over 5.5 hours (20,000 seconds) at 45 °C. The reference material in the presence of externally added base shows a stress relaxation response as well, although significantly slower than the dual synergistic CAN. Finally, the reference material without any base doesn't show a meaningful stress relaxation response under the tested conditions. To further consolidate these findings, we performed frequency sweeps at 45 °C (Figure 4.3d). Frequency sweeps have been shown in literature to be a good tool to identify and quantify self-healing behaviour.<sup>68</sup> An increase in  $\tan \delta$  towards lower frequencies indicates a liquid-like behaviour which is characteristic for self-healing materials.<sup>68</sup> Indeed, both the synergistic dual CAN, and the reference material in the presence of base do show self-healing behaviour at lower frequencies. Comparing the frequencies at which  $\tan \delta$  shows an inflection for the different materials (Figure 4.3d) demonstrates that the synergistic dual CAN is more readily self-healing with liquid-like behaviour up to approximately 30 rad/s, whereas the reference material in the presence of base already shows an inflection of  $\tan \delta$  at approximately 3 rad/s. The reference material without base doesn't show any self-healing behaviour in the tested frequency range. These findings indicate that the integration of DCv urea bonds into a DCv thiol-

maleimide network significantly improve self-healing at temperatures as low as 45 °C. More tests are needed with non-DCv crosslinks to test the role that the catalytic DCv urea bonds play in the improved self-healing. With a few further tests, we envision that this material can be utilised as a more readily self-healing CAN. In addition to the improved self-healing capabilities that we demonstrate in this work, it has been shown in literature that the utilised chemistry allows for ready degradability in the presence of monothiol, making this material a versatile candidate for applications where both self-healing at low temperatures, as well as simple degradability are required.<sup>55,59</sup>

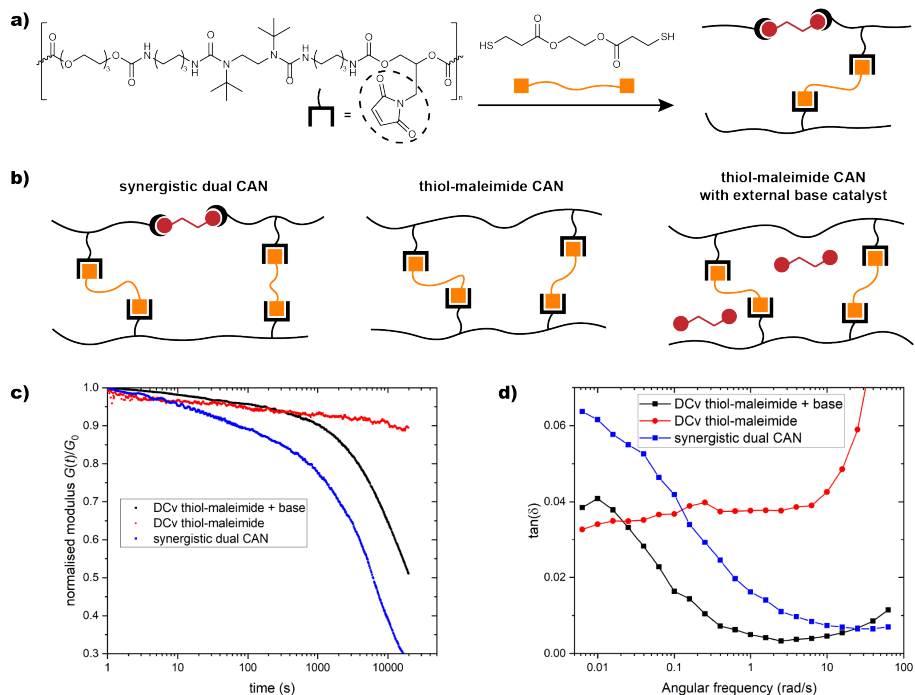


**Figure 4.3:** rheological comparison of the self-healing behaviour of an uncatalysed DCv thiol-maleimide network, a base-catalysed DCv thiol-maleimide network, and the synergistic dual CAN. **a)** scheme to show the crosslinking of the linear maleimide-functionalised DCv poly(ureaurethanes). **b)** schematic structures of the synergistic dual CAN and the two reference materials without DCv urea units. **c)** normalised stress relaxation curves at 45 °C for all three materials. **d)**  $\tan(\delta)$  of frequency sweeps for all three materials at 45 °C.

## Conclusion

Utilising two different DCv chemistries, we show how the species in the equilibrium of one bond can catalyse the exchange of the other in response to heat. This allows for a synergistic dual CAN with improved self-healing at lower temperatures compared to uncatalysed thiol-maleimide CANs. Further, we investigate how the bulkiness of DCv ureas can be used to tune the kinetics and responsiveness to changes in temperature of thiol-maleimide addition and exchange reactions, opening up yet another application for DCv ureas beyond self-healing alone. These findings offer a new level of flexibility over important self-healing parameters while overcoming crucial issues such as catalyst leaching or low stability at ambient conditions. We envision future applications where DCv bonds are combined with synergy in mind, to enable more flexible, adaptable, and degradable CANs with improved properties.

## Methods

### Polymer synthesis

The linear polymer containing DCv urea and maleimide units is synthesised by dissolving 803  $\mu$ L hexamethylene diisocyanate (5.0 mmol, 1.0 eq.) in 5 mL anhydrous 1,4-dioxane ( $c = 1$  M) under nitrogen in a dry round bottom flask. Under ice cooling and stirring, *N,N'*-di-*tert*-butylethylenediamine (0.05 eq.) is added dropwise. The ice bath is removed and the maleimide monomer (0.95 eq.), and triethylamine (0.1 eq.) are added. The reaction mixture is heated to 70 °C overnight under nitrogen (typically ~16 hours). The solvent and catalyst are removed immediately under high vacuum. The polymer is redissolved in approximately 5 mL anhydrous 1,4-dioxane and the solvent is removed once more under high vacuum to ensure full removal of all volatiles. For the reference polymer, 0.2 eq. maleimide monomer and instead of *N,N'*-di-*tert*-butylethylenediamine, 0.8 eq. triethyleneglycol are added to make a polymer containing only maleimide side chains and no DCv urea moieties.

### NMR kinetics

To ensure quantitative measurements, T1 measurements were taken for all compounds and the delay between scans is set to 5 times the longest T1 time (see SI). For thiol maleimide additions, a 25 mM solution of *N*-methylmaleimide, 25 mM ethyl 3-mercaptopropionate, and 12.5 mM of the catalyst (base or DCv urea) is prepared in dimethyl carbonate. A glass insert containing a 10 mM solution of sodium trimethylsilylpropanesulfonate in D<sub>2</sub>O is inserted into the NMR tube and the PRESAT measurements at different time intervals are started. Between each measurement, the tubes are placed in a water bath at 25 °C or 45 °C. For thiol maleimide exchange reactions, the same procedure is used, but the solvent mixture is 2/1 dimethylcarbonate/DMSO-*d*<sub>6</sub>.

## Rheology

For all rheological measurements, 10 %w/v solutions of the polymer are prepared by weighing out the final, purified polymer and dissolving it in the appropriate volume of an anhydrous mixture of 2/1 propylene carbonate/DMSO. The volume of the final solution is determined volumetrically to calculate the concentration of active maleimide units. For each rheology experiment, 650  $\mu$ L of the solution are mixed with 0.5 eq. of the bis-thiol relative to the amount of maleimide units (e.g. if a polymer batch with 1.0 mmol maleimide monomer yields 15 mL final 10 %w/v solution, then 650  $\mu$ L solution contain 0.043 mmol maleimide, and 0.022 mmol bis-thiol are added). The mixture is immediately applied to the rheometer plate (stainless steel stage with a 40 mm Peltier parallel plate) and the plate is lowered to the geometry gap of 500  $\mu$ m. The crosslinking process is tracked via a time oscillation experiment (1 % strain, 1 Hz) at 50 °C until a plateau is reached. Upon achieving full crosslinking, the material is equilibrated for 10 minutes at 45 °C. Stress relaxation tests (1 % strain, 0.01 s strain rise time), frequency sweeps (1 % strain, 0.001–10 Hz), and amplitude sweeps (1 Hz, 0.1–1000%) are performed at 45 °C as shown in the paper and supplementary information.

## Acknowledgments

This work has received funding from the European Union's Horizon 2020 research and innovation program under the Marie Skłodowska-Curie grant agreement No 812868.

## Competing interests

There are no conflicts to declare.

## References

1. Takashima, Y. & Harada, A. Self-Healing Polymers. in *Encyclopedia of Polymeric Nanomaterials* 1–6 (Springer Berlin Heidelberg, 2013). doi:10.1007/978-3-642-36199-9.
2. Yuan, Y. C., Yin, T., Rong, M. Z. & Zhang, M. Q. Self healing in polymers and polymer composites. Concepts, realization and outlook: A review. *Express Polym. Lett.* **2**, 238–250 (2008).
3. Aïssa, B., Therriault, D., Haddad, E. & Jamroz, W. Self-healing materials systems: Overview of major approaches and recent developed technologies. *Adv. Mater. Sci. Eng.* **2012**, 854203 (2012).
4. Kloxin, C. J. & Bowman, C. N. Covalent adaptable networks: Smart,

- reconfigurable and responsive network systems. *Chem. Soc. Rev.* **42**, 7161–7173 (2013).
5. Li, B., Cao, P.-F., Saito, T. & Sokolov, A. P. Intrinsically Self-Healing Polymers: From Mechanistic Insight to Current Challenges. *Chem. Rev.* **123**, 701–735 (2023).
  6. Denissen, W., Winne, J. M. & Du Prez, F. E. Vitrimers: Permanent organic networks with glass-like fluidity. *Chem. Sci.* **7**, 30–38 (2016).
  7. García, F. & Smulders, M. M. J. Dynamic covalent polymers. *J. Polym. Sci. Part A Polym. Chem.* **54**, 3551–3577 (2016).
  8. Zhang, Z. P., Rong, M. Z. & Zhang, M. Q. Polymer engineering based on reversible covalent chemistry: A promising innovative pathway towards new materials and new functionalities. *Prog. Polym. Sci.* **80**, 39–93 (2018).
  9. Podgórski, M., Fairbanks, B. D., Kirkpatrick, B. E., McBride, M., Martinez, A., Dobson, A., Bongiardina, N. J. & Bowman, C. N. Toward Stimuli-Responsive Dynamic Thermosets through Continuous Development and Improvements in Covalent Adaptable Networks (CANs). *Adv. Mater.* **32**, 1906876 (2020).
  10. Chakma, P. & Konkolewicz, D. Dynamic Covalent Bonds in Polymeric Materials. *Angew. Chem. Int. Ed.* **58**, 9682–9695 (2019).
  11. Kessler, M. R. & White, S. R. Self-activated healing of delamination damage in woven composites. *Compos. Part A Appl. Sci. Manuf.* **32**, 683–699 (2001).
  12. Matsuda, T., Kawakami, R., Namba, R., Nakajima, T. & Gong, J. P. Mechanoresponsive self-growing hydrogels inspired by muscle training. *Science.* **363**, 504–508 (2019).
  13. Chung, C., Roh, Y., Cho, S. & Kim, J. Crack Healing in Polymeric Materials via Photochemical [ 2 + 2 ] Cycloaddition The fatigue in plastics caused by constant or cyclic stress results in microcrack formation and propagation , ultimately leading to significant reduction in mechanical has been. *Chem. Mater.* **16**, 3982–3984 (2004).
  14. Lehn, J.-M. Constitutional dynamic chemistry: bridge from supramolecular chemistry to adaptive chemistry. *Top. Curr. Chem.* **322**, 1–32 (2012).
  15. Jin, Y., Yu, C., Denman, R. J. & Zhang, W. Recent advances in dynamic covalent chemistry. *Chem. Soc. Rev.* **42**, 6634–6654 (2013).
  16. Li, J., Carnall, J. M. A., Stuart, M. C. A. & Otto, S. Hydrogel formation upon photoinduced covalent capture of macrocycle stacks from dynamic combinatorial libraries. *Angew. Chem. Int. Ed.* **50**, 8384–8386 (2011).
  17. Nishiyabu, R., Kubo, Y., James, T. D. & Fossey, J. S. Boronic acid building blocks: tools for self assembly. *Chem. Commun* **47**, 1124–1150 (2011).
  18. Denissen, W., Rivero, G., Nicolay, R., Leibler, L., Winne, J. M. & Du Prez, F. E. Vinylogous urethane vitrimers. *Adv. Funct. Mater.* **25**, 2451–2457 (2015).

19. Fan, B., Zhang, K., Liu, Q. & Eelkema, R. Self-Healing Injectable Polymer Hydrogel via Dynamic Thiol-Alkynone Double Addition Cross-Links. *ACS Macro Lett.* **9**, 776–780 (2020).
20. Liu, W. X., Yang, Z., Qiao, Z., Zhang, L., Zhao, N., Luo, S. & Xu, J. Dynamic multiphase semi-crystalline polymers based on thermally reversible pyrazole-urea bonds. *Nat. Commun.* **10**, 4753 (2019).
21. Snyder, R. L., Fortman, D. J., De Hoe, G. X., Hillmyer, M. A. & Dichtel, W. R. Reprocessable Acid-Degradable Polycarbonate Vitrimers. *Macromolecules* **51**, 389–397 (2018).
22. Fortman, D. J., Brutman, J. P., Cramer, C. J., Hillmyer, M. A. & Dichtel, W. R. Mechanically Activated, Catalyst-Free Polyhydroxyurethane Vitrimers. *J. Am. Chem. Soc.* **137**, 14019–14022 (2015).
23. Rolph, M. S., Inam, M. & O'Reilly, R. K. The application of blocked isocyanate chemistry in the development of tunable thermoresponsive crosslinkers. *Polym. Chem.* **8**, 7229–7239 (2017).
24. Lee, D. S., Choi, Y.-S., Hwang, J. H., Lee, J.-H., Lee, W., Ahn, S., Park, S., Lee, J.-H., Kim, Y. S. & Kim, D.-G. Weldable and Reprocessable Biomimetic Polymer Networks Based on a Hydrogen Bonding and Dynamic Covalent Thiourea Motif. *ACS Appl. Polym. Mater.* **3**, 3714–3720 (2021).
25. Yang, M., Lu, X., Wang, Z., Fei, G. & Xia, H. A novel self-catalytic cooperative multiple dynamic moiety: towards rigid and tough but more healable polymer networks. *J. Mater. Chem. A* **9**, 16759–16768 (2021).
26. Stephenson, N. A., Zhu, J., Gellman, S. H. & Stahl, S. S. Catalytic transamidation reactions compatible with tertiary amide metathesis under ambient conditions. *J. Am. Chem. Soc.* **131**, 10003–10008 (2009).
27. Lu, Y.-X. & Guan, Z. Olefin metathesis for effective polymer healing via dynamic exchange of strong carbon-carbon double bonds. *J. Am. Chem. Soc.* **134**, 14226–14231 (2012).
28. Li, Q., Ma, S., Wang, S., Yuan, W., Xu, X., Wang, B., Huang, K. & Zhu, J. Facile catalyst-free synthesis, exchanging, and hydrolysis of an acetal motif for dynamic covalent networks. *J. Mater. Chem. A* **7**, 18039–18049 (2019).
29. Ying, H., Zhang, Y. & Cheng, J. Dynamic urea bond for the design of reversible and self-healing polymers. *Nat. Commun.* **5**, 3218 (2014).
30. Bakkali-Hassani, C., Berne, D., Bron, P., Irusta, L., Sardon, H., Ladmiral, V. & Caillol, S. Polymer Chemistry Polyhydroxyurethane covalent adaptable networks : looking for suitable catalysts. *Polym. Chem.* **14**, 3610–3620 (2023).
31. Diodati, L. E., Liu, S., Rinaldi-Ramos, C. M. & Sumerlin, B. S. Magnetic Nanoparticles Improve Flow Rate and Enable Self-Healing in Covalent Adaptable Networks. *ACS Appl. Mater. Interfaces* **15**, 32957–32966 (2023).
32. Wanasinghe, S. V., Dodo, O. J. & Konkolewicz, D. Dynamic Bonds: Adaptable

- Timescales for Responsive Materials. *Angew. Chem. Int. Ed.* **61**, e202206938 (2022).
33. Van Lijsebetten, F., Spiesschaert, Y., Winne, J. M. & Du Prez, F. E. Reprocessing of Covalent Adaptable Polyamide Networks through Internal Catalysis and Ring-Size Effects. *J. Am. Chem. Soc.* **143**, 15834–15844 (2021).
  34. Li, Q., Ma, S., Li, P., Wang, B., Yu, Z., Feng, H., Liu, Y. & Zhu, J. Fast Reprocessing of Acetal Covalent Adaptable Networks with High Performance Enabled by Neighboring Group Participation. *Macromolecules* **54**, 8423–8434 (2021).
  35. Yamawake, K. & Hayashi, M. The role of tertiary amines as internal catalysts for disulfide exchange in covalent adaptable networks. *Polym. Chem.* **14**, 680–686 (2023).
  36. Cuminet, F., Caillol, S., Dantras, É., Leclerc, É. & Ladmiral, V. Neighboring Group Participation and Internal Catalysis Effects on Exchangeable Covalent Bonds: Application to the Thriving Field of Vitriimer Chemistry. *Macromolecules* **54**, 3927–3961 (2021).
  37. Schoustra, S. K., Asadi, V., Zuilhof, H. & Smulders, M. M. J. Internal hydrogen bonding of imines to control and enhance the dynamic mechanical properties of covalent adaptable networks. *Eur. Polym. J.* **195**, 112209 (2023).
  38. Robinson, L. L., Taddese, E. S., Self, J. L., Bates, C. M., Read De Alaniz, J., Geng, Z. & Hawker, C. J. Neighboring Group Participation in Ionic Covalent Adaptable Networks. *Macromolecules* **55**, 9780–9789 (2022).
  39. Zhao, J., Zhang, Z., Wang, C. & Yan, X. Synergistic Dual Dynamic Bonds in Covalent Adaptable Networks. *CCS Chem.* (2023) doi:10.31635/ccschem.023.202303045.
  40. Crolais, A. E., Dolinski, N. D., Boynton, N. R., Radhakrishnan, J. M., Snyder, S. A. & Rowan, S. J. Enhancing the Equilibrium of Dynamic Thia-Michael Reactions through Heterocyclic Design. *J. Am. Chem. Soc.* **145**, 14427–14434 (2023).
  41. Chakma, P., Digby, Z. A., Via, J., Shulman, M. P., Sparks, J. L. & Konkolewicz, D. Tuning thermoresponsive network materials through macromolecular architecture and dynamic thiol-Michael chemistry. *Polym. Chem.* **9**, 4744–4756 (2018).
  42. Baldwin, A. D. & Kiick, K. L. Tunable degradation of maleimide-Thiol adducts in reducing environments. *Bioconjug. Chem.* **22**, 1946–1953 (2011).
  43. Chakma, P., Rodrigues Possarle, L. H., Digby, Z. A., Zhang, B., Sparks, J. L. & Konkolewicz, D. Dual stimuli responsive self-healing and malleable materials based on dynamic thiol-Michael chemistry. *Polym. Chem.* **8**, 6534–6543 (2017).
  44. Mukaiyama, T. On the Thermal Dissociation of Organic Compounds. VII. The Urea Linkage (1,3-Dibenzylurea and 1-isopropyl-3,3-diethylurea in Alcohols).

- Bull. Chem. Soc. Jpn.* **28**, 253–258 (1955).
45. Zhang, Q., Wang, S., Rao, B., Chen, X., Ma, L., Cui, C., Zhong, Q., Li, Z., Cheng, Y. & Zhang, Y. Hindered urea bonds for dynamic polymers: An overview. *React. Funct. Polym.* **159**, 104807 (2021).
  46. Khan, A., Huang, K., Sarwar, M. G., Cheng, K., Li, Z., Tuhin, M. O. & Rabnawaz, M. Self-healing and self-cleaning clear coating. *J. Colloid Interface Sci.* **577**, 311–318 (2020).
  47. Ying, H. & Cheng, J. Hydrolyzable polyureas bearing hindered urea bonds. *J. Am. Chem. Soc.* **136**, 16974–16977 (2014).
  48. Chen, M., Feng, X., Xu, W., Wang, Y., Yang, Y., Jiang, Z. & Ding, J. Pegylated polyurea bearing hindered urea bond for drug delivery. *Molecules* **24**, 1538 (2019).
  49. Jia, Y., Ying, H., Zhang, Y., He, H. & Cheng, J. Reconfigurable Poly(urea-urethane) Thermoset Based on Hindered Urea Bonds with Triple-Shape-Memory Performance. *Macromol. Chem. Phys.* **220**, 1900148 (2019).
  50. Allen, C. F. H., Fournier, J. O. & Humphlett, W. J. the Thermal Reversibility of the Michael Reaction: I. Nitriles. *Can. J. Chem.* **42**, 2616–2620 (1964).
  51. Zhang, B., Digby, Z. A., Flum, J. A., Chakma, P., Saul, J. M., Sparks, J. L. & Konkolewicz, D. Dynamic Thiol-Michael Chemistry for Thermoresponsive Rehealable and Malleable Networks. *Macromolecules* **49**, 6871–6878 (2016).
  52. Kuhl, N., Geitner, R., Bose, R. K., Bode, S., Dietzek, B., Schmitt, M., Popp, J., Garcia, S. J., van der Zwaag, S., Schubert, U. S. & Hager, M. D. Self-Healing Polymer Networks Based on Reversible Michael Addition Reactions. *Macromol. Chem. Phys.* **217**, 2541–2550 (2016).
  53. Shi, B. & Greaney, M. F. Reversible Michael addition of thiols as a new tool for dynamic combinatorial chemistry. *Chem. Commun* 886–888 (2005) doi:10.1039/b414300k.
  54. Zhong, Y., Xu, Y. & Anslyn, E. V. Studies of reversible conjugate additions. *European J. Org. Chem.* 5017–5021 (2013) doi:10.1002/EJOC.201300358.
  55. Kharkar, P. M., Kiick, K. L. & Kloxin, A. M. Design of thiol- and light-sensitive degradable hydrogels using Michael-type addition reactions. *Polym. Chem* **6**, 5565 (2015).
  56. Berne, D., Ladmiral, V., Leclerc, E. & Caillol, S. Thia-Michael Reaction: The Route to Promising Covalent Adaptable Networks. *Polymers (Basel)*. **14**, 4457 (2022).
  57. Nair, D. P., Podgórski, M., Chatani, S., Gong, T., Xi, W., Fenoli, C. R. & Bowman, C. N. The Thiol-Michael addition click reaction: A powerful and widely used tool in materials chemistry. *Chem. Mater.* **26**, 724–744 (2014).
  58. Zhang, B., Chakma, P., Shulman, M. P., Ke, J., Digby, Z. A. & Konkolewicz, D.

- Probing the mechanism of thermally driven thiol-Michael dynamic covalent chemistry. *Org. Biomol. Chem.* **16**, 2725–2734 (2018).
59. Baldwin, A. D. & Kiick, K. L. Reversible maleimide-thiol adducts yield glutathione-sensitive poly(ethylene glycol)-heparin hydrogels. *Polym. Chem.* **4**, 133–143 (2013).
  60. Spitzbarth, B. & Eelkema, R. On-Demand Release of Secondary Amine Bases for the Activation of Catalysts and Crosslinkers. *Chem. Eur. J.* **29**, e202203028 (2023).
  61. Nguyen, L. T. T., Gokmen, M. T. & Du Prez, F. E. Kinetic Comparison of 13 Homogeneous Thiol–X Reactions Published. *Polym. Chem.* **4**, 5527–5536 (2013).
  62. Huang, S., Kim, K., Musgrave, G. M., Sharp, M., Sinha, J., Stansbury, J. W., Musgrave, C. B. & Bowman, C. N. Determining Michael acceptor reactivity from kinetic, mechanistic, and computational analysis for the base-catalyzed thiol-Michael reaction. *Polym. Chem.* **12**, 3619–3628 (2021).
  63. Chan, J. W., Hoyle, C. E., Lowe, A. B. & Bowman, M. Nucleophile-initiated thiol-michael reactions: Effect of organocatalyst, thiol, and Ene. *Macromolecules* **43**, 6381–6388 (2010).
  64. Mather, B. D., Viswanathan, K., Miller, K. M. & Long, T. E. Michael addition reactions in macromolecular design for emerging technologies. *Prog. Polym. Sci.* **31**, 487–531 (2006).
  65. Okhay, N., Mignard, N., Jegat, C. & Taha, M. Diels-Alder thermoresponsive networks based on high maleimide- functionalized urethane prepolymers. *Des. Monomers Polym.* **16**, 475–487 (2013).
  66. Izraylit, V., Hommes-Schattmann, P. J., Neffe, A. T., Gould, O. E. C. & Lendlein, A. Polyester urethane functionalizable through maleimide side-chains and cross-linkable by polylactide stereocomplexes. *Eur. Polym. J.* **137**, 109916 (2020).
  67. Delebecq, E., Pascault, J. P., Boutevin, B. & Ganachaud, F. On the versatility of urethane/urea bonds: Reversibility, blocked isocyanate, and non-isocyanate polyurethane. *Chem. Rev.* **113**, 80–118 (2013).
  68. Shin, M., Shin, S. H., Lee, M., Kim, H. J., Jeong, J. H., Choi, Y. H., Oh, D. X., Park, J., Jeon, H. & Eom, Y. Rheological criteria for distinguishing self-healing and non-self-healing hydrogels. *Polymer.* **229**, 123969 (2021).

## Supporting Information

### General Information

1,4-Dioxane and DMSO were purchased from Fisher Scientific as extra dry solvents over molecular sieves. Dimethyl carbonate (DMC), ethylene glycol bis(3-mercaptopropionate), hexamethylene diisocyanate, maleic anhydride, furan, 3-amino-1,2-propanediol, *N,N'*-di-*tert*-butylethylenediamine and 4-trifluoromethyl benzenethiol were purchased from TCI. Benzyl isocyanate, xylene, ethyl 3-mercaptopropionate, and diisopropylamine were purchased from Sigma Aldrich. Ethanol and ethyl acetate were purchased from VWR. *N*-Methylmaleimide was purchased from Fluorochem. Deuterium oxide, DMSO-*d*<sub>6</sub>, and CDCl<sub>3</sub> were purchased from Eurisotop. Unless stated otherwise, all chemicals were used as received. For water-free experiments, anhydrous solvents were stored over 3 Å molecular sieves and pre-dried flasks were used. The DCv ureas TBEU and TBIPU were available from a previous study in our lab. For synthetic procedures refer to the supplementary information there.<sup>1</sup>

### NMR measurements

NMR spectra were measured on an Agilent-400 MR DD2 (400 MHz for <sup>1</sup>H, 101 MHz for <sup>13</sup>C) instrument. All measurements were performed at 298 K or 318 K, as stated for each experiment accordingly. T1 measurements were performed to ensure full relaxation of all signals of interest in kinetic qNMR studies. For this, we followed our previous procedure.<sup>2</sup> Briefly, sealed glass ampoules (NMR tubes with an outer diameter of 2.5 mm) were prepared, containing a 10 mM solution of sodium trimethylsilylpropanesulfonate (DSS) in D<sub>2</sub>O. They were added in the NMR tubes with the sample solution and the spectra were locked on D<sub>2</sub>O and PRESAT experiments were measured to suppress the DMC signal. For data analysis, the raw data was treated in Mestrenova V11.0. Here, all spectra were treated with baseline and phase correction. The 0.00 ppm signal of DSS was set to 1000 and the concentrations of the compounds in the reaction were derived from this integral and the known starting concentrations. All qNMR kinetic experiments were conducted in duplicates. For precise procedures refer to the Methods section in the main text.

### GPC measurements

GPC measurements were performed on a Shimadzu GPC equipped with a CTO-20AC column oven, a RID-10A RI detector, a SPD-20A UV-Vis detector and a Agilent PLGel MIXED-C 5 μm column with dimensions of 300 mm × 7.5 mm and a PLGel guard column (50 mm × 7.5 mm). The eluent was DMF with 25 mM LiBr and a flow rate of 1 mL/min.

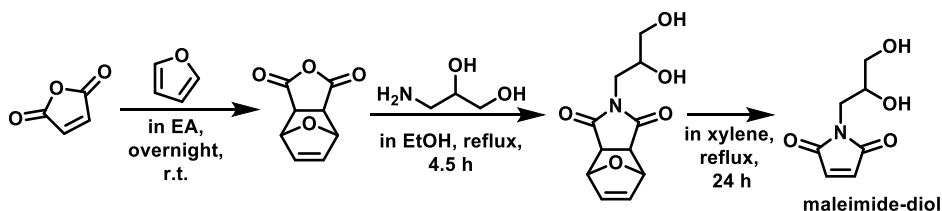
## Rheology measurements

Rheology was performed on a TA instruments AR-G2 rheometer equipped with a temperature-controlled stainless steel sample stage and a 40 mm stainless steel flat plate. All measurements were enclosed with a solvent trap. For precise procedures refer to the Methods section in the main text.

## ESI-LC/MS measurements

For LC/MS measurements, a Thermo Scientific LTQ XL was used. The spectrometer is equipped with a Supelco discovery C18 100 mm x 2.1 mm column with a particle size of 5  $\mu\text{m}$ . As eluent, a water and acetonitrile solutions with 0.1 vol% formic acid were used.

## Synthesis



The maleimide-diol monomer was synthesised according to several adapted literature procedures.<sup>3-6</sup>

In the first step, 5.00 g (51.0 mmol, 1.0 eq.) maleic anhydride were dissolved in 6.25 mL ethyl acetate. 4.95 mL (67.9 mmol, 1.33 eq.) furan were added and the solution was stirred overnight at room temperature. The next day, the mixture had solidified. The solid was filtered, washed twice with ethyl acetate, and dried under vacuum to yield 7.75 g (46.7 mmol, 92 %, literature 78.5 %) of 4,10-dioxatricyclo[5.2.1.0<sup>2,6</sup>]dec-8-ene-3,5-dione as a colourless solid. The spectroscopic data was found to be in accordance with literature.<sup>3</sup> Despite minor impurities of maleic anhydride and furan in the product, it was continued with the second step of the synthesis.

**<sup>1</sup>H-NMR (400 MHz, CDCl<sub>3</sub>):**  $\delta$  = 6.58 (s, 2H, *CHCO*), 5.46 (s, 2H, *CHO*), 3.17 (s, 2H, *CHC(O)O*).

In the second step, 6.65 g (40.0 mmol, 1.0 eq.) of the maleic anhydride furan adduct of step 1 were dissolved in 10 mL ethanol. Under stirring, a mixture of 3.195 mL (41.2 mmol, 1.03 eq.) 3-amino-1,2-propanediol and 2.5 mL ethanol were added dropwise to the solution under stirring. Subsequently, the solution was heated to reflux (85 °C oil bath temperature) for 4.5 hours. Upon cooling, the product was crystallised from the solution at -20 °C overnight. The colourless precipitate was filtered, washed with ice-cold ethanol and dried under vacuum to yield 4.47 g (18.8 mmol, 47 %, literature 49 %) of *N*-(2,3-dihydroxy-propyl)-10-oxa-4-aza-tricyclo[5.2.1.0<sup>2,6</sup>]-dec-8-ene-3,5-dione. The spectroscopic data was in accordance with literature.<sup>3</sup>

**<sup>1</sup>H-NMR (400 MHz, DMSO-*d*<sub>6</sub>):**  $\delta$  = 6.55 (d,  $J$  = 1.2 Hz, 2H, CHCHO), 5.12 (d,  $J$  = 1.1 Hz, 2H, CHO), 4.78 (d,  $J$  = 5.2 Hz, 1H, CHOH), 4.56 (t,  $J$  = 5.7 Hz, 1H, CH<sub>2</sub>OH), 3.67 (h,  $J$  = 5.9 Hz, 1H, CHOH), 3.35 (d,  $J$  = 2.0 Hz, 2H, NCH<sub>2</sub>), 3.29 – 3.23 (m, 2H, CH<sub>2</sub>OH), 2.95 – 2.89 (m, 2H, CH<sub>2</sub>C(O)N).

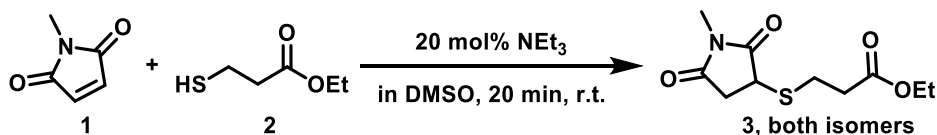
The third step caused significant issues in practice. Several differing procedures have been reported,<sup>3–6</sup> and we had to apply a combined approach of several procedures to yield a pure product that did not contain residual starting material. Of note, we found toluene not to work in our hands as a solvent due to its lower boiling point. At reflux, we could not achieve full conversions even over several days. We had to use xylene at reflux with vigorous bubbling and a short air condenser to drive the retro-Diels Alder reaction to completion.

Specifically, 10.0 g of the product of step 2 were suspended in 125 mL xylene in a three-necked round bottom flask fitted with a short air condenser and a syringe connected to an argon line. The mixture was heated to reflux (140 °C oil bath temperature) while stirring, under vigorous argon bubbling for 5 hours. At this time, all solids had dissolved and the clear solution had formed a second liquid phase with brown colour at the bottom of the flask. The biphasic mixture was reheated to 130 °C under stirring and the top clear xylene layer was decanted off. A fresh portion of xylene was added and decanted off after an additional 10 minutes of heating. This process was repeated three more times, the xylene fractions were combined, and the maleimide-diol was crystallised at –20 °C overnight. Filtration and drying under vacuum yielded 4.51 g (23.0 mmol, 55 %, literature 80.7 %) colourless powder. The spectroscopic data was in accordance with literature.<sup>3</sup>

**<sup>1</sup>H-NMR (400 MHz, DMSO-*d*<sub>6</sub>):**  $\delta$  = 7.00 (s, 2H, CHC(O)N), 4.82 (d,  $J$  = 5.4 Hz, 1H, CHOH), 4.60 (t,  $J$  = 5.7 Hz, 1H, CH<sub>2</sub>OH), 3.67 (p,  $J$  = 5.5 Hz, 1H, CHOH), 3.41 – 3.37 (m, 2H, NCH<sub>2</sub>), 3.36 – 3.24 (m, 2H, CH<sub>2</sub>OH).

**<sup>13</sup>C-NMR (101 MHz, DMSO-*d*<sub>6</sub>):**  $\delta$  = 171.61 (CO), 134.91 (CHC(O)), 68.86 (CHOH), 64.52 (CH<sub>2</sub>OH), 41.65 (NCH<sub>2</sub>).

**ESI-LC/MS (m/z):** calculated for [M+H]<sup>+</sup>: 172.1, found: 172.1; calculated for [M+Na]<sup>+</sup>: 194.0, found: 194.0.

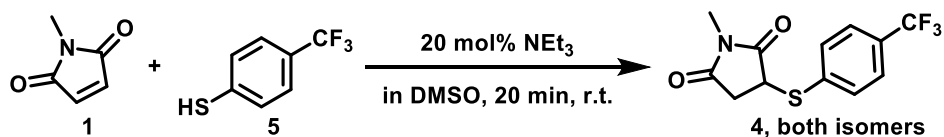


The adduct **3** of *N*-methylmaleimide **1** and ethyl 3-mercaptopropionate **2** was synthesised by dissolving 222.2 mg (2.0 mmol, 1.0 eq.) of *N*-methylmaleimide **1** in 10 mL DMSO. Thiol **2** (253.4  $\mu$ L, 2.0 mmol, 1.0 eq.) and 55.0  $\mu$ L triethylamine (0.4 mmol, 0.2 eq.) were added and the solution was stirred for 20 minutes at room temperature. An NMR-sample showed full conversion. The solution was lyophilised to yield 489 mg (2.0 mmol, quant.) of thiol-maleimide adduct **3** as a pale yellow oil.

**<sup>1</sup>H-NMR (400 MHz, CDCl<sub>3</sub>):** δ = 4.17 (q, *J* = 7.1 Hz, 2H, CH<sub>3</sub>CH<sub>2</sub>O), 3.80 (dd, *J* = 9.1, 3.8 Hz, 1H, *CHS*), 3.26 – 3.02 (m, 3H, CH<sub>2</sub>CHS (one of the two protons), SCH<sub>2</sub>CH<sub>2</sub>), 3.01 (s, 3H, NCH<sub>3</sub>), 2.71 (t, *J* = 7.0 Hz, 2H, SCH<sub>2</sub>CH<sub>2</sub>), 2.51 (dd, *J* = 18.7, 3.8 Hz, 1H, CH<sub>2</sub>CHS (one of the two protons)), 1.27 (t, *J* = 7.1 Hz, 3H, CH<sub>3</sub>CH<sub>2</sub>O).

**<sup>13</sup>C-NMR (101 MHz, CDCl<sub>3</sub>):** δ = 176.75 (NC(O)CH<sub>2</sub>), 174.74 (NC(O)CHS), 171.71 (C(O)OEt), 61.03 (OCH<sub>2</sub>CH<sub>3</sub>), 39.29 (CHS), 36.03 (CH<sub>2</sub>CHS), 34.56 (SCH<sub>2</sub>CH<sub>2</sub>), 27.08 (SCH<sub>2</sub>), 25.30 (NCH<sub>3</sub>), 14.35 (OCH<sub>2</sub>CH<sub>3</sub>).

**ESI-LC/MS (m/z):** calculated for [M+H]<sup>+</sup>: 246.1, found: 246.1; calculated for [M+Na]<sup>+</sup>: 268.1, found: 268.1.



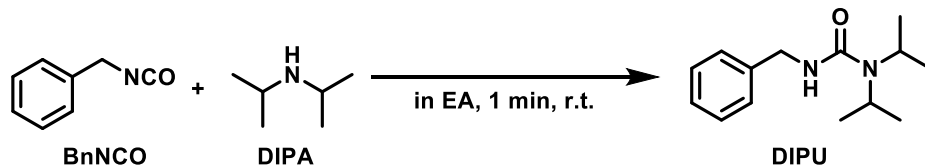
The adduct **4** of *N*-methylmaleimide **1** and 4-(trifluoromethyl)benzenethiol **5** was synthesised by dissolving 111.1 mg (1.0 mmol, 1.0 eq.) of *N*-methylmaleimide **1** in 10 mL DMSO. Thiol **5** (135.0 μL, 1.0 mmol, 1.0 eq.) and 27.8 μL triethylamine (0.2 mmol, 0.2 eq.) were added and the solution was stirred for 20 minutes at room temperature. An NMR-sample showed full conversion. The solution was lyophilised to yield 288 mg (1.0 mmol, quant.) of thiol-maleimide adduct **4** as a grey solid.

**<sup>1</sup>H-NMR (400 MHz, CDCl<sub>3</sub>):** δ = 7.61 (q, *J* = 8.5 Hz, 4H, CH<sub>aromatic</sub>), 4.16 (dd, *J* = 9.2, 4.2 Hz, 1H, CHSAr), 3.23 (dd, *J* = 18.7, 9.2 Hz, 1H, CH<sub>2</sub>SAr), 2.98 (s, 3H, NCH<sub>3</sub>), 2.69 (dd, *J* = 18.7, 4.3 Hz, 1H, CH<sub>2</sub>SAr).

**<sup>13</sup>C-NMR (101 MHz, CDCl<sub>3</sub>):** δ = 175.38 (NC(O)CHSAr), 174.10 (NC(O)CH<sub>2</sub>), 137.04 (C<sub>q</sub>S), 132.31 (CH<sub>aromatic</sub>), 130.76 (CH<sub>aromatic</sub>), 130.44 (CH<sub>aromatic</sub>), 126.26 (q, *J* = 3.8 Hz, CF<sub>3</sub>), 125.25 (CH<sub>aromatic</sub>), 122.54 (CH<sub>aromatic</sub>), 43.40 (CHSAr), 36.32 (CH<sub>2</sub>CHSAr), 25.44 (NCH<sub>3</sub>).

**<sup>19</sup>F-NMR (376 MHz, CDCl<sub>3</sub>):** δ = -62.83 (CF<sub>3</sub>).

**ESI-LC/MS (m/z):** calculated for [M+H]<sup>+</sup>: 290.0, found: 290.0.



DIPU was synthesised in the same manner as TBEU and TBIPU.<sup>1</sup> Briefly, 494 μL benzyl isocyanate (4.0 mmol, 1.0 eq.) and 673 μL DIPA (4.8 mmol, 1.2 eq.) were mixed in 4 mL

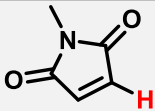
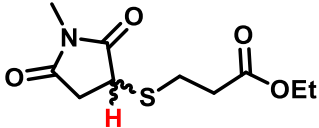
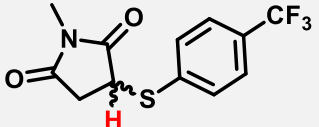
ethyl acetate. The solution was cooled down and filtered through a short silica plug to remove excess base. The solvent was removed under reduced pressure to yield 1.0 g (4.0 mmol, quant.) of DIPU as a colourless powder. The spectroscopic data was in accordance with literature.<sup>7</sup>

**<sup>1</sup>H-NMR (400 MHz, CDCl<sub>3</sub>):**  $\delta$  = 7.36 – 7.23 (m, 6H, CH<sub>aromatic</sub>, overlap with CDCl<sub>3</sub> signal), 4.45 (s, 2H, CH<sub>2</sub>NH), 3.90 (hept,  $J$  = 6.9 Hz, 2H, NCH(CH<sub>3</sub>)<sub>2</sub>), 1.25 (d,  $J$  = 6.9 Hz, 12H, NCH(CH<sub>3</sub>)<sub>2</sub>).

**<sup>13</sup>C-NMR (101 MHz, CDCl<sub>3</sub>):**  $\delta$  = 157.30 (NHC(O)), 140.05 (C<sub>q</sub>CH<sub>2</sub>NH), 128.74 (CH<sub>aromatic-meta</sub>), 127.81 (CH<sub>aromatic-ortho</sub>), 127.27 (CH<sub>aromatic-para</sub>), 45.33 (NCH(CH<sub>3</sub>)<sub>2</sub>), 45.00 (NCH<sub>2</sub>), 21.63 (NCH(CH<sub>3</sub>)<sub>2</sub>).

### T1 Measurements

To determine the d1 delay to use with the PRESAT measurements to ensure full relaxation of each signal to be integrated, inversion-recovery experiments were performed. The results were as follows:

Signal	T1 time (s)
	6.05
	1.87
	2.94

The d1 delay for the PRESAT measurements was set as 5 times the maximum determined T1 value for each experiment, minus 2.55 seconds (= acquisition time).

### Side Reactivity of DIPU

As stated in the main text, TBEU and DIPU did not show any significant side reactions, neither in the thiol-maleimide additions, nor in the exchange reactions. TBIPU on the other hand was abandoned upon measuring kinetics at 25 °C due to high side reactivity. As the least stable of the three DCv ureas, significant benzyl isocyanate is release in the DCv urea equilibrium. During the kinetic measurements, new signals were found:

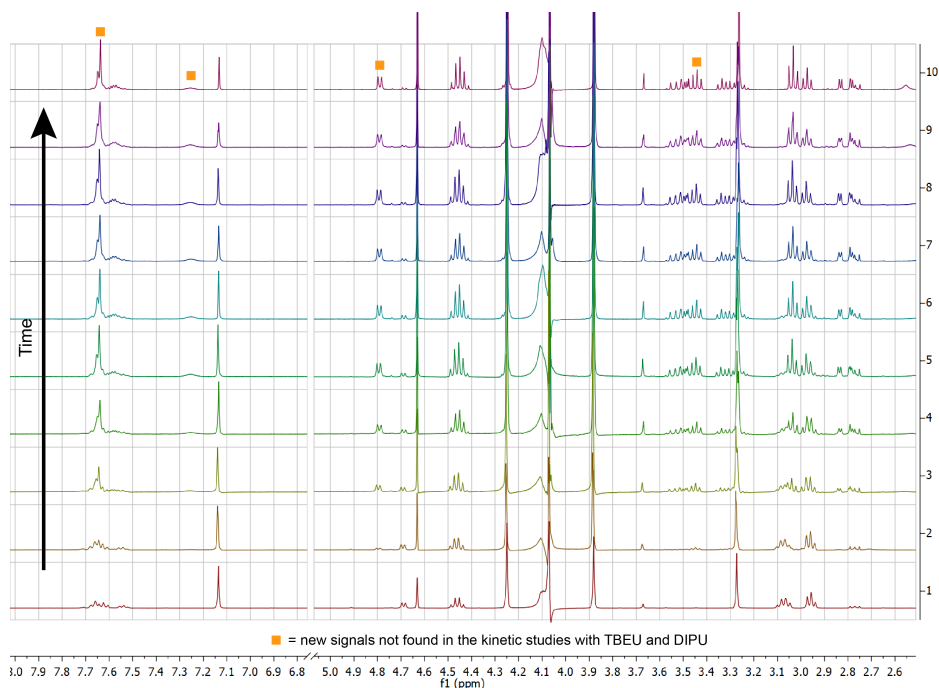


**Figure S4.1:** Conversion of a mixture of 25 mM *N*-methylmaleimide **1** with 25 mM thiol **2** and 12.5 mM DIPU in dimethyl carbonate. Orange squares indicate signal that are not found in the identical experiments with TBEU and DIPU.

We hypothesised that these signals belong to the *S*-thiocarbamate of thiol **2** and benzyl isocyanate release from DIPU over time. This would align with the release of DIPA over time which we also observed in the kinetics above (Figure S4.1). To assure that this is the case, we mixed benzyl isocyanate with thiol **2** and added a base (triethylamine). Indeed, the same signals as found in Figure S4.1 also appeared within minutes of adding triethylamine to a mixture of benzyl isocyanate and thiol **2** (Figure S4.2). These findings corroborate that TBIPU is not suitable as a temperature-triggered catalyst for thiol-maleimide addition and exchange reactions due to the formation of the *S*-thiocarbamate side product.

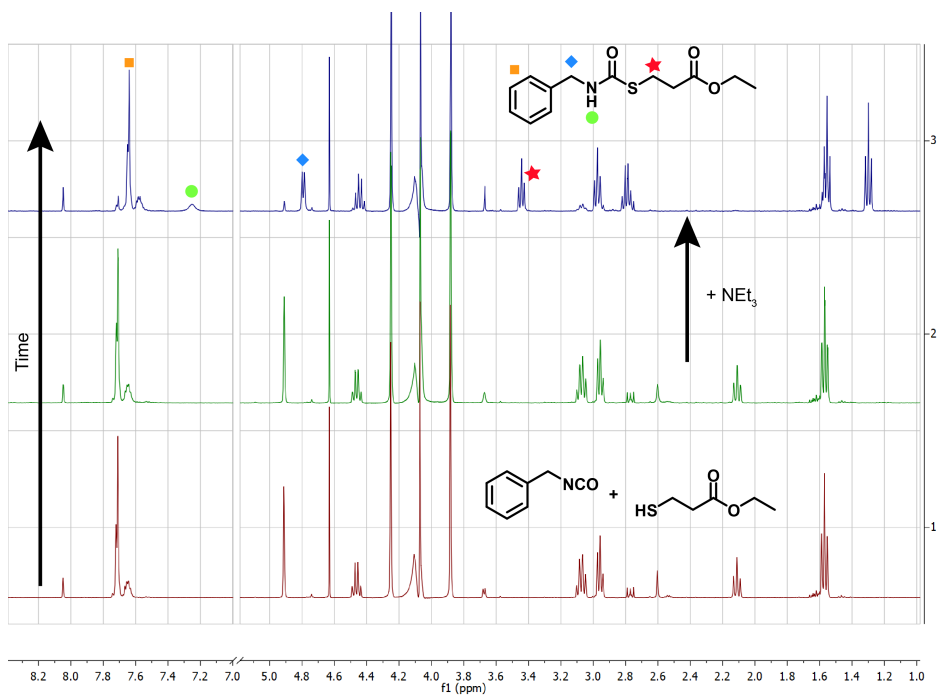


**Figure S4.2:** Mixture of 25 mM benzyl isocyanate and 25 mM thiol **2** in dimethyl carbonate. Upon addition of 12.5 mM triethyl amine, the *S*-thiocarbamate adduct forms within minutes.

## References

1. Spitzbarth, B. & Eelkema, R. On-Demand Release of Secondary Amine Bases for the Activation of Catalysts and Crosslinkers. *Chem. Eur. J.* **29**, e202203028 (2023).
2. Sharko, A., Spitzbarth, B., Hermans, T. M. & Eelkema, R. Redox-Controlled Shunts in a Synthetic Chemical Reaction Cycle. *J. Am. Chem. Soc.* **145**, 9672–9678 (2023).
3. Yu, S., Zhang, R., Wu, Q., Chen, T. & Sun, P. Bio-Inspired High-Performance and Recyclable Cross-Linked Polymers. *Adv. Mater.* **25**, 4912–4917 (2013).
4. Ouyang, C., Zhao, C., Li, W., Wu, X., Le, X., Chen, T., Huang, W., Gao, Q., Shan, X., Zhg, R. & Zhang, W. Super-Tough, Self-Healing Polyurethane Based on Diels-Alder Bonds and Dynamic Zinc–Ligand Interactions. *Macromol. Mater. Eng.* **305**, 2000089 (2020).
5. Fang, Y., Du, X., Cheng, X., Zhou, M., Du, Z. & Wang, H. Preparation of living and highly stable blended polyurethane emulsions for self-healing films with enhance toughness and recyclability. *Polymer* **188**, 122142 (2020).
6. Hartmann, R. W., Pijnappel, M., Nilvebrant, J., Helgudottir, H. R., Asbjarnarson, A., Traustadottir, G. A., Gudjonsson, T., Nygren, P.-Å., Lehmann, F. & Odell, L. R. The Wittig bioconjugation of maleimide derived, water soluble phosphonium ylides to aldehyde-tagged proteins. *Org. Biomol. Chem.* **19**, 10417–10423 (2021).
7. Lee, A., Kim, H. K. & Thompson, D. H. A Facile Method for the Preparation of Unsymmetrical Ureas Utilizing Zirconium(IV) Chloride. *Bull. Korean Chem. Soc.* **37**, 154–160 (2016).

# Chemical Reaction Networks based on Conjugate Additions on $\beta'$ -substituted Michael Acceptors

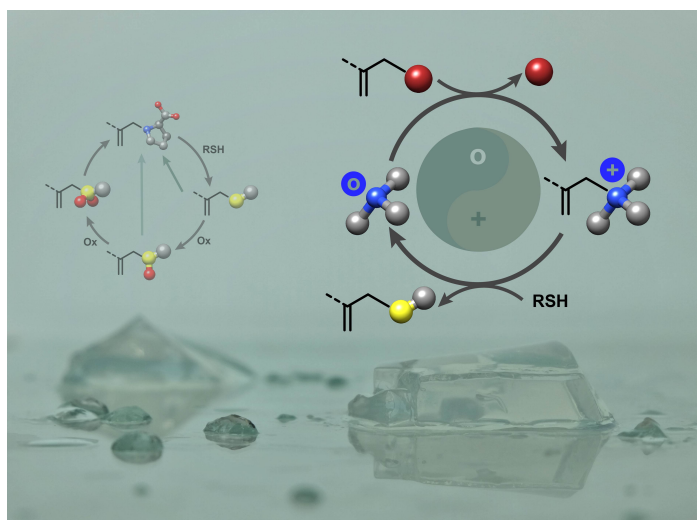
## Abstract

Over the last few decades, the study of more complex, chemical systems closer to those found in nature, and the interactions within those systems, has grown immensely. Despite great efforts, the need for new, versatile, and robust chemistry to apply in CRNs remains. In this Feature Article, we give a brief overview over previous developments in the field of systems chemistry and how  $\beta'$ -substituted Michael acceptors (MAs) can be a great addition to the systems chemist's toolbox. We illustrate their versatility by showcasing a range of examples of applying  $\beta'$ -substituted MAs in CRNs, both as chemical signals and as substrates, to open up the path to many applications ranging from responsive materials, to pathway control in CRNs, drug delivery, analyte detection, and beyond.

## Availability and Contributions

This chapter is based on a feature article published as: B. Spitzbarth, R. Eelkema. *Chem. Commun.* **59**, 11174–11187 (2023). It is reproduced from this reference with permission from the Royal Society of Chemistry. DOI: 10.1039/d3cc02126b

B.S. performed the literature search, wrote the manuscript draft, and designed all figures, schemes, and the *Chem. Commun.* Issue 75, 2023 back cover (see below). R.E. corrected the draft, aided with figure design, and secured funding.



## Introduction

### Systems chemistry: chemical toolbox to understand and mimic Nature

Systems chemistry initially evolved out of a desire to develop and study more complex chemical systems to bridge the large gap between traditional chemical processes and biochemical reaction networks.<sup>1</sup> As a result, over the last couple of decades, a wide range of artificial Chemical Reaction Networks (CRNs) have been developed.<sup>2</sup> They have many functions and can impart interesting properties such as transient formation, cargo release, or autonomous behaviour on other systems such as fuelled, transient materials (e.g. supramolecular assemblies,<sup>3,4</sup> micelles,<sup>5-8</sup> Complex Coacervate Core Micelles (C3Ms),<sup>9-12</sup> crosslinked hydrogels,<sup>13-15</sup> and sensors (e.g. pH switches<sup>16-19</sup> and light-controlled switches<sup>20-22</sup>),<sup>23</sup> among others. Such CRNs typically consist of a cycle of chemical reactions, starting from and ending with the same chemical species (Figure 5.1, left). In *autonomous cycles*, a stimulus (such as chemical fuel(s), changes in pH, or irradiation) is used to transform the starting material into a new species, which typically leads to an out-of-equilibrium situation (i.e. a situation in which the thermodynamic minimum of the system has not been established yet), where the back reaction recovers the starting material (Figure 5.1, light blue). The driving force of the cycle maintains the system in an out-of-equilibrium state until the stimulus is used up or not applied anymore. In *signal-induced cycles* a reagent is added that transforms state A into state B (Figure 5.1, dark blue). State B will then only be transformed back to state A when a second reagent (a signal) to initiate the back-reaction is added. Whether cycles can be run *autonomously* or in a *signal-induced* manner depends on several factors such as orthogonality of all stimuli and desired lifetime of state B.

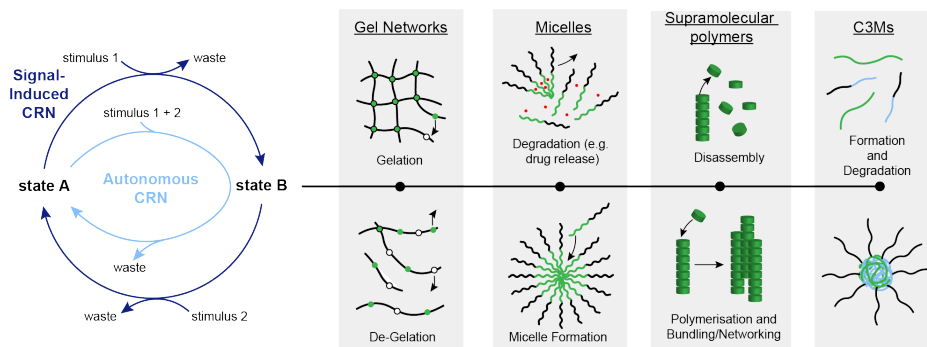
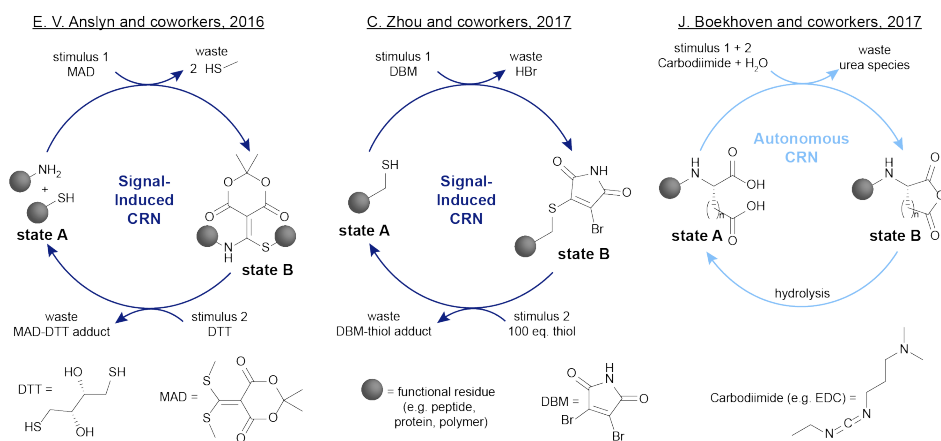


**Figure 5.1:** General Scheme 5. of a CRN. Under the influence of a stimulus, state A is transformed into state B which can perform a function, with some examples depicted on the right. A second stimulus can recover state A from state B.

Among the many systems introduced over the last decades, some have attracted considerable attention due to their versatile applications. One of such systems is the click-declick cycle of Anslyn and coworkers.<sup>24</sup> Here, a Meldrum's acid derivative (MAD) is used to selectively capture one equivalent of thiol and one equivalent of amine (Scheme 5.1, left). This strategy can be used to functionalise peptides,<sup>24</sup> or form cyclic peptides.<sup>25</sup>

Adding the thiol DTT can fully revert this reaction and release the initial thiol and amine. This system is *signal-induced* because the forward and backward process are two distinct steps for which the reagents are added subsequently. This is due to the cross-reactivity of MAD and DTT which prevents *autonomous* operation of this CRN. In another instance, Caddick, Baker, and coworkers show the reversible functionalisation of biomolecules such as proteins with a dibromomaleimide (DBM) (Scheme 5.1, centre).<sup>26</sup> Unlike the typical thiol-maleimide bond, this formation is fully reversible in the presence of a second thiol which makes this biofunctionalisation especially attractive. One of the downsides here is that to fully push the reaction back to the starting point, a large excess of second thiol is necessary. Contrasting these *signal-induced CRNs*, a prime example of *autonomous CRNs* are the EDC-driven systems pioneered by Boekhoven and colleagues,<sup>27</sup> as well as the group of C. Scott Hartley.<sup>28</sup> In Boekhoven's system, a glutamic or aspartic acid functionalised species can transiently be transformed into an uncharged anhydride with a carbodiimide such as EDC (Scheme 5.1, right). This anhydride will then spontaneously hydrolyse back to the starting acid, allowing for temporal control over the charge density in the system. The fact that only one reagent addition is necessary to fully cycle this system through an activated state B back to state A makes it *autonomous*. One of the downsides however is the poor control over the kinetics of the hydrolysis step.



**Scheme 5.1:** Recent examples of signal-induced and autonomous CRNs. Left: Ansyn and coworkers showed that Meldrum's acid derivative (MAD) can be used to selectively capture one thiol and one amine moiety which can be released again upon addition of DTT. Centre: Caddick, Baker, and coworkers demonstrated the reversible functionalisation of biologically relevant thiols with dibromomaleimides (DBM). Right: Boekhoven and coworkers introduced the transient formation of anhydrides from acids with carbodiimides such as EDC, leading to a temporal control over charge density.

Despite these promising works, CRNs controlled entirely through chemical signals remain relatively few, and still suffer from some common drawbacks such as waste accumulation and cross-reactivity.<sup>29–33</sup> Furthermore, the poor control over hydrolysis reactions as part of a CRN, common in the deactivation step of many CRN systems,<sup>27,30,34–38</sup> is one of the drawbacks that can be resolved in systems applying distinct reagents as

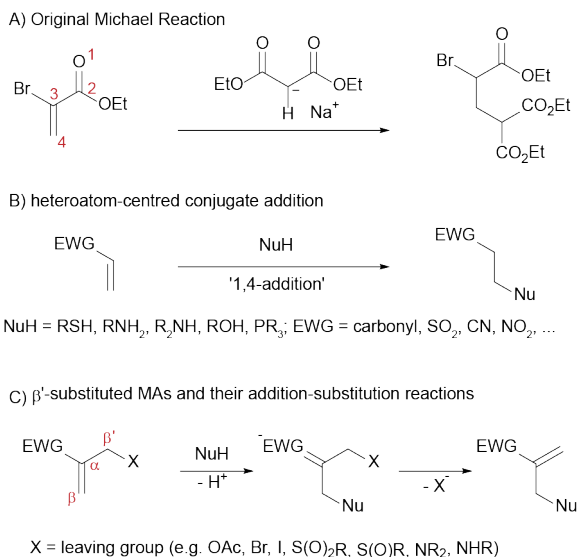
stimuli instead of relying on hydrolysis for the recovery of the starting compound. New chemical reactions are needed to design more robust, versatile and efficient CRNs that can respond to chemical signals. Additionally, if we aim to develop CRNs that are compatible with living systems, a novel approach is needed to find chemistry that is less toxic than commonly used fuels such as carbodiimides, or methylating agents such as methyl iodide.<sup>27,28,36,38,39</sup> We envisioned that conjugate additions could resolve many of these challenges and present a valuable extension of the systems chemists' toolbox for developing CRNs to enable new applications in material science, drug delivery, as well as fundamental science to study in depth how CRNs function and how we can bridge the gap between systems chemistry and much more complex, biological systems.

### **Versatility and drawbacks of conjugate additions**

Conjugate additions are of immense importance in the formation of carbon-carbon and carbon-heteroatom bonds. They have been investigated in depth over the last 150 years and comprise a large range of reactions that are indispensable in modern organic chemistry.<sup>40</sup> Among the large range of additions of different nucleophiles to different acceptors,<sup>40-43</sup> many of which can also be run with high enantioselectivity,<sup>40,44-46</sup> some of the key transformations are the Michael addition to form carbon-carbon bonds,<sup>47</sup> the Robinson annulation which is one of the key methods to close rings,<sup>48</sup> as well as the thiol-, aza-, and phospho-Michael additions, which enable the formation of carbon-sulfur, carbon-amine, and carbon-phosphorus bonds respectively, commonly applied in material science<sup>49-51</sup> and protein functionalisations.<sup>52-58</sup> Furthermore, nucleophilic conjugate additions are of biological relevance as the involved Michael acceptors possess high bioactivity due to their reactivity towards various nucleophiles, making them good candidates as covalent modifiers,<sup>59</sup> as well as warheads in activity-based probes.<sup>60</sup> Although their sometimes indiscriminate reactivity towards nucleophiles is responsible for the carcinogenicity and toxicity of some Michael acceptors,<sup>61</sup> precise tuning of their reactivity and substituents to precisely fit the pocket of the active sites of a biological target are commonly applied in the process of drug discovery.<sup>61,62</sup> Furthermore, cytotoxicity of even small-molecule Michael acceptors strongly depends on their structure, making biomedical applications possible depending on the choice of molecules.<sup>63</sup>

Conjugate additions always involve the attack of a carbon- or heteroatom-centred nucleophile, i.e. Michael donor, on an electron-poor, unsaturated electrophile, called the Michael acceptor (Scheme 5.2 A, B). These Michael acceptors are a wide class of compounds that consist of an electron-withdrawing group such as carbonyls, nitriles or sulfones in conjugation with one or more double or triple bonds. This wide substrate scope makes these reactions especially attractive in synthetic organic chemistry. There are several ways that nucleophiles can add to these Michael acceptors: in a 1,2-addition reaction which is especially relevant for carbonyls, in a 1,4-addition reaction which will be of central importance for this work (Scheme 5.2 B), and—in larger conjugated systems—also in a 1,(2n+2)-addition reaction ( $n > 1$ ). Upon searching the literature for these reactions, it becomes clear that the terms 'conjugate addition', 'Michael addition' and 'Michael reaction' are often used interchangeably. Strictly speaking however, only

the addition of carbon-centred nucleophiles to Michael acceptors is considered as a Michael addition, whereas the addition of stabilised carbon-centred nucleophiles is termed Michael reaction (Scheme 5.2 A). ‘Conjugate addition’ describes all such addition reactions of any nucleophile to an unsaturated, conjugated electrophile. Hence, we will refer to the addition reactions of heteroatom-centred nucleophiles to Michael acceptors (Scheme 5.2 B) simply as ‘conjugate additions’ throughout this article.



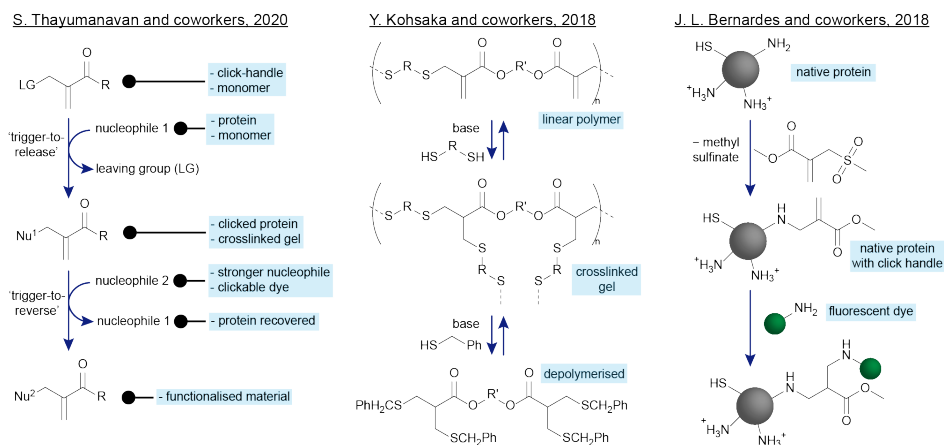
**Scheme 5.2:** A) The original Michael Reaction, discovered by A. Michael, comprises the addition of a malonate to a stabilised acrylate ester. B) The 1,4-addition of heteroatom-centred nucleophiles to Michael acceptors, which is of central importance to this work. C) β'-substituted Michael acceptors, which can undergo addition-substitution reactions, maintaining the active double bond moiety.

Despite the chemical versatility and often high yields and short reactions times, conjugate additions suffer from some drawbacks. Most notably, they are often difficult to reverse and the Michael-accepting functionality gets lost during the addition reaction, with some exceptions such as the Robinson annulation where the elimination of water follows the addition and ring closure steps, or the Morita-Baylis-Hillman reaction where the elimination of the catalyst regenerates the double bond, among others.<sup>48,64</sup> This loss of functionality is especially problematic if the Michael-accepting moiety is desirable for further addition- and substitution-reactions such as late-stage functionalisation procedures.

### β'-substituted Michael acceptors: addition-elimination reactions

To overcome this problem, the group of R. Lawton developed a special class of Michael acceptors that carry a leaving group in the β'-position (Scheme 5.2 C).<sup>65</sup> They are also commonly called α-substituted MAs,<sup>66,67</sup> however we will refer to them as β'-substituted to put emphasis on the presence of a leaving group in this position and distinguish them

from other  $\alpha$ -substituted species that cannot undergo the same reactions. Although these compounds also undergo the typical 1,4-addition reactions, the leaving group in  $\beta'$ -position enables an elimination reaction to take place upon conjugate addition of the nucleophile. This creates a new Michael-accepting double bond moiety (Scheme 5.2 C). This means that the MA moiety is retained in the molecule and is available for further conjugate addition-elimination reactions. In classical conjugate additions (Scheme 5.2 A, B), neither is the MA moiety retained, nor is the reaction reversible under such mild conditions.<sup>40</sup> For a second conjugate addition-elimination reaction to occur quantitatively on  $\beta'$ -substituted MAs, it is essential that the attacking nucleophile is stronger than the previous one, to enable the elimination of the first nucleophile as a new leaving group.<sup>68</sup> Furthermore, the feature of retaining the double bond upon eliminations allows for a dynamic exchange of nucleophile and leaving group on the  $\beta'$ -substituted MAs. This is why they are commonly referred to as ‘Equilibrium Transfer Alkylating Crosslink’ Reagents (ETACs).<sup>58,69</sup> Due to these favourable properties,  $\beta'$ -substituted MAs have since been applied as molecular yardsticks,<sup>69</sup> as tools for biofunctionalisations,<sup>54,57,58,70–73</sup> in chemical switches,<sup>68</sup> as well as in the random walk of small molecules.<sup>74</sup>



**Scheme 5.3:** Recent applications of  $\beta'$ -substituted MAs. Left: S. Thayumanavan and coworkers have performed in-depth kinetic studies on the addition-elimination reaction of these species and demonstrated their applications for crosslinkable gels, and as click handles. Centre: Y. Kohsaka and coworkers have shown different applications of  $\beta'$ -substituted MAs in polymer materials. One of them involves the fully reversible crosslinking of MA-based materials. Right: J. L. Bernardes and coworkers have demonstrated the chemoselective modification of native proteins on the most nucleophilic lysine residue(s) with a  $\beta'$ -substituted MA as a reactive click handle.

Of special note is the work of S. Thayumanavan and coworkers (Scheme 5.3, left). They have studied in depth the impact that different substituents have on the kinetics of addition-substitution reactions. Further, they showed that  $\beta'$ -substituted MAs can be used both as click handles for biofunctionalisations as well as monomers to make reversibly crosslinked networks.<sup>68</sup> Kohsaka and coworkers have performed several in depth studies on how to use these MAs in materials as well. In one of their works (Scheme 5.3, centre), they show how a linear polymer made of bisfunctional MAs and bis-thiols can be crosslinked with additional bis-thiols. They then demonstrate the fully reversible,

dynamic nature of these thiol-MA adducts by adding an excess of monofunctional thiol which leads to chain scission in the presence of catalytic base, making the polymer fully degradable in response to a chemical signal.<sup>75</sup> In another example, J. L. Bernardes and coworkers have demonstrated the chemoselectivity of  $\beta^{\prime}$ -substituted MAs (Scheme 5.3, right). By adding a MA with a sulfinate leaving group, they show a selective modification of the most nucleophilic lysine of a native protein, leaving cysteine and less nucleophilic lysines untouched. This work offers a strategy to chemoselectively introduce a clickable handle onto native proteins, which can further be functionalised with a fluorescent dye.<sup>72</sup> Despite their versatile applications,  $\beta^{\prime}$ -substituted MAs also suffer from some downsides, such as a loss of double bond functionality upon double additions.<sup>76</sup> Furthermore, the reactivity and high reversibility of these species may lead to a decreased stability of the desired products.<sup>58,76</sup> Lastly, double bonds typically tend to be relatively labile groups and may degrade over time thermally, in light, or in the presence of radical sources, making the addition of inhibitors required for prolonged storage.<sup>77,78</sup>

Besides these findings on  $\beta^{\prime}$ -substituted MAs, significant work has been undertaken on  $\alpha$ - and  $\beta$ -substituted MAs as well.<sup>66,67,75,79–82</sup> On the one hand, MAs with a leaving group in  $\alpha$ -position cannot undergo subsequent addition-elimination reactions.  $\beta$ -substituted MAs on the other hand can react similarly to  $\beta^{\prime}$ -substituted MAs. One famous example of  $\beta$ -substituted MAs are Meldrum's Acid derivatives developed by the group of Eric Anslyn mentioned above (Scheme 5.1, left),<sup>24</sup> commonly applied in the formation of cyclic peptides, as well as click-declick plastics.<sup>24,25,83</sup>

However, due to the steric hindrance that leaving groups in  $\beta$ -position present towards incoming nucleophiles, we decided to start working with the  $\beta^{\prime}$ -substituted analogues. We sought to use their interesting features to derive new out-of-equilibrium fuel-driven CRNs that can have potential applications in a wide range of fields.

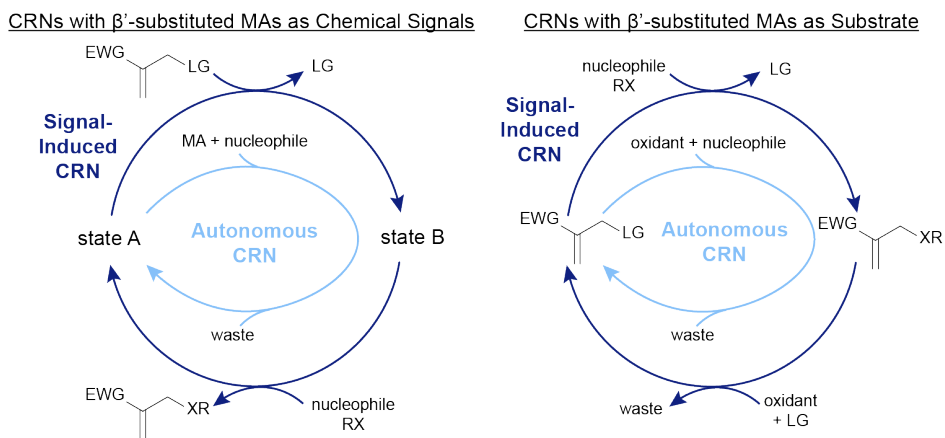


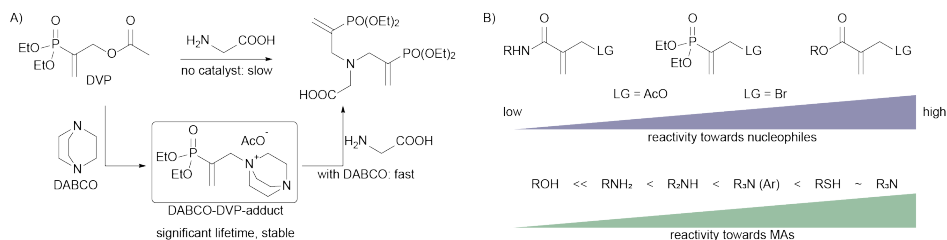
**Figure 5.2:** Signal-induced and autonomous CRNs in which the  $\beta^{\prime}$ -substituted MAs are used as A) chemical signals, and B) substrates. The different properties of state A and state B lead to various applications of these CRNs explained in detail below.

The following sections will showcase, in more detail, the progress we have made in applying this chemistry in the context of CRNs (Figure 5.2). We have grouped our works

by area of application. Figure 5.2 also gives a comprehensive summary of the nature of the systems we present: they can be classified by whether the  $\beta'$ -substituted MA is the chemical signal (top), or the substrate (bottom) of the CRN. Furthermore, a dark-blue colour indicates a signal-induced CRN, whereas light-blue colour indicates an autonomous CRN. We will start by giving a brief overview of how we conceived some of the ideas and concepts for these projects and what we learned about the reactivity of the species involved along the way.

### MAAs as a basis for CRN chemistry and their reactivity

We initially looked at  $\beta'$ -substituted MAAs through the lens of catalysis and host-guest chemistry. We studied how host-guest chemistry can be used to encapsulate 1,4-diazabicyclo(2.2.2)octane (DABCO), which catalyses the addition-substitution reaction of nucleophiles on  $\beta'$ -substituted vinylphosphonates, and hence tune catalytic rates.<sup>84</sup>  $\beta'$ -substituted vinylphosphonates and their reactions with nucleophiles have been studied previously,<sup>85,86</sup> and we found that cucurbit[7]uril (CB[7]) can indeed be used to tune the organocatalytic activity of DABCO.<sup>84</sup> Yet, what appeared in these experiments was that DABCO is a mediocre catalyst at best. We regularly observed a build-up of the catalytic DABCO-MA intermediate (Scheme 5.4A), which could even be isolated, due to its relatively low reactivity. Although these amine-MA adducts, their reactions, and applications in synthesis have been studied previously,<sup>87–89</sup> they have not been applied in the context of CRNs before. As these species are charged, have a significant lifetime and can react with other nucleophiles to recover the initial, uncharged amine species, we hypothesised that such catalytic intermediates could be excellent candidates as substrates in a CRN which can switch between uncharged (state A, Figure 5.1, 2A) and charged (state B, Figure 5.1, 2A) species in response to a chemical signal. This finding, that  $\beta'$ -substituted MAAs can be used to cycle tertiary amines between an uncharged and charged state reversibly, became the starting point for the projects outlined below.



**Scheme 5.4:** A) Diethyl( $\alpha$ -acetoxymethyl) vinylphosphonate (DVP) reacts slowly with glycine to form a double adduct of DVP on glycine. In the presence of DABCO, this reaction proceeds roughly 15-fold faster via a DABCO-DVP adduct, which possesses a significant lifetime and can be isolated. B) Depending on the electron-withdrawing group (EWG) and leaving group (LG), MAAs possess vastly different reactivity towards nucleophiles, just as different nucleophiles show different reactivity towards MAAs. These trends can act as a general guideline for the reader.

These early experiments with  $\beta'$ -substituted MAAs also revealed some general trends regarding stability and reactivity that became useful for future projects (Scheme 5.4B). Along those lines, extensive studies from the group of S. Thayumanavan, as well as in

our lab, showed that both the electron-withdrawing group (EWG) and leaving group on the MA, as well as the characteristics of the nucleophile strongly impact the overall kinetics of the reactions and stability of the involved species.<sup>13,63,68,76,84,90</sup> While allylic amides were relatively unreactive, diethyl( $\alpha$ -acetoxymethyl) vinylphosphonate (DVP) was found to have intermediate reactivity and allylic esters were found to be most reactive, with the acetate leaving group leading to slower addition-substitution reactions than the bromide leaving group (Scheme 5.4B, top). Among nucleophiles, we found aliphatic tertiary amines to react fastest, at comparable rates to thiols, which react faster than aromatic tertiary amines, secondary amines, primary amines, and lastly alcohols, which do not show any meaningful reactivity with  $\beta'$ -substituted MAs (Scheme 5.4B, bottom).

### MA-based CRNs for material applications

Inspired by the findings regarding lifetime and stability of DABCO-MA adducts, we proceeded to explore potential material applications for this new chemistry. While activation of building blocks to form transient materials with a chemical signal is common, deactivation reactions are most commonly driven by hydrolysis or pH changes.<sup>30,32,35</sup> We envisioned that the chemistry of  $\beta'$ -substituted MAs could be another valuable asset in the systems chemist's toolbox to chemically control both activation and deactivation reactions in a CRN coupled to a material's properties.

Starting from small molecule studies, we decided to work with DVP and tertiary amines. We found that apart from DABCO, pyridine is another especially suitable amine to react with DVP to yield a relatively stable, charged pyridine-DVP adduct, that can further react with other nucleophiles to recover the initial, uncharged pyridine species (Figure 5.3).<sup>13</sup> Furthermore, we found that strong nucleophiles, i.e. thiols, react very fast and with high yields with charged amine-DVP adducts, recovering the uncharged amine and forming a thiol-DVP adduct as waste. Mixing DVP with a substoichiometric amount of amine and adding the same amount of thiol in four portions led to a repeated cycling of the amine between its charged adduct and its free, uncharged state. Hence, tertiary amines such as DABCO and pyridine could be activated to yield a charged state through the addition of DVP and deactivated again to the uncharged state through addition of a thiol in a signal-induced CRN. Weaker nucleophiles such as threonine, a primary amine, react with the amine-DVP adduct much more slowly than thiols, and with somewhat lower yields, allowing for control over the lifetime of the activated species. This is due to the relatively high  $pK_a$  (9.1) of threonine,<sup>13</sup> which means that the majority is in its protonated state at physiological pH. Mixing DVP, pyridine and threonine, we observed an autonomous operation of the CRN, with a transient formation of the charged pyridine-DVP adduct. Varying the ratios between chemical signal, pyridine and threonine allowed for a control over the amplitude of the activation step.<sup>13</sup>

With the chemistry in hand for a new CRN that can switch between an uncharged state A and a charged state B, we applied these reactions on the material scale. We chose to apply this chemistry to micelles, which have been previously shown to undergo oscillatory behaviour and function as nanoreactors or stimuli-responsive drug delivery systems, in response to chemical signals within CRNs.<sup>5-8</sup> DMA-VP-block copolymers were used to

make amphiphilic micelles, confirmed via DLS and TEM. *N,N*-dimethylacrylamide (DMA) was used as the water-soluble block, while 4-vinylpyridine (VP) was used as the active block that can switch between a charged (Figure 5.3, top right) and uncharged state (Figure 5.3, top left). Vinylpyridine is especially attractive due to its  $pK_a$  of  $5.0 \pm 0.3$ , meaning that it is uncharged at physiological pH, making it the hydrophobic block in its non-activated state.<sup>13</sup> To probe the signal-induced (dis)assembly of the micelles, an excess of DVP was added to the micelle solutions. We found the micelles to degrade fully, due to the formation of charges in the hydrophobic block via reaction of pyridine units with DVP, within approx. 105 hours. Addition of thiol very swiftly (approx. 1 hour) leads to the reformation of the micelles, which then degraded again due to the presence of an excess of DVP. We repeated the disassembly-assembly cycle 4 times, until all of the DVP had depleted. <sup>1</sup>H-NMR studies revealed that even relatively low conversions of pyridine units to their charged pyridine-DVP adducts (approx. 28%) are sufficient to induce micellar disassembly due to charge repulsion.<sup>13</sup>

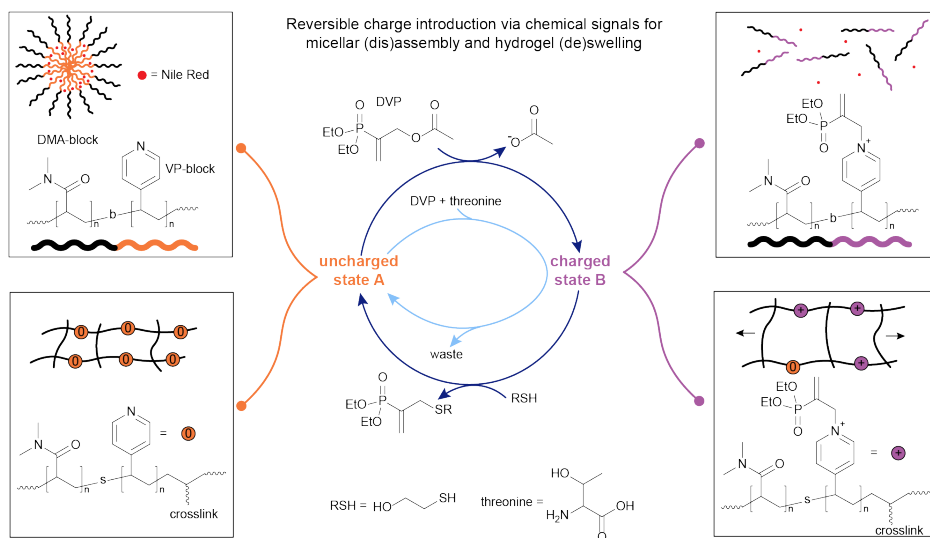


**Figure 5.3:** The addition of DVP on pyridine was applied to DMA-VP block copolymers (top left, uncharged state A) to trigger the disassembly of micelles encapsulating Nile Red (top left). A nucleophile (thiol or amine) was applied to switch from the disassembled charged state (top right, charged state B) back to state A. Also, this chemistry was applied to crosslinked, DMA-VP statistical copolymers (bottom left) to switch between a swollen (bottom right) and unswollen (bottom left) gel state. The letter b denotes a block-, the letter s a statistical copolymer. Experiments typically conducted in pH 7.4 phosphate buffer (0.1 M for signal-induced, 0.5 M for autonomous CRN).

Next, we tested whether loaded micelles can undergo the same (dis)assembly steps, leading to the release and re-uptake of a cargo. For this, Nile Red (NR) dye was chosen, due to its strong fluorescence in hydrophobic environments, which is quenched in water.<sup>91</sup> We managed to reproduce the behaviour found for the unloaded micelles: The loaded micelles released 95% of NR within 54 hours after introducing DVP, due to micellar disassembly, whereas fluorescence increases rapidly, within 4 hours, upon introduction

of a thiol, due to re-assembly of the micelles and incorporation of NR into the hydrophobic core (Figure 5.3, top left and right). Although repeated thiol additions led to repeated (dis)assembly cycles, the dampening of the fluorescence response was stronger than conversion-dampening in unloaded micelles, due to waste accumulation in the hydrophobic micelle blocks, leading to less NR uptake over several additions of DVP. Similar to the unloaded micelles, we tried to achieve a transient NR release with threonine as a nucleophile, instead of a thiol. Indeed, upon simultaneous addition of DVP and threonine to the loaded micelles, 83% cargo were released over the following 19 hours, upon which fluorescence started to increase again, indicating cargo-reuptake to near original levels over the following 19 days.<sup>13</sup>

In addition to the micellar system, we became interested in the (de)swelling of crosslinked hydrogels in response to the reversible introduction of a charge with this MA chemistry (Figure 5.3, bottom left and right). For this application, we synthesised statistical DMA-VP copolymers with blocks of bis(acrylamide) crosslinkers. These block-shaped gels swell in aqueous conditions (90wt% water), due to the presence of the hydrophilic DMA units. Upon introduction of equimolar amounts of DVP, relative to pyridine units, a size increase of  $106 \pm 16\%$  was observed over 96 hours, due to the introduction of charges in the network, leading to increased water uptake and charge repulsion. Upon addition of a thiol, deswelling was observed over a similar timescale, back to roughly the initial size of the gels, demonstrating the time-programmed deswelling of crosslinked hydrogels. Similarly, to showcase an autonomous (de)swelling behaviour, we introduced 2.1 eq. DVP and 8.0 eq. threonine simultaneously. Over 168 hours, the gels expanded by  $80 \pm 11\%$ , and reached initial dimensions after 504 hours.<sup>13</sup>

Concluding, these results show the successful applications of  $\beta'$ -substituted MAs for both the time-programmed, and autonomous introduction and removal of charges on tertiary amines in response to chemical signals. These findings were applied both to the (dis)assembly of micelles, showcasing the release and re-uptake of NR as a model cargo, as well as the (de)swelling of crosslinked hydrogels.

With a system in hand that offers precise and fully reversible control over charge introduction on tertiary amines, we decided to look at Complex Coacervate Core Micelles (C3M) as another interesting area in which to apply the chemistry of  $\beta'$ -substituted MAs (Figure 5.4).<sup>90</sup> C3Ms form via coacervation of positively and negatively charged polyelectrolytes, with neutral, water-soluble blocks attached to at least one of those polyelectrolytes.<sup>9-12</sup> Unlike traditional micelles, the hydrated, water-insoluble cores of C3Ms are capable of encapsulating, protecting, and releasing complex biomolecules for applications in stabilised dispersions, and therapeutic delivery systems, among others.<sup>92-94</sup> Although C3Ms have been extensively studied in the past,<sup>10</sup> precise control over their lifetime in response to chemical signals at physiological pH has not been achieved previously. We decided to work with a VP-co-DMA-b-DMA polymer (Figure 5.4) and apply the same addition-substitution chemistry we previously explored,<sup>13,84</sup> in the presence of polyanionic species. We decided to incorporate DMA units into the VP block as well, to avoid micelle formation in the uncharged state (Figure 5.4 left), as observed in the previous project.<sup>13</sup> This process starts by combining the uncharged polymer with a polyanion (in this case PSS, poly(sodium 4-styrenesulfonate), yielding a homogeneous polymer solution. Upon introducing positive charges on the polymer through addition of

a  $\beta'$ -substituted MA (DVP or ME), the charged copolymer can then form C3Ms with the polyanion in solution (Figure 5.4 right). The addition of different nucleophiles, i.e. a thiol or amine, can revert the C3Ms back to the disassembled state, in a signal-induced or an autonomous manner (Figure 5.4).<sup>90</sup> Mixing the neutral polymer with one equivalent of MA and a sulfonate-functionalised polyanion in buffer at physiological pH led to the formation of the charged polymer (Figure 5.4, charged state B). For this system, we studied two MA species, DVP and 2-(acetoxymethyl)acrylate (ME) (Figure 5.4), with different electrophilicities. With DVP, 65 % of the VP units were functionalised after 120 hours, whereas ME reacted with 80 % of VP units in just 5 hours. This shows that the reactivity of the chemical signal can be used to tune the kinetics of the forward reaction, introducing charges on the polymer. Upon this functionalisation, these block copolymers form C3Ms by complexation with the polyanion, which was confirmed via DLS and TEM. To study the signal-induced disassembly of these C3Ms, a thiol was added. This resulted in the swift recovery of the uncharged starting polymer within 5 minutes, with generation of the thiol-functionalised waste. This system was also run under physiological conditions at 37.5 °C. Furthermore, we found that both systems can be cycled between a solution and an assembled C3M state at least twice.<sup>90</sup>

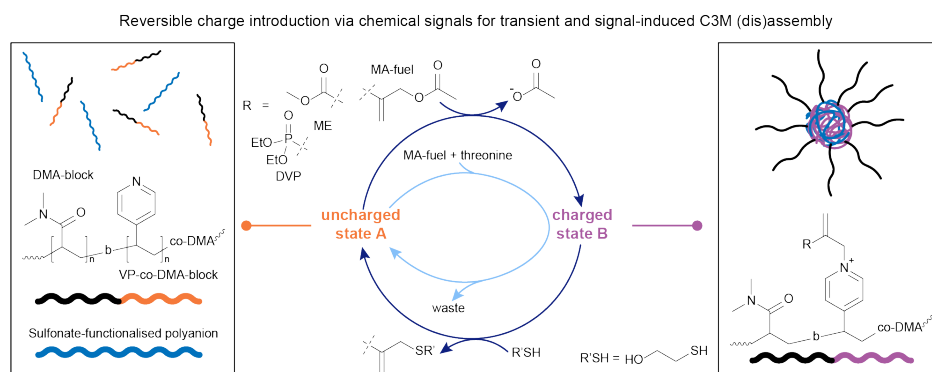


**Figure 5.4:** 2-(Acetoxymethyl)acrylate (ME) and DVP were applied to solution of DMA-VP block copolymers with sulfonate-functionalised polyanions (poly(sodium 4-styrenesulfonate), PSS) (left, uncharged state A) to form Complex Coacervate Core Micelles (C3Ms, right, charged state B). A nucleophile was applied to switch back to state A, both in a signal-induced and autonomous manner. The letter b denotes a block-copolymer. Experiments typically conducted in pH 7.4 phosphate buffer (0.1 M for signal-induced, 0.25 M for autonomous CRN).

Upon establishing that a signal-induced assembly and disassembly of C3Ms is possible by adding 1.0 eq. of MA-signal (assembly) and 1.0 eq. of a thiol (disassembly), we investigated the transient disassembly of C3Ms by adding an excess of MA-signal. Indeed, in the presence of 3.0 eq. of MA-signal, the addition of 1.0 eq. thiol resulted in the temporary disassembly of the C3Ms. Subsequently, the polymers autonomously returned to an assembled C3M state in 2 hours in the presence of ME. When DVP was used instead, this process took 193 hours. The cross-reactivity between thiol and MA species was minimal in both cases due to the preferred reactivity with the pyridine-MA adduct over the MA-signal, demonstrating that this system can also be run autonomously.

Vice versa, we found that adding an excess of a weak nucleophile, in this case threonine, with which the deionisation reaction is slower than the ionisation step, can lead to the transient assembly of C3Ms upon addition of small portions of MA. Again, DVP led to a more long-lived transient assembly of C3Ms than ME, allowing autonomous time control over the assembled regime.

After studying how  $\beta'$ -substituted MAs with different residues can be used in combination with nucleophiles of different strength to achieve the signal-induced, as well as autonomous assembly and disassembly of C3Ms, we decided to apply this knowledge to create injectable, coacervate polymer hydrogels (Figure 5.5). In this more recent work, we functionalised a DMA-polymer with VP-DMA-blocks on both ends. These reactive ends enable the formation of C3Ms in the presence of polyanions (in this case PAMPS<sub>236</sub>, poly(sodium 2-acrylamido-2-methylpropane sulfonate)), upon application of an MA, acting as crosslinks.<sup>63</sup> Although CRN-based control of coacervation has previously been shown and applied in different fields,<sup>95-97</sup> this is the first example that demonstrates chemically induced assembly and disassembly of C3Ms (Figure 5.5 right and left, respectively) under physiological conditions on a macroscopic scale, i.e. a gel. Similar to previous works, we found the triblock copolymer (Figure 5.5, left) to react with 1.0 eq. of ME to about 80 % conversion over 5 hours, with higher conversions achievable with an excess of ME. The deactivation step with pyrrolidine proceeded within five hours to yield approx. 90 % uncharged state A. Combining the triblock copolymers with a polyanion and adding 1.0 eq. of ME led to the formation of a macroscopic gel within 30 minutes, and a return to solution state within 5 minutes of adding pyrrolidine. We managed to cycle between the gel and sol states three times with subsequent additions of ME and pyrrolidine, and furthermore demonstrated an autonomous behaviour upon adding an excess of ME, followed by stoichiometric additions of pyrrolidine (Figure 5.5, central, light blue cycle). Additionally, adding larger amounts of ME leads both to stronger gels, as well as shorter gelation times (between 30 and 90 minutes), enabling a degree of control over gel properties by tuning the amount of chemical signal applied to the system, as well as the initial concentration of the triblock copolymer. Rheology measurements showed that the gels can also be destroyed with high strain (> 200 %), rapidly recovering to their initial strength upon lowering the strain back to 5 %, demonstrating the self-healing nature of these materials. This inspired us to apply these materials as injectable hydrogels. Indeed, we found that due to their destruction under high shear forces and rapid self-healing, the gels could be injected through needles ranging from 20G down to 26G (0.9 – 0.45 mm), making these materials good candidates for biomedical applications, such as drug delivery. Another important criterion is the degradability of the injected material under physiological conditions. We show that the gels easily degrade in cell culture medium at 37 °C within 2 hours, whereas their degradation in phosphate buffer is much slower (approx. 24 hours). Although their cytotoxicity is relatively high due to the presence of ME, we found that substituting ME with DVP resulted in a significantly lower cytotoxicity of the gel system.<sup>63</sup>

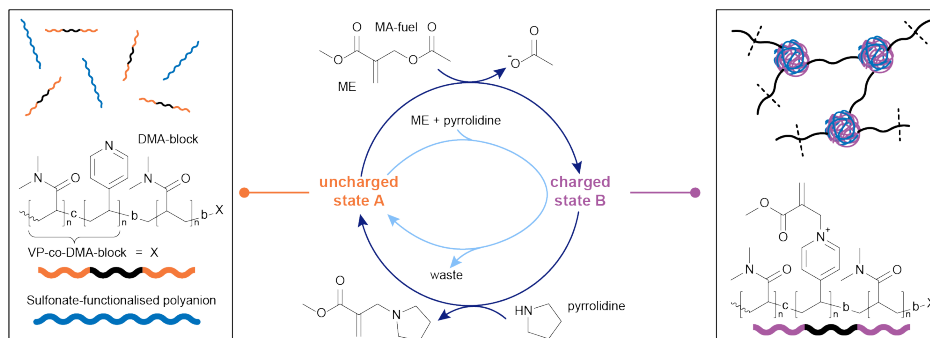


**Figure 5.5:** ME was applied to a solution of VP-DMA-block-DMA-block-VP-DMA triblock copolymers and sulfonate-functionalised polyanions (PAMPS<sub>236</sub>, poly(sodium 2-acrylamido-2-methylpropane sulfonate)) (left, uncharged state A) to yield a C3M-based, injectable, crosslinked hydrogel (right, charged state B). Pyrrolidine was applied, both in a signal-induced and autonomous manner, to return to the uncharged solution state A. The letter c denotes a copolymer, the letter b denotes a block-copolymer. Experiments typically conducted in 0.1 – 0.15 M pH 7.4 phosphate buffer.

In a follow-up work, we wanted to further demonstrate the relevance of this chemistry in cellular environments due to the low cytotoxicity of DVP. We became interested in looking at how reversible cationisation can be used to encapsulate plasmid DNA (pDNA) and shuttle it into cells, leading to enhanced gene expression. This work used polymers that had been cationised by reaction with a MA prior to complexation with DNA. Unlike the other results presented in this Feature Article, this work does not apply MA chemistry in the scope of a full CRN. The backward process, i.e. to decationisation of charged pyridine units, was used to selectively release pDNA in cells.<sup>98</sup> The core idea of this project is based on the relatively low concentration of nucleophiles in extracellular medium, whereas the concentration of amino acids and thiols, specifically glutathione, is much higher in intracellular medium, leading to the release of pDNA after transfer into the cell. We show in model experiments that pDNA can be released from the cationic polymer DNA complexes (polyplexes) within 4 hours in cell culture medium and within 1 hour in the presence of 1 mM glutathione.<sup>98</sup> Permanently cationised control polyplexes do not lead to a pDNA release in the presence of nucleophiles. Further, a range of micelles, polyplexes and lipopolyplexes were prepared. We found that the lipopolyplexes transfect cells and demonstrated with control experiments that decationisation in the cellular medium is responsible for the enhanced gene expression. Besides these findings, this work also shows the significantly reduced cytotoxicity of the reversibly cationised polyplexes, as well as the cationization reagent DVP, compared to permanent cations and other commonly applied reactants often applied in CRNs.<sup>98</sup> These results extend the scope of applications of MA chemistry beyond material applications into the biological realm, overcoming some of the previous challenges such as high cytotoxicity.

## MA-based CRNs for signal amplification

In more recent work, we looked at different applications beyond the material scope and focused on signal amplification. The amplification of chemical signals has many promising applications,<sup>99–101</sup> but systems driven only by simple, chemical reactions remain few and often some downsides remain such as high background reactivity or low sensitivity.<sup>99,102–106</sup> We chose to use  $\beta'$ -substituted MAs for the protection of phosphines ( $\text{PR}_3$ ), in the form of phosphonium salts. These salts can respond to a chemical signal (thiol), yielding a free phosphine which can reduce disulfides to the corresponding free thiols (Figure 5.6, see also Notes for explanation of thiol-adduct structure).<sup>107</sup> Due to the stoichiometry of the reduction of disulfides with phosphines, each phosphine can liberate two thiol molecules, of which one can in turn release a new phosphine, making this cycle self-propagating, amplifying the initial thiol signal and producing a thiol-functionalised MA and a phosphine oxide as waste species.

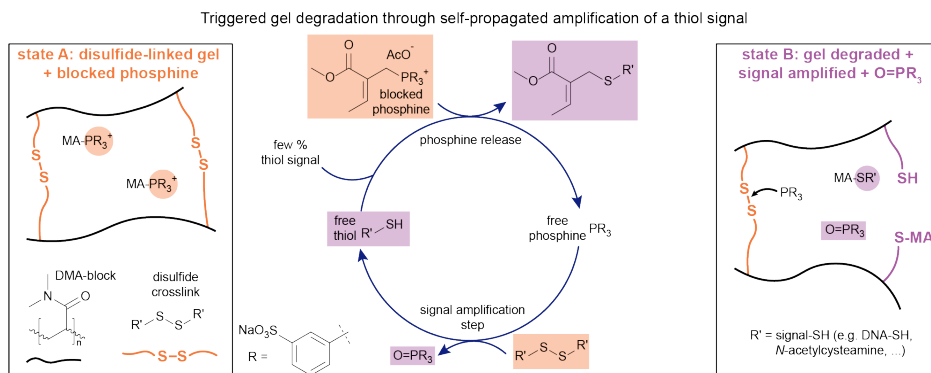


**Figure 5.6:** Blocked phosphine was applied in a crosslinked disulfide-based gel (state A). The addition of a thiol signal (the analyte) leads to the amplified release of phosphine and more thiol, degrading the network over time (state B), both in response to a chemical (thiol addition) and a mechanical signal (force-generated thiol radicals as a thiol). Experiments typically conducted in 0.1 M pH 7.6 phosphate buffer.

Kinetic studies on the system containing blocked phosphine and disulfide (Figure 5.6, state A), supported by modelling the kinetics, proved the concept and revealed the influence that the ratios of reagents have on the reaction progress.<sup>107</sup> The reaction was primarily tracked studying the amount of free phosphine over time, which is the transient species that gets first released upon introducing the thiol signal, then consumed by reducing the disulfide. We found that adding more signal to the system leads to an earlier and more pronounced peak of released phosphine ( $\text{PR}_3$ ). Having more disulfide present in the system at the start leads to an earlier, but less pronounced peak of free phosphine, while starting with more blocked phosphine leads to a bigger accumulation of free phosphine over time. Having understood the role that the chemical composition of the system plays, we synthesised a dimethylacrylamide network gel crosslinked by disulfide bonds, containing blocked phosphine. We used this gel to test whether these networks can degrade in response to a thiol signal, *N*-acetyl cysteamine in this case. Indeed, upon introducing 5 % of a thiol signal, gel degradation was observed within 168 hours, whereas

the reference gel remained stable for over 13 days. Equally, for several biologically relevant thiols, glutathione, bovine serum albumin, and thiol functionalized DNA, gel degradation was also observed with sensitivities ranging down to 0.132  $\mu\text{M}$  of thiol signal. Although lower signal concentrations (e.g. 0.001 % thiol functionalized DNA vs. 1 % glutathione) also led to slower kinetics, eventual degradation can still be observed at such low signal input. Finally, the impact of mechanical damage on the gels was investigated. We found that cutting the gels significantly shortens their time to full degradation. The results indicate that this is due to force-generated thiyl radicals which can abstract H-atoms from the solvent surroundings, generating a thiol signal in situ, or adding directly to the double bond of the blocked phosphine, generating a radical which can release the phosphine. This work demonstrates the potential of  $\beta^1$ -substituted MAs to be applied in signal amplification and as sensors for both chemical and mechanical signals.

### MA-based CRNs for oxidation-driven pathway control and MA recovery

In all the previously described works, the purpose of the MA was to (transiently) introduce a positive charge in the system. Upon addition of a nucleophile, the MA moiety is then transformed into a waste product. We wondered whether we can also use these  $\beta^1$ -substituted MAs as a substrate, maintaining the active MA moiety throughout the CRN and using it to affect product speciation, as well as maintain the active MA site for further modification reactions. Typically, these MAs can be applied in chemical switches,<sup>68</sup> however reverting back to the original state is challenging. As evident from our previous works, the reactions with strong nucleophiles such as thiols lead to a thermodynamic sink and the reaction with weaker nucleophiles such as amines to recover starting compounds is not possible.

Inspired by findings on protein functionalisations,<sup>57,58,72,73</sup> and our previous efforts to design a CRN with MAs as substrates,<sup>31</sup> we envisioned that oxidation chemistry can close the gap between  $\beta^1$ -thiol-functionalised and  $\beta^1$ -amine-functionalised MAs, by oxidising the thiol-functionalised species to a more electron-deficient MA, which enables the addition of an amine and recovery of the initial amine-MA (Figure 5.7, see also Chapter 6 of this Thesis).<sup>76</sup>

Starting from exploring the separate steps of this network, we found that proline, as well as other primary and secondary amines, can recover the amine-functionalised MA from the sulfoxide- and sulfone-MAs with yields of 55 to 83 %.<sup>76</sup> Combining all reactions in a signal-induced cycle, we found that in the presence of the strong oxidant Oxone, sulfone-MA forms and subsequently proline-MA recovers in a yield of 55 % (Figure 5.7, full cycle). This system can be run at least twice with similarly high recovery yields. Although this cycle works in a signal-induced manner, it cannot be run autonomously due to cross-reactivity of free thiol and oxidant. Even in the signal-induced sulfone cycle, we observed a range of side reactions such as oxidation of proline and proline-MA,<sup>76</sup> which made us wonder whether some of these reactions can be mitigated by employing weaker oxidants. Studying medium-strength oxidants such as  $\text{NaClO}_2$ , we found that indeed, proline-MA can also be recovered in yields of up to 83 % with fewer oxidative side reactions occurring (Figure 5.7, central pathway). Effectively, this creates a shunt to the full cycle in response

the chemical potential of the oxidant, endowing the system with an adaptability similar to that found in shunts in nature, such as the glyoxylate shunt or Cytochrome P450 shunt. To our surprise we found that even in the presence of weak oxidants such as  $\text{KBrO}_3$ , the system also recovers proline-MA, not through oxidation of the sulfide-MA, but through oxidation of free thiol from the equilibrium between the sulfide- and proline-MA (Figure 5.7, left pathway). Higher oxidation states and most of the side reaction found in the full cycle are completely bypassed in the presence of weak oxidants. Furthermore, the kinetics of the sulfide shunt are significantly slower than those found in the full cycle or the sulfoxide shunt.<sup>76</sup>

Redox-driven pathway bias in a CRN based on MA-substrates

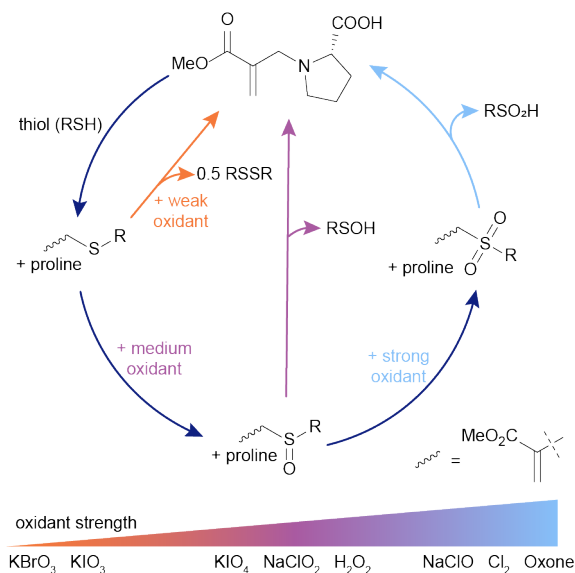


**Figure 5.7:** Proline-functionalised MA reacts with a thiol to form sulfide-MA. In the presence of strong oxidants, the sulfide-MA is activated towards nucleophilic attack via sulfone-MA, and proline-MA can be recovered (full cycle, light blue line). In the presence of weaker oxidants, two shunts open up, enabling the recovery of proline-MA via sulfoxide-MA (central pathway, purple line), as well as directly through sulfide-MA (left pathway, orange line), with different kinetics and side products compared to the full cycle. Experiments typically conducted in 9/1 0.5 M phosphate buffer (pH 7.0 – 8.0) / DMF.

This CRN enables the use of  $\beta'$ -substituted MAs as the substrate and hence allows for their recovery. Further, we observed the presence of two different shunts to the full cycle in response to the strength of the oxidant employed. This leads to different CRN kinetics, side reaction profiles, and product speciation in response to a chemical stimulus, similar to shunts found in nature. These findings promise new applications for the exploration of CRN behaviour, transient materials and catalyst release.

## Conclusions

Chemical Reaction Networks (CRNs) are a great tool for systems chemists to study the complexity, adaptability, and responsiveness found in nature. They give insights into the underlying principles and open up possibilities to implement these principles in synthetic materials. Although previous works in this area show great progress and many promising applications as a result, a lack of signal-responsiveness, operation under non-physiological conditions, side reactions, and waste accumulation remain common issues in many CRNs. We have applied a special group of Michael acceptors (MAs),  $\beta'$ -substituted MAs, to develop two new types of CRNs. Using  $\beta'$ -substituted MAs as a chemical signal, the first type of CRN presents a highly versatile way to reversibly introduce charges on tertiary amines, both in a signal-induced and autonomous manner, for the application in chemical signal-based control over the behaviour of block copolymer micelles, C3Ms, hydrogels, and DNA polyplexes. Further, we show how this chemistry can also be used for signal amplification, demonstrating applications in naked-eye analyte detection. In another type of CRN, we apply these MAs as a substrate instead of a chemical signal, and show precise redox-based control over the pathway the CRN takes, its kinetics, and side reaction profile. We believe that this chemistry is extremely versatile and the works we have presented here are only the start of more exciting applications in different areas. Further, we believe that the reduced cytotoxicity of these species, specifically DVP, compared to other commonly used reagents in CRNs, can act as an entry into interactions of synthetic CRNs with living systems. We are currently working on exploring further projects in the fields of host-guest chemistry, where we have recently demonstrated application in control over supramolecular aggregate formation,<sup>108</sup> triggered drug and catalyst release, transient materials, and beyond. We hope this overview can give researchers an understanding of the scope of applications and the reactivity of the involved species and aid in further discoveries based on novel CRNs that make use of this versatile chemistry.

## Conflicts of interest

There are no conflicts to declare.

## Acknowledgements

This work has received funding from the European Union's Horizon 2020 research and innovation programme under the Marie Skłodowska-Curie grant agreement No 812868, and the European Research Council (ERC Consolidator Grant 726381). Further, we would like to thank all the people involved in the projects discussed in this Feature Article: Benjamin Klemm, Reece W. Lewis, Irene Piergentili, Guotai Li, Mariano Macchione, Yucheng Wan, Bowen Fan, Bohang Wu, Ardeshir Roshanasan, Jan H. van Esch, Aswin Muralidharan, Pouyan E. Boukany (TU Delft), Anastasiia V. Shariko, Thomas M. Hermans (University of Strasbourg), Yifan Gao, Jianan Huang, Junyou Wang, Martien A. Cohen Stuart (East China University of Science and Technology).

## Notes

Note 1: The structure of the thiol-MA adduct in Figure 5. 6 may suggest a direct substitution of the phosphine on the  $\beta$ -carbon instead of on the  $\beta'$ -carbon like in the other projects. This is however not the case. The thiol attacks adjacent to the methyl group. As the product is dynamic however, it will slowly equilibrate to the thermodynamically more stable product depicted in Figure 5. 6 in the presence of free thiols. For more details, see the Supplementary Information of the cited work.

## References

1. Whitesides, G. M. & Ismagilov, R. F. Complexity in chemistry. *Science*. **284**, 89–92 (1999).
2. Ashkenasy, G., Hermans, T. M., Otto, S. & Taylor, A. F. Systems chemistry. *Chem. Soc. Rev.* **46**, 2543–2554 (2017).
3. De, S. & Klajn, R. Dissipative Self-Assembly Driven by the Consumption of Chemical Fuels. *Adv. Mater.* **30**, 1706750 (2018).
4. Sharko, A., Livitz, D., De Piccoli, S., Bishop, K. J. M. & Hermans, T. M. Insights into Chemically Fueled Supramolecular Polymers. *Chem. Rev.* **122**, 11759–11777 (2022).
5. Yoshizawa, T., Onoda, M., Ueki, T., Tamate, R., Akimoto, A. M. & Yoshida, R. Fabrication of Self-Oscillating Micelles with a Built-In Oxidizing Agent. *Angew. Chem. Int. Ed.* **59**, 3871–3875 (2020).
6. Würbser, M. A., Schwarz, P. S., Heckel, J., Bergmann, A. M., Walther, A. & Boekhoven, J. Chemically Fueled Block Copolymer Self-Assembly into Transient Nanoreactors. *ChemSystemsChem* **3**, e2100015 (2021).
7. Hao, X., Sang, W., Hu, J. & Yan, Q. Pulsating Polymer Micelles via ATP-Fueled Dissipative Self-Assembly. *ACS Macro Lett.* **6**, 1151–1155 (2017).
8. Rapoport, N. Physical stimuli-responsive polymeric micelles for anti-cancer drug delivery. *Prog. Polym. Sci.* **32**, 962–990 (2007).
9. Gucht, J. van der, Spruijt, E., Lemmers, M. & Cohen Stuart, M. A. Polyelectrolyte complexes: Bulk phases and colloidal systems. *J. Colloid Interface Sci.* **361**, 407–422 (2011).
10. Sing, C. E. & Perry, S. L. Recent progress in the science of complex coacervation. *Soft Matter* **16**, 2885 (2020).
11. Harada, A. & Kataoka, K. Formation of Polyion Complex Micelles in an Aqueous Milieu from a Pair of Oppositely-Charged Block Copolymers with Poly(ethylene glycol) Segments. *Macromolecules* **28**, 5294–5299 (1995).
12. Voets, I. K., de Keizer, A. & Cohen Stuart, M. A. Complex coacervate core micelles. *Adv. Colloid Interface Sci.* **147–148**, 300–318 (2009).

13. Klemm, B., Lewis, R. W., Piergentili, I. & Eelkema, R. Temporally programmed polymer – solvent interactions using a chemical reaction network. *Nat. Commun.* **13**, 6242 (2022).
14. Postma, S. G. J., Vialshin, I. N., Gerritsen, C. Y., Bao, M. & Huck, W. T. S. Preprogramming Complex Hydrogel Responses using Enzymatic Reaction Networks. *Angew. Chem. Int. Ed.* **56**, 1794–1798 (2017).
15. Su, B., Chi, T., Ye, Z., Xiang, Y., Dong, P., Liu, D., Addonizio, C. J. & Webber, M. J. Transient and Dissipative Host–Guest Hydrogels Regulated by Consumption of a Reactive Chemical Fuel. *Angew. Chem., Int. Ed.* e202216537 (2023) doi:10.1002/anie.202216537.
16. Krieg, E., Bastings, M. M. C., Besenius, P. & Rybtchinski, B. Supramolecular polymers in aqueous media. *Chem. Rev.* **116**, 2414–2477 (2016).
17. Frisch, H., Unsleber, J. P., Lüdeker, D., Peterlechner, M., Brunklaus, G., Waller, M. & Besenius, P. PH-switchable ampholytic supramolecular copolymers. *Angew. Chem. Int. Ed.* **52**, 10097–10101 (2013).
18. Panja, S., Patterson, C. & Adams, D. J. Temporally-Programmed Transient Supramolecular Gels. *Macromol. Rapid Commun.* **40**, 1900251 (2019).
19. Heuser, T., Weyandt, E. & Walther, A. Biocatalytic Feedback-Driven Temporal Programming of Self-Regulating Peptide Hydrogels. *Angew. Chem. Int. Ed.* **54**, 13258–13262 (2015).
20. Liu, Y., Chouai, A., Degtyareva, N. N., Lutterman, D. A., Dunbar, K. R. & Turro, C. Chemical control of the DNA light switch: Cycling the switch ON and OFF. *J. Am. Chem. Soc.* **127**, 10796–10797 (2005).
21. Mayer, G. & Heckel, A. Biologically Active Molecules with a “Light Switch”. *Angew. Chem. Int. Ed.* **45**, 4900–4921 (2006).
22. Bléger, D. & Hecht, S. Visible-Light-Activated Molecular Switches. *Angew. Chem. Int. Ed.* **54**, 11338–11349 (2015).
23. Fabbrizzi, L. & Poggi, A. Sensors and switches from supramolecular chemistry. *Chem. Soc. Rev.* **24**, 197–202 (1995).
24. Diehl, K. L., Kolesnichenko, I. V., Robotham, S. A., Bachman, J. L., Zhong, Y., Brodbelt, J. S. & Anslyn, E. V. Click and chemically triggered declck reactions through reversible amine and thiol coupling via a conjugate acceptor. *Nat. Chem.* **8**, 968–973 (2016).
25. Johnson, A. M. & Anslyn, E. V. Reversible Macrocyclization of Peptides with a Conjugate Acceptor. *Org. Lett.* **19**, 1654–1657 (2017).
26. Smith, M. E. B., Schumacher, F. F., Ryan, C. P., Tedaldi, L. M., Papaioannou, D., Waksman, G., Caddick, S. & Baker, J. R. Protein modification, bioconjugation, and disulfide bridging using bromomaleimides. *J. Am. Chem. Soc.* **132**, 1960–1965 (2010).

27. Tena-Solsona, M., Rieß, B., Grötsch, R. K., Löhner, F. C., Wanzke, C., Käsdorf, B., Bausch, A. R., Müller-Buschbaum, P., Lieleg, O. & Boekhoven, J. Non-equilibrium dissipative supramolecular materials with a tunable lifetime. *Nat. Commun.* **8**, 15895 (2017).
28. Kariyawasam, L. S. & Hartley, C. S. Dissipative Assembly of Aqueous Carboxylic Acid Anhydrides Fueled by Carbodiimides. *J. Am. Chem. Soc.* **139**, 11949–11955 (2017).
29. Morrow, S. M., Colomer, I. & Fletcher, S. P. A chemically fuelled self-replicator. *Nat. Commun.* **10**, 1011 (2019).
30. Van Rossum, S. A. P., Tena-Solsona, M., Van Esch, J. H., Eelkema, R. & Boekhoven, J. Dissipative out-of-equilibrium assembly of man-made supramolecular materials. *Chem. Soc. Rev.* **46**, 5519–5535 (2017).
31. Fan, B., Men, Y., van Rossum, S. A. P., Li, G. & Eelkema, R. A Fuel-Driven Chemical Reaction Network Based on Conjugate Addition and Elimination Chemistry. *ChemSystemsChem* **2**, e1900028 (2020).
32. Wang, G. & Liu, S. Strategies to Construct a Chemical-Fuel-Driven Self-Assembly. *ChemSystemsChem* **2**, e1900046 (2020).
33. Singh, N., Lopez-Acosta, A., Formon, G. J. M. & Hermans, T. M. Chemically Fueled Self-Sorted Hydrogels. *J. Am. Chem. Soc.* **144**, 410–415 (2022).
34. Kariyawasam, L. S., Hossain, M. M. & Hartley, C. S. The Transient Covalent Bond in Abiotic Nonequilibrium Systems. *Angew. Chem. Int. Ed.* **60**, 12648–12658 (2021).
35. Boekhoven, J., Brizard, A. M., Kowlgi, K. N. K., Koper, G. J. M., Eelkema, R. & Van Esch, J. H. Dissipative self-assembly of a molecular gelator by using a chemical fuel. *Angew. Chem. Int. Ed.* **49**, 4825–4828 (2010).
36. Boekhoven, J., Hendriksen, W. E., Koper, G. J. M., Eelkema, R. & Van Esch, J. H. Transient assembly of active materials fueled by a chemical reaction. *Science.* **349**, 1075–1080 (2015).
37. Debnath, S., Roy, S. & Ulijn, R. V. Peptide nanofibers with dynamic instability through nonequilibrium biocatalytic assembly. *J. Am. Chem. Soc.* **135**, 16789–16792 (2013).
38. Borsley, S., Leigh, D. A. & Roberts, B. M. W. Chemical fuels for molecular machinery. *Nat. Chem.* **14**, 728–738 (2022).
39. Moshnikova, A. B., Afanasyev, V. N., Proussakova, O. V., Chernyshov, S., Gogvadze, V. & Beletsky, I. P. Cytotoxic activity of 1-ethyl-3-(3-dimethylaminopropyl)-carbodiimide is underlain by DNA interchain cross-linking. *Cell. Mol. Life Sci.* **63**, 229–234 (2006).
40. Perlmutter, P. *Conjugate Addition Reactions in Organic Synthesis.* (Pergamon Press, 1992).

41. Fleming, F. F. & Wang, Q. Unsaturated nitriles: Conjugate additions of carbon nucleophiles to a recalcitrant class of acceptors. *Chem. Rev.* **103**, 2035–2077 (2003).
42. Csákÿ, A. G., De La Herrán, G. & Murcia, M. C. Conjugate addition reactions of carbon nucleophiles to electron-deficient dienes. *Chem. Soc. Rev.* **39**, 4080–4102 (2010).
43. Worch, J. C., Stubbs, C. J., Price, M. J. & Dove, A. P. Click Nucleophilic Conjugate Additions to Activated Alkynes: Exploring Thiol-yne, Amino-yne, and Hydroxyl-yne Reactions from (Bio)Organic to Polymer Chemistry. *Chem. Rev.* **121**, 6744–6776 (2021).
44. Almaşi, D., Alonso, D. A. & Nájera, C. Organocatalytic asymmetric conjugate additions. *Tetrahedron Asymmetry* **18**, 299–365 (2007).
45. Zheng, K., Liu, X. & Feng, X. Recent Advances in Metal-Catalyzed Asymmetric 1,4-Conjugate Addition (ACA) of Nonorganometallic Nucleophiles. *Chem. Rev.* **118**, 7586–7656 (2018).
46. Sibi, M. P. & Manyem, S. Enantioselective Conjugate Additions. *Tetrahedron* **56**, 8033–8061 (2000).
47. Tokoroyama, T. Discovery of the Michael Reaction. *Eur. J. Org. Chem.* **2010**, 2009–2016 (2010).
48. Rapson, W. S. & Robinson, R. 307. Experiments on the Synthesis of Substances related to the Sterols. Part II. A new General Method for the Synthesis of Substituted cycloHexenones. *J. Chem. Soc.* 1285–1288 (1935).
49. Nair, D. P., Podgórski, M., Chatani, S., Gong, T., Xi, W., Fenoli, C. R. & Bowman, C. N. The Thiol-Michael addition click reaction: A powerful and widely used tool in materials chemistry. *Chem. Mater.* **26**, 724–744 (2014).
50. Fan, B., Zhang, K., Liu, Q. & Eelkema, R. Self-Healing Injectable Polymer Hydrogel via Dynamic Thiol-Alkynone Double Addition Cross-Links. *ACS Macro Lett.* **9**, 776–780 (2020).
51. Berne, D., Ladmiral, V., Leclerc, E. & Caillol, S. Thia-Michael Reaction: The Route to Promising Covalent Adaptable Networks. *Polymers.* **14**, 4457 (2022).
52. Lee, Y.-J., Kurra, Y. & Liu, W. R. Phospha-Michael Addition as a New Click Reaction for Protein Functionalization. *ChemBioChem* **17**, 456–461 (2016).
53. Freedy, A. M., Matos, M. J., Boutureira, O., Corzana, F., Guerreiro, A., Akkapeddi, P., Somovilla, V. J., Rodrigues, T., Nicholls, K., Xie, B., Jiménez-Osés, G., Brindle, K. M., Neves, A. A. & Bernardes, G. J. L. Chemoselective Installation of Amine Bonds on Proteins through Aza-Michael Ligation. *J. Am. Chem. Soc.* **139**, 18365–18375 (2017).
54. Reddi, R. N., Rogel, A., Resnick, E., Gabizon, R., Prasad, P. K., Gurwicz, N., Barr, H., Shulman, Z. & London, N. Site-Specific Labeling of Endogenous Proteins Using CoLDR Chemistry. *J. Am. Chem. Soc.* **143**, 20095–20108 (2021).

55. Bejan, D. S., Sundalam, S., Jin, H., Morgan, R. K., Kirby, I. T., Siordia, I. R., Tivon, B., London, N. & Cohen, M. S. Structure-guided design and characterization of a clickable, covalent PARP16 inhibitor. *Chem. Sci.* **13**, 13898–13906 (2022).
56. Gabizon, R. *et al.* Efficient Targeted Degradation via Reversible and Irreversible Covalent PROTACs. *J. Am. Chem. Soc.* **142**, 11734–11742 (2020).
57. Mitra, S. & Lawton, R. G. Reagents for the crosslinking of proteins by equilibrium transfer alkylation. *J. Am. Chem. Soc.* **101**, 3097–3110 (1979).
58. Liberatore, F. A., Comeau, R. D., McKearin, J. M., Pearson, D. A., Belonga, B. Q., Brocchini, S. J., Kath, J., Phillips, T., Oswald, K. & Lawton, R. G. Site-Directed Chemical Modification and Cross-Linking of a Monoclonal Antibody Using Equilibrium Transfer Alkylating Cross-Link Reagents. *Bioconjug. Chem.* **1**, 36–50 (1990).
59. Jackson, P. A., Widen, J. C., Harki, D. A. & Brummond, K. M. Covalent Modifiers: A Chemical Perspective on the Reactivity of  $\alpha,\beta$ -Unsaturated Carbonyls with Thiols via Hetero-Michael Addition Reactions. *J. Med. Chem.* **60**, 839–885 (2017).
60. Heal, W. P., Dang, T. H. T. & Tate, E. W. Activity-based probes: discovering new biology and new drug targets. *Chem. Soc. Rev.* **40**, 246–257 (2010).
61. Mulliner, D., Wondrousch, D. & Schüürmann, G. Predicting Michael-acceptor reactivity and toxicity through quantum chemical transition-state calculations. *Org. Biomol. Chem.* **9**, 8400–8412 (2011).
62. Fell, J. B. *et al.* Identification of the Clinical Development Candidate MRTX849, a Covalent KRASG12C Inhibitor for the Treatment of Cancer. *J. Med. Chem.* **63**, 6679–6693 (2020).
63. Wu, B., Lewis, R. W., Li, G., Gao, Y., Fan, B., Klemm, B., Huang, J., Wang, J., Stuart, M. A. C. & Eelkema, R. Chemical signal regulated injectable coacervate hydrogels. *Chem. Sci.* **14**, 1512–1523 (2023).
64. Morita, K., Suzuki, Z. & Hirose, H. A Tertiary Phosphine-catalyzed Reaction of Acrylic Compounds with Aldehydes. *Bull. Chem. Soc. Jpn.* **41**, 2815 (1968).
65. Nelson, R. P. & Lawton, R. G. On the  $\alpha,\alpha'$  Annelation of Cyclic Ketones. *J. Am. Chem. Soc.* **88**, 3884–3885 (1966).
66. Kohsaka, Y., Akae, Y., Kawatani, R. & Kazama, A. Polymer chemistry of  $\alpha$ -substituted acrylates designed for functional-group synergy. *J. Macromol. Sci. Part A* **59**, 83–97 (2022).
67. Kohsaka, Y. Conjugate substitution reaction of  $\alpha$ -(substituted methyl)acrylates in polymer chemistry. *Polym. J.* **52**, 1175–1183 (2020).
68. Zhuang, J., Zhao, B., Meng, X., Schiffman, J. D., Perry, S. L., Vachet, R. W. & Thayumanavan, S. A programmable chemical switch based on triggerable Michael acceptors. *Chem. Sci.* **11**, 2103–2111 (2020).

69. Brocchini, S. J., Eberle, M. & Lawton, R. G. Molecular Yardsticks. Synthesis of Extended Equilibrium Transfer Alkylating Cross-link Reagents and Their Use in the Formation of Macrocycles. *J. Am. Chem. Soc.* **110**, 5211–5212 (1988).
70. Wang, T., Pfisterer, A., Kuan, S. L., Wu, Y., Dumele, O., Lamla, M., Müllen, K. & Weil, T. Cross-conjugation of DNA, proteins and peptides via a pH switch. *Chem. Sci.* **4**, 1889–1894 (2013).
71. Brocchini, S., Balan, S., Godwin, A., Choi, J.-W., Zloh, M. & Shaunak, S. PEGylation of native disulfide bonds in proteins. *Nat. Protoc.* **1**, 2241–2252 (2006).
72. Matos, M. J., Oliveira, B. L., Martínez-Sáez, N., Guerreiro, A., Cal, P. M. S. D., Bertoldo, J., Maneiro, M., Perkins, E., Howard, J., Deery, M. J., Chalker, J. M., Corzana, F., Jiménez-Osés, G. & Bernardes, G. J. L. Chemo- and Regioselective Lysine Modification on Native Proteins. *J. Am. Chem. Soc.* **140**, 4004–4017 (2018).
73. Reddi, R. N., Resnick, E., Rogel, A., Rao, B. V., Gabizon, R., Goldenberg, K., Gurwicz, N., Zaidman, D., Plotnikov, A., Barr, H., Shulman, Z. & London, N. Tunable Methacrylamides for Covalent Ligand Directed Release Chemistry. *J. Am. Chem. Soc.* **143**, 4979–4992 (2021).
74. Campaña, A. G., Leigh, D. A. & Lewandowska, U. One-dimensional random walk of a synthetic small molecule toward a thermodynamic sink. *J. Am. Chem. Soc.* **135**, 8639–8645 (2013).
75. Kohsaka, Y., Miyazaki, T. & Hagiwara, K. Conjugate substitution and addition of  $\alpha$ -substituted acrylate: a highly efficient, facile, convenient, and versatile approach to fabricate degradable polymers by dynamic covalent chemistry. *Polym. Chem.* **9**, 1610–1617 (2018).
76. Sharko, A., Spitzbarth, B., Hermans, T. M. & Eelkema, R. Redox-Controlled Shunts in a Synthetic Chemical Reaction Cycle. *J. Am. Chem. Soc.* **145**, 9672–9678 (2023).
77. Kirch, L. S., Kargol, J. A., Magee, J. W. & Stuper, W. S. Stability of acrylic monomers. *Plant/Operations Prog.* **7**, 270–274 (1988).
78. Becker, H. & Vogel, H. Stabilization of Acrylic Esters. *Chem. Eng. Technol.* **27**, 1122–1126 (2004).
79. Nenajdenko, V. G., Krasovskiy, A. L. & Balenkova, E. S. The chemistry of sulfinyl and sulfonyl enones. *Tetrahedron* **63**, 12481–12539 (2007).
80. Imada, M., Takenaka, Y., Tsuge, T. & Abe, H. Copolymers incorporated with  $\beta$ -substituted acrylate synthesized by organo-catalyzed group-transfer polymerization. *Polym. J.* **53**, 989–999 (2021).
81. Hatada, K., Kitayama, T., Ute, K. & Nishiura, T. Polymers of  $\alpha$ - and  $\beta$ -substituted acrylates with controlled structures. *Macromol. Symp.* **89**, 465–478 (1995).
82. Ding, R., Zhang, Q.-C., Xu, Y.-H. & Loh, T.-P. Preparation of highly substituted

- ( $\beta$ -acylamino)acrylates via iron-catalyzed alkoxycarbonylation of N-vinylacetamides with carbazates. *Chem. Commun.* **50**, 11661–11664 (2014).
83. Wu, T., Liang, T., Hu, W., Du, M., Zhang, S., Zhang, Y., Anslyn, E. V. & Sun, X. Chemically Triggered Click and Declick Reactions: Application in Synthesis and Degradation of Thermosetting Plastics. *ACS Macro Lett.* **10**, 1125–1131 (2021).
84. Li, G., Trausel, F., van der Helm, M., Klemm, B., Breve, T., van Rossum, S., Hartono, M., Gerlings, H., Lovrak, M., van Esch, J. & Eelkema, R. Tuneable control over organocatalytic activity through host guest chemistry. *Angew. Chem. Int. Ed.* **60**, 14022–14029 (2021).
85. Seingeot, A., Charmasson, Y., Attolini, M. & Maffei, M. Organocatalyzed synthesis of functionalized vinylphosphonates in water. *Heteroat. Chem.* **28**, e21352 (2017).
86. Garzon, C., Attolini, M. & Maffei, M. Synthesis of  $\beta$ -aminovinylphosphonates by organocatalytic nucleophilic displacement of acetate with amines. *Tetrahedron Lett.* **51**, 3772–3774 (2010).
87. Baidya, M., Remennikov, G. Y., Mayer, P. & Mayr, H. SN2' versus SN2 reactivity: Control of regioselectivity in conversions of Baylis-Hillman adducts. *Chem. Eur. J.* **16**, 1365–1371 (2010).
88. Chen, G.-Y., Zhong, F. & Lu, Y. Highly Enantioselective and Regioselective Substitution of Morita-Baylis-Hillman Carbonates with Nitroalkanes. *Org. Lett.* **13**, 6070–6073 (2011).
89. Kim, J. N., Lee, H. J., Lee, K. Y. & Gong, J. H. Regioselective Allylic Amination of the Baylis-Hillman Adducts: An Easy and Practical Access to the Baylis-Hillman Adducts of N-Tosylimines. *Synlett* 173–175 (2002) doi:10.1055/S-2002-19360.
90. Lewis, R. W., Klemm, B., Macchione, M. & Eelkema, R. Fuel-driven macromolecular coacervation in complex coacervate core micelles. *Chem. Sci.* **13**, 4533–4544 (2022).
91. Greenspan, P. & Fowler, S. D. Spectrofluorometric studies of the lipid probe, Nile red. *J. Lipid Res.* **26**, 781–789 (1985).
92. Mills, C. E., Obermeyer, A., Dong, X., Walker, J. & Olsen, B. D. Complex Coacervate Core Micelles for the Dispersion and Stabilization of Organophosphate Hydrolase in Organic Solvents. *Langmuir* **32**, 13367–13376 (2016).
93. Shi, B., Zheng, M., Tao, W., Chung, R., Jin, D., Ghaffari, D. & Farokhzad, O. C. Challenges in DNA Delivery and Recent Advances in Multifunctional Polymeric DNA Delivery Systems. *Biomacromolecules* **18**, 2231–2246 (2017).
94. Uchida, S. & Kataoka, K. Design concepts of polyplex micelles for in vivo therapeutic delivery of plasmid DNA and messenger RNA. *J. Biomed. Mater.*

*Res. Part A* **107**, 978–990 (2019).

95. Donau, C., Späth, F., Sosson, M., Kriebisch, B. A. K., Schnitter, F., Tena-Solsona, M., Kang, H.-S., Salibi, E., Sattler, M., Mutschler, H. & Boekhoven, J. Active coacervate droplets as a model for membraneless organelles and protocells. *Nat. Commun.* **11**, 5167 (2020).
96. Späth, F., Donau, C., Bergmann, A. M., Kränzlein, M., Synatschke, C. V., Rieger, B. & Boekhoven, J. Molecular Design of Chemically Fueled Peptide–Polyelectrolyte Coacervate-Based Assemblies Fabian. *J. Am. Chem. Soc* **143**, 4782–4789 (2021).
97. Deng, J. & Walther, A. Programmable ATP-Fueled DNA Coacervates by Transient Liquid-Liquid Phase Separation. *Chem* **6**, 3329–3343 (2020).
98. Lewis, R. W., Muralidharan, A., Klemm, B., Boukany, P. E. & Eelkema, R. Nucleophile responsive charge-reversing polycations for pDNA transfection. *Polym. Chem.* 1591–1601 (2023) doi:10.1039/d3py00075c.
99. Scrimin, P. & Prins, L. J. Sensing through signal amplification. *Chem. Soc. Rev* **40**, 4488–4505 (2011).
100. Yoshii, T., Onogi, S., Shigemitsu, H. & Hamachi, I. Chemically reactive supramolecular hydrogel coupled with a signal amplification system for enhanced analyte sensitivity. *J. Am. Chem. Soc.* **137**, 3360–3365 (2015).
101. Lee, D.-H., Valenzuela, S. A., Dominguez, M. N., Otsuka, M., Milliron, D. J. & Anslyn, E. V. A self-degradable hydrogel sensor for a nerve agent tabun surrogate through a self-propagating cascade. *Cell Reports Phys. Sci.* **2**, 100552 (2021).
102. Cho, D.-G. & Sessler, J. L. Modern reaction-based indicator systems. *Chem. Soc. Rev* **38**, 1647–1662 (2009).
103. Sun, X., Dahlhauser, S. D. & Anslyn, E. V. New Autoinductive Cascade for the Optical Sensing of Fluoride: Application in the Detection of Phosphoryl Fluoride Nerve Agents. *J. Am. Chem. Soc* **139**, 4635–4638 (2017).
104. Sella, E., Lubelski, A., Klafner, J. & Shabat, D. Two-Component Dendritic Chain Reactions: Experiment and Theory. *J. Am. Chem. Soc* **132**, 3945–3952 (2010).
105. Mohapatra, H., Schmid, K. M. & Phillips, S. T. Design of small molecule reagents that enable signal amplification via an autocatalytic, base-mediated cascade elimination reaction. *Chem. Commun.* **48**, 3018–3020 (2012).
106. Gianneschi, N. C., Nguyen, S. T. & Mirkin, C. A. Signal Amplification and Detection via a Supramolecular Allosteric Catalyst. *J. Am. Chem. Soc* **127**, 1644–1645 (2005).
107. Klemm, B., Roshanasan, A., Piergentili, I., Esch, J. H. Van & Eelkema, R. Naked-eye thiol analyte detection via self-propagating, amplified reaction cycle. *ChemRxiv* (2023) doi:https://doi.org/10.26434/chemrxiv-2023-4cdx6-v2.
108. Li, G., Wan, Y., Lewis, R. W., Fan, B. & Eelkema, R. Signal-dependent reactivity

of host-guest complexes controls supramolecular aggregate formation. *Cell Reports Phys. Sci.* **4**, 101309 (2023).

# Redox-controlled shunts in a synthetic chemical reaction cycle

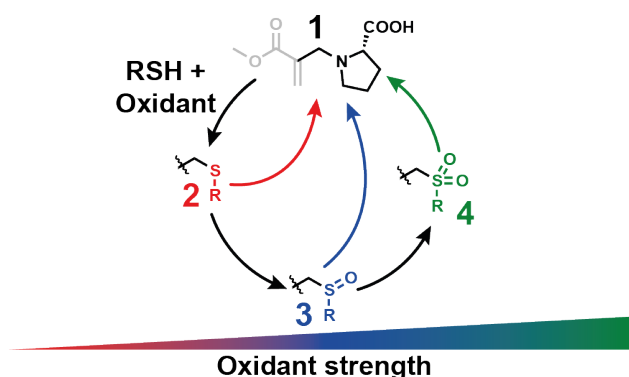
## Abstract

Shunts, alternative pathways in chemical reaction networks, are ubiquitous in Nature, enabling adaptability to external and internal stimuli. We introduce a chemical reaction network (CRN) in which the recovery of a Michael-accepting species is driven by oxidation chemistry. Using weak oxidants can enable access to two shunts within this CRN with different kinetics and a reduced number of side reactions compared to the main cycle that is driven by strong oxidants. Further, we introduce a strategy to recycle one of the main products under flow conditions to partially reverse the CRN and control product speciation throughout time. These findings introduce new levels of control over artificial CRNs, driven by redox chemistry, narrowing the gap between synthetic and natural systems.

## Availability and Contributions

This chapter is based on an article published as: A. Sharko,<sup>§</sup> B. Spitzbarth,<sup>§</sup> T. M. Hermans, R. Eelkema. *J. Am. Chem. Soc.* **145**, 9672–9678 (2023). (§ contributed equally) It is reprinted with permission from this reference. Copyright 2023 American Chemical Society. DOI: 10.1021/jacs.3c00985

A.S. and B.S. developed the project idea and equally participated in planning and conducting experiments, writing the paper draft, supplementary information, and designing the figures and schemes. R.E. supervised the research conducted at TU Delft. T.M.H. supervised the research conducted at University of Strasbourg, especially the flow experiments. R.E. and T.M.H. aided in development of the project idea, corrected the manuscript draft, helped with figure design, and secured funding.



## Introduction

Nature has evolved myriad ways of performing chemical conversions to regulate living organisms. Such conversions often are done in chemical reaction networks (CRNs), where intricate connections between reactants and products exist. One of the key reaction cycles to control cellular respiration is the Krebs cycle, in which high-energy molecules (NADH, GTP, and QH<sub>2</sub>) are generated by transforming acetyl-CoA into carbon dioxide in eight consecutive reactions;<sup>1</sup> however, under oxidative stress or carbon feedstock shortage, three of them are bypassed. This alternative pathway that allows respiration to continue is called the glyoxylate shunt.<sup>2</sup> Similar shunts, such as the P450 peroxide shunt,<sup>3</sup> GABA shunt,<sup>4</sup> and pentose phosphate shunt,<sup>5</sup> among others,<sup>1,6</sup> are ubiquitous in metabolism and are responsible for its adaptive regulation. A distinct feature of natural shunts is that they offer control over product speciation in response to external stimuli or the organism's internal needs.<sup>7-10</sup> Although there are numerous artificial reaction networks of various complexity,<sup>11-20</sup> shunts have not yet been explored in the context of Systems Chemistry.

Here we show how two alternative pathways in an artificial reaction cycle (i.e., shunts) can be accessed depending on the oxidant strength (Figure 6.1). For the sake of clarity in the following discussion, we define shunt as: *an alternative pathway in a chemical reaction network with distinct intermediate species that becomes available or even dominant upon changing external conditions (e.g., reactant concentration, catalytic activity, oxidant strength, pH, but excluding temperature or pressure)*. In our current reaction cycle, we start from a Michael acceptor (MA) that reacts with a thiol to release proline. The thiol adduct is subsequently oxidized to the sulfoxide and further to the sulfone, allowing the proline to re-attack and recover the original MA species. Strong oxidants provide access to all oxidation states of the sulfur species, i.e., sulfide, sulfoxide, and sulfone, defining the maximum speciation of the network (Figure 6.1a). For weaker oxidants, the sulfone pathway becomes less dominant, which we refer to as the 'sulfoxide shunt' (Figure 6.1b). For the weakest oxidants, only the sulfide is available (i.e., the 'sulfide shunt', Figure 6.1c), which leads to the smallest CRN with the fewest side reactions and the slowest kinetics (Table S6.2). Lastly, we show how a reductant can partially reverse the sulfoxide shunt by recycling the disulfide product, resembling the partial reversibility<sup>21-23</sup> of the Krebs cycle in the presence of primordial reducing agents such as cyanide or hydrogen.

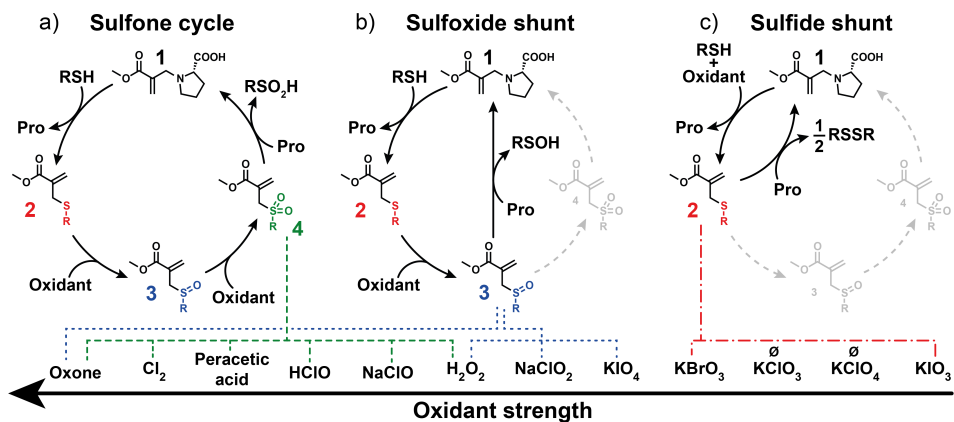


**Figure 6.1:** Simplified CRN schemes; Depending on the oxidant strength, proline-MA 1 recovery goes via the Sulfone cycle (a) with strong oxidants and two different shunts (b, c) with weaker oxidants, leading to different sulfur product speciation. Here, Pro is L-proline, and R = 4-carboxyphenyl.

## Results and Discussion

### Choice of chemistry and reagents

Conjugate additions to MAs have been employed for efficient functionalization reactions in a vast range of applications, such as in material science and biofunctionalizations.<sup>24–31</sup> In their previous work, the Eelkema group attempted to design a redox-controlled reaction cycle for the recovery of Michael acceptors based on thiol-addition and -elimination chemistry. Although the steps of this cycle worked well in isolation, combining them led to challenges such as over-oxidation and significant side reactivity of the waste products.<sup>32</sup> We decided to work with different oxidants to overcome the challenges faced previously and to look at a different class of Michael acceptors.  $\beta'$ -Substituted MAs are especially attractive due to their ability to retain the reactive double bond upon the addition of a nucleophile and subsequent elimination of a leaving group in the  $\beta'$ -position.<sup>33–38</sup> The group of Thayumanavan demonstrated the addition of thiols on amine-functionalized  $\beta'$ -MAs for application in chemical switches.<sup>39</sup> Further, it was found that the more oxidized sulfone adducts are electron-deficient enough to react with amines to form amine-functionalized MAs.<sup>34,35,40</sup> Therefore, we hypothesized that oxidation of the thiol-functionalized MA would enable the completion of a reaction *cycle*, where the initial MA is recovered (Figure 6.1).

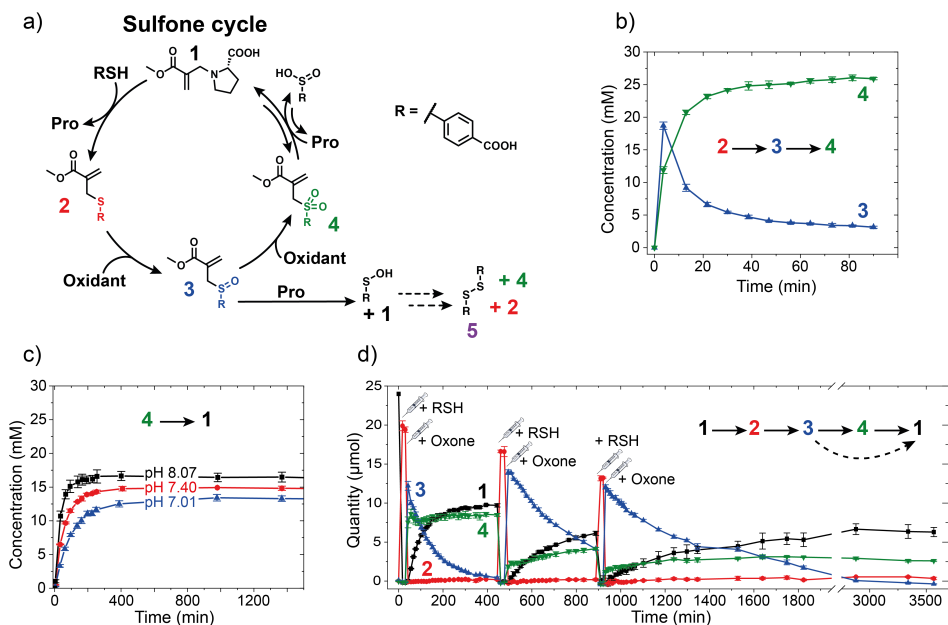


**Figure 6.2:** Sulfone reaction network. a) General scheme of the sulfone reaction network; b) Oxidation of sulfide-MA 2 by Oxone at pH 8; c) proline-MA 1 recovery from the reaction of sulfone-MA 4 with proline at different pH; d) Stepwise addition of RSH and Oxone to proline-MA 1, the system is refueled 2 times. All kinetic measurements were performed in the same conditions: 10% DMF in 0.5 M phosphate buffer at 20°C. Error bars represent one standard deviation over three independent experiments.

## Sulfone cycle

One of the oxidants of choice to oxidize sulfides to sulfones is Oxone (i.e., the complex salt of potassium peroxymonosulfate).<sup>41,42</sup> As a thiol, we chose water-soluble 4-mercaptobenzoic acid (RSH) due to its high thiol acidity, which makes it both a good nucleophile and stabilized leaving group. We studied the steps of this CRN separately: thiol substitution ( $1 \rightarrow 2$ ), sulfide oxidation ( $2 \rightarrow 3 \rightarrow 4$ ), and sulfone substitution ( $4 \rightarrow 1$ ) (Figure 6.2a). The first step ( $1 \rightarrow 2$ ) proceeds fast and with high yield (typically above 90% in <1 min, Table S6.2). The sulfide oxidation  $2 \rightarrow 4$  proceeds smoothly within 1.5 hours via 3 (Figure 6.2b). Varying the pH from 7.0 to 8.0 does not influence this step (Figure S6.1, this pH range was found experimentally where the ester of 1 is stable to hydrolysis and nucleophiles react fast with 4). For the sulfone substitution ( $4 \rightarrow 1$ ), we studied a range of amines and alcohols (Figures S6.2–S6.6) and the stability of the resulting adducts (Figure S6.7). We found l-proline (Pro) to react fast ( $t_{1/2} = 30$  min, at pH 8.0, Figure 6.2c, Table S6.2) and with a relatively high yield to proline-MA 1, which is stable over the observed time. Hence, we decided to proceed with proline as a nucleophile for this CRN. The substitution step  $4 \rightarrow 1$  was found to be pH-dependent, proceeding faster and with higher yields at increased pH (pH 7:  $t_{1/2} = 75$  min, 45% yield;

pH 7.4:  $t_{1/2} = 45$  min, 49% yield; pH 8:  $t_{1/2} = 30$  min, 56% yield, Figure 6.2c). This effect is likely due to the increased nucleophilicity of proline at higher pH. As shown in Figure 6.2c, even at higher pH, the conversions are not quantitative, likely because the substitution step  $4 \rightarrow 1$  is an equilibrium reaction. The displaced sulfinate can act as a nucleophile in the reverse reaction  $1 \rightarrow 4$  (Figure S6.8). Having studied all separate CRN steps in detail, we combined them into one system. Starting from a proline-MA **1** solution, we initiated the cycle by adding RSH, followed after three to five minutes by the addition of Oxone. We found all reactions in the cycle to proceed subsequently, recovering approximately 50% of the original amount of proline-MA **1** (Figure 6.2d, a line with black squares at 440 min). The system can be run at least three times. After the second addition of thiol and oxidant, significant dampening of the recovery of proline-MA **1** is observed, whereas, after the third addition, proline-MA **1** is recovered at a similar yield as after the second addition, although over a longer timescale (Figure 6.2d, a line with black squares around 3500 min). We found several side reactions that influence the recovery, such as double additions, hydrolysis of substrate **1** over long timescales, and proline oxidation (Scheme S6.1). Apart from the sulfone substitution ( $4 \rightarrow 1$ ), proline-MA **1** recovery can also occur via the addition-substitution of proline on sulfoxide-MA **3** ( $3 \rightarrow 1$ ) (Figure 6.d). This reaction will be discussed in detail in the following section. Furthermore, upon adding RSH, a sharp decrease of sulfone-MA **4** and sulfoxide-MA **3** occurs because both species can react with RSH swiftly—being the better nucleophile than proline—recovering sulfide-MA **2** in the process (Figure S6.9–S6.11). Contrary to the stepwise addition experiment in Figure 6.2d, the simultaneous addition of RSH and Oxone does not lead to a significant recovery of **1** (Figure S6.12). This is due to the rapid consumption of RSH by Oxone to form RSH-disulfide **5**. Furthermore, Oxone can also directly oxidize proline-MA **1** to form oxidized proline-MA and proline to form the corresponding nitron (Scheme S6.1, Figures S6.13–S6.15). Despite some off-cycle side reactions when simultaneously adding RSH and oxidant, these results show that with a stepwise manner of addition, we can successfully run the sulfone cycle at least three times, recovering the initial Michael-accepting species mediated by oxidation chemistry, producing the sulfinate and sulfonate of RSH as side products.

### Sulfoxide shunt

Starting from the observation that proline can also react with sulfoxide-MA **3** (Figure 6.d), we hypothesized that the formation of sulfone-MA **4** can be suppressed in favor of **3** by using a weaker oxidant, avoiding some of the problematic side reactions of the sulfone cycle (see Scheme S6.1). This would allow access to a shunt with different yields, timescales, and products in response to the properties of the employed oxidant. We found that oxidants such as hypochlorite and hydrogen peroxide, which are only slightly weaker than Oxone (as judged by their oxidation potentials<sup>43</sup>, Figure 6.1), still yielded sulfone-MA **4**, along with the side reactions associated with this CRN (Figure S6.16). Potassium periodate, on the other hand, being even weaker, is commonly applied for the selective synthesis of sulfoxides from sulfides and hence should be a good candidate for running the CRN primarily via sulfoxide-MA **3**.<sup>44</sup> The steps of this CRN were again studied separately. To our surprise, subjecting sulfide-MA **2** to  $\text{KIO}_4$  (oxidation step  $2 \rightarrow 3$ )

yielded not only sulfoxide-MA **3**, but also small amounts of sulfone-MA **4** (Figure 6.3c). Upon the formation of sulfoxide-MA **3**, we found that, unlike sulfone-MA **4**, **3** is not stable in aqueous media for a prolonged time. Under basic conditions (pH 8), water can attack and displace sulfenic acid (Figure S6.17). This highly reactive species is responsible for a complex cascade of reactions, which can lead to the formation of sulfide-MA **2**, sulfone-MA **4**, and disulfide **5**, among others (Figure 6.3a, Scheme S6.1). This suggests that the sulfone-MA **4** formed in Figure 6.3c is not due to oxidation with  $\text{KIO}_4$  but due to a degradation reaction of the formed sulfoxide-MA **3** instead. This was further confirmed by subjecting sulfoxide-MA **3** to proline (sulfoxide substitution  $\mathbf{3} \rightarrow \mathbf{1}$ , Figure 6.3d). Even without any oxidant, we found disulfide **5**, sulfide-MA **2**, and sulfone-MA **4** side products forming over time due to the degradation pathways of the sulfenic acid (Figure 6.2a). Further, we found a higher recovery of proline-MA **1** (~ 83%, Figure 6.3d) compared to the sulfone substitution (~ 55%,  $\mathbf{4} \rightarrow \mathbf{1}$ , Figure 6.2c). We achieved similar results for sodium chlorite, which also proceeds primarily through the sulfoxide pathway. Combining stepwise RSH addition and oxidation by  $\text{NaClO}_2$  gave good recovery yields of proline-MA **1** and the transient formation of sulfoxide-MA **3** (Figure 6.3e). Furthermore, we did not observe the oxidation of proline as we had seen previously with stronger oxidants such as Oxone. As expected, when attempting to run this system with the simultaneous addition of RSH and oxidant, we encountered the same challenge as with stronger oxidants: a rapid consumption of RSH to exclusively form disulfide **5**. However, the stepwise addition experiments demonstrate that our CRN can be run via a shunt, mostly avoiding sulfone-MA **4**. Similar to the peroxide shunt of P450 enzymes, where stronger oxidants lead to the degradation of the heme center,<sup>3,45</sup> the sulfoxide shunt results in a reduced number of side reactions. Unlike the sulfone cycle, the sulfoxide shunt leads to sulfenic acid as the dominant sulfur side product, which disproportionates to produce thiol and sulfinic acid (Figure S6.17). Thiol can be further oxidized to disulfide **5**, whereas sulfinic acid can react with **1** to produce sulfone-MA **4** (Figure 6.a, d).

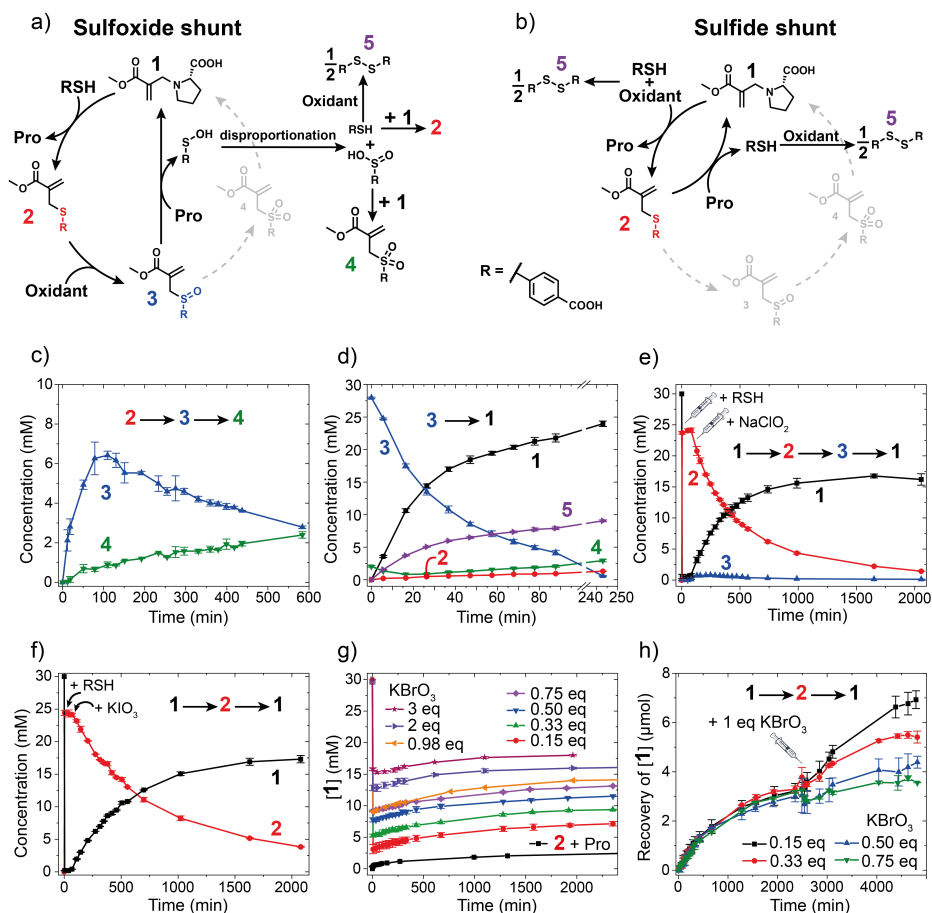


**Figure 6.3:** Sulfoxide (a) and sulfide (b) reaction networks. c) Oxidation of sulfide-MA **2** with  $\text{KIO}_4$ ; d) Sulfoxide-MA **3** + 1 eq. proline; e) Stepwise addition of RSH and  $\text{NaClO}_2$  to proline-MA **1**; f) Stepwise addition of RSH and  $\text{KIO}_3$  to proline-MA **1**; g) Reaction cycle experiments with different amounts of  $\text{KBrO}_3$ ; h) Differences in the recovery of proline-MA **1** after addition of another 1 eq. of  $\text{KBrO}_3$  to different reaction cycle experiments. Error bars represent one standard deviation over two (c, e, f, g, h) or three (d) independent experiments.

### Sulfide shunt

We hypothesized that employing even weaker oxidants might further reduce side reactions and potentially enable us to run the CRN with the simultaneous addition of RSH and oxidant. To our surprise, when testing oxidants such as bromates and iodates, which are too weak to oxidize sulfide-MA **2** to sulfoxide-MA **3** (Figure S6.18–S6.19), we still observed a significant recovery of proline-MA **1** with the stepwise addition of RSH and oxidant, creating a second shunt to the original sulfone cycle (Figure 6.1c, Figure 6.3f). While in the first two CRNs (Figure 6.1a, b) the recovery of **1** is driven by direct

oxidation, i.e., activation, of sulfide-MA **2**, in this case, the weaker oxidants remove RSH from the equilibrium between **2** and **1**, forming disulfide **5** as waste (Figure S6.20) and driving the recovery  $2 \rightarrow 1$  forward. While we found similarly high recoveries with  $\text{KIO}_3$  compared to the sulfone CRN (approximately 55%), the timescale of recovery through the sulfide shunt is roughly 5-fold longer, 2000 min (Figure 6.3f, Table S6.2). This shunt shows even fewer side reactions than the sulfoxide shunt: the only two significant side reactions are double additions of thiol and hydrolysis of substrate **1** over time (Figure S6.7, S6.21, Scheme S6.1). Furthermore, when adding RSH and  $\text{KBrO}_3$  to proline-MA **1** simultaneously, we found that, indeed, some recovery of **1** could be observed (approximately 10%), depending on how much oxidant is added (Figure 6.3g). Adding a large excess of  $\text{KBrO}_3$  leads to lower recoveries, as the direct oxidation of RSH to disulfide is favored over its substitution reaction with **1**. Interestingly, we found that the recovery rates are mostly limited by the lifetime of  $\text{KBrO}_3$  in solution, as adding an excess of oxidant at a later stage leads to increased recoveries, with the highest recoveries being observed with low initial doses of oxidant (Figure 6.3h). This effect is because a low initial dose of  $\text{KBrO}_3$  allows more sulfide-MA **2** to form. The sulfide shunt offers yet another pathway for recovery of **1** with fewer side reactions over a longer timescale. Recoveries in the case of stepwise addition are similar to those of the sulfone CRN, while unlike for the sulfone and sulfoxide pathways, in the sulfide shunt low recovery levels are possible even when RSH and oxidant are added simultaneously. This shunt produces disulfide **5** as the only sulfur side product, avoiding other species and degradation pathways found in the sulfone cycle and sulfoxide shunt. Comparing the kinetics of the three pathways, we find that the sulfone cycle proceeds fastest, with the addition of proline to sulfone-MA **4** to recover **1** as the rate-determining step (Figure 6.2c, Table S6.2). In both the sulfoxide and sulfide shunt, oxidation is the rate-determining step, with the sulfide shunt being the slowest pathway to recover **1** (Figure 6.3e, h). This decrease in kinetics goes hand in hand with fewer side reactions. Interestingly, the yields of the recovery of **1** are similar for each of the available pathways, with the potential to increase the recovery yields with additional portions of oxidant in the sulfide shunt (Figure 6.h).

### Reversibility and recycling strategy

Metabolic pathways are not always unidirectional.<sup>22,46,47</sup> The Krebs cycle for example can run in reverse, in the reduction mode, with autotrophic carbon dioxide fixation depending on whether organic or inorganic carbon sources are available.<sup>21,46</sup> Reversibility is an important aspect of adaptability and is difficult to implement in synthetic systems, especially in redox reactions, as forward and backward processes are usually not orthogonal.

In this context, we explored the recovery of RSH from disulfide **5**, which is the major product in both the sulfoxide and sulfide shunts. This allows a partial reversal of the CRN, leading to the formation of sulfide-MA **2** from **1**, driving the main cycle forward again. Phosphines are widely used for disulfide reduction.<sup>48,49</sup> For this system, we decided to use  $\text{NaClO}_2$  as an oxidant due to its high solubility and stability in water, and tris(2-carboxyethyl)phosphine (TCEP) as a phosphine (Figure 6.4a). We used a flow setup to efficiently switch the system between an excess of sulfide-MA **2** and an excess of proline-

MA 1. Depending on the flow rate, the apparent reaction rates can be tuned. We start from a solution of proline-MA **1** and explore four different flow regimes. In the first flow regime, i) an 8/1 excess of thiol relative to oxidant is flowed. This leads to the formation of sulfide-MA **2**, as well as the formation of disulfide **5** due to the cross-reactivity of the thiol with the oxidant (Figure 6.4a). In flow regime ii), both thiol and oxidant flows are stopped, and TCEP is flowed. TCEP reduces **5** to free thiol, which leads to the formation of yet more **2**, consuming **1**. In the third phase iii), an 8/1 excess of oxidant is flowed relative to the thiol. This primarily leads to the oxidation of **2** to form sulfoxide-MA **3**, which can react with free proline to recover **1**. Furthermore, **5** is formed both as a side product from the released sulfenic acid, as well as the direct reaction of thiol and oxidant. In the fourth flow regime iv), these trends continue, but as only oxidant (NaClO<sub>2</sub>) is flowed, disulfide **5** is exclusively generated as a side product of sulfenic acid degradation. The last flow regime v) is equal to regime ii), aiming to reduce disulfide **5** to recover RSH. One of the downsides of using phosphines in this system is that the addition to **1** is possible, yielding phosphine-MA as a side product (Figure S6.22). These findings show that recycling the major product of the sulfoxide shunt, disulfide **5**, is possible using phosphines, enabling control over CRN speciation under flow conditions over time.

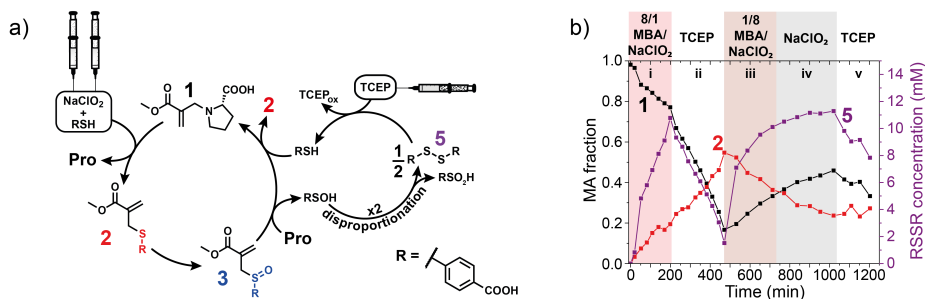


**Figure 6.4:** a) Disulfide recycling with phosphines in the sulfoxide shunt b) evolution of proline-MA **1**, sulfide-MA **2**, and disulfide **5** over time under different flow conditions.

## Conclusions

We introduce the use of shunts in an artificial CRN, offering three distinct pathways toward the recovery of a Michael acceptor using oxidation chemistry. The oxidant strength dictates if the full CRN or any of the two shunts will preferentially be used without a compromise in recovery yields. The shortest (sulfide) shunt leads to the slowest reaction kinetics and fewest side reactions. Using a flow setup, we can recycle the disulfide product and partially reverse the reaction cycle. Implementing shunts in artificial CRNs will provide more control over chemical speciation and steering of fluxes along different pathways. Our approach mimics Nature, where shunts are common to achieve precise control over metabolic processes in response to external and/or internal stimuli. Shunts could help Systems Chemists to engineer more adaptive chemical reaction

networks, with possible applications in triggered catalyst release, transient materials, or artificial metabolic networks.

### Acknowledgment

This work has received funding from the European Union's Horizon 2020 research and innovation program under the Marie Skłodowska-Curie grant agreement No 812868. We thank Dr. Stephen Eustace for his help with the NMR measurements.

### Conflict of Interest

There are no conflicts to declare.

### References

1. Jeremy M. Berg, John L. Tymoczko, Lubert Stryer. *Biochemistry*. (W. H. Freeman, 1995).
2. Dolan, S. K. & Welch, M. The Glyoxylate Shunt, 60 Years On. *Annu. Rev. Microbiol.* **72**, 309–330 (2018).
3. Munro, A. W., Girvan, H. M., Mason, A. E., Dunford, A. J. & McLean, K. J. What makes a P450 tick? *Trends in Biochemical Sciences* **38**, 140–150 (2013).
4. Ansari, M. I., Jalil, S. U., Ansari, S. A. & Hasanuzzaman, M. GABA shunt: a key-player in mitigation of ROS during stress. *Plant Growth Regul* **94**, 131–149 (2021).
5. Stincone, A. *et al.* The return of metabolism: biochemistry and physiology of the pentose phosphate pathway. *Biol Rev Camb Philos Soc* **90**, 927–963 (2015).
6. David L. Nelson, Michael M. Cox. *Lehninger Principles Of Biochemistry*, 4th ed.; W. H. Freeman, 2004, pp. 657–668; 804–805.
7. Erkut, C., Gade, V. R., Laxman, S. & Kurzchalia, T. V. The glyoxylate shunt is essential for desiccation tolerance in *C. elegans* and budding yeast. *eLife* **5**, e13614 (2016).
8. Ahn, S., Jung, J., Jang, I.-A., Madsen, E. L. & Park, W. Role of Glyoxylate Shunt in Oxidative Stress Response. *Journal of Biological Chemistry* **291**, 11928–11938 (2016).

9. Shulman, R. G. & Rothman, D. L. The “glycogen shunt” in exercising muscle: A role for glycogen in muscle energetics and fatigue. *Proc. Natl. Acad. Sci. U.S.A.* **98**, 457–461 (2001).
10. Crousilles, A., Dolan, S. K., Brear, P., Chirgadze, D. Y. & Welch, M. Gluconeogenic precursor availability regulates flux through the glyoxylate shunt in *Pseudomonas aeruginosa*. *Journal of Biological Chemistry* **293**, 14260–14269 (2018).
11. De, S. & Klajn, R. Dissipative Self-Assembly Driven by the Consumption of Chemical Fuels. *Advanced Materials* **30**, 1706750 (2018).
12. Nitschke, J. R. Molecular networks come of age. *Nature* **462**, 736–738 (2009).
13. Das, K., Gabrielli, L. & Prins, L. J. Chemically Fueled Self-Assembly in Biology and Chemistry. *Angew. Chem.* **133**, 20280–20303 (2021).
14. Whitesides, G. M. & Ismagilov, R. F. Complexity in chemistry. *Science* **284**, 89–92 (1999).
15. Chen, J. L.-Y., Maiti, S., Fortunati, I., Ferrante, C. & Prins, L. J. Temporal Control over Transient Chemical Systems using Structurally Diverse Chemical Fuels. *Chemistry – A European Journal* **23**, 11549–11559 (2017).
16. Rieß, B., Grötsch, R. K. & Boekhoven, J. The Design of Dissipative Molecular Assemblies Driven by Chemical Reaction Cycles. *Chem* **6**, 552–578 (2020).
17. Ashkenasy, G., Hermans, T. M., Otto, S. & Taylor, A. F. Systems chemistry. *Chem. Soc. Rev.* **46**, 2543–2554 (2017).
18. Mattia, E. & Otto, S. Supramolecular systems chemistry. *Nature Nanotech* **10**, 111–119 (2015).
19. Singh, N., Formon, G. J. M., De Piccoli, S. & Hermans, T. M. Devising Synthetic Reaction Cycles for Dissipative Nonequilibrium Self-Assembly. *Advanced Materials* **32**, 1906834 (2020).
20. Sharko, A., Livitz, D., De Piccoli, S., Bishop, K. J. M. & Hermans, T. M. Insights into Chemically Fueled Supramolecular Polymers. *Chem. Rev.* **122**, 11759–11777 (2022).
21. Yadav, M., Pulletikurti, S., Yerabolu, J. R. & Krishnamurthy, R. Cyanide as a primordial reductant enables a protometabolic reductive glyoxylate pathway. *Nat. Chem.* **14**, 170–178 (2022).
22. Steffens, L., Pettinato, E., Steiner, T. M., Mall, A., König, S., Eisenreich, W. & Berg, I. A. High CO<sub>2</sub> levels drive the TCA cycle backwards towards autotrophy. *Nature* **592**, 784–788 (2021).

23. Rauscher, S. A. & Moran, J. Hydrogen Drives Part of the Reverse Krebs Cycle under Metal or Meteorite Catalysis. *Angew. Chem. Int. Ed.* **61**, e202212932 (2022).
24. Diehl, K. L., Kolesnichenko, I. V., Robotham, S. A., Bachman, J. L., Zhong, Y., Brodbelt, J. S. & Anslyn, E. V. Click and chemically triggered declick reactions through reversible amine and thiol coupling via a conjugate acceptor. *Nature Chem* **8**, 968–973 (2016).
25. Campaña, A. G., Leigh, D. A. & Lewandowska, U. One-Dimensional Random Walk of a Synthetic Small Molecule Toward a Thermodynamic Sink. *J. Am. Chem. Soc.* **135**, 8639–8645 (2013).
26. Jones, M. W., Strickland, R. A., Schumacher, F. F., Caddick, S., Baker, James. R., Gibson, M. I. & Haddleton, D. M. Polymeric Dibromomaleimides As Extremely Efficient Disulfide Bridging Bioconjugation and Pegylation Agents. *J. Am. Chem. Soc.* **134**, 1847–1852 (2012).
27. Wu, T., Liang, T., Hu, W., Du, M., Zhang, S., Zhang, Y., Anslyn, E. V. & Sun, X. Chemically Triggered Click and Declick Reactions: Application in Synthesis and Degradation of Thermosetting Plastics. *ACS Macro Lett.* **10**, 1125–1131 (2021).
28. Brocchini, S. J., Eberle, Martin. & Lawton, R. G. Molecular yardsticks. Synthesis of extended equilibrium transfer alkylating cross-link reagents and their use in the formation of macrocycles. *J. Am. Chem. Soc.* **110**, 5211–5212 (1988).
29. Wang, T., Pfisterer, A., Kuan, S. L., Wu, Y., Dumele, O., Lamla, M., Müllen, K. & Weil, T. Cross-conjugation of DNA, proteins and peptides via a pH switch. *Chem. Sci.* **4**, 1889 (2013).
30. Brocchini, S., Balan, S., Godwin, A., Choi, J.-W., Zloh, M. & Shaunak, S. PEGylation of native disulfide bonds in proteins. *Nat Protoc* **1**, 2241–2252 (2006).
31. Nair, D. P., Podgórski, M., Chatani, S., Gong, T., Xi, W., Fenoli, C. R. & Bowman, C. N. The Thiol-Michael Addition Click Reaction: A Powerful and Widely Used Tool in Materials Chemistry. *Chem. Mater.* **26**, 724–744 (2014).
32. Fan, B., Men, Y., Rossum, S. A. P., Li, G. & Eelkema, R. A Fuel-Driven Chemical Reaction Network Based on Conjugate Addition and Elimination Chemistry. *ChemSystemsChem* **2**, (2020).
33. Nelson, R. P. & Lawton, R. G. On the a,a' Annelation of Cyclic Ketones. 2.
34. Mitra, S. & Lawton, R. G. Reagents for the crosslinking of proteins by equilibrium transfer alkylation. *J. Am. Chem. Soc.* **101**, 3097–3110 (1979).

35. Liberatore, F. A., Comeau, R. D., McKearin, J. M., Pearson, D. A., Belonga, B. Q., Brocchini, S. J., Kath, J., Phillips, T., Oswell, K. & Lawton, R. G. Site-directed chemical modification and crosslinking of a monoclonal antibody using equilibrium transfer alkylating crosslink reagents. *Bioconjugate Chem.* **1**, 36–50 (1990).
36. Reddi, R. N., Resnick, E., Rogel, A., Rao, B. V., Gabizon, R., Goldenberg, K., Gurwicz, N., Zaidman, D., Plotnikov, A., Barr, H., Shulman, Z. & London, N. Tunable Methacrylamides for Covalent Ligand Directed Release Chemistry. *J. Am. Chem. Soc.* **143**, 4979–4992 (2021).
37. Lewis, R. W., Klemm, B., Macchione, M. & Eelkema, R. Fuel-driven macromolecular coacervation in complex coacervate core micelles. *Chem. Sci.* **13**, 4533–4544 (2022).
38. Klemm, B., Lewis, R. W., Piergentili, I. & Eelkema, R. Temporally programmed polymer – solvent interactions using a chemical reaction network. *Nat Commun* **13**, 6242 (2022).
39. Zhuang, J., Zhao, B., Meng, X., Schiffman, J. D., Perry, S. L., Vachet, R. W. & Thayumanavan, S. A programmable chemical switch based on triggerable Michael acceptors. *Chem. Sci.* **11**, 2103–2111 (2020).
40. Matos, M. J., Oliveira, B. L., Martínez-Sáez, N., Guerreiro, A., Cal, P. M. S. D., Bertoldo, J., Maneiro, M., Perkins, E., Howard, J., Deery, M. J., Chalker, J. M., Corzana, F., Jiménez-Osés, G. & Bernardes, G. J. L. Chemo- and Regioselective Lysine Modification on Native Proteins. *J. Am. Chem. Soc.* **140**, 4004–4017 (2018).
41. Ligon, S. C., Seidler, K., Gorsche, C., Griesser, M., Moszner, N. & Liska, R. Allyl sulfides and  $\alpha$ -substituted acrylates as addition-fragmentation chain transfer agents for methacrylate polymer networks. *J. Polym. Sci. Part A: Polym. Chem.* **54**, 394–406 (2016).
42. Wang, Y., Jiang, W. & Huo, C. One-Pot Synthesis of  $\beta$ -Hydroxysulfones and Its Application in the Preparation of Anticancer Drug Bicalutamide. *J. Org. Chem.* **82**, 10628–10634 (2017).
43. Haynes, W. M. *CRC Handbook of Chemistry and Physics, 91st Edition*; Taylor & Francis, 2010, pp. 8.23–8.33.
44. Leonard, N. J. & Johnson, C. R. Periodate Oxidation of Sulfides to Sulfoxides. Scope of the Reaction. *J. Org. Chem.* **27**, 282–284 (1962).
45. Rittle, J. & Green, M. T. Cytochrome P450 Compound I: Capture, Characterization, and C-H Bond Activation Kinetics. *Science* **330**, 933–937 (2010).

46. Nunoura, T. *et al.* A primordial and reversible TCA cycle in a facultatively chemolithoautotrophic thermophile. *Science* **359**, 559–563 (2018).
47. Hanson, R. W. & Owen, O. E. Gluconeogenesis. in *Encyclopedia of Biological Chemistry (Second Edition)* (eds. Lennarz, W. J. & Lane, M. D.) 381–386 (Academic Press, 2013). doi:10.1016/B978-0-12-378630-2.00040-2.
48. Jocelyn, P. C. Chemical reduction of disulfides. in *Methods in Enzymology* vol. 143 246–256 (Elsevier, 1987).
49. Mizhiritskii, M., Shpernat, Y. & Ashkenazi, B. Methods for the reduction of disulfide bonds. (2004).

## Supporting Information

### General Information

Methyl (2-hydroxymethyl)acrylate and L-Proline were purchased from Fluorochem. Methyl (2-bromomethyl)acrylate, Oxone (potassium peroxydisulfate), and sodium hypochlorite were purchased from TCI Europe. Acetonitrile, DMF, potassium hydrogen phosphate, potassium hydroxide, acetyl chloride, trimethylamine, anhydrous DCM, DSS, sodium chlorite, potassium iodate, potassium periodate, MMPP, SDCI, potassium chlorate, and potassium perchlorate were purchased from Sigma Aldrich. DCM (technical grade) was purchased from VWR International. D<sub>2</sub>O, MeOD, CDCl<sub>3</sub>, and DMSO-*d*<sub>6</sub> were purchased from Eurisotop. Deionized (milliQ) water was made in our laboratory. Unless stated otherwise, all chemicals were used as received. For water-free experiments, anhydrous solvents and pre-dried flasks were used.

### NMR measurements

NMR spectra were recorded on an Agilent-400 MR DD2 (400 MHz for <sup>1</sup>H, 101 MHz for <sup>13</sup>C) instrument. All measurements were taken at 298 K. For qNMR measurements, sealed ampoules (short NMR tubes with an outer diameter of 3 mm, purchased from VWR International) were prepared, containing a 10 mM solution of sodium trimethylsilylpropanesulfonate (DSS) in D<sub>2</sub>O to ensure i) no potential reaction between standard and sample and ii) no presence of deuterated solvent in the sample to avoid a change in kinetics due to isotope effects. **All qNMR measurements were conducted in a 9/1 mixture of 0.5 M pH 8.0 potassium phosphate buffer and DMF unless stated otherwise.** For data analysis, the raw data was treated in Mestrenova V11.0. The 0.0 ppm signal of DSS was integrated and set to 1000, and the sample concentrations were derived accordingly based on the known starting concentrations. To ensure full relaxation of all protons, T1 measurements (see Table S6.1) were performed, and the scan time was set to 5xT1 for the slowest relaxing signal in each experiment, respectively. All kinetic studies were performed using PRESAT experiments with 8 scans and suppression of the H<sub>2</sub>O peak.

### LC-HRMS measurements

LC-HRMS was performed with a ThermoFisher Scientific UltiMate 3000 RSLCnano UHPLC System coupled with EMT Thermo OrbiTrap Mass analyzer. The ionization used was ESI using a Hypersil GOLD column, 50 x 2.1 mm, 1.9 μm.



- i) Direct oxidation of proline, first to *N*-hydroxyproline,<sup>2</sup> and subsequently under decarboxylation to the corresponding nitron as shown in literature.<sup>3</sup> We observed the characteristic double bond signal of said nitron (see Figure S6.13).
- ii) Oxidation of proline-MA to oxidized proline-MA (Ox-Proline-MA in Scheme S6.1) which can degrade under double addition or re-form proline-MA **1** via substitution with proline under release of *N*-hydroxyproline (Figure S6.15).
- iii) Oxidation of free thiol to form disulfide and subsequently higher oxidized species.

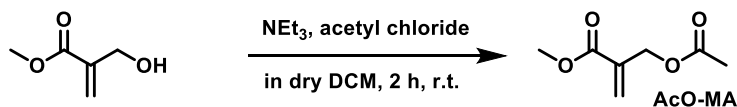
Continuing on the main route of the CRN, the remaining Oxone can now oxidize sulfide-MA **2** to sulfoxide-MA **3** and sulfone-MA **4**. Oxone is a capable reagent for this task, as it can efficiently oxidize sulfides to sulfones, leaving the allylic double bond untouched, as previously shown in literature.<sup>4</sup> While Oxone can generally oxidize alkenes, this is only possible with electron-rich alkenes in the presence of ketones.<sup>5</sup> One of the minor side reactions that can occur at each stage of sulfide-MA **2**, sulfoxide-MA **3**, and sulfone-MA **4** is the addition of proline under loss of double bond functionality. The double adduct species were identified by LC-HRMS.

At the stage of sulfoxide-MA **3**, proline can now undergo an addition-substitution reaction, expelling the corresponding sulfenic acid under the generation of starting proline-MA **1**. This step is irreversible, as sulfenic acids are notorious for their high reactivity,<sup>6</sup> leading to their swift degradation. They can either be directly oxidized to sulfinates (and sulfonates subsequently) or dimerize under the release of water to form thiosulfinates. These thiosulfinates can either comproportionate with sulfinates to form thiosulfonates, or, more likely under our conditions, hydrolyze (under sulfide-catalysis) to yield a thiol and a sulfinate, as shown in literature.<sup>6,7</sup> The thiol formed in this process can either be oxidized by free Oxone or react with proline-MA **1** to generate more sulfide-MA **2**. We confirmed these pathways by reacting sulfoxide-MA **3** with proline and identifying the proposed side products (Figure 6.3d, main text).

At the last stage of the main route, sulfone-MA **4** is present and can directly react with proline to recover proline-MA **1** under the generation of free sulfinate. This last step has been shown before in literature for the functionalization of lysine residues.<sup>8</sup> We propose that this reaction is an equilibrium (see Figure S6.8) and will only lead to high yields if the released sulfinate is further oxidized to inert sulfonate, which presents the final waste species.

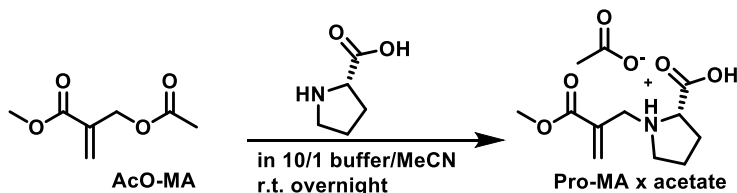
The cycle is closed, and the recovered proline-MA **1** can now undergo the same reactions again upon the addition of new portions of thiol and oxidant (see repeated oxidant additions in Figure 6.2d, main text).

## Synthesis



Methyl (2-acetoxymethyl)acrylate (AcO-MA) was synthesized according to a literature procedure.<sup>9</sup> Briefly, 1.161 g (1.030 mL, 10.0 mmol, 1.0 eq.) methyl (2-hydroxymethyl)acrylate were dissolved in 20 mL anhydrous DCM under argon. The solution was cooled to 0 °C in an ice bath. 1.113 g (1.525 mL, 11.0 mmol, 1.1 eq.) triethylamine were added, followed by the dropwise addition of 0.785 g (0.714 mL, 10.0 mmol, 1.0 eq.) acetyl chloride. The ice bath was removed, and a colorless precipitate formed within approximately one minute. After stirring at r.t. for two hours, the mixture was filtered, and the filter was rinsed with additional DCM. The organic phase was washed with 20 mL water twice and with 20 mL brine once. The organic phase was dried over MgSO<sub>4</sub>, and the solvent was removed under reduced pressure. The crude, yellow liquid was purified via a short silica plug (gradient 10/1 → 8/1 PE/EA) to yield 1.32 g (8.5 mmol, 85%) as a colorless oil.

<sup>1</sup>H-NMR (400 MHz, CDCl<sub>3</sub>): δ = 6.36 (s, 1H, C=CH<sub>2</sub>), 5.84 (s, 1H, C=CH<sub>2</sub>), 4.80 (s, 2H, CH<sub>2</sub>OAc), 3.78 (s, 3H, OCH<sub>3</sub>), 2.10 (s, 3H, O(O)CCH<sub>3</sub>). The spectroscopic data was found to be in accordance with the literature data.<sup>9</sup>



**Note:** This synthesis proved to be challenging. A synthesis starting from Br-MA was not feasible as the product would contain bromide as a counterion which can react with some oxidants, forming oxidized bromine species. The bromide counterion proved difficult to remove. Hence, a switch to AcO-MA was necessary to introduce the inert acetate counterion. Also, using a buffer is crucial to avoid acidification from the release of acetic acid over time which would halt the reaction by protonating free proline. Furthermore, the pH MUST NOT exceed 8.0 as this will lead to swift hydrolysis of the methyl ester moiety. Hence, the use of other strong, sacrificial bases instead of the buffer is also not feasible. The product was not isolated from the buffer salts and was used as a stock solution, the concentration of which was determined by adding a known amount of pure 4-mercaptobenzoic acid (MBA) and comparing the signals of remaining Proline-MA and sulfide-MA.

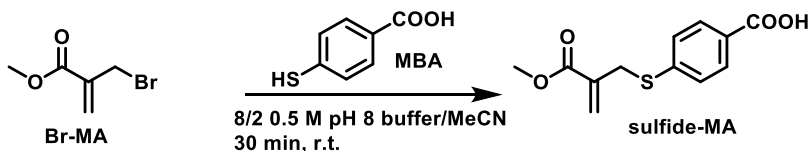
(2-(methoxycarbonyl)allyl)-L-proline (proline-MA **1**) was synthesized by dissolving 229.30 mg (2.0 mmol, 1.0 eq.) L-proline in a mixture of 10 mL 0.5 M pH 7.4 potassium

phosphate buffer and 1 mL acetonitrile. (**Note:** acetonitrile is not necessary, however, it speeds up the reaction by aiding the dissolution of hydrophobic AcO-MA.) 647.6 mg (585.0  $\mu$ L, 2.4 mmol, 1.2 eq.) AcO-MA were added dropwise. The mixture was vigorously stirred at room temperature overnight, upon which the suspension cleared up. The excess AcO-MA was removed by extracting with 15 mL EtOAc twice. The acetonitrile was removed under reduced pressure, and the water was removed by lyophilizing. The resulting colorless powder was dissolved in 9/1 0.5 M potassium phosphate buffer/DMF (pH dependent on the experiment) to yield a 70 mM stock solution. The yield, determined by NMR, usually exceeded 90 %, depending on the batch. **Note:** The following spectra were taken of a batch without acetate as a counterion.

**$^1\text{H-NMR}$  (400 MHz, MeOD):**  $\delta$  = 6.56 (s, 1H, C=CH<sub>2</sub>), 6.28 (s, 1H, C=CH<sub>2</sub>), 4.20 – 4.08 (m, 2H, C<sub>q</sub>CH<sub>2</sub>N, **Note:** we found that the observed multiplicity of these CH<sub>2</sub> signals strongly depends on the solvent.), 3.93 (ddd, J = 9.6, 5.2, 1.7 Hz, 1H, NCHCOOH), 3.83 (s, 3H, C(O)OCH<sub>3</sub>), 3.72 (ddd, J = 11.8, 8.3, 5.1 Hz, 1H, NCH<sub>2</sub>CH<sub>2</sub>), 3.26 – 3.14 (m, 1H, NCH<sub>2</sub>CH<sub>2</sub>), 2.52 – 2.38 (m, 1H, NCH(COOH)CH<sub>2</sub>), 2.22 – 2.04 (m, 2H, NCH(COOH)CH<sub>2</sub>, NCH<sub>2</sub>CH<sub>2</sub>), 1.94 (dq, J = 13.2, 8.5 Hz, 1H, NCH<sub>2</sub>CH<sub>2</sub>).

**$^{13}\text{C-NMR}$  (101 MHz, MeOD):**  $\delta$  = 173.13 (COOH), 167.05 (COOMe), 135.58 (C<sub>q</sub>=CH<sub>2</sub>), 132.74 (C<sub>q</sub>=CH<sub>2</sub>), 70.64 (NCHCOOH), 56.61 (C<sub>q</sub>CH<sub>2</sub>N), 55.99 (NCH<sub>2</sub>CH<sub>2</sub>), 53.25 (C(O)OCH<sub>3</sub>), 30.18 (NCH(COOH)CH<sub>2</sub>), 24.64 (NCH<sub>2</sub>CH<sub>2</sub>).

**ESI-LC/HRMS (m/z):** calculated for [C<sub>10</sub>H<sub>16</sub>NO<sub>4</sub>]<sup>+</sup>: 214.1074, found: 214.1065; calculated for [C<sub>10</sub>H<sub>14</sub>NO<sub>4</sub>]<sup>-</sup>: 212.0928, found: 212.0923.

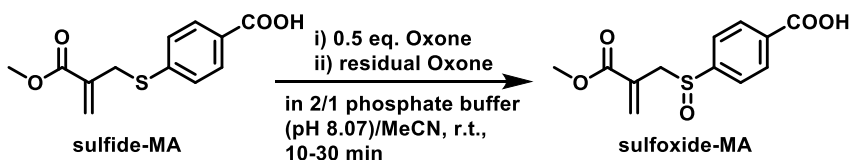


4-((2-(methoxycarbonyl)allyl)thio)benzoic acid (sulfide-MA **2**) was synthesized by dissolving 154.18 mg (1.0 mmol, 1.0 eq.) 4-mercapto benzoic acid (MBA) in 10 mL of an 8/2 mixture of 0.5 M pH 8 potassium phosphate buffer and acetonitrile. 179.01 mg (119.34  $\mu$ L, 1.0 mmol, 1.0 eq.) of Br-MA were added dropwise. After stirring at room temperature for 30 minutes, the acetonitrile was mostly removed under reduced pressure, upon which the solution turned cloudy. (**Note:** Unlike sulfoxide- and sulfone-MA, sulfide-MA is not soluble in pure buffer even at elevated pH. Hence, it is important to add the reactants in a 1:1 ratio as precisely as possible, as washing the aqueous phase will extract excess Br-MA and sulfide-MA even before acidification.) The aqueous phase was then diluted with approximately 10 mL water, acidified to pH 1 with approximately 5 mL 1 M HCl, and extracted with 20 mL EtOAc thrice. The combined organic phases were dried over MgSO<sub>4</sub>, and the solvent was removed under reduced pressure to yield 227.1 mg (0.9 mmol, 90%) sulfide-MA **2** as a pale-yellow powder.

**<sup>1</sup>H-NMR (400 MHz, MeOD):**  $\delta$  = 7.95 – 7.87 (m, 2H,  $CHC_qCOOH$ ), 7.41 – 7.35 (m, 2H,  $CHC_qS$ ), 6.17 (s, 1H,  $C=CH_2$ ), 5.76 (s, 1H,  $C=CH_2$ ), 3.92 (s, 2H,  $CH_2S$ ), 3.77 (s, 3H,  $C(O)OCH_3$ ).

**<sup>13</sup>C-NMR (101 MHz, MeOD):**  $\delta$  = 169.39 (COOH), 167.85 (COOMe), 144.02 ( $C_qCOOH$ ), 137.52 ( $C_qS$ ), 131.16 ( $CHC_qCOOH$ ), 129.33 ( $C_q=CH_2$ ), 129.12 ( $CHC_qS$ ), 127.74 ( $C_q=CH_2$ ), 52.62 (COOMe), 34.55 ( $CH_2S$ ).

**ESI-LC/HRMS (m/z):** calculated for [ $C_{12}H_{11}O_4S$ ]: 251.0384, found: 251.0382.

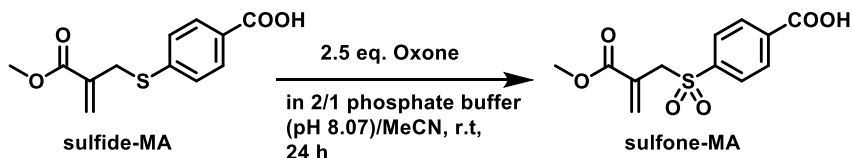


4-((2-(methoxycarbonyl)allyl)sulfinyl)benzoic acid (sulfoxide-MA **3**) was synthesized by dissolving 47.58 mg (0.189 mmol, 1.0 eq.) sulfide-MA in 6 mL of a 2/1 mixture of 0.5 M pH 8.07 potassium phosphate buffer and acetonitrile. 28.97 mg (94.25  $\mu$ mol, 0.5 eq.) Oxone was dissolved in 1 mL of water and added to the MA-sulfide solution. The solution was stirred at room temperature for 10 minutes. Upon NMR measurement, it was determined that 44.6 % of sulfide-MA had reacted to sulfoxide-MA. Hence, it was calculated that 35.2 mg Oxone were needed to achieve full conversion. This amount was weighed out, added as a solution in 1 mL water, and it was stirred for a further 30 minutes. After completion, the reaction mixture was diluted with 15 mL water and acidified to pH 1 with approximately 5 mL 1 M HCl. Upon acidification, a thick, colorless precipitate formed. The milky suspension was extracted with 20 mL chloroform thrice. The combined organic layers were washed with 10 mL 1 M HCl and dried over  $MgSO_4$ . The solvent was removed under reduced pressure to yield 42.38 mg (0.158 mmol, 84%) of sulfoxide-MA **3** as a colorless powder. **Note:** Unlike sulfide-MA **2** and sulfone-MA **4**, which we found to be stable over months at room temperature, sulfoxide-MA **3** tends to degrade and needs to be stored in the fridge or preferably the freezer and be used up within several days.

**<sup>1</sup>H-NMR (400 MHz, MeOD):**  $\delta$  = 8.22 – 8.16 (m, 2H,  $CHC_qCOOH$ ), 7.76 – 7.71 (m, 2H,  $CHC_qSO$ ), 6.43 (d,  $J$  = 0.9 Hz, 1H,  $C=CH_2$ ), 5.78 – 5.76 (m, 1H,  $C=CH_2$ ), 4.02 (dd,  $J$  = 12.9, 1.0 Hz, 1H,  $CH_2SO$ , **Note:** we found that the multiplicity of these  $CH_2$  protons strongly depends on the solvent.), 3.91 (dd,  $J$  = 12.9, 0.8 Hz, 1H,  $CH_2SO$ , **Note:** we found that the multiplicity of these  $CH_2$  protons strongly depends on the solvent.), 3.62 (s, 3H,  $C(O)OCH_3$ ).

**<sup>13</sup>C-NMR (101 MHz, MeOD):**  $\delta$  = 168.43 (COOH), 167.17 (COOMe), 148.22 ( $C_qCOOH$ ), 135.09 ( $C_qSO$ ), 133.45 ( $C_q=CH_2$ ), 131.36 ( $CHC_qCOOH$ ), 130.20 ( $C_q=CH_2$ ), 125.79 ( $CHC_qSO$ ), 59.08 ( $CH_2SO$ ), 52.73 ( $C(O)OCH_3$ ).

**ESI-LC/HRMS (m/z):** calculated for  $[C_{12}H_{11}O_5S]^-$ : 267.0333, found: 267.0333; calculated for  $[C_{12}H_{13}O_5S]^+$ : 269.0478, found: 269.0468.



4-((2-(methoxycarbonyl)allyl)sulfonyl)benzoic acid (sulfone-MA **4**) was synthesized by dissolving 47.58 mg (0.189 mmol, 1.0 eq.) sulfide-MA in 6 mL of a 2/1 mixture of 0.5 M pH 8.07 potassium phosphate buffer and acetonitrile. 144.85 mg (0.471 mmol, 2.5 eq.) Oxone were dissolved in 1 mL of water and added to the MA-sulfide solution. A further 2 mL water were added to dissolve the Oxone fully. The solution was stirred at room temperature for 24 hours. After completion, the reaction mixture was diluted with 15 mL water and acidified to pH 1 with approximately 5 mL 1 M HCl. Upon acidification, a thick, colorless precipitate formed. The milky suspension was extracted with 20 mL chloroform thrice. The combined organic layers were washed with 10 mL 1 M HCl and dried over  $MgSO_4$ . The solvent was removed under reduced pressure to yield 40.68 mg (0.143 mmol, 76%) of sulfone-MA **4** as a colorless powder.

**$^1H$ -NMR (400 MHz, MeOD):**  $\delta$  = 8.23 (d,  $J$  = 8.0, 2H,  $CHC_qCOOH$ ), 7.96 (d,  $J$  = 8.0, 2H,  $CHC_qSO_2$ ), 6.45 (s, 1H,  $C=CH_2$ ), 5.85 (s, 1H,  $C=CH_2$ ), 4.33 (s, 2H,  $CH_2SO_2$ ), 3.60 (s, 3H,  $C(O)OCH_3$ ).

**$^{13}C$ -NMR (101 MHz, MeOD):**  $\delta$  = 167.88 ( $COOH$ ), 166.80 ( $COOMe$ ), 143.40 ( $C_qCOOH$ ), 137.19 ( $C_qSO_2$ ), 134.41 ( $C_q=CH_2$ ), 131.37 ( $CHC_qCOOH$ ), 130.59 ( $C_q=CH_2$ ), 130.05 ( $CHC_qSO_2$ ), 58.28 ( $CH_2SO_2$ ), 52.83 ( $C(O)OCH_3$ ).

**ESI-LC/HRMS (m/z):** calculated for  $[C_{12}H_{11}O_6S]^-$ : 283.0282, found: 283.0282; calculated for  $[C_{12}H_{13}O_6S]^+$ : 285.0427, found: 284.0417.

## Supplementary experiments

### T1 measurements

To allow for qNMR measurements to be conducted, we measured the T1 times for compounds to be quantified via inversion-recovery experiments. Measurements were performed under the same conditions (i.e. solvent, concentration, and temperature) as in the kinetic studies. T1 times were extracted for the double bond signals of MA species and can be found tabulated below.

**Table S6.1:** Compounds that were used in qNMR, the signal of the nucleus that was used for quantification, and its calculated T1 time.

Compound	Signal (ppm)	T1 time (s)
Sulfone-MA <b>4</b>	6.35	0.85
Sulfoxide-MA <b>3</b>	6.25	0.80
Proline-MA <b>1</b>	7.40	1.04
Sulfide-MA <b>2</b>	5.93	1.40
TCEP-MA adduct	6.45	0.73
Disulfide <b>5</b>	7.62	1.96
Morpholine-MA	6.22	1.09
Piperidine-MA	6.53	0.99
Lysine-MA	5.92	1.45
4-amino benzoic acid-MA	5.65	0.74
ATMA-MA	6.09	0.86
<i>N</i> -methyl taurine-MA	6.22	0.92
Aspartic acid-MA	6.27	0.82

### Half-lives of individual CRN reactions

We have extracted the apparent half-lives from the graphs of separately studied reactions wherever possible. Although the half-lives of these individually studied reactions do not necessarily reflect the kinetics of the whole network, they are convenient to compare experiments with each other.

Comparing the proline reaction with sulfone-MA **4**, sulfoxide-MA **3**, and sulfide-MA **2** separate from the full network (Proline-MA **1** formation in entries # 2, 3, and 4), one can see that reaction with sulfoxide-MA **3** is slightly faster than with sulfone-MA **4** (20 min vs. 28 min). It is the slowest with sulfide-MA **4** (413 min).

The recovery rate of proline-MA **1** is increased in the reaction with sulfide-MA **4** by adding an oxidant KIO<sub>3</sub> (329 min, entry # 7).

Proline-MA **1** recovery in separate steps is faster than within the full network (28 min vs. 31 min, entries # 2, 5) and sulfoxide shunt (20 min vs. 202 min, entries # 3, 6).

Proline-MA **1** recovery is faster in the full cycle (via the sulfone, 31 min, entry # 5) than in the sulfoxide shunt (202 min, entry # 6) and the sulfide shunt (329 min, entry # 7).

Finally, in the sulfide shunt, adding thiol and oxidant simultaneously or stepwise also influences the rate of proline-MA **1** recovery (643 vs. 329 min).

**Table S6.2:** Half-lives of different reactions of the whole CRN and the two shunts, determined from <sup>1</sup>H-NMR experiments, with standard deviations.

#		Reaction	Half-life, t <sub>1/2</sub> , min
1	Sulfide oxidation	Sulfide-MA 2 oxidation with 2.5 eq. Oxone at pH 8	Sulfoxide-MA 3 consumption 9.3±0.5 min Sulfone-MA 4 formation 4.9±0.2 min
2	Sulfone + Pro	Sulfone-MA 4 + 1.0 eq. Proline at pH 8	Sulfone-MA 4 consumption 26±1 min Proline-MA 1 formation 28±1 min
3	Sulfoxide + Pro	Sulfoxide-MA 3 + 1.0 eq. Proline at pH 8	Sulfoxide-MA 3 consumption 25±4 min Proline-MA 1 formation 20±3 min
4	Sulfide + Pro	Sulfide-MA 2 + 1.0 eq. Proline at pH 8	Sulfide-MA 2 consumption 1480±172 min Proline-MA 1 formation 413±100 min
5	Sulfone cycle stepwise	Sulfide-MA 2 + 1.0 eq. Proline + 2.5 eq. Oxone at pH 8	Proline-MA 1 formation 31±1 min
6	Sulfoxide cycle stepwise	Sulfide-MA 2 + 1.0 eq. Proline + 2.5 eq. NaClO <sub>2</sub> at pH 8	Sulfide-MA 2 consumption 283±10min Proline-MA 1 formation 202±7 min
7	Sulfide cycle stepwise	Sulfide-MA 2 + 1.0 eq. Proline + 2.5 eq. KIO <sub>3</sub> at pH 8	Sulfide-MA 2 consumption 541±1min Proline-MA 1 formation 329±29 min
8	Sulfide cycle simultaneous addition	Sulfide-MA 2 + 1.0 eq. Proline + 0.33 eq. KBrO <sub>3</sub> at pH 8	Sulfide-MA 2 consumption 941±11 min Proline-MA 1 formation 643±7 min

## Sulfide Oxidation at different pH values

We tested the oxidation of sulfide-MA **2** to sulfone-MA **4** with 2.5 equivalents of Oxone at different pH values (Figure S6.1). Firstly, it is apparent that the oxidation happens via sulfoxide-MA **3** and that this step is relatively fast, showing the highest conversions within several minutes. Sulfoxide-MA **3** then gets further oxidized to sulfone-MA **4** within roughly one hour. Furthermore, in the pH range we tested, we did not see a significant impact of the pH value on the oxidation rates. This is plausible, as the  $\text{HSO}_5^-$  anion, which is the most abundant form at this pH value, has a  $\text{pK}_a$  value of 9.88. Hence, the  $\text{SO}_5^{2-}$  form with a lower oxidation potential only becomes the dominant species at pH values above 10.<sup>10</sup>

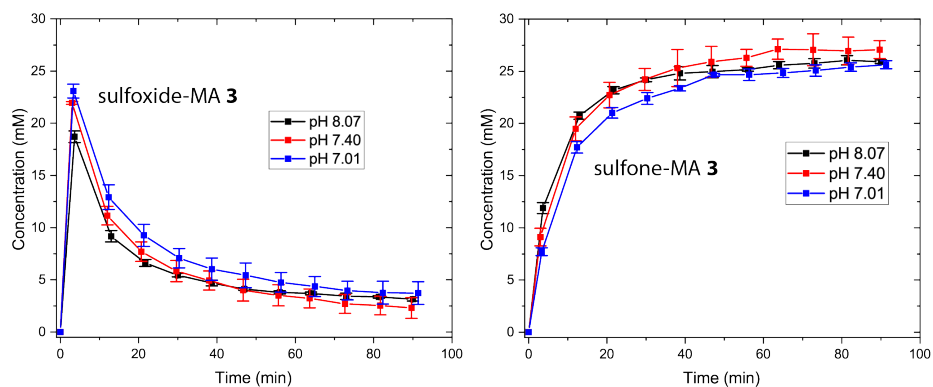


**Figure S6.1:** The oxidation of sulfide-MA **2** to sulfone-MA **4** via sulfoxide-MA **3** in the presence of 2.5 eq. of Oxone.

## Sulfone-MA + nucleophiles

To determine which nucleophile is most suitable to run the addition-substitution reaction on sulfone-MA **4**, we tested a range of primary and secondary amines as these species are most likely to be able to undergo this reaction (Figure S6.2). We found that, in general, amines, both primary and secondary, react well with sulfone-MA **4**. Especially for morpholine, we found swift, high conversions (red line), however, the product is not stable over time. We found similar results for the reaction of sulfone-MA **4** with *N*-methyltaurine, piperidine, and (2-aminoethyl)trimethylammonium chloride hydrochloride (ATMA), although their degradation was somewhat slower than that of the morpholine-MA adduct. The addition with 3-aminobenzoic acid also proceeds smoothly, although over a relatively long timescale with lower conversions. Hence, we found that proline is the best nucleophile candidate due to the relatively fast product formation and stability over time (dark grey line with squares, Figure S6.2, Figure S6.7).

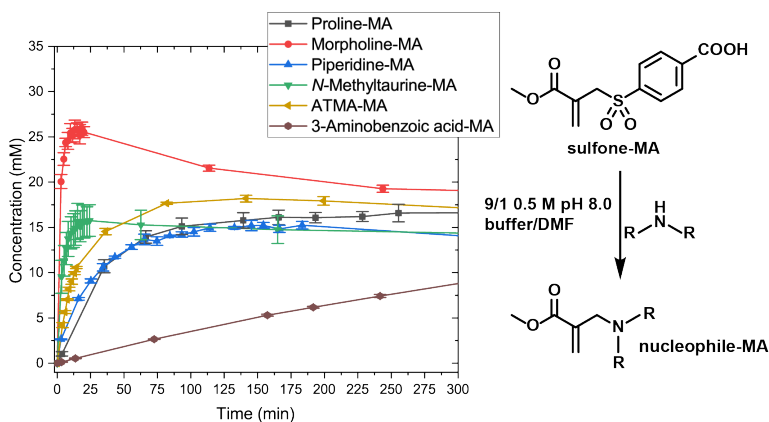


**Figure S6.2:** Reaction of different amine nucleophiles with sulfone-MA **4** to yield nucleophile-substituted MAs.

Apart from the nucleophiles that can substitute on sulfone-MA **4** discussed above, we tested several other nucleophiles. We found that phenol, tertiary amines such as trimethylamine, and pyrroles such as pyrrole-2-carboxylic acid do not react with sulfone-MA. It has been shown in the literature that aliphatic alcohols can substitute sulfone MAs under certain conditions (in the presence of  $K_2CO_3$ , see compound **5**, condition iii. in reference).<sup>11</sup> Our rationale was that phenols, which are more acidic than aliphatic alcohols, should be able to act as nucleophiles under our conditions as well. However, no substitution took place (see Figure S6.3). Furthermore, in accordance with the literature, we found that tertiary amines cannot substitute on sulfone-MA (Figure S6.4) due to the lack of the hydrogen-bonding motif.<sup>8</sup> Pyrrole-2-carboxylic acid can likely not participate in a substitution reaction due to the nitrogen's free electron pair being involved in aromaticity (Figure S6.5). We also tested the reaction of several other nucleophiles that successfully substituted on sulfone-MA. The conversion plots for these nucleophiles were left out in the main text for clarity reasons and the presence of some side reactions that will be discussed below.

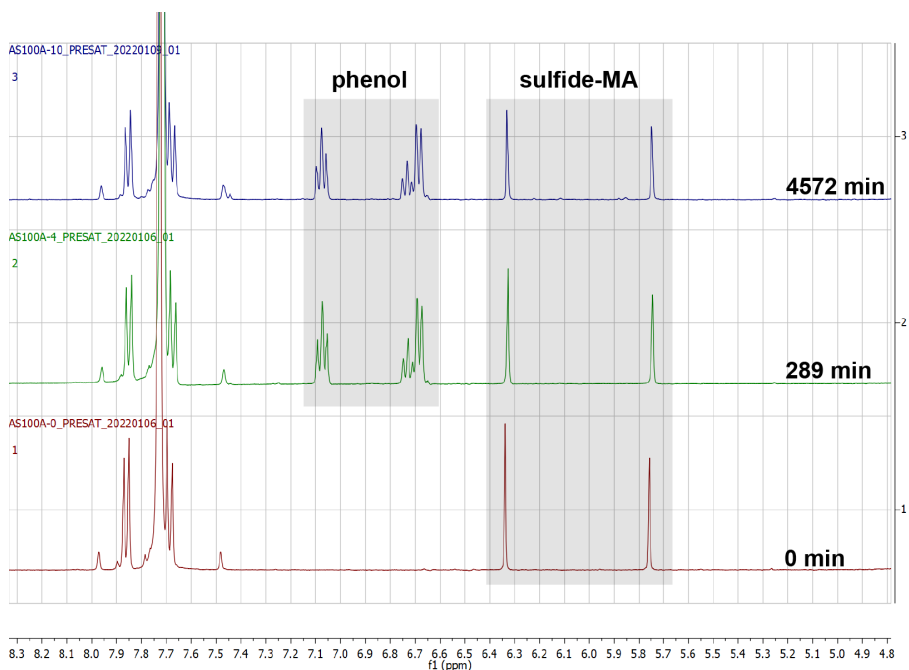


**Figure S6.3:** <sup>1</sup>H-NMR cutout; bottom: sulfide-MA **2** reference; middle and top: sulfide-MA **2** after addition of 1.0 eq. phenol. No reaction could be observed. As stated in the general section, standard NMR conditions were used (i.e. 9/1 0.5 M pH 8.0 phosphate buffer/DMF) unless stated otherwise.

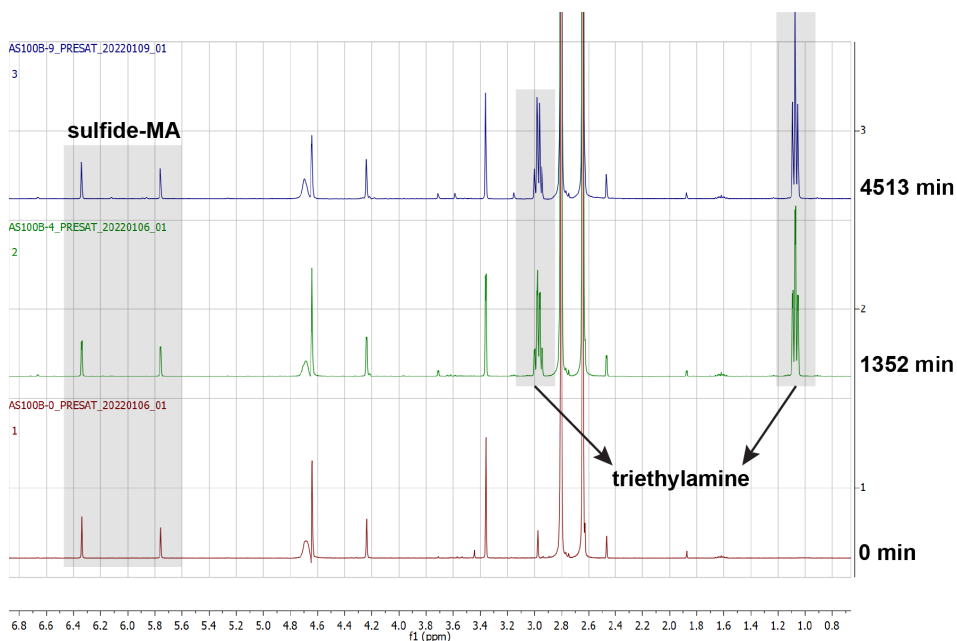


**Figure S6.4:** <sup>1</sup>H-NMR cutout; bottom: sulfide-MA **2** reference; middle and top: sulfide-MA **2** after addition of 1.0 eq. triethylamine. No reaction could be observed.

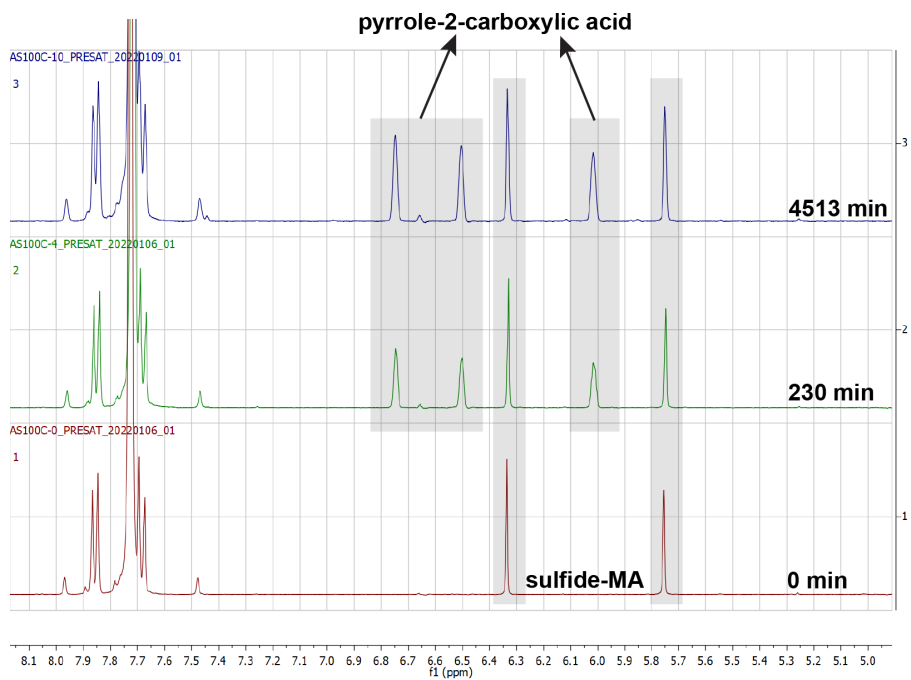


**Figure S6.5:** <sup>1</sup>H-NMR cutout; bottom: sulfide-MA **2** reference; middle and top: sulfide-MA **2** after addition of 1.0 eq. pyrrole-2-carboxylic acid. No reaction could be observed.

The reaction of sulfone-MA **4** with the primary amines aspartic acid and *N*-acetyl lysine (Figure S6.6) showed the formation of double addition products, which made these species not suitable. Interestingly, the third primary amine we tested, ATMA, did not show this double addition (Figure S6.2).

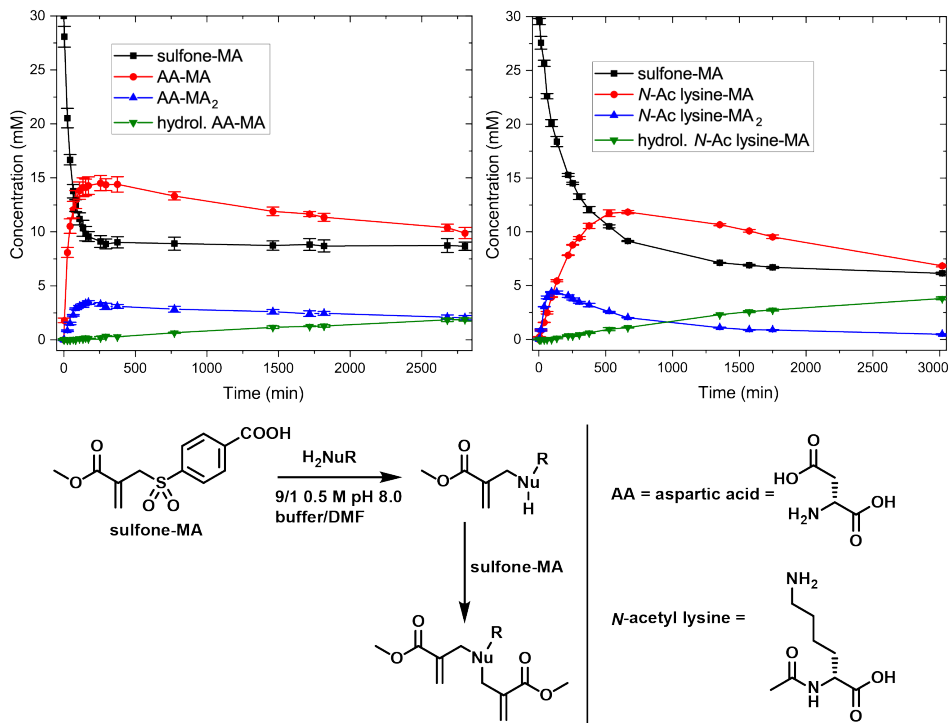


**Figure S6.6:** Reaction of sulfone-MA **4** with aspartic acid (left) and *N*-acetyl lysine (right). The graph shows the consumption of sulfone-MA **4** over time, along with the formation of the mono- and bis-adducts over time. The green line shows the hydrolysis of the mono-adducts over time.

Apart from comparing the kinetics to choose which nucleophile would best suit our system, we also looked at any potential side reactions. The main side reaction we found (besides the double addition of primary amines) was the hydrolysis of the substituted products (Figure S6.7). The comparatively slow hydrolysis of proline-MA was one of the points that made it a favorable candidate for our CRNs.

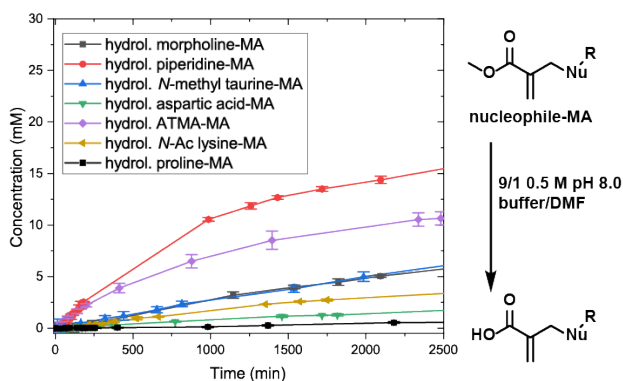


**Figure S6.7:** Hydrolysis of nucleophile-MAs (products of sulfone-MA **4** + nucleophile) over time. 3-amino benzoic acid is not shown, as no hydrolysis product was detected over this time scale.

### Sulfone-MA **4** + additional proline: substitution reversibility and the fate of the sulfinate

As can be seen for the reaction of sulfone-MA **4** + nucleophiles (Figure S6.2 and Figure S6.6), different nucleophiles give different yields of nucleophile-MA, yet some sulfone-MA **4** always remains unreacted. We hypothesize that the substitution of sulfone-MA **4** under the release of the corresponding sulfinate salt is an equilibrium reaction. The sulfinate anion is nucleophilic enough to re-attack the nucleophile-MAs, displacing an amine. This would explain the lower yields with the less-nucleophilic amines (e.g., proline-MA **1** vs. morpholine-MA). To further support this hypothesis, upon the reaction of sulfone-MA **4** with 1 eq. proline, a further 5 eq. of proline were added to examine how the system behaves. We indeed found an increase in the yield of proline-MA **1**, suggesting the presence of an equilibrium between sulfone-MA **4** and nucleophile-MA. However, as demonstrated in Figure S6.8, an excess of nucleophiles should be avoided, as the increase in yield is negligible compared to the loss of active MA moieties due to the double addition adducts.

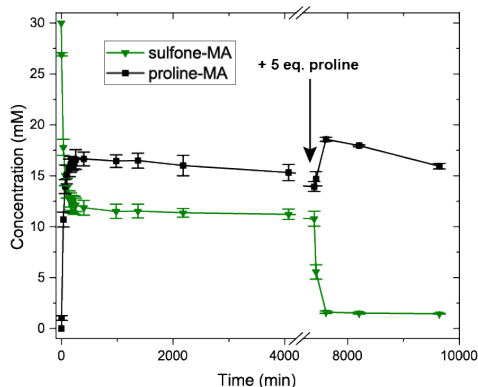


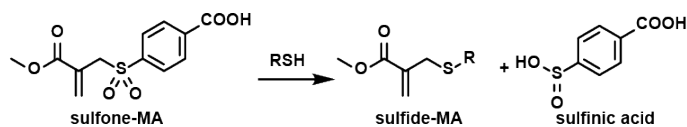
**Figure S6.8:** Reaction of sulfone-MA with 1.0 eq. proline and the addition of a further 5.0 eq. proline.

Apart from these experiments, we managed to confirm the presence of the sulfinate of MBA via HRMS: found for  $[M-H^+]^-$  184.9907 (expected: 184.9914).

Furthermore, we found the sulfonate of MBA: found for  $[M-H^+]^-$  200.9858 (expected: 200.9863). It remains unclear whether the sulfonate formed during analysis in the LC-HRMS, or whether oxidation to sulfonate occurred before analysis due to the presence of atmospheric oxygen. In general, sulfinates (and even more so sulfinic acids) are prone to oxidation; however, aromatic sulfinates have been found to be somewhat more stable than their aliphatic counterparts.<sup>12</sup> In general, we assume that the sulfinate of MBA is relatively stable in solution. Otherwise, in the reaction of sulfone-MA **4** with nucleophiles, more nucleophile-MA would form over time as the released sulfinate degrades to yield sulfonate, which is not in equilibrium anymore.

### Sulfone-MA **4** + thiol(s)

As expected, we found that not only amines can displace sulfinates by undergoing a substitution reaction with sulfone-MA **4**, but also thiols—as they are the stronger nucleophiles—giving sulfide-MA **2** and a sulfinate salt in the process (Scheme S6.2). This reaction is fast compared to the reaction with amines (i.e. full conversion within minutes). We chose an aromatic thiol (MBA, Figure S6.9) and an aliphatic thiol (3-mercaptopropionic acid, Figure S6.10) to demonstrate this point.



**Scheme S6.2:** Reaction of sulfone-MA with a thiol (RSH) to yield sulfide-MA and sulfonic acid (effectively sulfinate at pH 8).

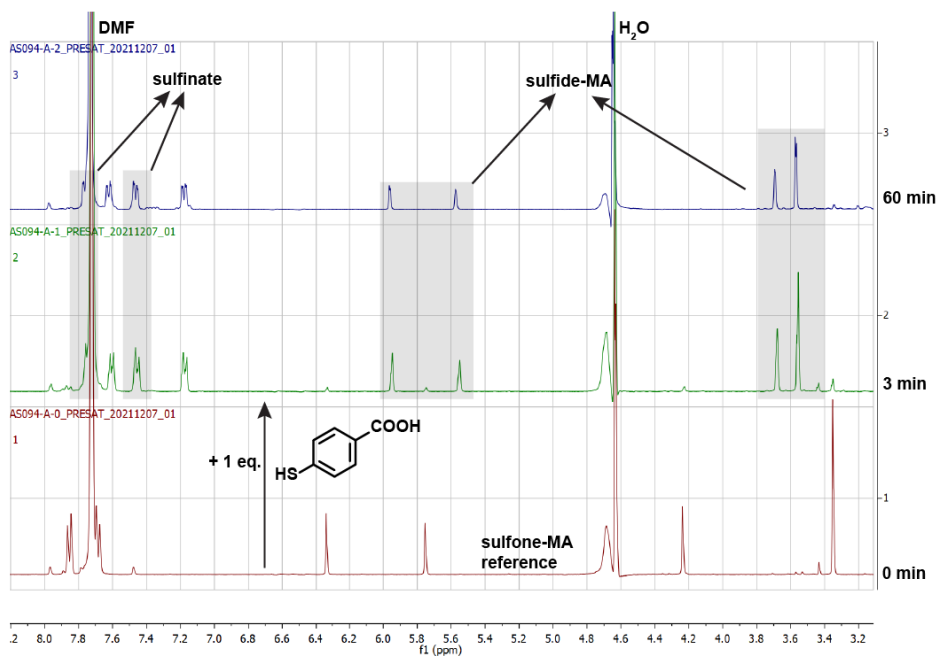


**Figure S6.9:** Reaction of sulfone-MA 4 with 1.0 eq. of MBA to yield sulfide-MA 2 and sulfinate. **Note:** The downfield aromatic sulfinate signal overlaps with the DMF signal.

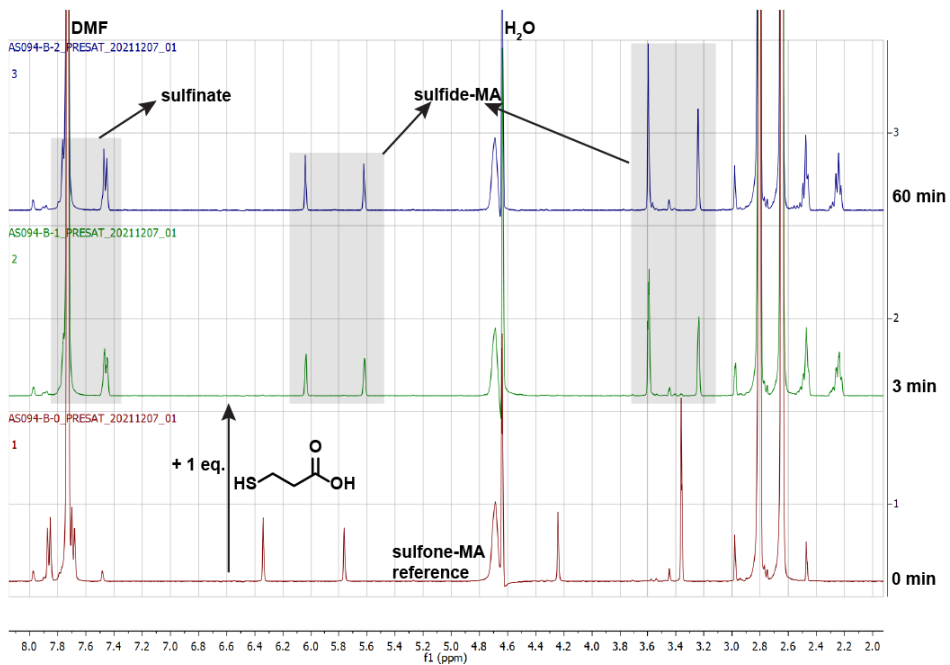


**Figure S6.10:** Reaction of sulfone-MA 4 with 1.0 eq. of 3-mercapto propionic acid to yield sulfide-MA 2 and sulfinate. **Note:** The downfield aromatic sulfinate signal overlaps with the DMF signal.

## Sulfoxide-MA 3 + thiol

Analogously to the reaction between sulfone-MA 4 and thiols, the reaction between sulfoxide-MA 3 and thiols can also proceed, yielding a sulfide-MA 2 and a sulfenic acid which will further react according to Scheme S6.1 (see Figure S6.11). The same side products (i.e. sulfone-MA 4, disulfide 5) can also be found in the reaction of sulfoxide-MA 3 with proline (Figure 6.3d).

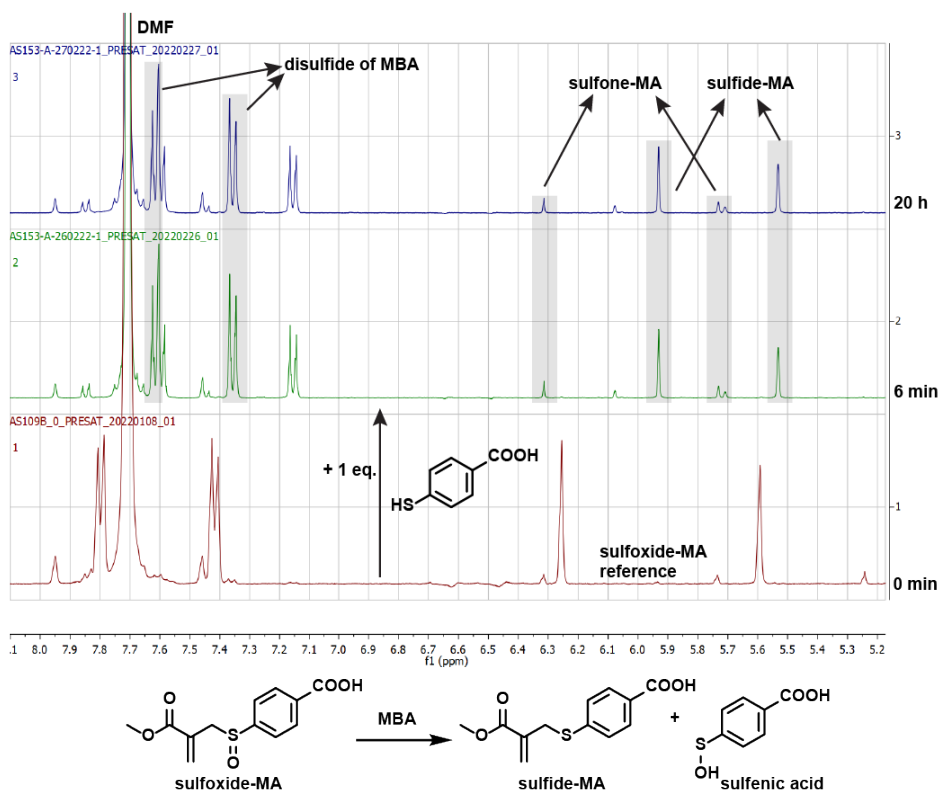


**Figure S6.11:** Reaction of sulfoxide-MA 3 with 1.0 eq. MBA to yield sulfide-MA 2, along with the disulfide of MBA 5 (from the degradation of sulfenic acid) and small amounts of sulfone-MA 4 (from the degradation of sulfenic acid and further reaction with sulfoxide-MA 3).

## Sulfone network: simultaneous addition of MBA and Oxone

Unlike the stepwise addition experiments we tested in the main text (e.g. Figure 6.2d), we also decided to test a simultaneous addition of MBA and Oxone to see if the sulfone system can be run as a reaction cycle with strong oxidants. We found minimal recoveries of proline-MA 1 due to the swift reaction of Oxone with MBA to form the corresponding disulfide 5. Furthermore, Oxone reacted both with proline and proline-MA 1 to form the nitron and oxidized proline-MA, respectively (compare Scheme S6.1). This also explains why, even though proline-MA 1 can be recovered from oxidized proline-MA, the actual recoveries are minimal.

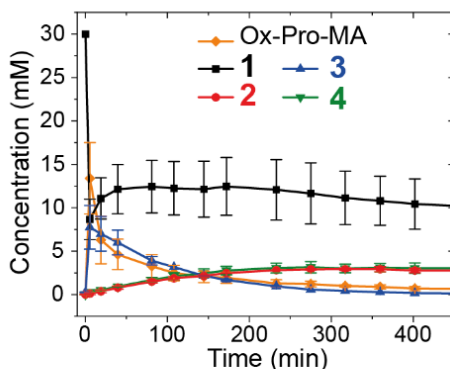


**Figure S6.12:** evolution of different species in the CRN upon simultaneous addition of MBA and Oxone to a solution of proline-MA **1**. The oxidation of thiol, proline, and proline-MA **1** outcompetes the conjugate addition and elimination of thiol to proline-MA **1**.

### Oxone: reference reactions

To demonstrate potential side reactions of our sulfone CRN, we performed several reference reactions of some species with Oxone. Here, we show how proline and proline-MA **1** react with Oxone. Furthermore, we show that acetate (side product of proline-MA **1** formation) and the used solvent mixture (i.e. buffer/DMF) are compatible with Oxone. First, we subjected proline to 2.5 eq. Oxone. It has been shown in the literature that the oxidation of amino acids and subsequent decarboxylation to nitrones typically proceeds via *N*-hydroxylamino acids and a short-lived intermediate dihydroxylated species before decarboxylating.<sup>13</sup> It has also been shown that Oxone specifically is capable of producing a nitron from proline.<sup>3</sup> In agreement with the literature data, we found the formation of the nitron upon oxidation of proline. However, we were unable to achieve full conversion even with 2.5 eq. Oxone. Furthermore, we were unable to observe any potential intermediate species as the conversion occurred too fast to be tracked appropriately via <sup>1</sup>H-NMR (Figure S6.13).

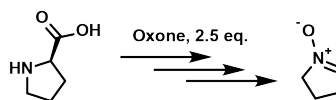
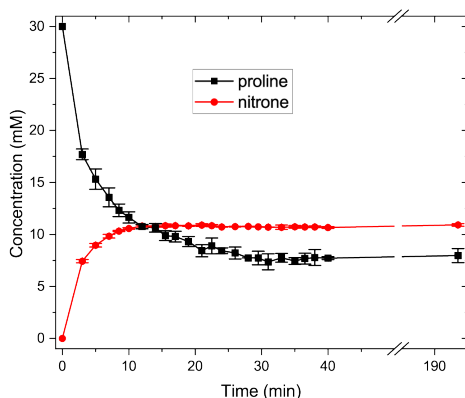


**Figure S6.13:** Reaction of proline with 2.5 eq. Oxone. The formation of nitron was observed, tracked by the appearance of the characteristic double bond signal at ~ 7 ppm.

Besides the NMR results, we also managed to confirm the nitron via HRMS from the reaction of proline-MA **1** with Oxone as a side product:

**ESI-LC/HRMS (m/z):** calculated for  $[C_4H_8NO^+]$  86.0600, found: 86.0606.

Next, we subjected proline-MA **1** to Oxone. It can be seen that a swift oxidation of proline-MA **1** upon the addition of Oxone takes place to form Ox-Proline-MA (see Figure S6.14, see also Scheme S6.1). We also managed to confirm this oxidized species via HRMS:

**ESI-LC/HRMS (m/z):** calculated for  $[C_{10}H_{16}NO_5^+]$  230.1023, found: 230.1015.

In alignment with the mechanism proposed in literature,<sup>13</sup> a decarboxylation, as in the oxidation of free proline, cannot take place due to the tertiary nature of the amine in the proline-MA **1** species. Therefore, the oxidation stops at the stage of the quaternary oxidized proline-MA.

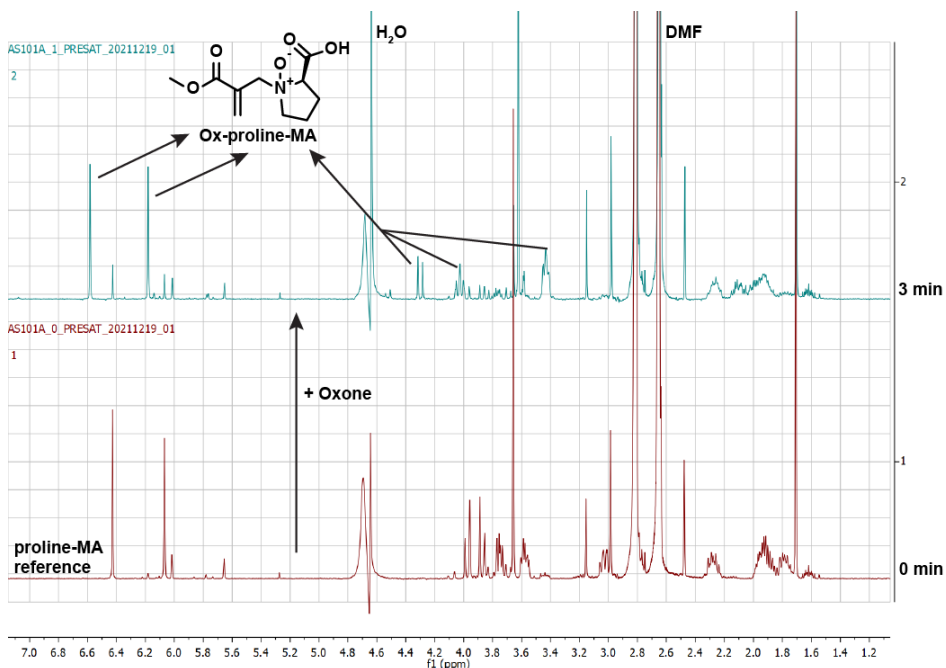


**Figure S6.14:** Reaction of proline-MA **1** with Oxone to yield oxidized proline-MA.

Lastly, we also subjected sodium acetate, as well as our solvent mixture (9/1 0.5 M pH 8.0 potassium phosphate buffer/DMF), to Oxone. Neither of those experiments showed any changes over time, ruling out any potential cross-reactivity between acetate (side product of proline-MA **1** preparation) and Oxone, as well as the used solvent and Oxone.

## Recovery of Proline-MA **1** from Ox-Proline-MA

As shown in Scheme S6.1, we have added a backward arrow leading back from oxidized Proline-MA to proline-MA **1**. We have found that upon oxidation of proline-MA **1**, the oxidized species becomes electron-deficient, and hence proline can re-attack, leading to the recovery of proline-MA **1**. As can be seen in Figure S6.15, proline-MA **1** quickly gets oxidized to form oxidized proline-MA (compare Scheme S6.1). Further, this signal decreases in intensity, and a new signal appears. We hypothesize that the oxidized proline-MA undergoes isomerization via nucleophilic attack of the amine-*N*-oxide on a second oxidized proline-MA to yield the *O*-bonded form as the thermodynamic product.

Upon addition of proline, proline-MA **1** gets recovered quickly from the oxidized proline-MA species via nucleophilic attack and substitution of *N*-hydroxyproline. The reason why this recovery is less efficient when trying to run the Oxone CRN as a reaction cycle (Figure S6.12) is the fact that proline, which is needed for the recovery of proline-MA **1**, also gets consumed by the Oxone that is added to the reaction mixture.

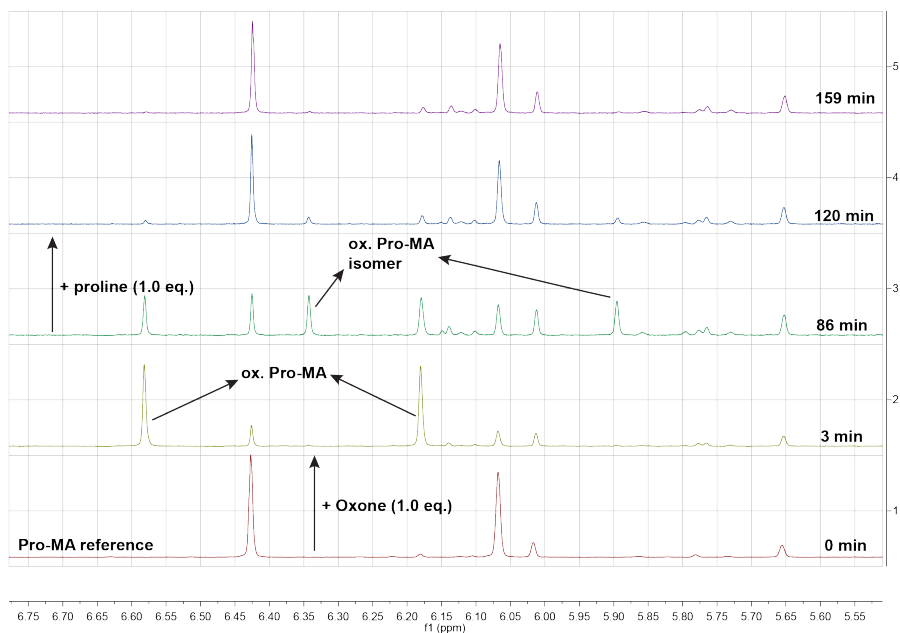


**Figure S6.15:** Oxidation of Proline-MA **1** with Oxone and subsequent addition of proline to recover Proline-MA **1**.

### Stepwise addition: comparison of oxidants

To directly compare the efficiency of different oxidants of recovering proline-MA **1** over time, we plotted the recoveries of proline-MA **1** over time from stepwise addition experiments, adding 2.5 eq. of oxidant in each case. In each case, we started from the usual 30 mM proline-MA **1** stock solution and added 1.0 eq. MBA, followed by adding a certain amount of oxidant (specified below).

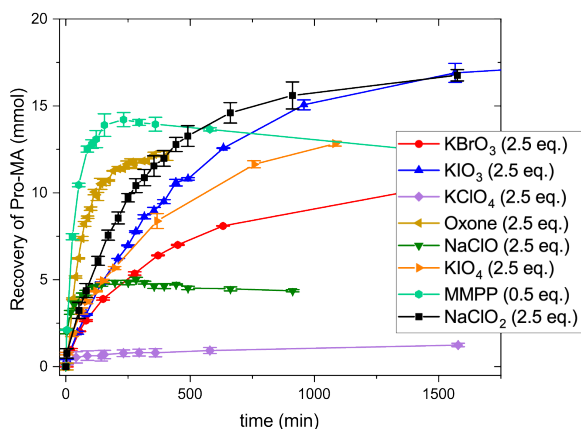


**Figure S6.16:** Comparison of different oxidants in the recovery of proline-MA **1** upon addition of 1.0 eq. of MBA to a 30 mM proline-MA stock solution, followed by the addition of the oxidant.

It can clearly be seen that the rates of recovery, the maximum level of recovery, and the product stability over time all vary widely, depending on the oxidant.  $\text{KClO}_4$  (violet line with diamonds) and  $\text{KClO}_3$  (omitted for clarity) do not work in recovering proline-MA **1** from sulfide-MA **2**, likely due to their weak oxidation strength under the used conditions compared to the other oxidants used.  $\text{KBrO}_3$  and  $\text{KIO}_3$  recover proline-MA **1** relatively slowly, as the recovery mechanism proceeds purely via oxidation of free thiol from equilibrium. As the concentration of free thiol and the rate of equilibration limit the overall rate of recovery, precise control of the recovery kinetics via variation of the oxidant quantity is not possible in the sulfide pathway. The oxidants that can oxidize sulfide-MA **2** to sulfoxide-MA **3** and/or sulfone-MA **4** lead to a more rapid recovery of proline-MA **1**, as the recovery of **1** depends on the direct displacement of sulfenic and/or sulfinic acid by proline instead of release of MBA. As we have shown, proline-MA **1** can be recovered similarly fast from sulfoxide-MA **3** and sulfone-MA **4**.

As the formation of sulfoxide-MA **3** is faster than that of sulfone-MA **4** with strong oxidants, the amount of oxidant used is another crucial factor. A good example is MMPP. While adding 2.5 eq. (omitted for clarity) led to a whole range of side reactions, as well as low and slow recovery rates, the use of 0.5 eq. led to a fast recovery of proline-MA **1**. However, the stability of recovered proline-MA was low over time. Likewise, for sodium hypochlorite, we also observed side reactivity, low recovery rates, and low stability of recovered proline-MA **1** over time. Oxone, on the other hand, led to a relatively fast recovery rate, high recovery level, and improved stability over time.

Hence, it can be concluded that by varying the applied oxidant, one has control over which pathway the recovery will take (i.e. slow sulfide pathway vs the much faster sulfoxide and sulfone pathways). Furthermore, the amount of strong oxidant (i.e. sulfone pathway) used can kinetically bias the pathway; using stoichiometric or substoichiometric amounts of oxidant can bias recovery mode more towards the sulfoxide pathway while using an excess of oxidant will bias the recovery mode more towards the sulfone pathway. These factors strongly influence side products, recovery rates, and the kinetics of the recovery.

## Sulfoxide-MA stability study

Unlike sulfide-MA **2** and sulfone-MA **4**, sulfoxide-MA **3** was neither stable in its pure form nor in solution for prolonged periods of time. We found a comparatively swift degradation of sulfoxide-MA **3** in solution (9/1 buffer/DMF), likely either via a solvent-induced addition-substitution SN2' reaction or a two-step process in which a [2,3]-sigmatropic rearrangement to yield a sulfenate ester is followed by hydrolysis. Both of these mechanisms yield the same products. Accordingly, we observed HO-MA as the main side product, along with the common sulfenic acid degradation products mentioned previously (i.e. sulfide-MA **2**, sulfone-MA **4**, disulfide of MBA **5**). Furthermore, this degradation (Figure S6.17) also explains why oxidants that should selectively proceed via the sulfoxide pathway (main text, Figure 6.1, center) also show the formation of minor amounts of sulfone-MA **4** over time—not due to over-oxidation but due to sulfoxide-MA degradation instead. This sulfone-MA **4** formation may, however, be somewhat suppressed in the presence of oxidants compared to the free degradation of sulfoxide-MA **3**, as oxidants can react with the sulfenic acid, reducing the formation of its degradation products that would otherwise form in a non-oxidizing environment such as in this experiment (Figure S6.17).

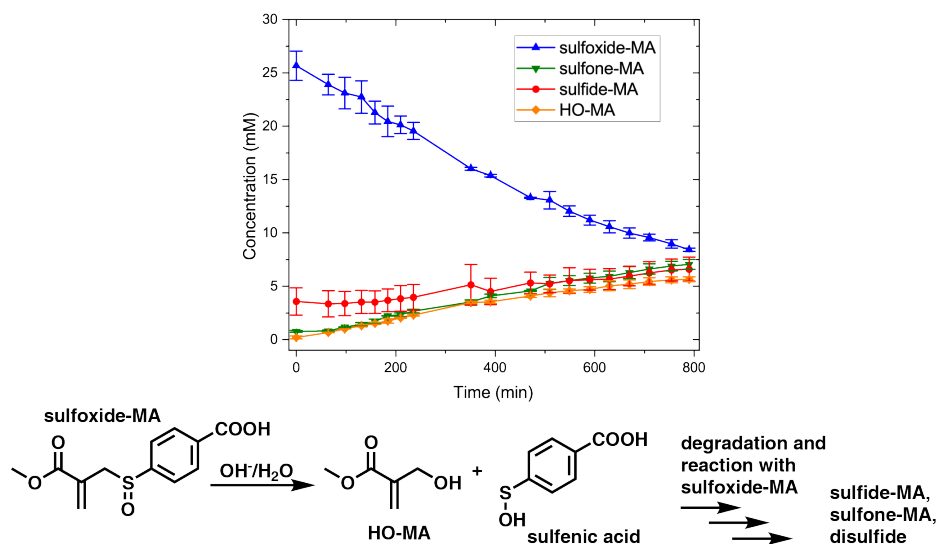


**Figure S6.17:** Degradation of sulfoxide-MA **3** in 9/1 0.5 M pH 8.0 buffer/DMF. Unlike sulfide-MA **2** and sulfone-MA **4**, sulfoxide-MA **3** is unstable in solution and degrades to yield HO-MA and the common side products of sulfenic acid degradation (refer to Scheme S6.1). **Note:** The initial presence of sulfide-MA **2** is due to incomplete oxidation of this batch of sulfoxide-MA **3**. However, this likely plays no role in the degradation of sulfoxide-MA **3**.

## Bromate: reference reactions

To further corroborate the way in which the third CRN proceeds (Figure 6.1, right scheme, main text), we reacted potassium bromate with sulfide-MA, with MBA, and with proline. We found that, unlike stronger oxidants, bromate is incapable of oxidizing sulfide-MA, neither to sulfoxide-MA nor sulfone-MA (see Figure S6.18). This was expected, as bromate is typically not the active oxidizer but requires acidic conditions and the presence of bromide ions to comproportionate into the more reactive bromine. At pH 8 and without bromide ions, these conditions are not given. Also, unlike Oxone, bromate does not react with proline (see Figure S6.19), avoiding the side reaction of forming oxidized proline-MA as it is found with stronger oxidants. However, bromate efficiently oxidizes the thiol MBA to form the corresponding disulfide of MBA **5** (see Figure S6.20).

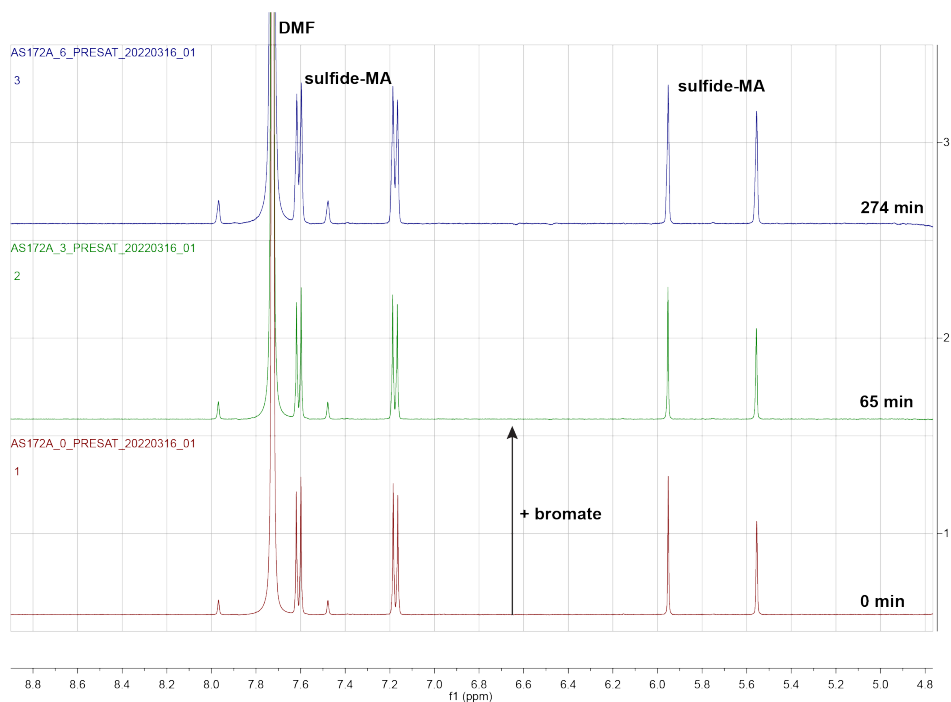


**Figure S6.18:** sulfide-MA **2** with 2.5 eq. potassium bromate. No oxidation of sulfide-MA **2** could be observed at pH 8.0 over the observed timeframe.

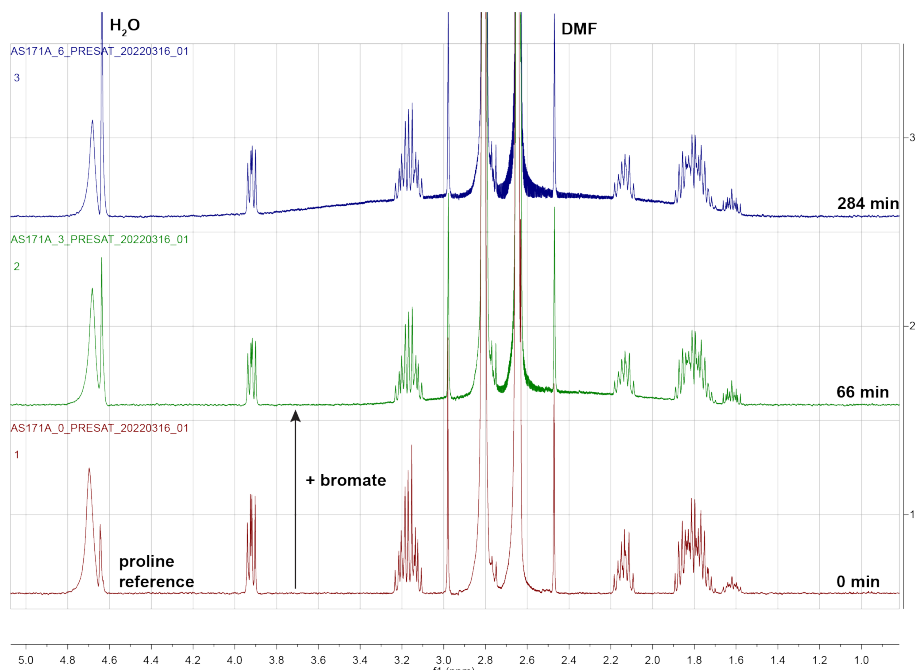


**Figure S6.19:** proline with 2.5 eq. potassium bromate. No oxidation of proline could be observed at pH 8.0 over the observed timeframe.

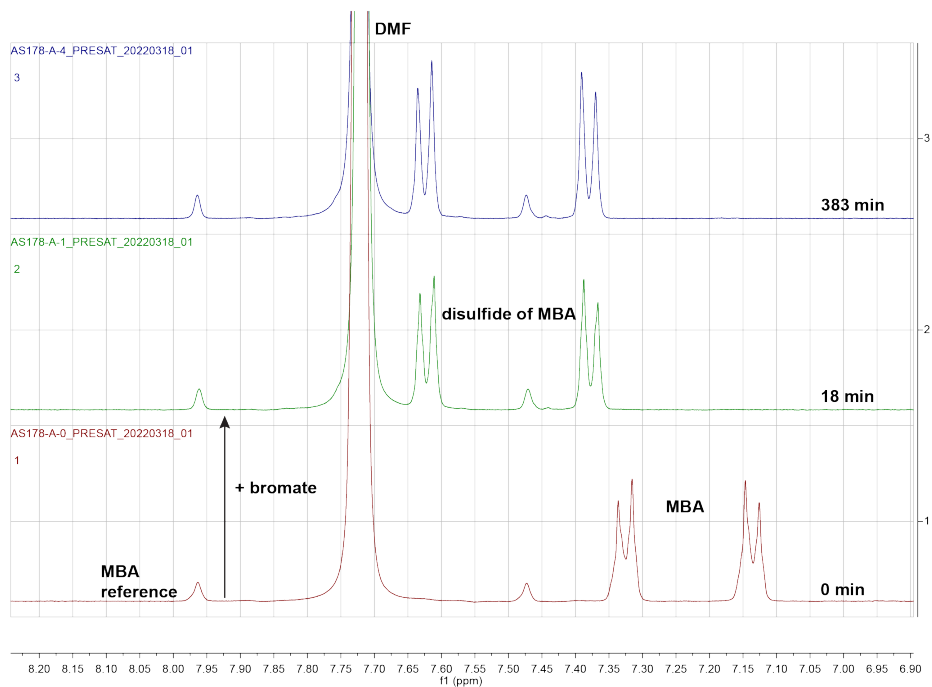


**Figure S6.20:** MBA with 2.5 eq. potassium bromate. MBA was quickly oxidized to the corresponding disulfide of MBA 5.

### Addition reactions without substitution: Loss of double bond functionality

As can be seen in Scheme S6.1, one of the side reactions which causes a loss of double bond functionality is the addition of a nucleophile (amine, thiol) to any MA-species without a substitution (i.e. expelling of leaving group) taking place. This side reaction is difficult to track via NMR due to the absence of acrylic signals and the strong overlap of the remaining signals. Hence, we resorted to HRMS to prove the formation of double adducts.

First, we investigated to the behavior of Proline-MA **1** over time in the presence of 1.0 eq. free proline (Figure S6.21). We found a decrease of roughly 15 % in total MA-moiety concentration over 29 h when adding 1.0 eq. proline to a 30 mM solution of Proline-MA **1**. Quantifying the double adduct via NMR is challenging due to the strong overlap and absence of acrylic signals. However, we managed to identify the double adduct via HRMS as the main side product:

ESI-LC/HRMS (m/z): calculated for  $[C_{15}H_{24}N_2O_6]^+$  329.1707, found: 329.1693.

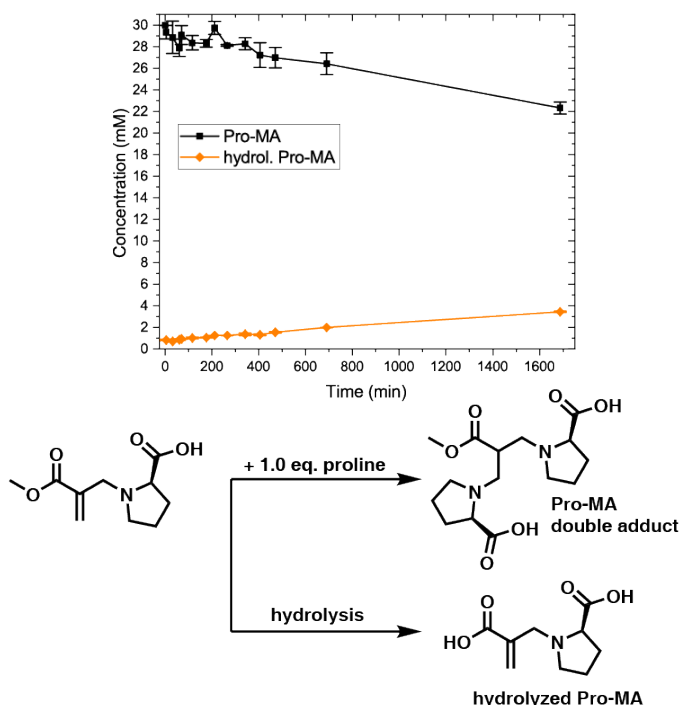


**Figure S6.21:** Double addition of proline to proline-MA **1**, along with background hydrolysis. The overall concentration of double bond moieties (i.e. proline-MA **1** + hydrolyzed Proline-MA) decreases from 30.0 mM to 25.8 mM.

Next, we tested the behavior of sulfoxide-MA **3** and sulfone-MA **4** in the presence of 2.0 eq. free proline. As the reaction of **3** with proline will also generate sulfide-MA **2** in the process, these experiments also serve to probe for the double addition to **2**. This also explains the non-quantitative yield of proline-MA **1** + MBA in stepwise additions; a part (usually ~ 10 %) gets lost due to the addition side reaction. Indeed, we managed to confirm all species proposed in Scheme S6.1 via HRMS:

- Addition of proline to sulfoxide-MA **3**:  
**ESI-LC/HRMS (m/z)**: calculated for  $[C_{17}H_{22}NO_7S]^+$  384.1111, found: 384.1153.
- Addition of proline to sulfone-MA **4**:  
**ESI-LC/HRMS (m/z)**: calculated for  $[C_{17}H_{22}NO_8S]^+$  400.1061, found: 400.1046; calculated for  $[C_{17}H_{20}NO_8S]^-$  398.0915, found: 398.0918.
- Addition of 4-mercapto benzoic acid (MBA) to sulfide-MA **2**:  
**ESI-LC/HRMS (m/z)**: calculated for  $[C_{19}H_{17}O_6S_2]^-$  405.0472, found: 405.0475.
- Addition of MBA to sulfoxide-MA **3**:  
**ESI-LC/HRMS (m/z)**: calculated for  $[C_{19}H_{19}O_7S_2]^+$  423.0567, found: 423.0550; calculated for  $[C_{19}H_{17}O_7S_2]^-$  421.0421, found: 421.0425.
- Addition of MBA to sulfone-MA **4**:  
**ESI-LC/HRMS (m/z)**: calculated for  $[C_{19}H_{19}O_8S_2]^+$  439.0516, found: 439.0502; calculated for  $[C_{19}H_{17}O_8S_2]^-$  437.0370, found: 437.0373.

### Phosphine + MA

One of the most dominant side reactions we found in the flow experiments with TCEP was the addition of proline-MA **1** to form a TCEP-MA adduct. To confirm this, we measured a reference  $^{31}P$  spectrum of TCEP and added 1.0 eq. Br-MA. We found the same signals as in the flow experiments, both in  $^1H$  and  $^{31}P$  spectra. Interestingly, two phosphorus signals appeared upon the addition of Br-MA, with close chemical shifts. We hypothesize that these are the mono- and double-adduct of TCEP to Br-MA. Other reagents, such as borohydrides, may be an alternative recovery reagent in batch conditions, however, preparing stock solutions for flow experiments is difficult due to their *in situ* degradation.<sup>14,15</sup>

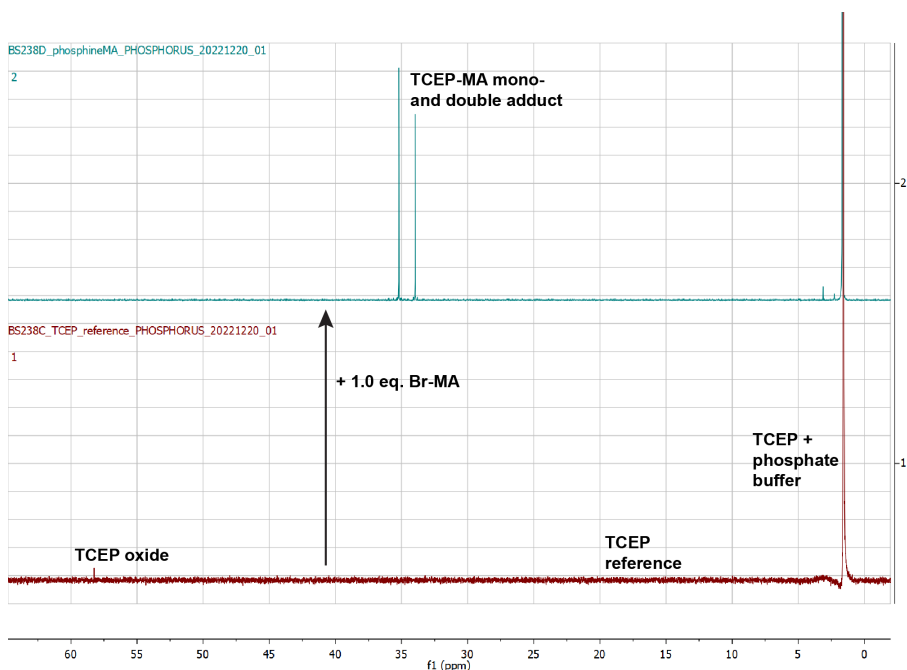


**Figure S6.22:** Addition of 1.0 eq. Br-MA to TCEP, yielding two new signals of TCEP-MA adducts, likely the mono- and bis-adducts.

### Bromate RC with aliphatic thiol

After we managed to identify satisfying conditions for our bromate RC with our typically employed thiol MBA and proline, we tested the influence of using a different thiol. We started the cycle with proline but using an aliphatic thiol—3-mercaptopropionic acid—instead of MBA.

We found that with 3-mercaptopropionic acid (3MPra), unlike with MBA, no significant recovery could be observed (see Figure S6.23). We hypothesize that this has to do with the acidity of the employed thiol. Under nucleophilic attack from proline, MBA is a much better leaving group due to the high charge stabilization of its thiolate. The much lower acidity probably pushes the equilibrium between proline-MA **1** and 3MPra-MA even further toward the side of the sulfide, strongly disfavoring the thiolate as a leaving group and hence not leading to any recovery of initial proline-MA **1** over the observed timescale.

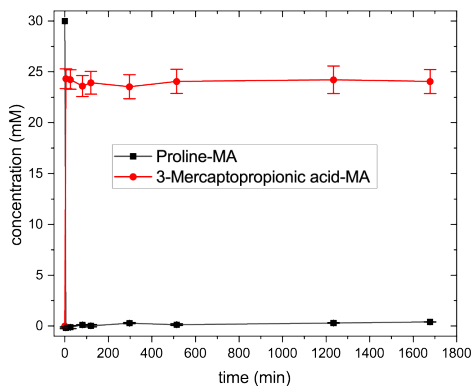


**Figure S6.23:** simultaneous addition of 1.0 eq. of 3MPrA and 2.5 eq. potassium bromate to a 30 mM solution of proline-MA **1**. While the sulfide-MA **2** forms efficiently and fast, as with MBA, no recovery of proline-MA **1** can be observed over time.

## References

1. Koo, B. S., Lee, C. K. & Lee, K. J. Oxidation of benzyl alcohols with Oxone® and sodium bromide. *Synth. Commun.* **32**, 2115–2123 (2002).
2. Murahashi, S.-I. & Shiota, T. Short-Step Synthesis of Amino Acids And N-Hydroxyamino Acids From Amines. *Tetrahedron Lett.* **28**, 5241–5244 (1987).
3. Gella, C., Ferrer, È., Alibés, R., Busqué, F., De March, P., Figueredo, M. & Font, J. A metal-free general procedure for oxidation of secondary amines to nitrones. *J. Org. Chem.* **74**, 6365–6367 (2009).
4. Ligon, S. C., Seidler, K., Gorsche, C., Griesser, M., Moszner, N. & Liska, R. Allyl sulfides and  $\alpha$ -substituted acrylates as addition-fragmentation chain transfer agents for methacrylate polymer networks. *J. Polym. Sci. Part A Polym. Chem.* **54**, 394–406 (2016).
5. Denmark, S. E., Forbes, D. C., Hays, D. S., DePue, J. S. & Wilde, R. G. Catalytic Epoxidation of Alkenes with Oxone. *J. Org. Chem.* **60**, 1391–1407 (1995).
6. Nagy, P. & Winterbourn, C. C. Redox chemistry of biological thiols. *Adv. Mol. Toxicol.* **4**, 183–222 (2010).
7. Kice, J. L., Venier, C. G., Large, G. B. & Heasley, L. Mechanisms of Reactions of Thiolsulfonates (Sulfenic Anhydrides). III. The Sulfide-Catalyzed Disproportionation of Aryl Thiosulfonates. *J. Am. Chem. Soc.* **91**, 2028–2035 (1969).
8. Matos, M. J., Oliveira, B. L., Martínez-Sáez, N., Guerreiro, A., Cal, P. M. S. D., Bertoldo, J., Maneiro, M., Perkins, E., Howard, J., Deery, M. J., Chalker, J. M., Corzana, F., Jiménez-Osés, G. & Bernardes, G. J. L. Chemo- and Regioselective Lysine Modification on Native Proteins. *J. Am. Chem. Soc.* **140**, 4004–4017

- (2018).
9. White, D. H., Noble, A., Booker-Milburn, K. I. & Aggarwal, V. K. Diastereoselective Photoredox-Catalyzed [3 + 2] Cycloadditions of N-Sulfonyl Cyclopropylamines with Electron-Deficient Olefins. *Org. Lett.* **23**, 3038–3042 (2021).
  10. Spiro, M. The standard potential of the peroxosulphate/sulphate couple. *Electrochim. Acta* **24**, 313–314 (1979).
  11. Challenger, S., Derrick, A., Mason, C. P. & Silk, T. V. Stereoselective Synthesis of a Cadoxatril Intermediate via Asymmetric Hydrogenation. *Tetrahedron Lett.* **40**, 2187–2190 (1999).
  12. Truce, W. E. & Roberts, F. E. A Convenient Synthesis of Aromatic and Aliphatic Sodium Sulfinates. *J. Org. Chem.* **28**, 593–594 (1963).
  13. Murahashi, S.-I., Imada, Y. & Ohtake, H. Tungstate-Catalyzed Decarboxylative Oxidation of N-Alkyl- $\alpha$ -amino Acids: An Efficient Method for Regioselective Synthesis of Nitrones. *J. Org. Chem.* **59**, 6170–6172 (1994).
  14. Stahl, C. R. & Siggia, S. Determination of Organic Disulfides by Reduction with Sodium Borohydride. *Anal. Chem.* **29**, 154–155 (1957).
  15. Duane Brown, W. Reduction of protein disulfide bonds by sodium borohydride. *Biochim. Biophys. Acta* **44**, 365–367 (1960).

# Summary

Nature has inspired countless researchers in their quest to understand the phenomena we observe and utilise their findings to develop new technologies. This becomes especially apparent in systems chemistry, which heavily draws inspiration from natural systems in its pursuit for the understanding and development of chemical reaction networks (CRNs) with interesting properties. Today, CRNs play a big role in many sensors, amplification systems, transient materials, and more.

Despite major advances in the field of CRNs, there is still a need for additional robust, versatile chemistries to allow for more diverse applications, both within systems chemistry and in other fields beyond, such as material science. This thesis aims to explore new applications of Dynamic Covalent Chemistry (DCvC)—typically utilised to make self-healing materials—in CRNs to allow for new applications drawing from the versatile chemistry used in DCv systems.

In **chapter 1**, we supply a general introduction to CRNs and DCvC and explain the research goals of this work in more detail.

In **chapter 2** of this thesis, we provide a literature overview about DCv ureas. We have outlined their historical development, their properties, both on a molecular as well as material scale, given a comprehensive guide to the reader on how to design DCv ureas with different stabilities, summarised their applications, and given an outlook on potential future applications.

In **chapter 3**, we have applied DCv ureas in a new context. Beyond their typical use in self-healing materials, we have shown that the amine present in the equilibrium of DCv ureas can be applied as a latent catalytic species, as well as equimolar reagent. More specifically, we have demonstrated that DCv ureas can be used as heat- and solvent-triggered moieties to catalyse Fmoc-deprotections, leading to the release of a catalyst and subsequently the catalysis of acylhydrazone formation on demand. Further, DCv ureas can be used as heat-triggered reagents to release nitrile-*N*-oxides from chlorooximes to make organogels on demand. These findings expand the field of applications of DCv ureas and show their use as triggered catalysts in reaction cascades.

In **chapter 4**, we have expanded on the findings of chapter 3 and demonstrated that DCv ureas can form synergistic, self-healing materials with thiol-maleimide units. Thiol-maleimide networks have been shown previously to be self-healing. DCv ureas, however, can be implemented into these networks to improve the exchange reaction between thiol-maleimide units through base-catalysis of the self-healing process. Just like in chapter 3, the base present in the DCv urea equilibrium is the catalytically active species, demonstrating the application of this concept in the context of material science.

In **chapter 5**, the start of the second part of this thesis, we provide a literature review of the chemistry and applications of  $\beta'$ -substituted Michael acceptors (MA). They are species which are capable of undergoing exchange reactions with different nucleophiles such as amines and thiols. This allows them to be used in CRNs. We have summarised

their most recent applications in different CRNs and given an outlook on their potential future applications.

Finally, in **chapter 6**, we demonstrate a new application of  $\beta'$ -substituted MAs. Typically, these MAs have been used as stimuli in CRNs. We show a CRN where  $\beta'$ -substituted MAs can act as the substrates, creating a system where the MA moiety is retained throughout the cycle through the use of different nucleophiles and oxidation chemistry. Moreover, we show that the oxidant is not only essential in activating the substrate to allow for recovery of the starting material, but can also be used to tune the pathway that the CRN takes, as well as the scope of side reactions and its kinetics. Further, we demonstrate that under flow conditions, the waste species, a disulfide, can be recovered, and the CRN can be cycled between different states.

Concluding, we have shown that DCv ureas and DCv Michael acceptors have different applications beyond their typical scope of use. We have demonstrated the application of DCv ureas as triggered catalysts and reagents, and shown that they can form synergistic self-healing networks with thiol-maleimide units. We have also introduced DCv Michael acceptors into a CRN and shown that they can effectively be recovered via oxidation chemistry, while offering control over the CRN pathway and kinetics. Together, these findings show that great potential lies within chemistry that has already been studied in detail. More efforts are warranted to come up with new, creative ways to apply the chemistry that we already know and understand to new areas via an interdisciplinary approach. While we managed to show applications in synergistic self-healing networks, CRN control, and triggered catalytic cascades, we believe that DCvC will find many more applications in different fields in the future, in ways which we have not yet envisioned.

# Samenvatting

De natuur heeft talloze onderzoekers geïnspireerd in hun zoektocht om de fenomenen die we waarnemen te begrijpen en hun conclusies te gebruiken om nieuwe technologieën te ontwikkelen. Dit wordt vooral duidelijk in de systeemchemie, die zich sterk laat inspireren door natuurlijke systemen in haar streven naar begrip en ontwikkeling van chemische reactienetwerken (CRN's) met interessante eigenschappen. Tegenwoordig spelen CRN's een grote rol in veel sensoren, versterkingssystemen, tijdelijke materialen en nog veel meer.

Ondanks de grote vooruitgang op het gebied van CRN's, is er nog steeds behoefte aan aanvullende robuuste, veelzijdige chemie om meer diverse toepassingen mogelijk te maken, zowel binnen de systeemchemie als in andere gebieden daarbuiten, zoals de materiaalkunde. Dit proefschrift heeft als doel om nieuwe toepassingen van Dynamische Covalente Chemie (DCvC)—die gewoonlijk gebruikt wordt om zelfhelende materialen te maken—in CRN's te onderzoeken, om nieuwe toepassingen mogelijk te maken die gebruik maken van de veelzijdige chemie die gebruikt wordt in DCv-systemen.

In **hoofdstuk 1** geven we een algemene inleiding tot CRNs en DCvC en leggen we de onderzoeksdoelen van dit werk in meer detail uit.

In **hoofdstuk 2** van dit proefschrift geven we een literatuuroverzicht over DCv urea's. We hebben hun historische ontwikkeling geschetst, hun eigenschappen, zowel op moleculaire als op materiële schaal, een uitgebreide handleiding gegeven aan de lezer voor het ontwerpen van DCv urea's met verschillende stabiliteiten, hun toepassingen samengevat en een vooruitblik gegeven op mogelijke toekomstige toepassingen.

In **hoofdstuk 3** hebben we DCv urea's in een nieuwe context toegepast. Naast hun typische gebruik in zelfherstellende materialen, hebben we laten zien dat het amine dat aanwezig is in het evenwicht van DCv urea's kan worden toegepast als een latente katalysator, evenals equimolair reagens. Meer specifiek hebben we aangetoond dat DCv urea's kunnen worden gebruikt als warmte- en oplosmiddelgeïnitieerde verbindingen om Fmoc-ontschermingen te katalyseren, wat leidt tot het vrijkomen van een katalysator en vervolgens de katalyse van acylhydrazonvorming op verzoek. Verder kunnen DCv-urea's worden gebruikt als door warmte geïnitieerde reagentia om nitril-*N*-oxiden vrij te maken uit chlooroximen om organogels te maken op verzoek. Deze bevindingen breiden het toepassingsgebied van DCv urea's uit en tonen hun gebruik als initieerbare katalysatoren in reactiecascade.

In **hoofdstuk 4** hebben we de bevindingen van hoofdstuk 3 uitgebreid en aangetoond dat DCv urea's synergetische, zelfherstellende materialen kunnen vormen met thiol-maleimide eenheden. Van thiol-maleimidenetwerken is eerder aangetoond dat ze zelfhelend zijn. DCv-urea's kunnen echter in deze netwerken worden geïmplementeerd om de uitwisselingsreactie tussen thiol-maleimide-eenheden te verbeteren door basekatalyse van het zelfgenezingsproces. Net als in hoofdstuk 3 is de base die aanwezig

is in het DCv urea evenwicht de katalytisch actieve soort, waarmee de toepassing van dit concept in de context van de materiaalkunde wordt aangetoond.

In **hoofdstuk 5**, de start van het tweede deel van dit proefschrift, geven we een literatuuroverzicht van de chemie en toepassingen van  $\beta'$ -gesubstitueerde Michaelacceptoren (MA). Dit zijn soorten die in staat zijn om uitwisselingsreacties te ondergaan met verschillende nucleofielen zoals amines en thiolen. Hierdoor kunnen ze worden gebruikt in CRN's. We hebben hun meest recente toepassingen in verschillende CRN's samengevat en een vooruitblik gegeven op hun mogelijke toekomstige toepassingen.

Tot slot laten we in **hoofdstuk 6** een nieuwe toepassing van  $\beta'$ -gesubstitueerde MA's zien. Gewoonlijk zijn deze MA's gebruikt als stimuli in CRN's. We laten een CRN zien waarbij  $\beta'$ -gesubstitueerde MA's als substraat kunnen fungeren, waardoor een systeem ontstaat waarbij het MA deeltje gedurende de hele cyclus behouden blijft door het gebruik van verschillende nucleofielen en oxidatiechemie. Bovendien laten we zien dat het oxidatiemiddel niet alleen essentieel is voor de activering van het substraat, zodat het uitgangsmateriaal kan worden teruggewonnen, maar ook kan worden gebruikt om de route die de CRN volgt af te stemmen, evenals de omvang van de nevenreacties en de kinetiek. Verder laten we zien dat onder stromingsomstandigheden de afvalsoort, een disulfide, kan worden teruggewonnen en de CRN kan worden heen en weer geslingerd tussen verschillende toestanden.

Concluderend hebben we aangetoond dat DCv urea's en DCv Michaelacceptoren verschillende toepassingen hebben buiten hun typische toepassingsgebied. We hebben de toepassing van DCv ureas als getriggerde katalysatoren en reagentia aangetoond en laten zien dat ze synergetische zelfherstellende netwerken kunnen vormen met thiol-maleimide eenheden. We hebben ook DCv Michaelacceptoren geïntroduceerd in een CRN en aangetoond dat ze effectief kunnen worden teruggewonnen via oxidatiechemie, terwijl ze controle bieden over de CRN route en kinetiek. Samen laten deze bevindingen zien dat er een groot potentieel ligt binnen chemie die al in detail is bestudeerd. Er zijn meer inspanningen nodig om nieuwe, creatieve manieren te bedenken om de chemie die we al kennen en begrijpen toe te passen op nieuwe gebieden via een interdisciplinaire aanpak. Hoewel we erin geslaagd zijn om toepassingen te laten zien in synergetische zelfhelende netwerken, CRN-besturing en getriggerde katalytische cascades, geloven we dat DCvC in de toekomst nog veel meer toepassingen zal vinden op verschillende gebieden, op manieren die we nog niet hebben voorzien.

*This translation was performed with the help of Uitmuntend (German-Dutch online dictionary (see <https://www.uitmuntend.de/>) and the free version of DeepL (see <https://www.deepl.com/translator>), accessed in October 2023.*

# Acknowledgement

First and foremost, I would like to thank **Rienk** for hiring me to work on such an interesting range of projects. Thank you for the lessons I learned from you: all the scientific discussions, corrections of paper drafts, figures, and schemes, and countless group meetings. Thanks to your valuable input, I went from receiving > 100 corrections on a paper draft to only a handful over the last few years and I am very grateful for all the skills I learned; especially those of non-scientific nature such as writing, presenting, project management, leadership, independence, and more. I would also like to thank you for your relaxed, open, and empathic attitude towards me. I can recall at least two difficult situations due to some health issues in my first year where you gave me all the space to breathe that I needed, so that I could get better without unnecessary pressure. I highly appreciate this. Thank you!

Next, I would like to thank **Jan** for being my co-promotor and for proof-reading my thesis. Our discussions were always fruitful and I appreciate the shared dinners during the arrival or departure of students.

Also, my sincere gratitude goes to the whole **thesis committee** for taking their time to examine this work and test me during my defence and to **Thomas Hermans** for hosting and supervising me during my stay at the University of Strasbourg and the many extremely fruitful and educative, although sometimes frustrating, discussions we had in writing the paper about this amazing project (chapter 6); I learned tons in the process!

To the whole **ASM and Eelkema group**, thank you for the warm welcome and the great time. I immediately felt part of the team and the working environment was always very pleasant. I enjoyed all the shared food and after-work activities, despite the unfortunately long break due to the pandemic restrictions. Thank you to **Reece & Sarah** for our shared coffee adventures and game nights, **Peggy** for our cooperation on the peptide project and the many talks about work, life, and the future, **Sietse and Aleksandra** for all your help in the lab with maintenance, ordering of chemicals, student supervision, and more, **Stephen** for the shared coffees and talks about the world, philosophy, politics, languages, travel, and of course your help with NMR measurements and your trust in me for backup maintenance, **Guotai, Juncheng, and Bohang** for our shared tea in the office and many interesting talks about Chinese language, culture, and your plans for the future, **Irene and Benjamin** for fruitful project discussions, your company and cooperation during long NMR weekends, and of course Irene's expertise for getting the best pizza delivered to the TU, **Tobias** for the cooperation on the mechanoresponsive polymer; despite not being very successful, I enjoyed it a lot, **Mariano** for the help in the lab and the nice discussions about life and career, **Marcel Bus** for the recommendation of the Dutch class with your wife, and the nice discussions we had (and always greeting everybody by name, which is a small detail, but feels very nice!), and my students **Siebe, Lukas, Lotte, Laura, Steffen, Melodie, and all LO2 students**, you were wonderful to supervise and I learned a lot about communication, management, and leadership in the process.

**Georgy**, you have a special place in my heart! You are among the most knowledgeable, eccentric, and direct people I have ever met. I learned a lot from our discussions, and I cherish your hands-on, get-it-done approach to work. Meh!

**Ardeshir**, thank you for being such a wonderful colleague over those four years. I enjoyed every talk with you and your relaxed, patient, mindful attitude was helpful to me many times. I enjoyed our shared adventures, all the way to Rome (toppoli).

**Elmira**, I feel very blessed that we met and managed to have very deep, insightful, philosophical discussions throughout the past years. I enjoyed all our shared dinners, adventures, the trip to Italy, and I immensely appreciate your trust! Thank you for being such a great friend and for all the guguli maguli!

**Hendrik**, without you, the whole PhD journey would have only been half the fun. From the day I entered the office, I felt like we will have a great bond. Thank you so much for all the fun we had together in the office and lab. The shared road trips, cooking sessions, visits at countless restaurants in the surrounding cities, and more. Especially the last year of living together is an experience I will never forget. This has only been possible in large part due to your spontaneity and open-mindedness, and I can say for sure that you taught me to be more flexible, relaxed, and patient. I never thought I would say this, but thank you for offering me so much marble to heat.

**Nastia**, we met pretty much exactly when this whole PhD journey started, in Israel in December 2019. I had many different fears, thoughts, and hopes before embarking on the road to PhD, but in none of the scenarios I envisioned, it went like this. Having the first date in Brussels one week before complete lockdown and starting a relationship by living together on 24 m<sup>2</sup> with a curfew, and then reverting back to a distance relationship is basically the opposite (and more!) of what most couples go through. However, it has shown us in the most immediate way possible that it just works; and I will forever cherish our story. Words cannot express how grateful I am for your support throughout those years. I am beyond excited for the years to come, and I cannot wait to see you grow, and to grow myself, at your side, throughout the challenges that the future has in stock for us!

Dank gilt nicht zuletzt **meinen Eltern**: ohne eure Unterstützung, Liebe und Offenheit hätte ich niemals Chemie studiert und meinen Doktorgrad erreicht. Die diversen Wochenenden und Feiertage bei euch während der letzten vier Jahre waren stets ein Energiebooster, der Nastia und mir die Kraft gegeben hat, weiter unsere Projekte zu bewältigen. Danke für eure bedingungslose Unterstützung. Ihr seid die besten Eltern!

Last but not least, thank you to my friends **Alex and Lisa**: your continued support throughout the last decade has helped me to pursue my goals and overcome struggles. I am blessed to have you.

## About the author

Benjamin Spitzbarth was born in 1994 in Frankfurt am Main, Germany. Upon graduating from school in 2014, he pursued his studies in chemistry at the University of Mainz, Germany. Here, he finished his B.Sc. in the group of Prof. Pol Besenius in 2017. He continued his studies in chemistry at the University of Mainz, and was awarded with the German Scholarship (“Deutschlandstipendium”) and PROMOS Scholarship. During a 6-months internship in Prof. Rein Ulijn’s laboratory at the City University New York, he researched transient biocatalytic self-assemblies. Back in Germany, he did his Master thesis in the group of Prof. Till Opatz, developing a photoredox-catalysed 4-component reaction. Upon finishing his thesis in 2019, he graduated with a M.Sc. in chemistry in the top 10%. In November 2019, he joined the group of Dr. Rienk Eelkema at TU Delft as a Marie Curie Fellow in the CReaNet Innovative Training Network (ITN). Here, as well as during an internship at the University of Strasbourg with Prof. Thomas M. Hermans, he has been working on the application of Dynamic Covalent bonds in Chemical Reaction Networks.

## List of Publications

**Spitzbarth, B.** & Eelkema, R. Chemical reaction networks based on conjugate additions on  $\beta$ -substituted Michael acceptors. *Chem. Commun* **59**, 11174–11187 (2023).

Sharko, A.<sup>#</sup>, **Spitzbarth, B.**<sup>#</sup>, Hermans, T. M. & Eelkema, R. Redox-Controlled Shunts in a Synthetic Chemical Reaction Cycle. *J. Am. Chem. Soc.* **145**, 9672–9678 (2023). (# authors contributed equally)

**Spitzbarth, B.** & Eelkema, R. On-Demand Release of Secondary Amine Bases for the Activation of Catalysts and Crosslinkers. *Chem. Eur. J.* **29**, e202203028 (2023).

Kammer, L. M., Krumb, M.<sup>#</sup>, **Spitzbarth, B.**<sup>#</sup>, Lipp, B., Kühlborn, J., Busold, J., Mulina, O. M., Terentev, A. O. & Opatz, T. Photoredox-Catalyzed Four-Component Reaction for the Synthesis of Complex Secondary Amines. *Org. Lett.* **22**, 3318–3322 (2020). (# authors contributed equally)

